12-2013

Synthesis and Characterization of Three New Tetrakis(N-phenylacetamidato) Dirhodium(II) Nitrile Complexes

Nkongho Atem-Tambe
East Tennessee State University

Recommended Citation

Synthesis and Characterization of Three New Tetrakis(N-phenylacetamidato) Dirhodium(II)

Nitrile Complexes

_____

A thesis

presented to

the faculty of the Department of Chemistry

East Tennessee State University

In partial fulfillment

of the requirements for the degree

Master of Science in Chemistry

_____

by

Nkongho Atem-Tambe

December 2013

_____

Dr. Cassandra T. Eagle

Dr. Scott Kirkby

Dr. Ningfeng Zhao

Keywords: Tetrakis, Paddlewheel, X-ray, Dirhodium, Nitrile, Polymer, Rh_2L_4

ABSTRACT

Synthesis and Characterization of Three New Tetrakis(N-phenylacetamidato) Dirhodium(II)

Nitrile Complexes

by

Nkongho Atem-Tambe

Three new tetrakis [$Rh_2(PhNCOCH_3)_4 \cdot xNCR$] (R = {2-CH_3}C_6H_4 (x=2), R = {3-CH_3}C_6H_4 (x=1), R = (3-CN)C_6H_4 (x=1)) complexes have been synthesized and characterized. These complexes were characterized by IR and ^{1}H NMR spectroscopies and X-ray crystallography that solved with $R_1 < 0.05$.

[$Rh_2(PhNCOCH_3)_4 \cdot 2NC\{2\text{-}CH_3\}C_6H_4$] was triclinic (a=9.79Å, b=14.79Å, c=16.36Å, α=103.84^0, β=99.17^0, γ=99.77^0, P-1(#2), µCN=2227.78cm^{-1}, Rh-Rh=2.42Å, N-C=1.13Å, 1.14Å, Rh-N=2.34Å, 2.35Å, Rh-N-C=151.6^0, 152.5^0, Rh-Rh-N=173.0^0, 174.6^0).

[$Rh_2(PhNCOCH_3)_4 \cdot NC\{3\text{-}CH_3\}C_6H_4$] was triclinic (a=11.71Å, b=13.02Å, c=13.40Å, α=72.34^0, β=66.78^0, γ=82.74^0, P-1(#2), µCN=2241.28cm^{-1}, Rh-Rh=2.40Å, N-C=1.14Å, Rh-N=2.16Å, Rh-N-C=166.3^0, Rh-Rh-N=175.9^0).

[$Rh_2(PhNCOCH_3)_4 \cdot 2NC\{3\text{-}CN\}C_6H_4$]$_\infty$ was triclinic (a=11.88Å, b=13.30Å, c=14.88Å, α=77.98^0, β=74.61^0, γ=65.48^0, P-1(#2), µCN=2233.57cm^{-1}, Rh-Rh=2.41Å, N-C=1.13Å, 1.13Å, Rh-N=2.18Å, 2.38Å, Rh-N-C=166.8^0, 127.7^0, Rh-Rh-N=178.4^0, 175.4^0).

The bond distances, bond angles and bonding interactions (σ and π) are similar to the metal-carbene bond formed during carbenoid transformations catalyzed by dirhodium(II) compounds.

DEDICATION

This thesis is dedicated to the Almighty Father, to my family, and to my friends.

ACKNOWLEDGEMENTS

I thank Dr. Cassandra Theresa Eagle for her able mentorship and incredible patience with me over these semesters we have had together. Working under her supervision, I have acquired increased understanding, leadership, wisdom, and guidance that should has shaped a lifetime ahead. I will forever say thank you for continued belief in me.

I thank my dad (Salvador J. A. Tambe), mom (Elizabeth Subi-Ngai Tambe), siblings (Bisong, Arrah, Bakaw, Ntoh, and Njui), family, and friends for never ceasing to support and believe in me. The pressure to make you proud is why I am here.

I thank Dr. Lee Daniels of Rigaku America for training in X-ray Crystallography and on the X-ray Diffractometer.

I thank all the professors and staff in the Chemistry Department at ETSU for making this journey a memorable one.

I thank God Almighty for His blessings and strength and for holding me up when I was falling down.

TABLE OF CONTENTS

LIST OF TABLES

LIST OF FIGURES

LIST OF ABBREVIATIONS

Ac   Acyl

Acam   Acetamide or Acetamidato

CCD   Charge Coupled Device

CPK   Corey, Pauling, Kulton

Et   Ethyl

IR   Infrared

Me   Methyl

MPLC   Medium Pressure Liquid Chromatography

NMR   Nuclear Magnetic Resonance

OAc   Acetate or Acetato

ORTEP   Oak Ridge Thermal Ellipsoid Plot

Ph   Phenyl

THF   Tetrahydro furan

TLC   Thin Layer Chromatography

TMS   Tetramethyl silane

UV   Ultraviolet

CHAPTER 1

INTRODUCTION

The purpose of this research was to understand the relationship between the rhodium –
carbene bond and the analogous rhodium- nitrile bond. By analyzing solid state crystal structures
of compounds where there is coordination of a nitrile containing ligand to a tetrakis (N-
phenylacetamidato) rhodium(II) complex, a better understanding of the rhodium – carbene bond
may be achieved. A major tool for the completion of this research was single crystal x-ray
diffraction from which information about bond lengths, bond angles, and unit cell parameters
may be obtained. Single crystal x-ray diffraction and other characterization techniques were
useful in providing structural information about these complexes.

X-ray Crystallography – The Technique

History and Discovery

By the late 18th century, many scientists worked on the emissions generated from the
cathode ray tube invention of the English scientist William Crookes, known as Crookes tubes.[1]
Johann Hittorf, a coinventor of these tubes, found that unexposed photographic plates placed
near these Crookes tubes where flawed by shadows.[1,2] He, however, did not investigate the
effect. In 1887, Nikola Tesla began investigation of these emissions using high voltage tubes he
had invented as well as Crookes tubes. By 1892, Nikola Tesla had performed several
experiments but did not categorize these emissions. Philipp Lenard, a student of Heinrich Hertz,
built his own version of the Crookes tubes, later called Lenard tubes, with a window in the end
made of thin aluminium facing the cathode so that the cathode rays would strike it.[1,3] He found
that some rays passed through the tube and when photographic plates were exposed to them

caused fluorescence. He measured the penetrating power of these rays, which he called Lenard rays, using several different materials. The Lenard rays were later discovered to consist of a variety of wavelengths.

Wilhelm Conrad Rontgen performed similar experiments as those of Lenard and Crookes.[1,2,3,4] While experimenting on Lenard and Crookes tubes, he observed cathode rays produced in free air; the same results as Lenard did. He further performed another experiment using a Rhumkoff induction coil to produce a large potential difference between the cathode and anode. He noticed an image was cast out of his cathode ray generator that was projected far beyond the possible range of cathode rays. After setting up several of these experiments, he found that the unknown radiation was generated at a point of contact of the cathode ray tube on the interior of the vacuum tube. After experimenting with several materials these unknown rays, which he called X-rays, he discovered that they were not deflected by a magnetic field nor were they stopped by the various kinds of materials used.

Rontgen kept working on this new, unknown type of radiation and was shortly able to convince the public of this radiation when he produced an x-ray photograph of his wife's (Bertha Rontgen) left hand that clearly showed her bones and wedding ring. This was an indication of the medical uses of X-rays. He was later awarded the Rumford gold medal of the U.K. Royal Society in 1896 and later in 1901 he received a Nobel Prize for physics.

X-rays and Bragg's Law

Applications of X-rays were soon found in crystallography. Max von Laue suggested that the periodic structure of a crystal may diffract X-rays in the same way the diffraction grating does with visible light. This was based on three assumptions:[5]

1. Crystals were periodic

2. X-rays were waves

3. The wavelengths of the X-rays, λ, were of the same magnitude as the repeat distance in the crystals

William Harris Bragg and William Lawrence Bragg (father and son), in 1913, discovered that crystalline solids produced diffracted patterns of X-rays due to diffraction of these rays off of crystal or lattice planes, also called Miller planes. These Miller planes are parallel to one another, equally spaced, and contain identical atomic arrangements. They found that the 3-dimensional arrangement of the crystal structure is perpendicular to the family of Miller planes within the crystal.[5] Figure 1 shows incident X-rays being diffracted off of Miller planes in the crystal lattice with interplanar spacing of d.[6] The X-rays (1, 2, 3) are incident on the set of Miller planes through an angle θ. These X-rays are scattered through the same angle θ. They exit parallel to one another as 1', 2', 3' for constructive interference (diffraction).
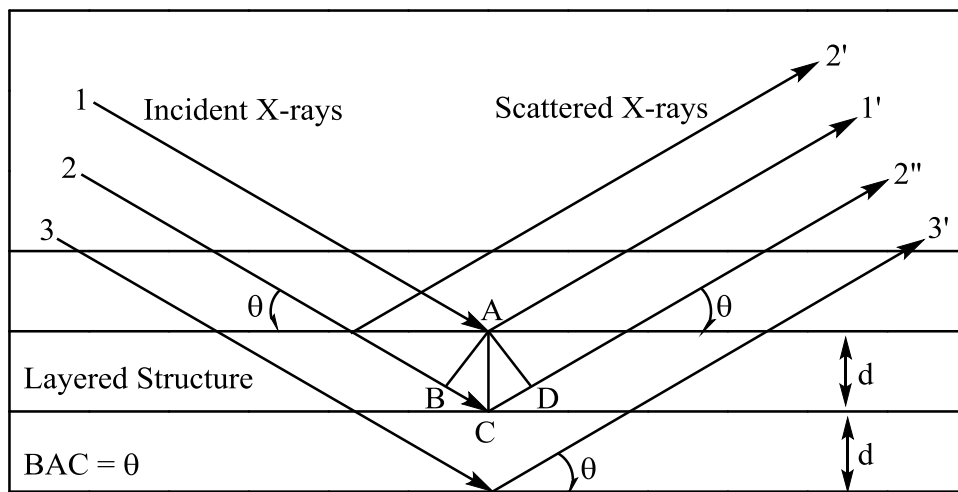
Figure 1. X-rays diffracted on a set of planes with interplanar spacing of d with and angle θ.(adapeted from [6])

When rays 1 and 2 reach the Miller plane at positions A and C, they are scattered through the angle θ. Constructing right angle triangles from point A to ray 2 (incident and scattered) generates points B and D for which angle BAC = angle CAD = θ because AC bisects the angle BAD = 2θ. Therefore, by trigonometry, $BC = CD = d\sin\theta$.

Thus, for diffraction;

$$n\lambda = 2d\sin\theta \tag{1}$$

where; d = lattice interplanar spacing within crystal

θ = X-ray angle of incidence (Bragg angle)

λ = wavelength of characteristic X-rays

n = positive interger (1, 2, 3 …)

The above is known as the Bragg condition and Equation 1 is known as Bragg's law.

Applications and Historical Success

Crystallographic applications have been seen over the years; Kathleen Longsdale in 1928, showed the planarity of the benzene ring by determining the structure of hexamethylbenzene.[7] Dorothy Crowfoot Hodgkin determined the structures of cholesterol (1937),[8] Vitamin B12 (1945),[8] penicillin (1954),[8] and Insulin (1969).[8] Max Perutz and Sir John Cowdery Kendrew determined the structure of Sperm whale myoglobin in 1959.[8]

X-ray diffraction was used by Rosalind Franklin who provided the crystallographic data that demonstrated the double stranded structure of DNA.[8] She provided the X-ray diffraction

image for DNA (which she also called, photo 51) that was used by James D. Watson and Francis Crick to build the double helical chemical model for DNA.

Paddlewheel Dirhodium(II) compounds

The Rh – Rh Bond

Four atomic orbitals are responsible for the bonding within the dirhodium(II) complex. They are d_{z2}, d_{xz}, d_{yz} and d_{xy}. These atomic orbitals combine to form the various molecular orbitals of the M – M bond. The positive overlap of 2 d_{z2} orbitals along the z-axis gives rise to a σ-bonding molecular orbital. A corresponding negative overlap of these orbitals gives rise to a σ*-antibonding molecular orbital. The overlaps of $d_{xz} + d_{xz}$ and $d_{yz} + d_{yz}$ give rise to 2 degenerate, orthogonal π-bonding molecular orbitals. Similarly, their negative overlaps give rise to 2 π*-antibonding molecular orbitals. The last pair of orbitals, a δ-bonding and δ*-antibonding orbital are formed from the positive and negative overlaps of the 2 d_{xy} atomic orbitals. The molecular orbitals and their atomic orbital contributors are shown in Figure 2.
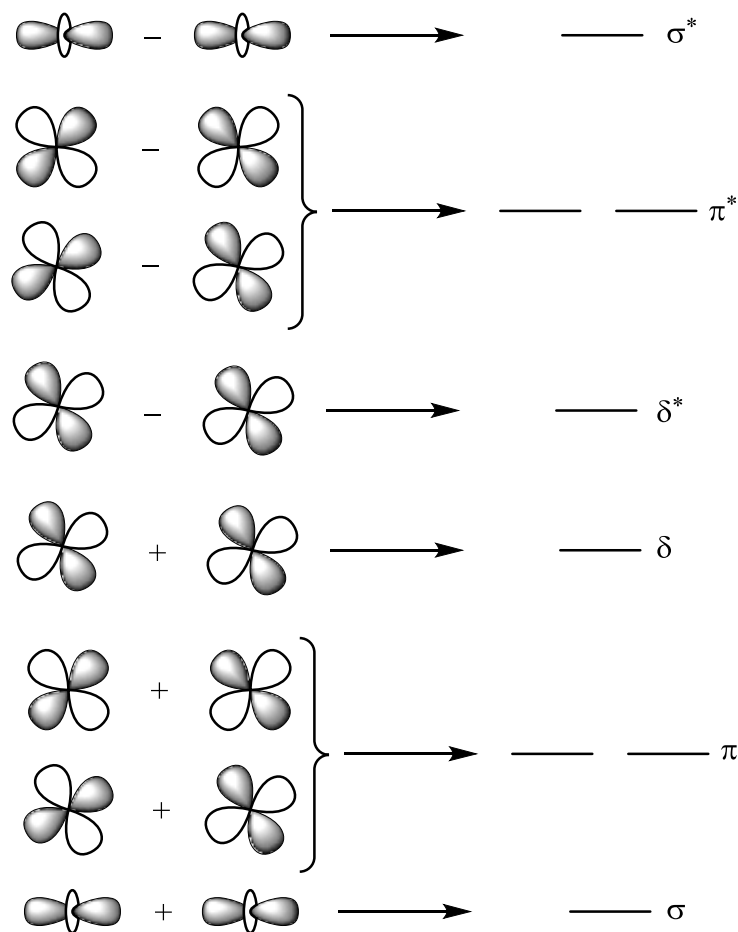
Figure 2. A simple molecular diagram showing overlap of d-orbitals in Rh – Rh complexes.[10]

The length of the Rh – Rh bond generally is between 2.35 – 2.45 Å.[9,10] Because each bridging ligand has a negative charge, each rhodium has a positive two charge. Thus, the dirhodium(II) compounds usually have Rh_2^{4+} cores and there are 7 d electrons per rhodium atom.[10] A simplified molecular orbital diagram for the dirhodium(II) unit shows its 14 electrons distributed in the σ-, π-, δ-orbitals and the remaining 6 electrons occupy the π*- and δ*-orbitals. This results in a net bond order of one and no unpaired electrons. The single bond has an electronic configuration of $\sigma^2\pi^4\delta^2\delta*^2\pi*^4$.

Structure of the Paddlewheel

Paddlewheel compounds generally possess 1 or 2 axial (ax) ligands that, by definition, lie along the z-axis. However, the Rh – Rh bond is insensitive to the presence of σ-donor axial ligands.[8] A $Rh_2(CO_2CH_3)_4$ compound has been synthesized that showed a tetrakis(tetracarboxylate) dirhodium(II) compound that completely lacks axial coordination by any ligand species[9] (see Figure 3 below). The compound contains 4 acetate ligands that each bridge 2 rhodium metal atoms (dirhodium core). Each acetate ligand also has a 1- charge that is resonance stabilized.
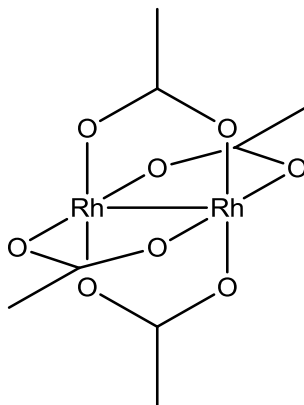
Figure 3. A paddlewheel structure for $Rh_2(CO_2CH_3)_4$.

There exists a 4-fold rotation axis (along the z-axis) and 4 perpendicular 2-fold rotation axes. In addition, there exists a horizontal and 4 vertical mirror planes. Thus, the tetrakis(tetracarboxylate) dirhodium(II) belongs to the D_{4h} point group. For convenience in this discussion, we will refer to this D_{4h} symmetry point group as the Paddlewheel structure.

Carboxylates to Carboxamidates

The tetrakis(carboxamidate) dirhodium(II) compounds may be prepared by refluxing the dirhodium(II) carboxylates in the presence of the carboxamidate ligand. The tetrakis(carboxylate) dirhodium(II) compounds, however, are synthesized from $RhCl_3$.

$$RhCl_3.H_2O \xrightarrow[\text{EtOH/reflux, N}_2]{CH_3CO_2H + CH_3CO_2Na} Rh_2(CH_3CO_2)_4.xEtOH$$

(2)
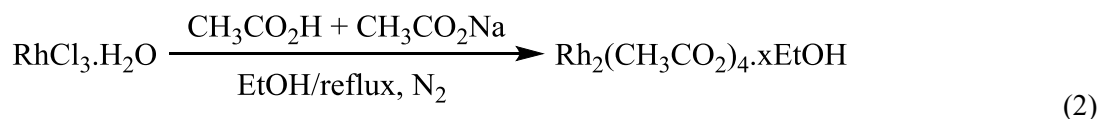
$RhCl_3$ is refluxed under N_2 in a mixture of sodium acetate, acetic acid, and ethanol.[10,11] The red solution of Rh(III) became dark dark green after one hour of reflux and the green solid precipitated out of solution. The product was then recrystallized from methanol. The yields for this process were between 80 – 85 %, and prolonged refluxing resulted in decomposition or reduction of $RhCl_3$ to rhodium metal.

The tetrakis(carboxamidate) dirhodium(II) compounds are produced by refluxing the tetrakis(carboxylate) dirhodium(II) compound in excess carboxamidate ligand boiling in chlorobenzene. The reaction is driven to completion by the use of a soxhlet extractor in which a thimble is filled with sodium carbonate and sand to trap the evolved acetic acid. Generally, there are 4 possible isomers that may be formed, as shown in Figure 4 below. The first is the 2,2-cis isomer that has 2 nitrogen atoms and 2 oxygen atoms on each rhodium atom. Both nitrogen atoms on each rhodium are 90^0 (cis) to one another. The second is the 2,2-trans isomer that has 2 nitrogen atoms and 2 oxygen atoms on each rhodium atom. Both nitrogen atoms on each rhodium are 180^0 (trans) to one another. The third is the 3,1- isomer that has 3 nitrogen atoms and 1 oxygen atom on 1 rhodium atom (sometimes referred to as the "three" side); 1 nitrogen atom and 3 oxygen atoms on the other rhodium atom (sometimes referred to as the "one" side).

The fourth is the 4,0- isomer that has 4 nitrogen atoms on 1 rhodium atom and 4 oxygen atoms on the other rhodium atom.

2,2-*cis*; C_{2h} 2,2-*trans*; D_{2d} 3,1; C_s 4,0; C_{4v}
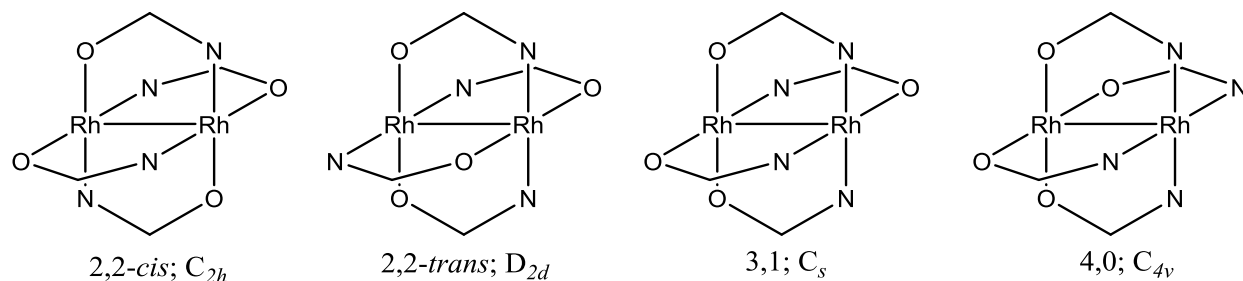
Figure 4. The different isomers of the tetrakis(carboxamidate) dirhodium(II) and the point group symmetries of their skeletal structures.[10]

Eagle and coworkers successfully synthesized tetrakis(N-phenylacetamidato) dirhodium(II) and observed the 2,2-cis, 2,2-trans, and 3,1- isomers but not the 4,0- isomer.[12] They have also reported the synthesis and characterization of the 2,2-trans isomer.[13] Bear, Kadish, and coworkers reported the presence of the 2,2-cis and 3,1- isomers.[14,15] Doyle and coworkers successfully isolated and obtained solid state structures for the chiral 3,1- isomer[16] and the 4,0- isomer.[17]

A detailed study of the reaction to form the tetrakis(carboxamidate) dirhodium(II) in Figure 4 has been done to explain the formation of the various isomers. Using oxoimidazolidinate as the carboxamidate ligand, the proposed mechanism is shown in Scheme 1.

N
HOAc   LH   N   LH   HOAc   N
Ac—Rh—Ac ←——— Ac—Rh—Ac ←——— Ac—Rh—Ac
O   Ac   N

LH   LH
                          LH
HOAc   HOAc
HOAc

N   N   N
Ac—Rh—N   Ac—Rh—O   Ac—Rh—N
O   N   N

LH   LH   LH

HOAc   HOAc   HOAc

N   N   N
O—Rh—N ⇌ LH ⇌ N—Rh—N ←—LH— N—Rh—N
O   O   N
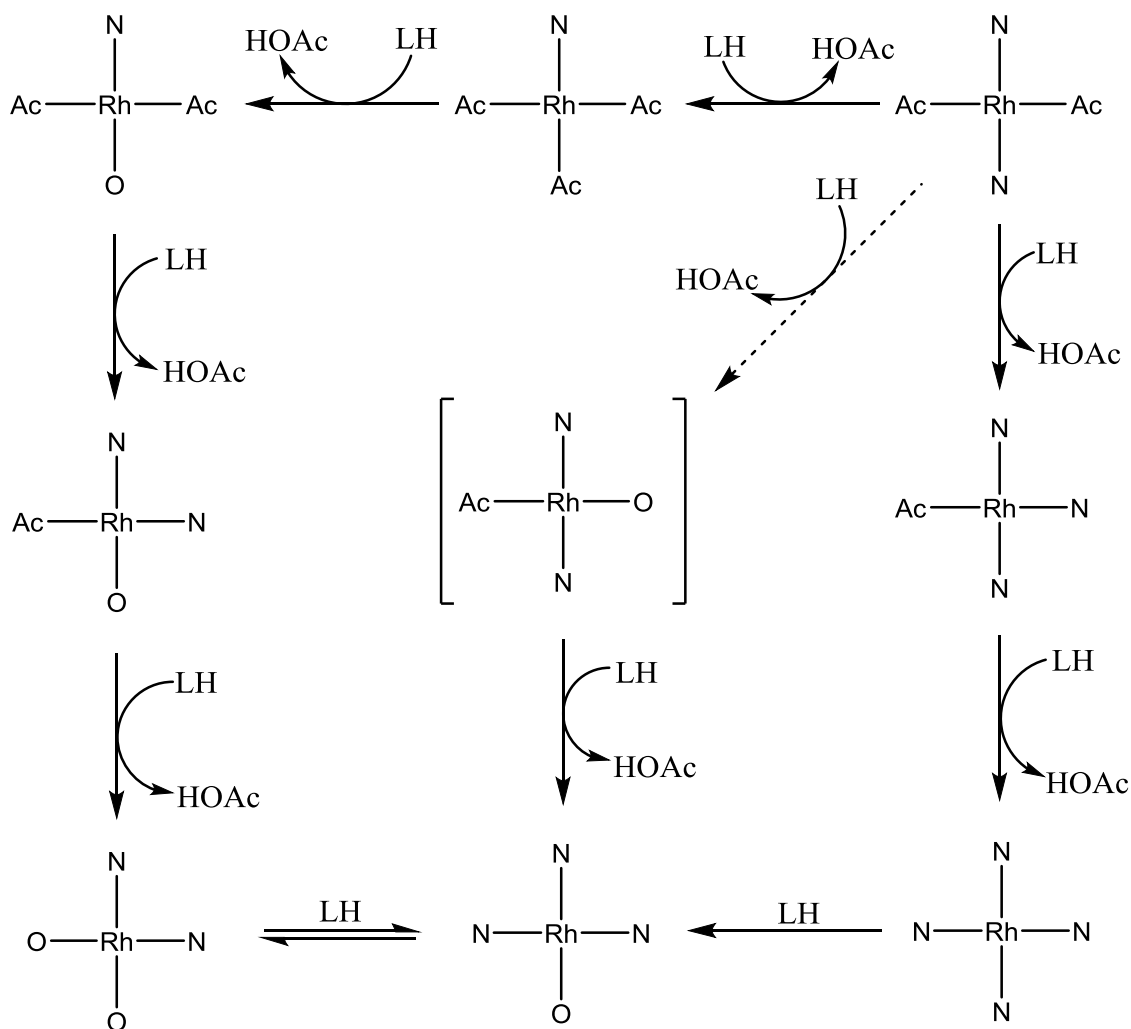
Scheme 1. Mechanism for the formation of tetrakis(carboxamidate) dirhodium(II) isomers.[10]

Ligand substitution is initiated through coordination of the carboxamidate to the

$Rh_2(COOCH_3)_4$ at the axial site (not shown in the above scheme). This then replaces an acetate

ligand, forming the structure in the top middle of the scheme above. The replacement of acetate

by the first carboxamidate ligand activates the acetate that is trans to the carboxamidate for the

second substitution (from top middle, follow right arrow). In some situations steric

considerations can lead directly to the formation of the 2,2-cis isomer (from top middle, follow

arrow to left) or the 4,0 isomer can be formed (bottom right), followed by isomerization to the

3,1- and 2,2-cis isomers (from bottom right, follow arrow to left). The stepwise exchange

reaction can be summarized as shown below.

$$Rh_2(OAc)_4 + Acam \rightarrow Rh_2(OAc)_3(Acam) + OAc \qquad (3)$$

$$Rh_2(OAc)_3(Acam) + Acam \rightarrow Rh_2(OAc)_2(Acam)_2 + OAc \qquad (4)$$

$$Rh(OAc)_2(Acam)_2 + Acam \rightarrow Rh_2(OAc)(Acam)_3 + OAc \qquad (5)$$

$$Rh_2(OAc)(Acam)_3 + Acam \rightarrow Rh_2(Acam)_4 + OAc \qquad (6)$$
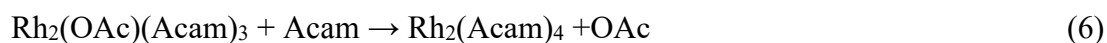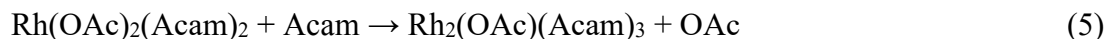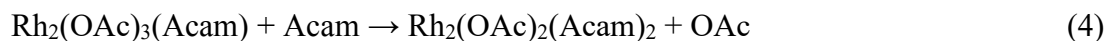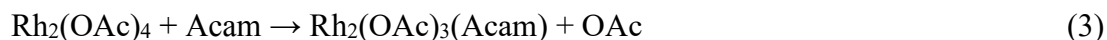
The product of Equation 3 has only one geometric isomer, the products of Equation 4 and

Equation 6 have 4 possible geometric isomers and the product of Equation 5 has 3 geometric

isomers.[18,19]

Doyle and coworkers have synthesized chiral tetrakis(carboxamidate) dirhodium(II)

complexes.[20-22] The structures typically have paddlewheel arrangements defined by 4 bridging

carboxamidate ligands about an Rh_2^{4+} core, with 2 nitrogen atoms and 2 oxygen atoms bound to

1 rhodium atom and the other 2 nitrogen atoms and 2 oxygen atoms bound to the other. The 2

nitrogen atoms or oxygen atoms were cis to one another as shown in Figure 5;
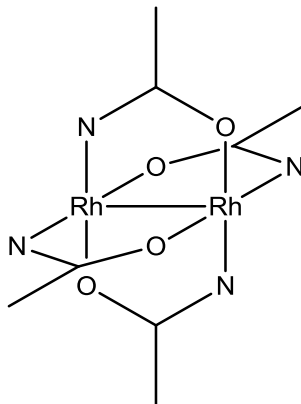
Figure 5. A typical paddlewheel arrangement for a tetrakis(carboxamidate) dirhodium(II)

(2,2 cis).

With acetonitrile or benzonitrile coordinated in the axial positions, these air stable

complexes typically crystallize as red solids. These axial ligands, usually introduced by the

solvent from which the complex was crystallized, can be easily removed by vacuum or by using

a poorly coordinating solvent like dichloromethane to crystallize the complex where blue species

are formed.

Applications

Tetrakis(carboxylate) and tetrakis(carboxamide) dirhodium(II) compounds are generally

used as catalysts. Their major use in catalysis has been in the transformation of diazo compounds

as seen in Scheme 2 below. $L_nM = Rh_2L_4$ represents the dirhodium(II) carboxamidate catalyst

and CZR represents the carbene. In the scheme below, the metallocarbene (middle structure) is

generated via the initial reaction of the diazo compound with the catalyst L_nM (left of scheme,

follow arrow to right). The metallocarbene intermediate may then facilitate the insertion of the

carbene into an A − H bond (middle structure, follow arrow to top scheme). The carbene may

also be added to an alkene, forming a cyclopropane ring (middle structure, follow arrow to top-

right scheme). Also, the carbene may be added to an alkyne, forming a cyclopropene ring (middle structure, follow arrow to bottom-right scheme). Finally, the carbene may be added to a species containing a lewis base, forming an ylide species (middle structure, follow arrow to bottom scheme).

$A = R_3C, R_2N, RO, R_3Si, RS$

$Z = H, \text{alkyl}, COR, CO_2R, CONR_2$

$R = H, \text{alkyl}, COR, CO_2R$
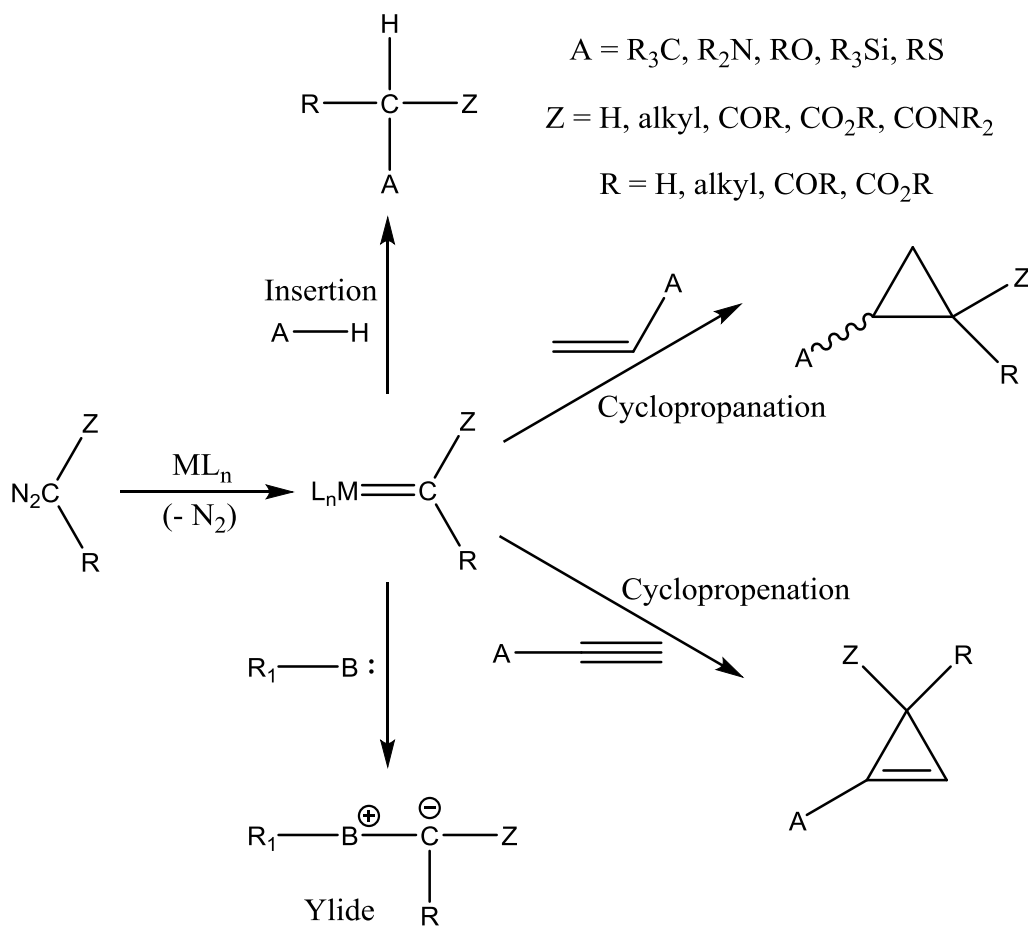
Scheme 2. Applications for catalytic reactions of diazo compounds.[10]

For catalysis involving cyclopropanation reactions (top right of scheme), stereoselectivity is achieved where there may be formation of the cis or trans cyclopropanes isomers. However, there are usually greater yields of trans cyclopropane isomers than cis cyclopropane isomers.[21]

Two mechanisms have been proposed for the formation of *cis* or *trans* cyclopropane isomers.

- Doyle proposed the alkene approaches the metallocarbene species with its double bond parallel to the carbene.[10]
- Kodadek proposed that the alkene approaches perpendicular to the metallocarbene and has a transient intermediate with the orientation being determined by the size of the space of the catalytic site (axial site of dirhodium(II) compound) available due to bulk on the catalyst.[22]

Both mechanisms above are based on the Fischer carbene mechanism where the diazo compound forms a double bond with the rhodium atom producing an electrophilic metal stabilized carbene which may then react with the alkene to form the cyclopropane ring.

- Hoye proposed that one of the bridging ligands on the metallocarbene complex first dissociates, creating an open coordination site. Hence, the incoming alkene then attaches directly to the rhodium atom in the vacant site forming a metallocyclobutane ring with the carbene.[23]

With the use of tetrakis(carboxamidate) dirhodium(II) compounds, Eagle and coworkers made attempts to increase the steric bulk closer to the catalytic site (axial site) of the carbene formation without blocking it. They used N-phenylacetamide as the carboxamidate to create bulk (due to the phenyl rings on the nitrogen atoms) around the dirhodium(II) catalytic site. In theory, this should force the reacting alkene to approach the metallocarbene complex with the orientation of its bulky group away from the steric group on the ligand. This was predicted to result in the production of high percentages of the cis cyclopropane isomers.

Tetrakis(N-phenylacetamidato) dirhodium(II) isomers have extra bulk around the dirhodium core provided for by the presence of the bulky phenyl group. In theory, this bulk could cause the formation of higher yields of *cis* cyclopropanes compared to *trans* cyclopropanes. Because of this, the 3,1-tetrakis(N-phenylacetamidato) dirhodium(II) isomer is of most interest. This research aims at synthesizing a compound that has the most steric bulk close to the metal carbene center (preferably, the 3,1- isomer), compared to the other 2 isomers (2,2-cis and 2,2-trans), and yet leave the dirhodium(II) catalytic site open for the possibility of cis cyclopropanation. The 4,0- isomer is of least interest because the bulky substituent on the N-phenylacetamide will most probably completely block the initial formation of the metal-carbene complex. However, the metal carbene complex can form on the three-nitrogen side as well as form on the one-nitrogen side of the 3,1-$Rh_2(NRCOCH_3)_4$ isomer.

Therefore, it is important to use ligands that will block the one-nitrogen side and will disfavor the metal – carbene complex at the one-nitrogen side as well as favor the metal – carbene formation on the three-nitrogen side. This study may be carried out by reacting the dirhodium(II) compound with bridging ligands and characterizing the product formed.

Other applications that may be realized using the dirhodium(II) compounds as catalysts include;

The hydrosilylation of alkynes and alkenes yielding alkene and alkane species respectively, see Equations 7[10] and 8[10] (pfb = perfluorobutyrate).[24,25]

$$CH_3(CH_2)_5C\equiv\!\!\equiv\!\!CH + Et_3SiH \xrightarrow[\substack{CH_2Cl_2 \\ 90\%}]{Rh_2(pfb)_4} CH_3(CH_2)_4CH\equiv\!\!\equiv\!\!\equiv CHCH_2SiEt_3$$

(alkyne added to silane) $E/Z = 2.0$

$$(7)$$

$$PhCH_2CH{=}CH_2 + Et_3SiH \xrightarrow[\substack{CH_2Cl_2 \\ 52\%}]{Rh_2(pfb)_4} PhCH_2CH_2CH_2SiEt_3$$

(alkene added to silane)

(8)
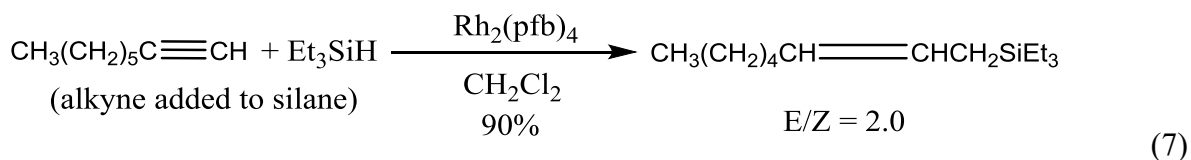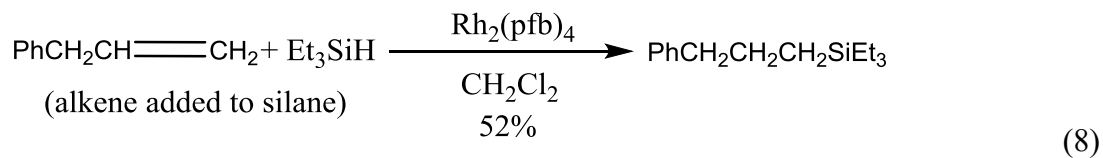
Organosilane alcoholysis, see Equation 9[10] (pfb = perfluorobutyrate).[26]

(9)
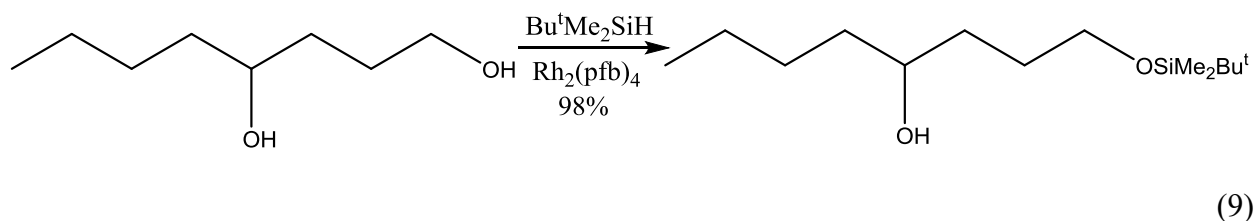
Silylformaylation, see Equation 10[10] (pfb = perfluorobutyrate).[27]

$$MeOCH_2C{\equiv}CH + Et_3SiH \xrightarrow[\substack{Rh_2(pfb)_4 \\ CH_2Cl_2 \\ 87\%}]{CO\ (1atm)}$$

Z/E = 14

(10)
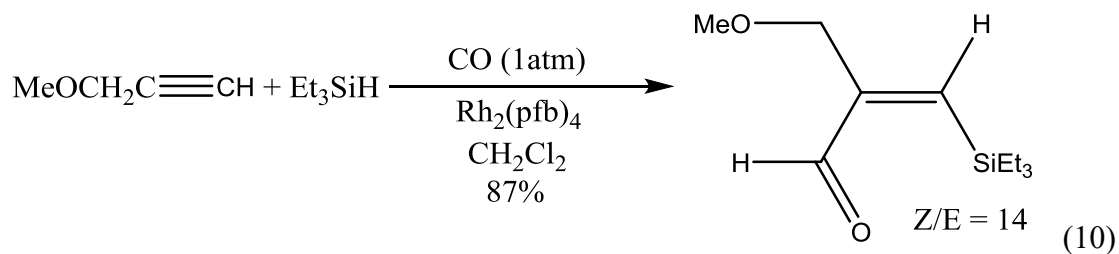
Hetero-Diels-Alder reactions, see Equation 11[10] where the dirhodium(II) catalyst acts as a Lewis acid.[28]

(11)
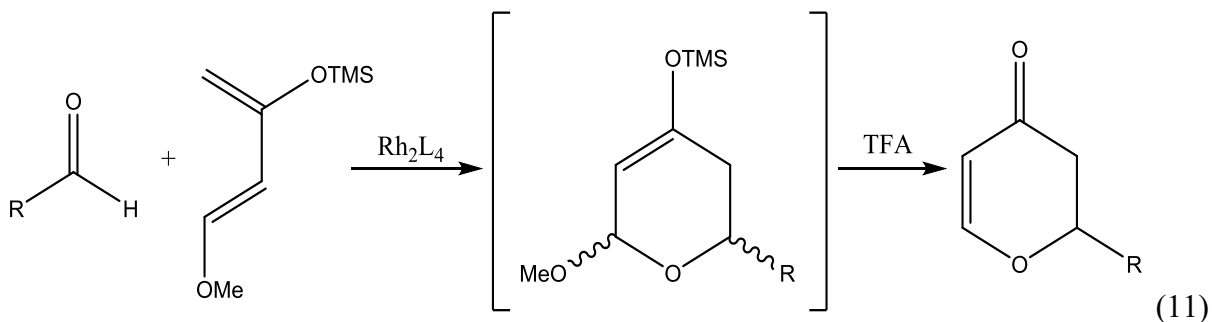
Carbene – Rhodium Bond

A carbene is a species with an electron rich divalent carbon atom. Usually, this carbene can donate its electron density to an empty orbital of a metal to form a σ-bond (see Figure 6).
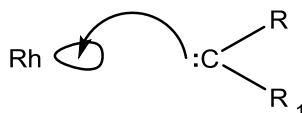
Figure 6. A σ bond from a carbene species to a Rhodium metal.

The carbene species has empty p-orbitals that may also accept electron density from the filled d-orbitals of the metal to form a π-back bond. This is called π-back bonding because there is a "back donation" of electron density from the metal to the carbene species (see Figure 7).
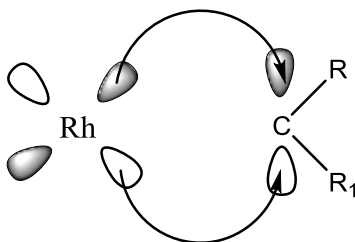
Figure 7. A π-back bond from a Rhodium metal to a carbene species.

Nitrile – Rhodium Bond

Carbonyls, nitriles, and isonitriles, like carbenes, have the capabilities of undergoing σ-bonding as well as π-back bonding with the rhodium atom.[29,30] In the case of nitriles, there is donation of the lone pair electron on the nitrogen atom of the nitrile to the Rhodium metal to form a σ-bond. In return, there is a π-back donation of electron density from the Rhodium metal

to the π*-antibonding orbital of the nitrile to form a π-back bond. Figure 8, below, shows the similarity of a Rhodium – nitrile bond to a Rhodium – carbene bond.

Figure 8. The similarity between the rhodium – carbene bond and rhodium – nitrile bond showing the orbitals involved in π-back bonding.

Effects of Pi-Back Bonding

In theory, because there is movement of electrons from the filled d-orbitals of the metal into the π*-antibonding orbital of the nitrile, there is a decrease in bond order. Thus, the C≡N bond becomes longer and weaker. This weakening of the C≡N bond can usually be seen as a decrease in stretching frequency using infrared spectroscopy (bathochromic shift in the energy of C≡N bond). Bear, Kadish, and coworkers found evidence for the existence of π-back bonding in $Rh_2(OAc)_n(HNOAc)_{4-n} \cdot CO$ complexes (n = 0 – 4; OAc = Acetate).[31] Also, with increased π-back bonding, the Rh – nitrile bond becomes shorter.[32]

Binding Modes

Tetrakis dirhodium(II) compounds have 2 open axial sites. This gives room for 1 or 2 ligands to be coordinate in either axial (see Figure 9) site or both sites (see Figure 10). With the use of a monodendate ligand, we can achieve monosubstitution (Figure 9) or disubstitution (Figure 10).
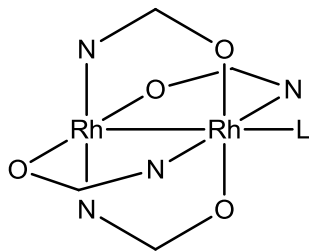
Figure 9. A [Rh$_2$]L – 1:1 coordination complex.
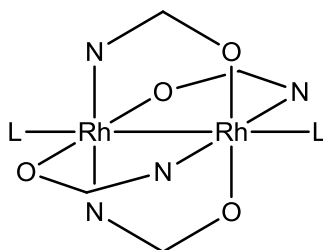
Figure 10. A [Rh$_2$]L$_2$ – 1:2 coordination complex.

However, with the use of bidendate bridging ligands such as 1,3-dicyanobenzene, 1,4-dicyanobenzene we can link 2 or more dirhodium(II) cores together (see Figures 11 and 12).
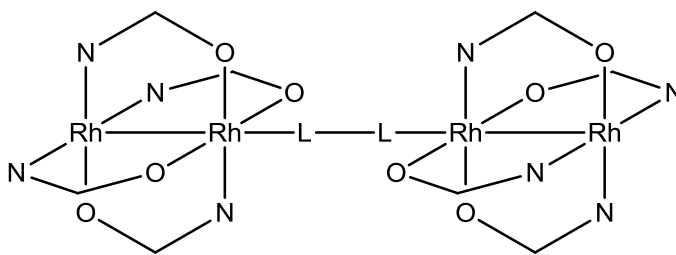
Figure 11. A 3,1-tetrakis(carboxamidate) dirhodium(II) bridged by L – L ligand on the '1' side.
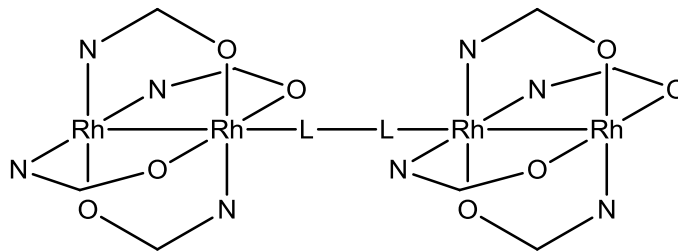
Figure 12. A 3,1-tetrakis(carboxamidate) dirhodium(II) bridged by L – L ligand on the '3' and

'1' side.

Some dirhodium(II) compounds with bridging L – L ligands have been synthesized in

various solvents and characterized.

Niu and coworkers prepared a series of tetrakis(acetate) dirhodium(II) adducts with 1,4-

dicyanobenzene in 5 different solvents (acetone, methanol, ethanol, THF, and benzene).[37]

Structural solutions were obtained for the crystals from all solutions except in ethanol. Even

though a structure solution was not obtained for the reaction in ethanol, the unit cell was

determined by X-ray crystallography. Through other methods[37] the structure solution was

obtained as $[Rh_2(O_2CCH_3)_4(NCPhCN)\cdot CH_3CH_2OH]$. X-ray crystallographic discoveries showed

that there was incorporation of a solvent molecule (**1**, **3,** and **4**), or 2 solvent molecules (**2**) in the

unit cell. X-ray crystallography has also shown that the structure of the compounds, bond

distances and bond angles varied with the different solvents used. Niu proposed that the

electronic interactions of the solvents with the compound acts in such a manner to maximize the

packing in these crystal lattices. Reported in Table 1 are some selected bond distances and angles

for the prepared compounds. The Rh – Rh – N bond angles were fairly linear in these

compounds. However, although the Rh – N – C$_{(axial)}$ bond angles were fairly linear, this angle

became more bent (168.7^0 and 150.6^0) in the cases with the ring structured solvents (THF and

benzene). For compound **3**, the lone pair electrons on the oxygen of the THF have a weak

interaction with the phenyl ring of the 1,4-dicyanobenzene ligand while for compound **4**, the

benzene solvent stacked parallel with the phenyl ring of the 1,4-dicyanobenzene ligand through

π-π interactions. All compounds formed a continuous one-dimensional straight chain polymer.

Table 1. Dirhodium(II) carboxylates with L – L bridging ligands[33]

Compound ID	Dirhodium(II) compound	Rh – Rh – N$_{(axial)}$ bond angle	Rh – N – C$_{(axial)}$ bond angle	C – N$_{(axial)}$ bond distance	Rh – N$_{(axial)}$ bond distance	Rh – Rh bond distance
1	$Rh_2(O_2CCH_3)_4(NCPhCN) \cdot CH_3COCH_3$	178.2(2)°	178.1(5)°	1.128(8) Å	2.239(5) Å	2.3910(10) Å
2	$Rh_2(O_2CCH_3)_4(NCPhCN) \cdot 2CH_3OH$	179.00(13)°	177.8(5)°	1.122(7) Å	2.236(4) Å	2.3910(8) Å
3	$Rh_2(O_2CCH_3)_4(NCPhCN) \cdot THF$	177.85(8)°	168.7(3)°	1.140(5) Å	2.226(3) Å	2.3830(10) Å
4	$Rh_2(O_2CCH_3)_4(NCPhCN) \cdot C_6H_6$	173.78(4)°	150.6(2)°	1.137(3) Å	2.237(2) Å	2.3887(4) Å

The structures for compounds **1, 2, 3** and **4** were determined by X-ray Crystallography.[37]

Crystal Growth

Definitions

   Crystal. Crystals are long-range ordered 3-dimensional arrangements of atoms or

molecules.

   Unit cell. A unit cell, defined by a, b, c, α, β, and γ, is the smallest repeating unit within

the long range ordered repeating 3-dimensional setup.

   Twinning. Term refers to 2 or more identical single crystals joined together in a

symmetrical manner to form a single entity.[34] This single entity is called a twinned crystal.

Residual Value. The residual value, also called R value, is defined mathematically as

$$R = \frac{\sum|Fo-Fc|}{\sum|Fo|}$$ (12)

Where;   Fo = Observed structural factors

Fc = Calculated structural factors

The R value indicates a model to data ratio. An R value less than 5% allows one to speculate to a reasonable degree of certainty that the structure is correct.

Crystal Systems

There are 7 known crystal systems. They are Triclinic, Monoclinic, Orthorhombic, Tetragonal, Trigonal, Hexagonal, and Cubic. Table 2, below, summarizes the various crystal systems and their restrictions on the unit cell parameters.

Table 2. Seven crystal systems

Crystal System	Cell axes	Cell angles
Triclinic	$a \neq b \neq c$	$\alpha \neq \beta \neq \gamma \neq 90^0$
Monoclinic	$a \neq b \neq c$	$\alpha = \gamma = 90^0, \beta > 90^0$
Orthorhombic	$a \neq b \neq c$	$\alpha = \beta = \gamma = 90^0$
Tetragonal	$a = b \neq c$	$\alpha = \beta = \gamma = 90^0$
Trigonal	$a = b = c$	$\alpha = \beta = \gamma$
Hexagonal	$a = b \neq c$	$\alpha = \beta = 90^0, \gamma = 120^0$
Cubic	$a = b = c$	$\alpha = \beta = \gamma = 90^0$

Geometry of the Paddlewheel

As indicated earlier (Figure 3), the paddlewheel consists of 4 bridging ligands on the dirhodium core. It has a 4-fold axis of rotation and 4 corresponding 2-fold axes. It has a horizontal mirror plane. Therefore, the point group of the paddlewheel structure is D_{4h}.

Growth Technique

Crystals may be grown by a variety of methods including; slow evaporation, slow cooling, vapor diffusion, and liquid-liquid diffusion techniques.

Among these techniques, the vapor diffusion technique has worked best for crystal growth during this research. A saturated solution is placed in a small vial. This small vial is then placed into a bigger vial containing another solvent that could be more volatile or less volatile and the setup is capped.

If the solvent in the outer vial is more volatile than that in the inner vial (saturated solution with compound), this solvent diffuses into the saturated solution and begins to dilute it. Due to the difference in the solubility of the compound in both solvents, crystals begin forming at the liquid-vapor interface of where the more volatile solvent meets the less volatile one.

If the solvent in the outer vial is less volatile than that in the inner vial (saturated solution with compound), the solvent in the saturated solution starts diffusing out of the inner vial into the outer vial, leaving behind an even more concentrated solution and crystals will begin to form over time.

The goal of this research was to synthesize adducts of the 2,2-tetrakis(N-phenylacetamidato) dirhodium(II) with benzonitrile, 2-methylbenzonitrile and 3-methylbenzonitrile. An adduct of 3,1-tetrakis(N-phenylacetamidato) dirhodium(II) with 1,3-dicyanobenzene was also synthesized. These compounds were analyzed and characterized by X-ray Crystallography.

The Rh – Rh bond, the Rh – N$_{(axial)}$ bond, the C≡N (nitrile) bond distances and their associated environments were studied. This information will be used in future studies to predict successful catalysts for carbenoid transformations.

CHAPTER 2

EXPERIMENTAL

The research was performed in 4 broad parts;

1. Synthesis of tetrakis(N-phenylacetamido) dirhodium(II)

2. Characterization of tetrakis(N-phenylacetamido) dirhodium(II)

3. Synthesis of tetrakis(N-phenylacetamido) dirhodium(II) adduct with nitrile

4. Characterization of the tetrakis(N-phenylacetamido) dirhodium(II) – nitrile adduct

Solvents and Reagents

1,3 dicyanobenzene ($C_6H_4(CN)_2$)

    1,3 dicyanobenzene (98%) was purchased from Acros Organics and used as supplied.

2-methyl benzonitrile (o-tolunitrile)

    2-methyl benzonitrile (98%) was purchased from Acros Organics and was used as supplied.

3-methyl benzonitrile (m-tolunitrile)

    3-methyl benzonitrile (99%) was purchased from Acros Organics and was used as supplied.

Acetone (CH_3COCH_3)

    Acetone (99.9%) was purchased from VWR International and was used as supplied.

Acetonitrile (CH$_3$CN)

Acetonitrile (99.9%) was purchased from Fischer Scientific and was used as supplied.

Benzonitrile (PhCN)

Benzonitrile (99.8%) was purchased from Alfa Aesar and was used as supplied.

Chlorobenzene (PhCl)

Chlorobenzene (99.8%) was purchased from Fischer Scientific and was further dried by adding anhydrous magnesium sulfide then filtered prior to use.

Chloroform-d (CDCl$_3$)

Chloroform-d (99.8 atom D%, 1.0 v/v% TMS) was purchased from Acros Organics and was used as supplied. It was stored in a refrigerator at all times.

Dichloromethane (CH$_2$Cl$_2$)

Dichloromethane (99.5%) was purchased from Fischer Scientific and was used as supplied.

Ethanol (EtOH)

Ethanol (99.9%) was purchased from VWR International and was used as supplied.

Ethyl acetate (EtOAc)

Ethyl acetate (99.5%) was purchased from VWR International and was used as supplied.

Hexane (C_6H_{12})

Hexane (60% n-Hexane, 98.5% total C6 isomers) was purchased from Fischer Scientific and VWR International. The quality of both sources was determined as equivalent. It was dried by adding anhydrous magnesium sulfate then filtered prior to use.

Magnesium Sulfate ($MgSO_4$)

Anhydrous magnesium sulfate was purchased from Fischer Scientific and was kept in a dry environment at all times.

Methanol (MeOH)

Methanol (99.9%) was purchased from Fischer Scientific and VWR International and the quality of both chemicals was determined as equivalent. It was used as supplied.

N-phenyl acetamide ($HNPhCOCH_3$)

N-phenyl acetamide (solid flakes) was purchased from Fischer Scientific and used as supplied.

Sand

Sand obtained from a stock bottle was washed with chlorobenzene and dried in the fume hood prior to use.

Sodium Carbonate monohydrate ($Na_2CO_3·H_2O$)

Sodium Carbonate monohydrate (soda crystals) was purchased from Fischer Scientific and stored in a dry area.

Tetrakis(acetato) dirhodium(II) (Rh$_2$(CH$_3$CO$_2$)$_4$)

Tetrakis(acetato) dirhodium(II) was synthesized from a supply of rhodium trichloride (RhCl$_3$).

Toluene (PhCH$_3$)

Toluene (99.5%) was purchased from Fischer Scientific and was further dried by adding anhydrous magnesium sulfide then filtered prior to use.

Physical Techniques

Infrared Spectroscopy

Infrared (IR) spectroscopy was done on an IRPrestige-21 Infrared spectrophotometer with 4 cm^{-1} resolution. 320 scans were done (typically 32 scans were used on this instrument but no decent results were obtained, so 32 * 10 = 320 scans were used) over the range 4000 cm^{-1} to 400 cm^{-1}. The samples were crushed to powder and then mounted on the ATR sample cup.

Medium Pressure Liquid Chromatography

A flash chromatography (MPLC) column was used to separate the various tetrakis(N-phenylacetamido) dirhodium(II) (Rh$_2$(PhNCOCH$_3$)$_4$) isomers that were formed during synthesis. Ethyl acetate, hexanes, and mixtures of ethyl acetate:hexanes were the solvents used to elute the products. The column was packed with flash silica gel (230 – 400 mesh, 60 Å), which was purchased from Fischer Scientific.

Nuclear Magnetic Resonance Spectroscopy

Proton (^{1}H) nuclear magnetic resonance spectroscopy (NMR) spectra were obtained on a

JOEL AS400 FT-NMR spectrophotometer. Spectra of tetrakis(N-phenylacetamide)

dirhodium(II) complexes, as well as tetrakis(N-phenylacetamide) dirhodium(II) – nitrile adducts,

were dissolved in chloroform-d (CDCl$_3$) with the 0.2% residual chloroform (CHCl$_3$) solvent

chemical shift appearing at 7.24 ppm. The spectra were referenced to Tetramethyl Silane (TMS)

at 0 ppm.

Thin Layer Chromatography

Thin layer chromatography (TLC) was used to see if the products from the MPLC

column were pure and to see if all the excess HNPhCOCH$_3$ had been removed. This technique

was also employed to monitor if the reaction had gone to reasonable completion during the

course of the synthesis of [Rh$_2$(PhNCOCH$_3$)$_4$] from [Rh$_2$(CH$_3$CO$_2$)$_4$]. Samples where dissolved

in CH$_2$Cl$_2$ and spotted on TLC plates. The plates were developed in 1 of 2 chambers using 50:50

mixture of ethyl acetate:hexane and the other using 70:30 ethyl acetate:hexane mixtures as the

mobile phase. The choice of chamber used depended on the polarity of the product isomer.

Ultraviolet (UV) light was used to further view the TLC plates.

X-ray Diffractometry

The crystal structure solution was obtained by mounting a single crystal on a Rigaku

Mercury 375R/M CCD diffractometer purchased from Rigaku Americas (Manufactured in May,

2011). The X-rays were produced by a Molybdenum source and were focused using a graphite

monochromatic collimator unto the crystal mounted on a mitogen loop on a mounting pin

attached to a goniometer with a magnetic base cup (this combination of mitogen loop, mounting

pin, and goniometer is called a sample holder). The diffracted X-rays were then captured by a

Charge Couple Device (CCD) detector. The initial unit cell was determined after collecting 12

images. Data collection consisted of 3 shells of images that were collected using Crystal Clear

software and analyzed. The unit cell parameters as well as Space and Laue groups were

calculated using Crystal Clear. The feed information from Crystal Clear software[35] was further

processed by Crystal Structure software[36] running on SHELX[37] platform, for which direct

methods were used for further interpreting the data and solving the crystal structure.

Synthesis and Purification of Tetrakis(N-phenylacetamidato) Dihrodium(II)

A condenser, soxhlet extractor, stir bar, 250 mL round bottom flask were washed and

dried in an oven at 125 ^{0}C for 12 hours. The apparatus was assembled on a heating mantle (to

serve as heat source) then cooled under nitrogen. 150.006 g of sand and 150.007 g of

$Na_2CO_3 \cdot H_2O$ was used to pack 9 thimbles ¾ full, followed by a layer of sand. The thimbles were

dried in an oven for 3 days at 125 ^{0}C, and then cooled under nitrogen (N_2) gas in the soxhlet

extractor.

Under nitrogen, 10.002 g of $HNPhCOCH_3$ was placed in the round bottom flask. 0.499 g

of $[Rh_2(CH_3CO_2)_4]$ was also placed in the same round bottom flask. 100 mL of PhCl was added

to the round bottom flask. The reaction was started by setting mixture to stir and the heating

mantle turned on under N_2 gas. The heat provided by the heating mantle was adjusted until the

mixture started to reflux at a rate of 20 min/cycle, at a temperature of 132^{0}C (the boiling point

for PhCl). Glass wool insulation and aluminium foil were used to wrap around the round bottom

flask and soxhlet extractor to provide insulation. The reaction was left to run for 7 days during

which the bright green colored solution of $[Rh_2(CH_3COO)_4]$ was replaced by a dark green/purple

colored solution with some precipitate. The thimble was exchanged for another fresh dry thimble packed with sodium carbonate and sand every 24 hours at the start of every new thimble cycle. When the thimble was changed, the heating mantle was turned off and the reaction was cooled under nitrogen. After thimble replacement, the reaction was reheated under N_2 gas. During the course of reaction, the volume of PhCl was always maintained at between 100 mL to 125 mL.

After 2 days, the reaction was cooled under N_2 gas and a small sample withdrawn from the mixture in the round bottom flask using a Pasteur pipette. A thin layer chromatography, TLC was performed using 30% ethyl acetate/ 70% hexane as eluent (mobile phase) in one developing chamber and 50% ethyl acetate/ 50% hexane as the eluent in another developing chamber to check the reaction progress. The visualization was done using a UV lamp and it was seen that a higher retention factor, R_f for each spot on the TLC plate was achieved with the second developing chamber.

After 6 days, another sample was withdrawn from the round bottom flask with a pasteur pipette. The sample was then cospotted against a known sample of $[Rh_2(C_6H_5NCOCH_3)_4]$. The TLC chromatogram showed spots at the origin and 4 others spots above the origin, corresponding to possible decomposed material (at the origin), the tetra-, tri-, di-, mono-substituted products. The reaction was then stopped and cooled under N_2 gas.

The excess $HNC_6H_5COCH_3$ solid was then filtered out (7.367 g) and the PhCl solvent was removed by rotary evaporation for which white crystalline solid of the $HNC_6H_5COCH_3$ formed alongside green $[Rh_2(C_6H_5NCOCH_3)_4]$ solid. The contents of the flask were evaporated to dryness and later dried under vacuum for 3 hours.

MPLC was used to separate and purify the various [Rh$_2$(C$_6$H$_5$NCOCH$_3$)$_4$] products. A column was prepared to be used for the MPLC. A glass wool plug was placed at the bottom of the column (burette). A 1-inch layer of sand was placed on the glass wool plug followed by a 22-inch layer of silica gel slurry then another 1-inch layer of sand. The column was packed with 98% hexane in acetone. The nitrogen gas tank was attached to the top of the column to provide for medium pressure. The Rh$_2$(C$_6$H$_5$NCOCH$_3$)$_4$ crude product was dissolved with 2 mL CH$_2$Cl$_2$ and was loaded unto the column. Hexane was first run through the column and 3 bands were observed; blue-green (turquoise), blue, emerald green, dirty blue. The first band which was blue-green was eluted with 20:80 ethyl acetate:hexane solvent mixture at a flow rate of one inch per minute. The second band which was blue was eluted with 30:70 and 40:60 ethyl acetate:hexane solvent mixtures at one inch per minute. The third emerald green band was eluted using 50:50 to 90:10 ethylacetate:hexane solvent mixtures at a rate of one inch per minute. The fourth band, dirty blue in color overlapped with some of the emerald green third band was eluted along with the other remaining bands on the column with a 50:50 methanol:ethylacetate solvent mixture at a rate of one inch per minute.

TLC was used to determine the purity of each fraction. All fractions were cospotted against pure N-phenylacetamide and the reaction mixture. 50:50 ethylacetate:hexane was used as eluent (mobile phase) for fraction I that showed only one spot corresponding to one of the rhodium isomers. 90:10 ethylacetate:hexane solvent mixture was used as eluent for fractions II – IV. Fraction II showed one spot with a small cap-like protrusion on top. The bulk of the spot resembled the spot for the N-phenylacetamide. This corresponded to Fraction II with some amounts of N-phenylacetamide leftover. Fraction III showed only one spot corresponding to one of the isomers. Fraction IV showed one spot but no movement up the TLC plate. Comparisons of

TLC chromatograms of Fractions III and IV showed that some amount of Fraction III may have been in Fraction IV. Fraction II was collected in 2 parts; one part containing N-phenylacetamide and the other without N-phenylacetamide.

The solvents from Fractions I – IV after the MPLC were removed by rotary evaporation, after which these fractions were further dried under vacuum for 3 hours. The flasks were scraped and the various fractions were transferred into clean, dry ½ dram vials. They were further dried overnight in vacuum at 25 in Hg under ambient pressure. Fraction I, which was a green solid turned mustard yellow in color. Fraction II, which was a dark green solid, turned lighter green in color. Fraction III, which were green flaky solids, turned yellowish green.

The ^{1}H NMR of each fraction was done in CDCl$_3$ (99.8 atom D%, 1.0 v/v% TMS). The ^{1}H NMR spectra further provided evidence that Fraction I contained only one isomer, Fraction II contained another isomer with some N-phenylacetamide, and Fraction III contained only one isomer. The samples were further dried at $70 - 80$ ^{0}C for 4 hours under vacuum (28.5 inHg). Fraction II was further purified by sublimation of the N-phenylacetamide. The flask was heated to 90 ^{0}C under vacuum over a 2-week period. Each fraction gave a unique ^{1}H NMR spectrum (see Figures 13 – 18 and Discussion Section)

The weights of Fractions I, II, and III were 147 mg, 192 mg and 229 mg respectively giving the experimental percent yield of the synthesis reaction to be 56.7%.

Characterization of the various isomers was done using ^{1}H NMR spectroscopy. An initial NMR of the CDCl$_3$ (1.0% v/v% TMS) solvent was first taken in clean, dry NMR tubes to ensure that the tubes were clean. These spectra showed peaks as expected (TMS at 0 ppm and the CHCl$_3$ at 7.263 ppm). The CDCl$_3$ from these NMR tubes with known spectra was then used to dissolve about 10 mg of the various Fractions (I, II, and III) and spectra were collected by coadding 300 scans for each fraction on a JOEL AS400 FT-NMR spectrophotometer. The spectra for each fraction are shown below in Figures 13 – 18.

Fraction I ^{1}H NMR

Figures 13 and 14, below, show the ^{1}H NMR spectrum for Fraction I (see Figure 47 for labelling).
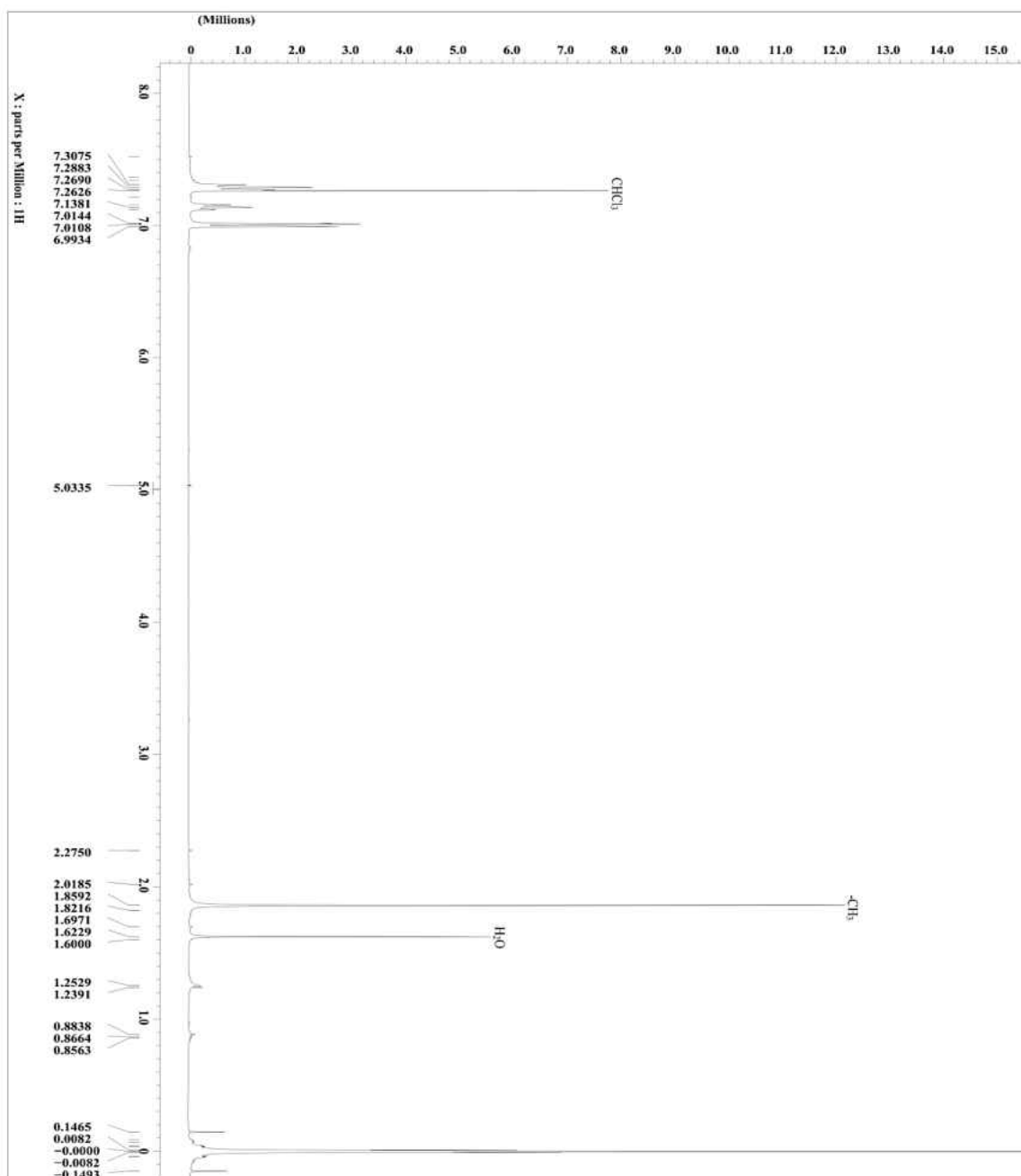
Figure 13. The ^{1}H NMR spectrum of Fraction I of $Rh_2(C_6H_5NCOCH_3)_4$.
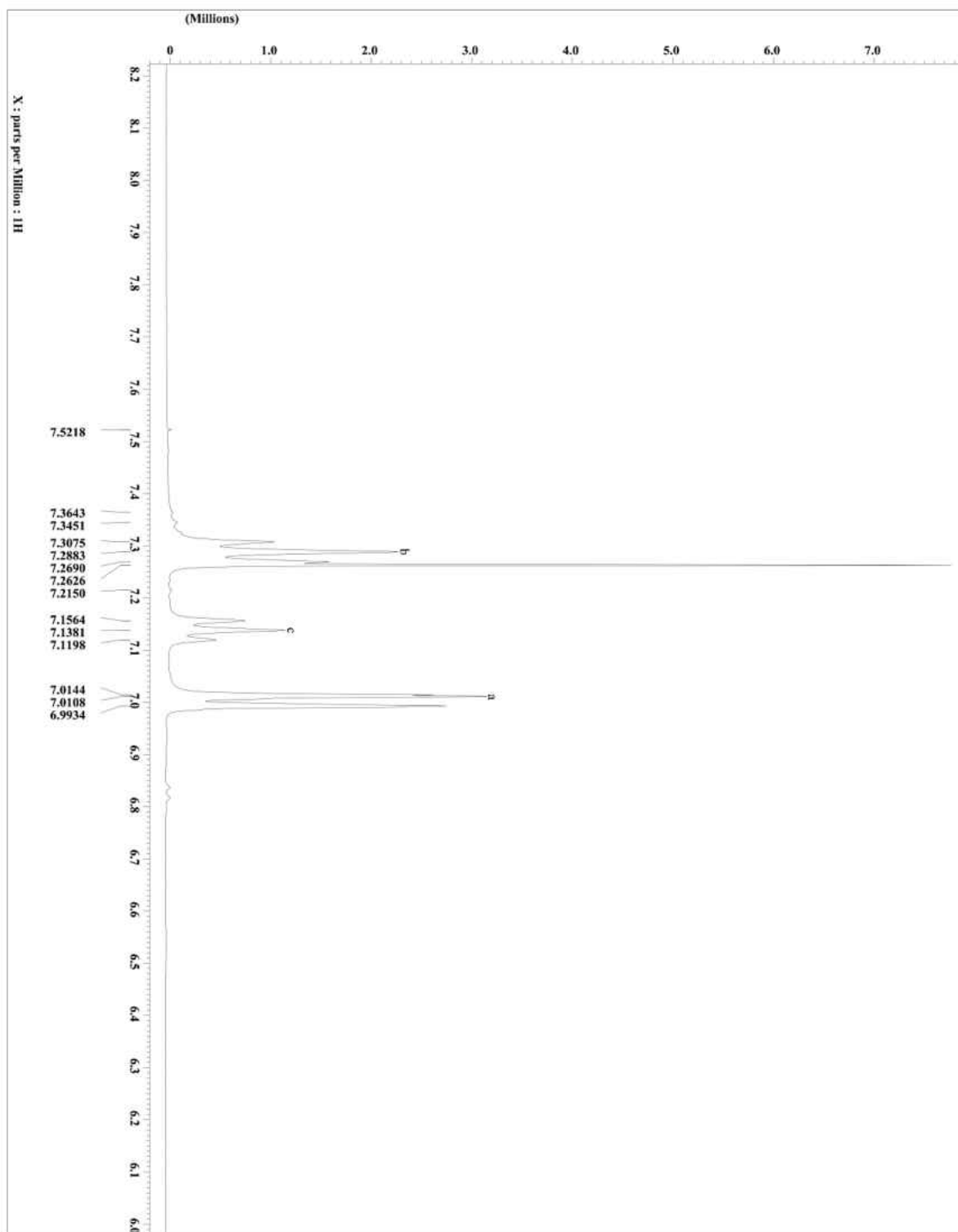
Figure 14. The ^{1}H NMR spectrum of Fraction I showing the chemical shift region from 6.0 ppm to 8.2 ppm.

Fraction II ^{1}H NMR

Figures 15 and 16, below, show the ^{1}H NMR spectrum for Fraction II (see Figure 48 for labelling).
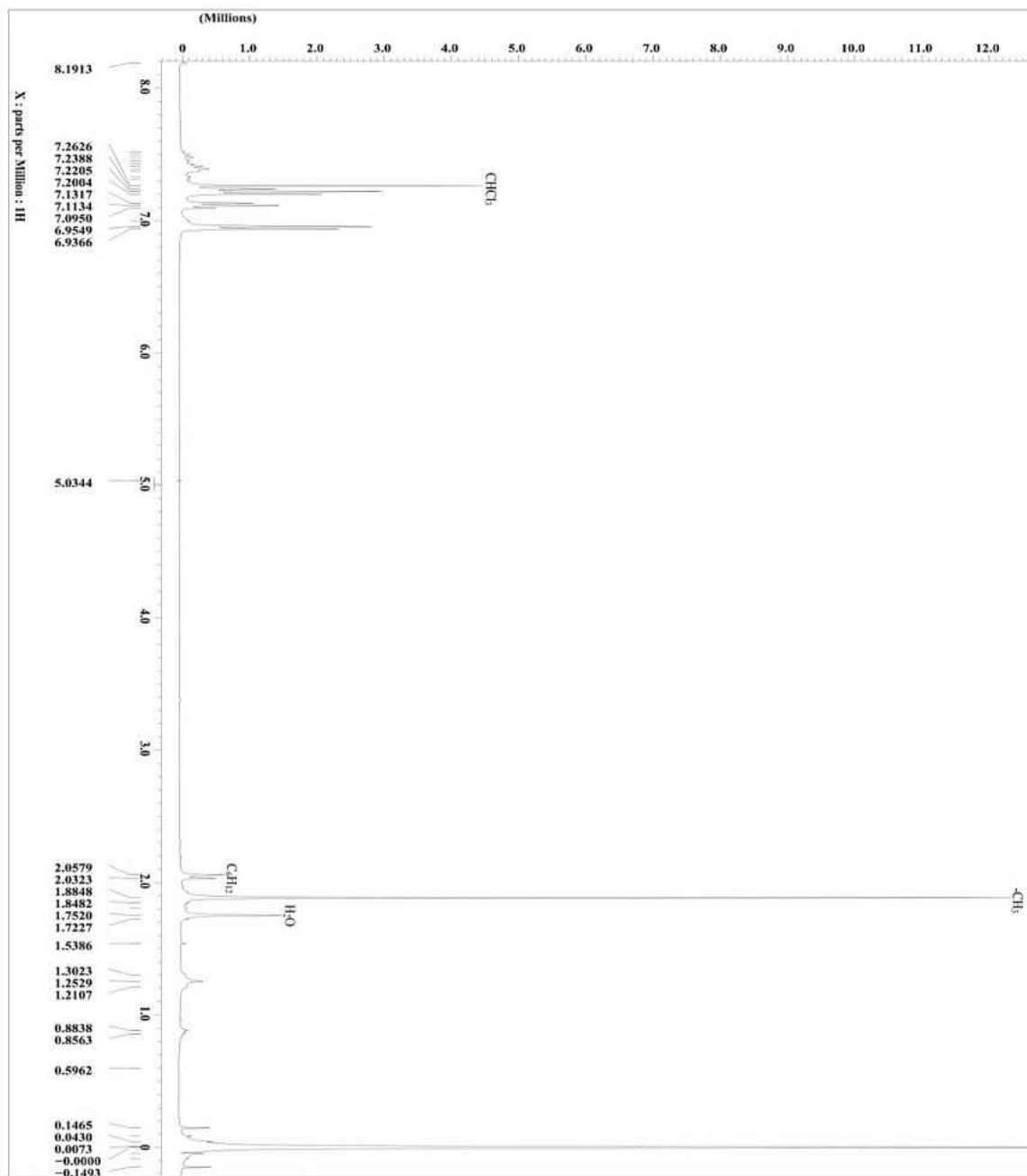
Figure 15. The ^{1}H NMR spectrum of Fraction II of $Rh_2(C_6H_5NCOCH_3)_4$.
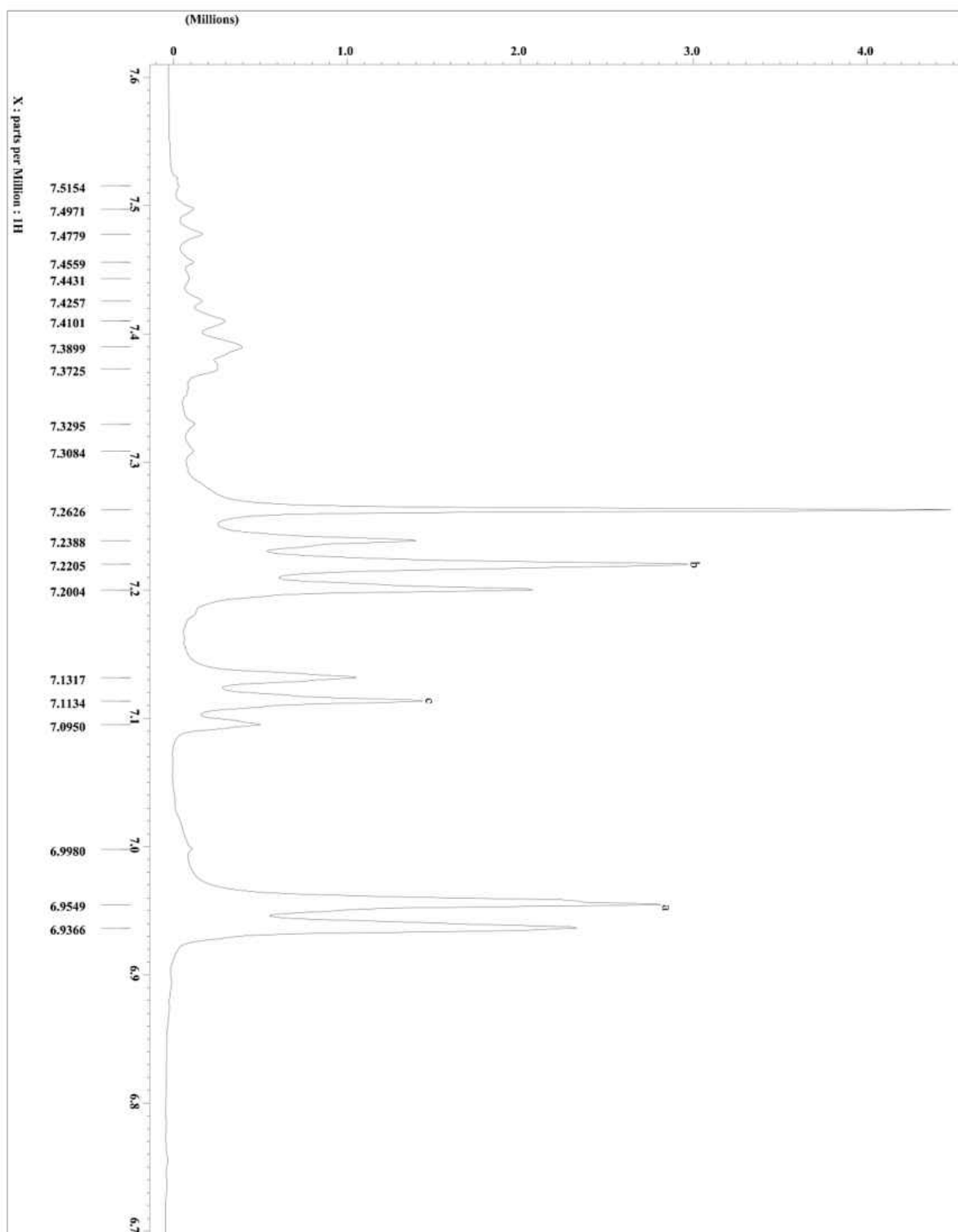
Figure 16. The ^{1}H NMR spectrum of Fraction II showing the chemical shift region from 6.7 ppm

to 7.6 ppm.

Fraction III ^{1}H NMR

Figure 17 and 18, below, show the ^{1}H NMR spectrum for Fraction III (see Figure 49 for labelling).
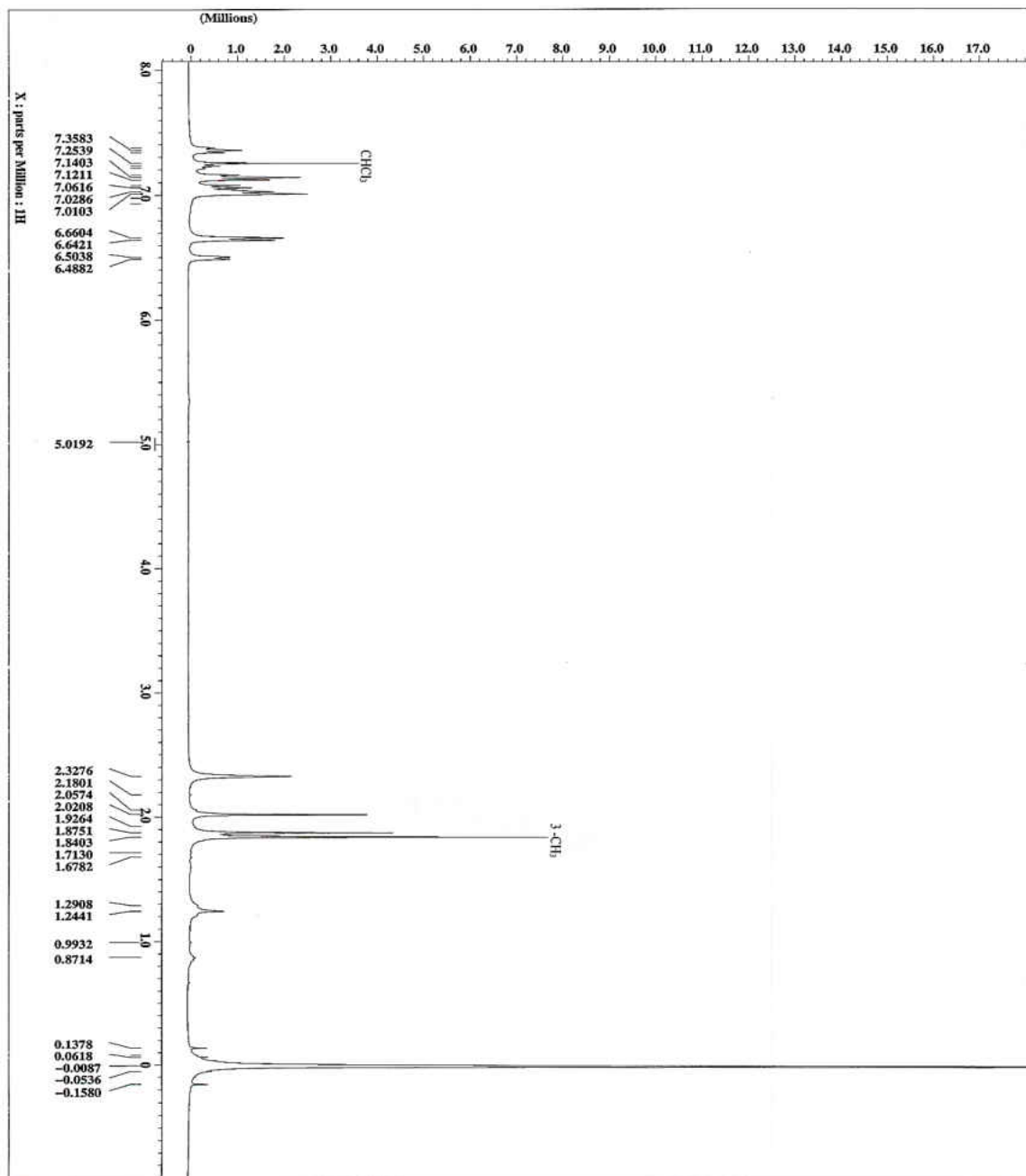
Figure 17. The ^{1}H NMR spectrum of Fraction III of $Rh_2(C_6H_5NCOCH_3)_4$.
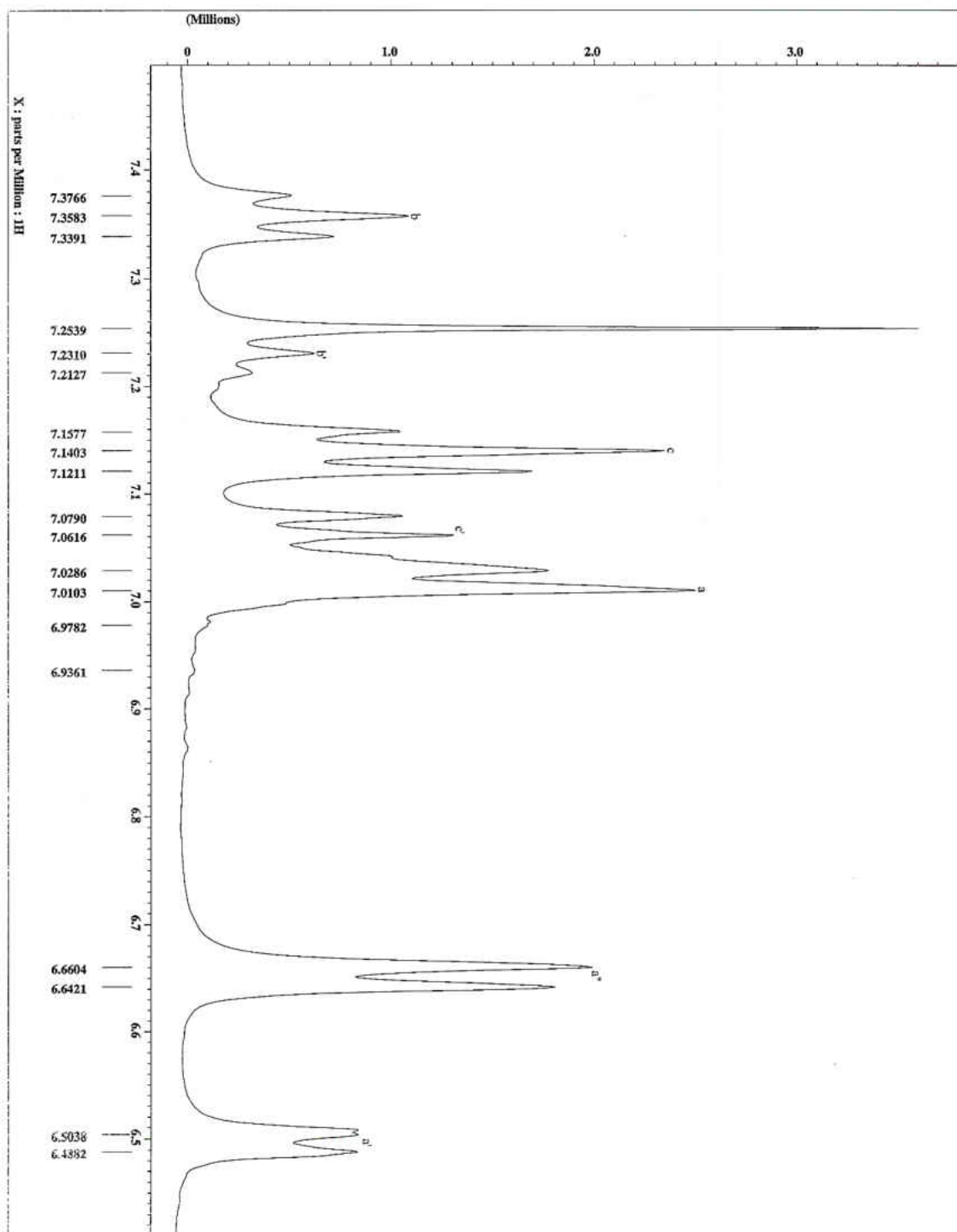
Figure 18. The ^{1}H NMR spectrum of Fraction III showing the chemical shift region from 6.6 ppm to 7.4 ppm.

Formation of the Nitrile Adducts

The glassware used for the formation of the nitrile adducts (25 mL round bottom flasks and stir bars) were washed with water, rinsed with acetone, and dried in the oven at 120 ^{0}C overnight prior to use. Benzonitrile, 2-methyl benzonitrile (o-tolunitrile) and 3-methyl benzonitrile (m-tolunitrile) were used to react with *trans-2,2*-tetrakis(N-phenylacetamido) dirhodium(II) isomer (fraction I) to form the *trans*-2,2-Rh$_2$(C$_6$H$_5$NCOCH$_3$)$_4$·xNitrile adducts (x = 1, 2). 1,3-dicyanobenzene was used to react with the 3,1-tetrakis(N-phenylacetamido) dirhodium(II) isomer (Fraction III) to form the 3,1-[Rh$_2$(C$_6$H$_5$NCOCH$_3$)$_4$·1,3-dicyanobenzene]$_\infty$ adduct. The setup was a round bottom flask containing a stir bar clamped over a magnetic stirrer. These reactions were carried out in CH$_2$Cl$_2$ solvent. The rhodium isomer was placed in the round bottom flask and dissolved with 5 mL of CH$_2$Cl$_2$ solvent. The appropriate number of moles of nitrile ligand that gave a desired ratio of rhodium isomer to nitrile ligand was calculated and were added slowly via a gas tight syringe for each reaction synthesis while stirring. The color of the solution was observed to change depending on the ligand that was added as each incoming nitrile axial ligand creates a different crystal field splitting. Growing the crystals was done by vapor diffusion techniques for which a second set of solvents (acetone, acetonitrile, ethanol, ethyl acetate, hexane, methanol, toluene, and water) were used to assist the vapor diffusion process. The reaction mixture was placed in a ½ dram vial that was then put in a 6 dram vial with another solvent and capped. This setup was left to stand undisturbed over a period of time until crystals grew. Each crystal grew with varying difficulty or varying time periods.

Trans-2,2-tetrakis(N-phenylacetamido) dirhodium(II) – Benzonitrile: Synthesis and Crystal Growth

0.02 g (0.027 mmol) of *trans*-2,2-[$Rh_2(C_6H_5NCOCH_3)_4$] was dissolved in 5 mL CH_2Cl_2 in a 50 mL round bottom flask and clamped to a stand over a magnetic stirrer. 6.31 μL (0.061 mmol) of benzonitrile was added (to achieve a 1:2 reaction) via a gas tight syringe while stirring. The solution turned from a green color to a blue color.

The reaction solution was divided into 7 portions and placed in separate ½ dram vials. These vials were placed in bigger 6 dram vials containing acetone, acetonitrile, ethanol, ethyl acetate, methanol, toluene, and water. These vials were capped and left to stand undisturbed. As the solvent from the inner (½ dram) vial diffused and mixed with the solvent in the outer (6 dram) vial, the volume of solvent in the bigger vial caused the inner vial to tilt over. The inner vial was recentered using a pair of tweezers and the vial recapped. The crystals grew over a 2-week period.

Trans-2,2-tetrakis(N-phenylacetamido) dirhodium(II) – o-Tolunitrile: Synthesis and Crystal Growth

0.02 g (0.027 mmol) of tetrakis *trans*-2,2-[$Rh_2(C_6H_5NCOCH_3)_4$] was dissolved in 5 mL CH_2Cl_2 in a 50 mL round bottom flask and clamped to a stand over a magnetic stirrer. 6.38 μL (0.054 mmol) of 2-methyl benzonitrile was added (to achieve a 1:2 reaction) via a gas tight syringe while stirring. The solution turned from a green color to a blue color.

The reaction solution was divided into 7 portions and placed in separate ½ dram vials. These vials were placed in bigger 6 dram vials containing acetone, acetonitrile, ethanol, ethyl acetate, methanol, toluene, and water. These vials were capped and left to stand undisturbed. As

the solvent from the inner (½ dram) vial diffused and mixed with the solvent in the outer (6 dram) vial, the volume of solvent in the bigger vial caused the inner vial to tilt over. The inner vial was recentered using a pair of tweezers and the vial recapped. The crystals grew over a 2-week period.

Trans-2,2-tetrakis(N-phenylacetamido) dirhodium(II) – m-Tolunitrile: Synthesis and Crystal Growth

0.02 g (0.027 mmol) of tetrakis *trans*-2,2-[$Rh_2(C_6H_5NCOCH_3)_4$] was dissolved in 5 mL CH_2Cl_2 in a 50 mL round bottom flask and clamped to a stand over a magnetic stirrer. 6.50 µL (0.054 mmol) of 3-methyl benzonitrile was added (to achieve a 1:2 reaction) via a gas tight syringe while stirring. The solution turned from a green color to a blue color.

The reaction solution was divided into 7 portions and placed in separate ½ dram vials. These vials were placed in bigger 6 dram vials containing acetone, acetonitrile, ethanol, ethyl acetate, methanol, toluene, and water. These vials were capped and left to stand undisturbed. As the solvent from the inner (½ dram) vial diffused and mixed with the solvent in the outer (6 dram) vial, the volume of solvent in the bigger vial caused the inner vial to tilt over. The inner vial was recentered using a pair of tweezers and the vial recapped. The crystals grew over a 2-week period.

The crystals that grew here were starburst in nature and were not suitable for X-ray diffractometry because they were long, thin, and did not diffract the incident X-rays properly. A second trial using the same quantities for synthesis was done still applying vapor diffusion techniques for crystal growth. This mixture was divided into 6 portions and the solvents used in the outer vials were acetone, acetonitrile, ethanol, ethyl acetate, methanol, and water that resulted

in the same observations; starburst crystals for which no structure solution could be obtained by X-ray diffractometry analysis (unfortunately, the instrument used cannot collect a powder diffraction pattern, so these data were not accessible).

To achieve X-ray quality crystals, the ½ dram vials containing crystals were dried by blowing nitrogen gas over them. These crystals were dissolved in about 5 drops of acetone and placed back into their respective 6 dram vials. The vials were capped and left to stand undisturbed. Big block crystals grew over a period of 1 week.

3,1-tetrakis(N-phenylacetamido) dirhodium(II) – 1,3-dicyanobenzene: Synthesis and Crystal Growth

0.02 g (0.027 mmol) of tetrakis 3,1-[$Rh_2(C_6H_5NCOCH_3)_4$] was dissolved in 5 mL CH_2Cl_2 in a 50 mL round bottom flask and clamped to a stand over a magnetic stirrer. 0.034 g of 1,3-dicyanobenzene was then dissolved in 9 mL CH_2Cl_2. 1 mL (0.029 mmol) of this solution was added (to achieve a 1:1 reaction) to the round bottom flask while stirring. The solution turned from a light green color to a dark blue color. Dissolving the nitrile ligand in 9 mL instead of 10 mL introduced an error as slightly over 1:1 ratio was used.

The reaction solution was divided into 7 portions and placed in separate ½ dram vials. These vials were placed in bigger 6 dram vials containing acetone, acetonitrile, ethanol, ethyl acetate, methanol, toluene, and water. These vials were capped and left to stand undisturbed. As the solvent from the inner (½ dram) vial diffused and mixed with the solvent in the outer (6 dram) vial, the volume of solvent in the bigger vial caused the inner vial to tilt over. The inner vial was recentered using a pair of tweezers and the vial recapped. The crystals grew over a 2-week period.

Infrared Spectrophotometry

    Trans-2,2-tetrakis(N-phenylacetamido) dirhodium(II) – Benzonitrile. Prior to taking the IR spectrum for the complex, the spectrum of the free benzonitrile ligand was first taken. The IR spectrum of the free ligand was obtained by placing a liquid sample on the ATR sample cup (crystal through which IR laser hits the sample).

    The IR spectrum of the *trans*-2,2-tetrakis(N-phenylacetamido) dirhodium(II) – Benzonitrile complex was obtained by grinding a small amount of the sample and placing the powder on the ATR sample cup. A background scan was first taken then the spectra for the benzonitrile ligand as well as that for the 2,2-*trans*-[$Rh_2(C_6H_5NCOCH_3)_4$·benzonitrile] were taken.

    Figures 19 and 20, below, show the FT-IR spectra for the free benzonitrile ligand and the *trans*-2,2-tetrakis(N-phenylacetamido) dirhodium(II) – Benzonitrile complex respectively.
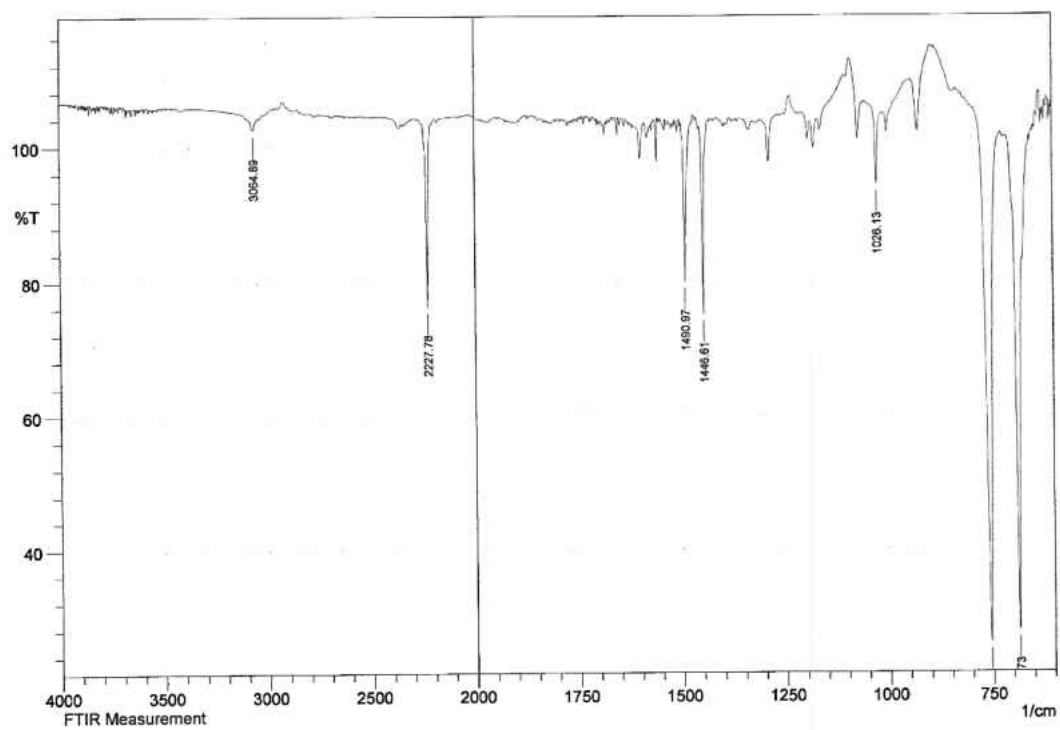
	Peak	Intensity	Corr. Intensity	Base (H)	Base (L)	Area	Corr. Area
1	684.73	27.795	59.864	713.66	675.09	5.257	3.815
2	754.17	26.005	77.344	788.89	725.23	6.694	7.644
3	1026.13	94.125	11.231	1041.56	1010.7	-0.378	0.321
4	1446.61	75.097	28.002	1454.33	1435.04	0.436	0.697
5	1490.97	79.946	23.611	1498.69	1469.76	0.346	0.821
6	2227.78	76.382	27.323	2252.86	2191.13	0.494	1.483
7	3064.89	102.609	1.724	3097.68	3043.67	-0.848	0.152

Figure 19. The FT-IR spectrum of benzonitrile showing the C≡N stretching frequency at

2227.78 cm^{-1}.
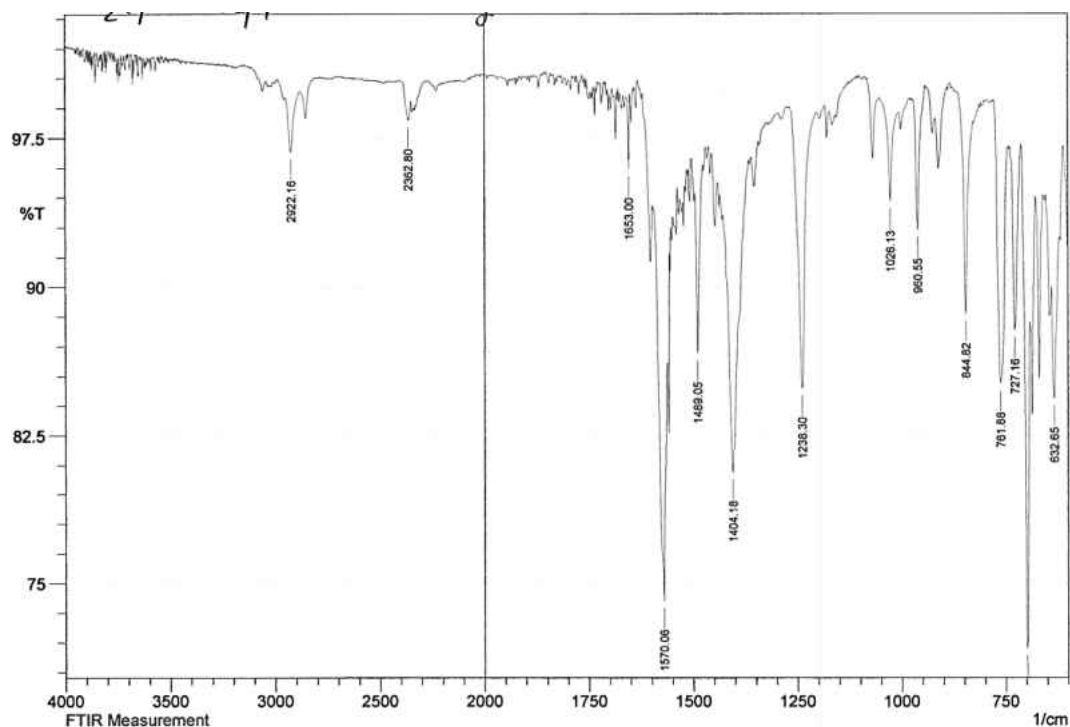
No.	Peak	Intensity	Corr. Intensity	Base (H)	Base (L)	Area	Corr. Area
1	632.65	84.38	6.423	638.44	619.15	1.063	0.3
2	698.23	71.742	19.76	711.73	690.52	1.568	0.861
3	727.16	87.843	9.302	738.74	711.73	0.833	0.494
4	761.88	85.149	13.238	777.31	742.59	1.328	1.061
5	844.82	88.635	10.388	864.11	827.46	0.667	0.517
6	960.55	92.927	6.734	970.19	943.19	0.326	0.299
7	1026.13	94.333	4.801	1051.2	1004.91	0.413	0.244
8	1238.3	84.898	14.021	1267.23	1205.51	1.548	1.253
9	1404.18	80.639	14.031	1427.32	1365.6	3.11	1.737
10	1489.05	86.677	8.491	1494.83	1475.54	0.694	0.304
11	1570.06	74.13	14.331	1593.2	1560.41	2.637	1.132
12	1653	95.958	3.76	1658.78	1651.07	0.054	0.043
13	2362.8	98.43	0.189	2395.59	2360.87	0.066	-0.017
14	2922.16	96.847	2.837	2949.16	2877.79	0.411	0.324

Figure 20. The FT-IR spectrum of *trans*-2,2-[$Rh_2(C_6H_5NCOCH_3)_4 \cdot 2$benzonitrile] showing the

C≡N stretching frequency at 2362.8 cm^{-1}.

Trans-2,2-tetrakis(N-phenylacetamido) dirhodium(II) – 2-methyl benzonitrile. Prior to

taking the IR spectrum for the complex, the spectrum of the free o-tolunitrile ligand was first

taken. The IR spectrum of the free ligand was obtained by placing a liquid sample on the ATR

sample cup (crystal through which IR laser hits the sample).

The IR spectrum of the *trans*-2,2-tetrakis(N-phenylacetamido) dirhodium(II) – 2-methyl benzonitrile complex was obtained by grinding a small amount of the sample and placing the powder on the ATR sample cup. A background scan was first taken then the spectra for the o-tolunitrile ligand as well as that for the *trans*-2,2-[Rh$_2$(C$_6$H$_5$NCOCH$_3$)$_4$·o-tolunitrile] were taken.

Figures 21 and 22, below, show the FT-IR spectra for the free 2-methyl benzonitrile ligand and the *trans*-2,2-tetrakis(N-phenylacetamido) dirhodium(II) – 2-methyl benzonitrile complex respectively.

	Peak	Intensity	Corr. Intensity	Base (H)	Base (L)	Area	Corr. Area
1	711.73	58.992	37.893	725.23	692.44	1.891	1.458
2	758.02	28.935	68.841	808.17	729.09	8.251	7.643
3	1487.12	80.063	17.802	1504.48	1473.62	0.936	0.672
4	2223.92	77.664	25.596	2262.5	2183.42	0.33	1.432
5	2926.01	102.549	0.978	2939.52	2893.22	-0.651	0.077
6	3064.89	102.867	0.976	3093.82	3051.39	-0.641	0.081
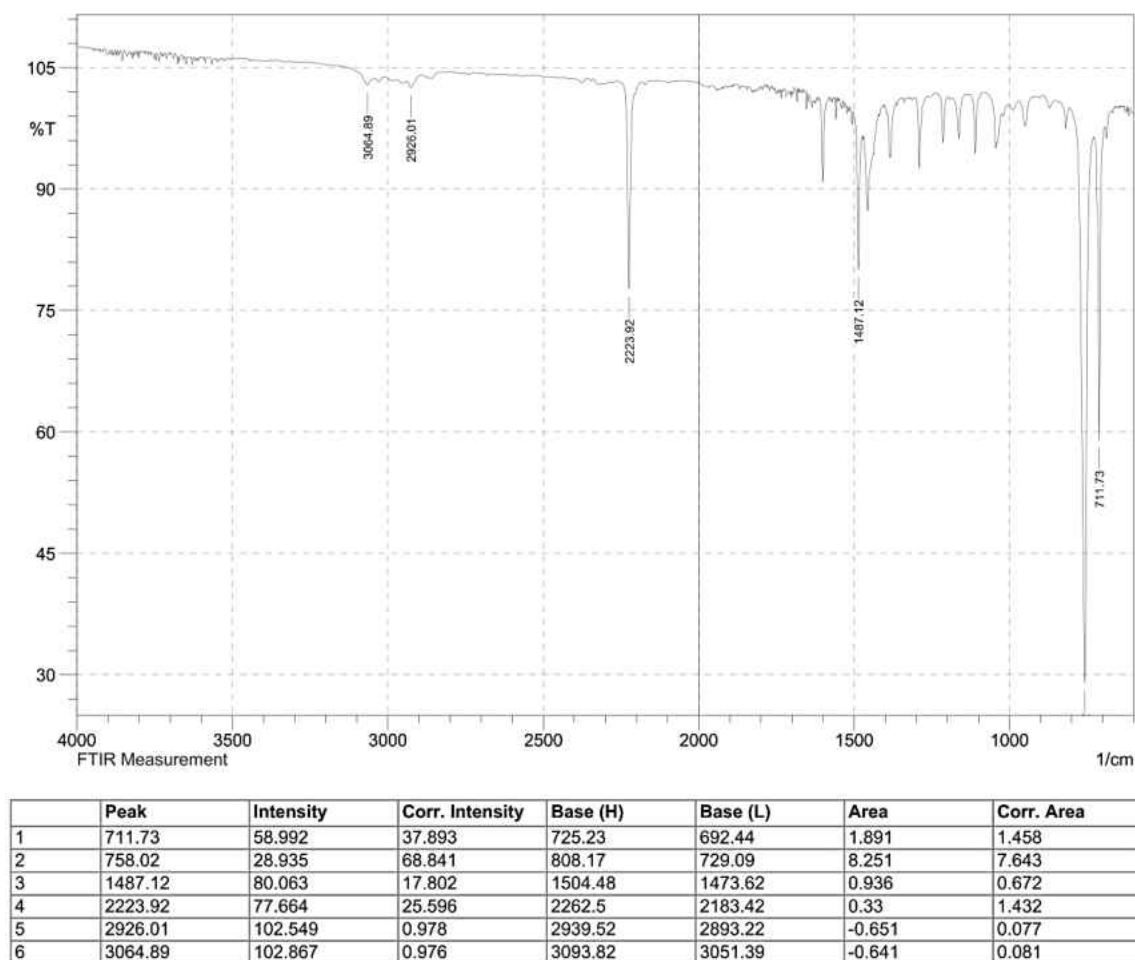
Figure 21. FT-IR spectrum of o-tolunitrile showing the C≡N stretching frequency at 2223.92 cm^{-1}.
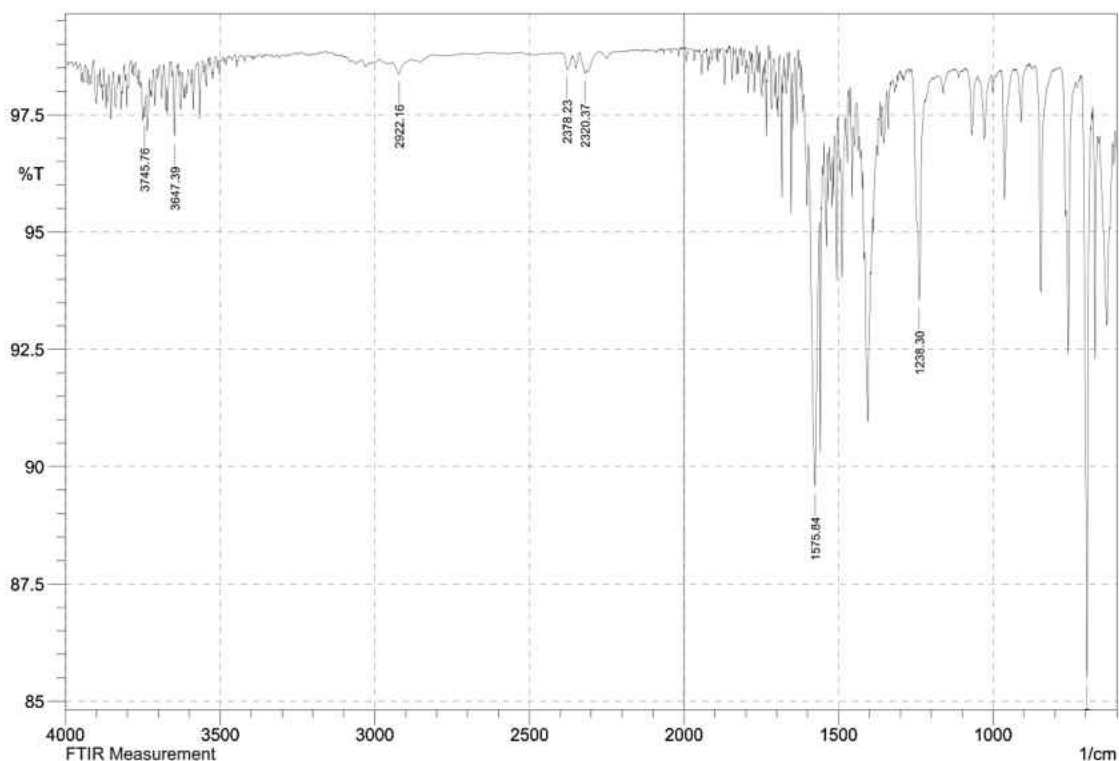
	Peak	Intensity	Corr. Intensity	Base (H)	Base (L)	Area	Corr. Area
1	696.3	85.489	12.187	713.66	684.73	0.851	0.57
2	1238.3	93.538	4.547	1263.37	1220.94	0.687	0.342
3	1575.84	89.575	6.337	1597.06	1560.41	1.175	0.532
4	2320.37	98.383	0.159	2337.72	2314.58	0.145	0.007
5	2378.23	98.463	0.297	2395.59	2364.73	0.184	0.018
6	2922.16	98.365	0.25	2943.37	2900.94	0.277	0.02
7	3647.39	97.036	1.452	3653.18	3639.68	0.125	0.036
8	3745.76	97.436	0.31	3747.69	3739.97	0.08	0.006

Figure 22. The FT-IR spectrum of *trans*-2,2-[Rh$_2$(C$_6$H$_5$NCOCH$_3$)$_4$·2o-tolunitrile] showing the

C≡N stretching frequency at 2320.37 cm^{-1}.

Trans-2,2-tetrakis(N-phenylacetamido) dirhodium(II) – 3-methyl benzonitrile. Prior to

taking the IR spectrum for the complex, the spectrum of the free m-tolunitrile ligand was first

taken. The IR spectrum of the free ligand was obtained by placing a liquid sample on the ATR

sample cup (crystal through which IR laser hits the sample).

The IR spectrum of the *trans*-2,2-tetrakis(N-phenylacetamido) dirhodium(II) – 3-methyl

benzonitrile complex was prepared by grinding a small amount of the sample and placing the

powder on the ATR sample cup. A background scan was first taken then the spectra for the m-tolunitrile ligand as well as that for the *trans*-2,2-[Rh$_2$(C$_6$H$_5$NCOCH$_3$)$_4$•m-tolunitrile] were taken.

Figures 23 and 24, below, show the FT-IR spectra for the free 3-methyl benzonitrile ligand and the *trans*-2,2-tetrakis(N-phenylacetamido) dirhodium(II) – 3-methyl benzonitrile complex respectively.

	Peak	Intensity	Corr. Intensity	Base (H)	Base (L)	Area	Corr. Area
1	684.73	29.868	67.105	700.16	655.8	4.368	3.799
2	785.03	45.976	52.331	823.6	746.45	6.167	5.595
3	1496.76	95.449	0.626	1502.55	1494.83	0.127	0.006
4	2227.78	73.912	26.241	2264.43	2185.35	1.341	1.395
5	2924.09	97.885	1.297	2941.44	2887.44	0.272	0.106
6	3647.39	98.076	2.31	3653.18	3639.68	0.033	0.056
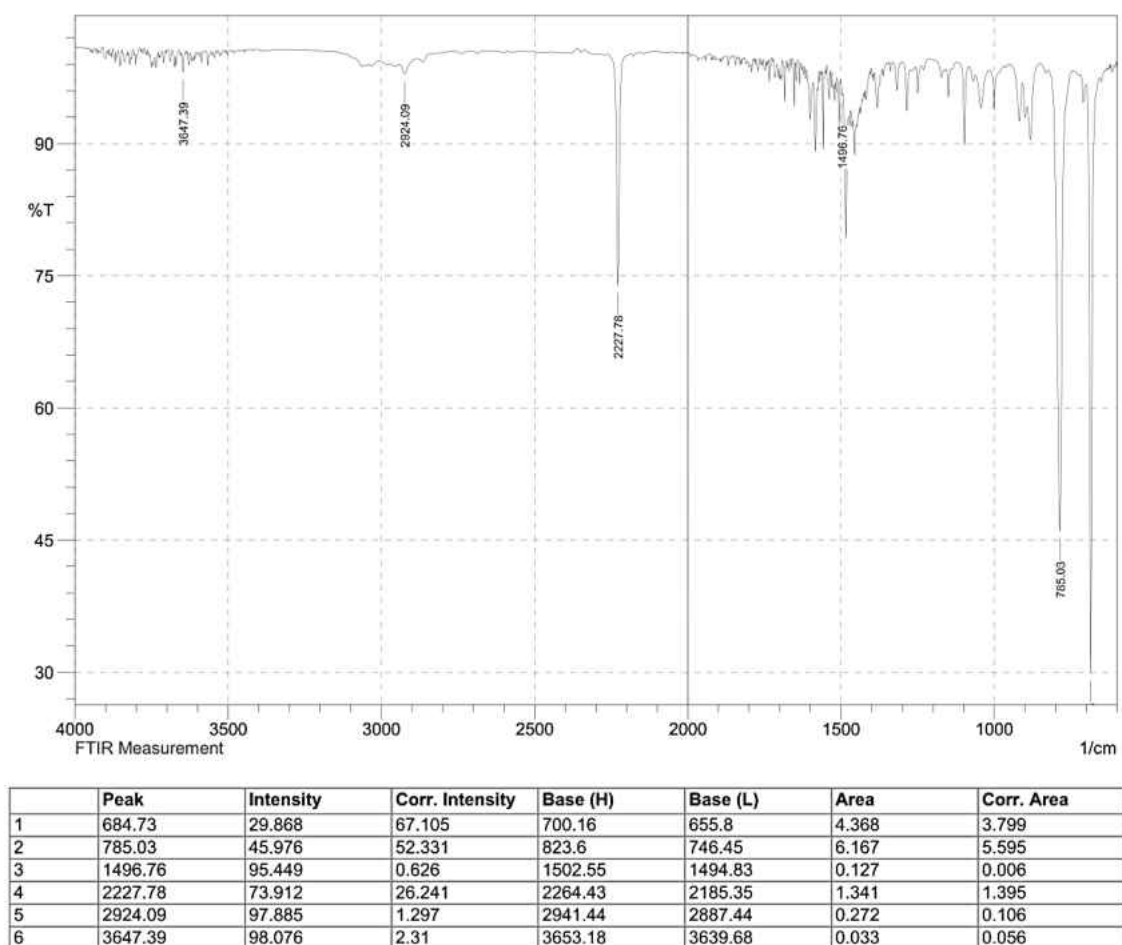
Figure 23. The FT-IR spectrum of m-tolunitrile showing the C≡N stretching frequency at 2227.78 cm^{-1}.

	Peak	Intensity	Corr. Intensity	Base (H)	Base (L)	Area	Corr. Area
1	1402.25	90.126	6.254	1419.61	1361.74	1.578	0.696
2	1571.99	90.438	0.632	1577.77	1570.06	0.297	0.005
3	2241.28	98.536	0.132	2249	2229.71	0.117	0.005
4	2310.72	98.538	0.037	2314.58	2287.58	0.165	0.002
5	2349.3	98.514	0.099	2357.01	2341.58	0.096	0.003
6	2852.72	98.313	0.246	2870.08	2812.21	0.37	0.017
7	2924.09	97.798	0.627	2945.3	2877.79	0.525	0.067
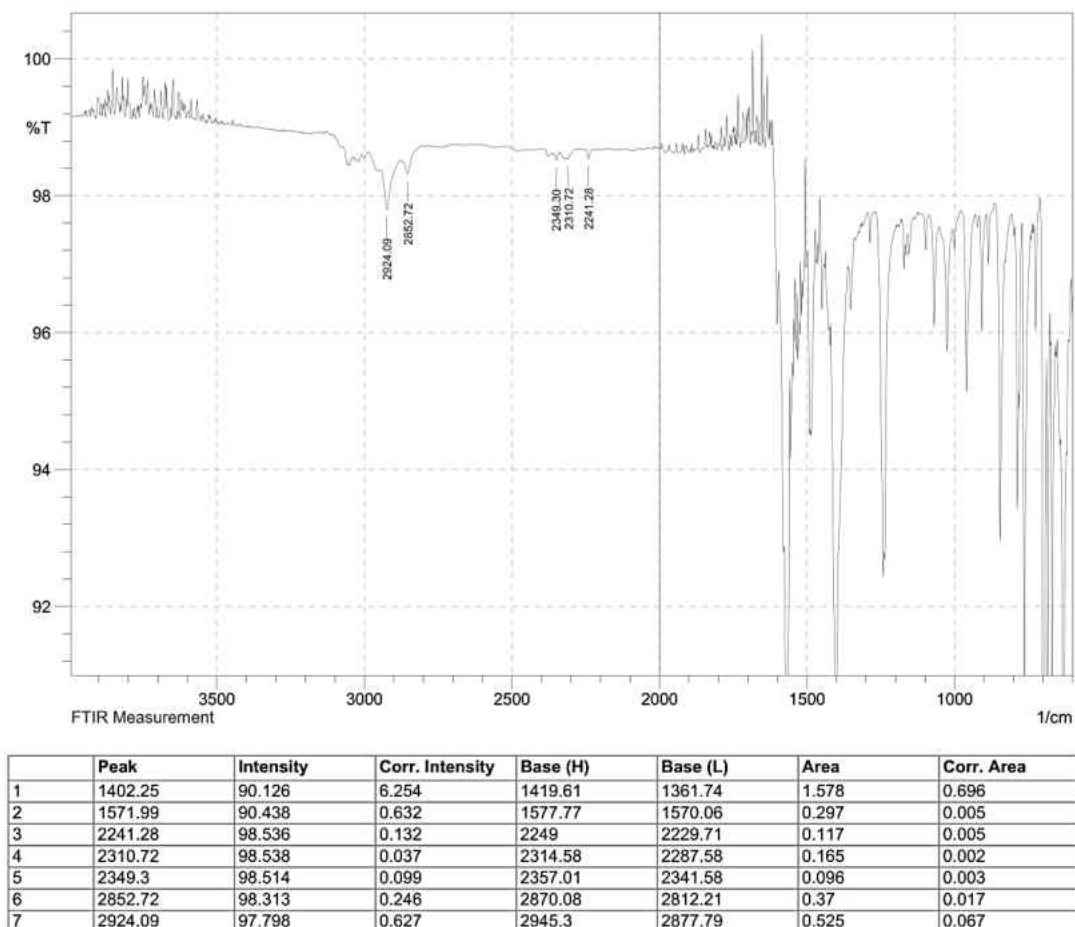
Figure 24. The FT-IR spectrum of *trans*-2,2-[Rh$_2$(C$_6$H$_5$NCOCH$_3$)$_4$·m-tolunitrile] showing the

C≡N stretching frequency at 2241.28 cm^{-1}.

3,1-tetrakis(N-phenylacetamido) dirhodium(II) – 1,3-dicyanobenzene. Prior to taking the

IR spectrum for the complex, the spectrum of the free 1,3-dicyanobenzene ligand was first taken.

The IR spectrum of the free ligand was obtained by placing a liquid sample on the ATR sample

cup (crystal through which IR laser hits the sample).

The IR spectrum of the 3,1-tetrakis(N-phenylacetamido) dirhodium(II) – 1,3-

dicyanobenzene complex was prepared by grinding a small amount of the sample and placing the

powder on the ATR sample cup. A background scan was first taken then the spectra for the 1,3-

dicyanobenzene ligand as well as that for the 3,1-[Rh$_2$(C$_6$H$_5$NCOCH$_3$)$_4$·1,3-dicyanobenzene] were taken.

Figures 25 and 26, below, show the FT-IR spectra for the free 1,3-dicyanobenzene ligand and the 3,1-tetrakis(N-phenylacetamido) dirhodium(II) – 1,3-dicyanobenzene complex respectively.

	Peak	Intensity	Corr. Intensity	Base (H)	Base (L)	Area	Corr. Area
1	678.94	93.723	9.447	686.66	657.73	0.002	0.373
2	804.32	96.425	6.967	821.68	779.24	-0.239	0.361
3	904.61	101.201	3.599	929.69	896.9	-0.63	0.093
4	1481.33	101.153	2.91	1485.19	1467.83	-0.208	0.092
5	2233.57	100.968	3.796	2249	2212.35	-0.585	0.151
6	3078.39	105.392	0.235	3093.82	3074.53	-0.484	-0.003
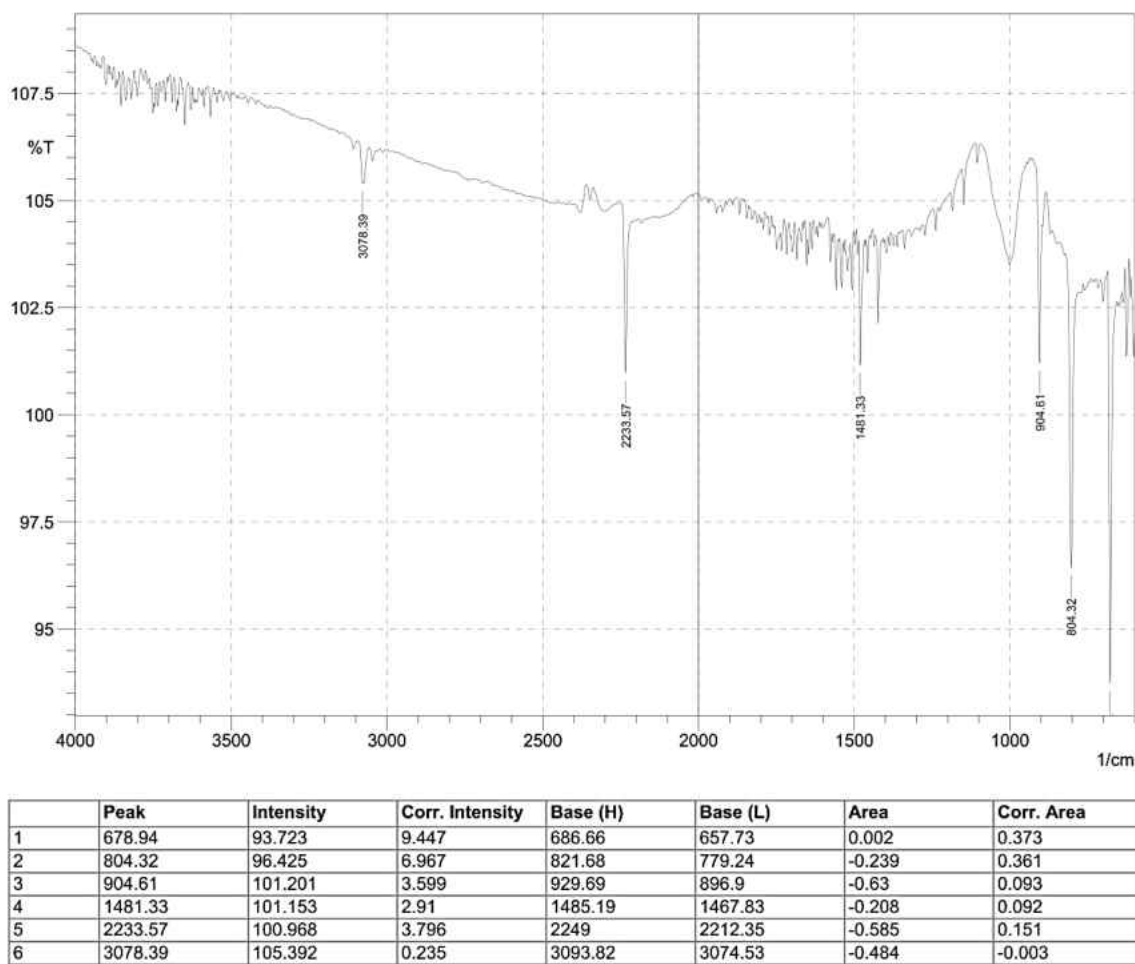
Figure 25. The FT-IR spectrum of 1,3-dicyanobenzene showing the C≡N stretching frequency at 2233.57 cm^{-1}.
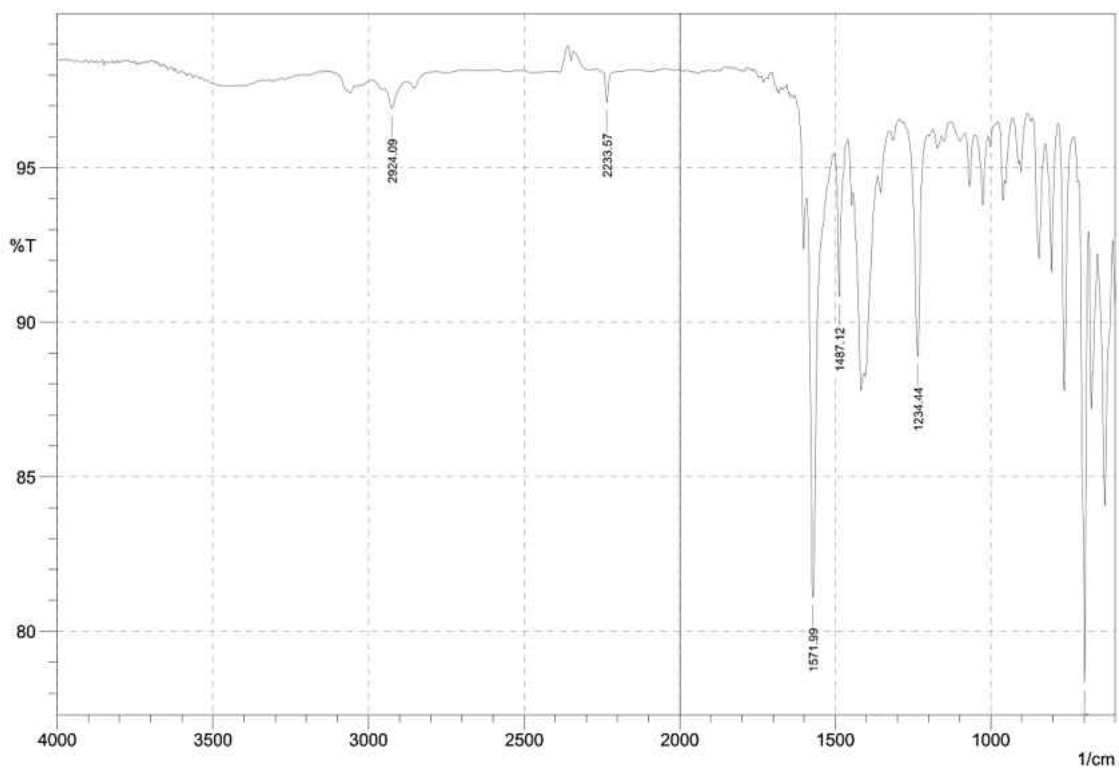
	Peak	Intensity	Corr. Intensity	Base (H)	Base (L)	Area	Corr. Area
1	698.23	78.328	15.285	717.52	684.73	1.88	0.962
2	1234.44	88.889	7.352	1278.81	1201.65	2.01	0.737
3	1487.12	90.817	4.8	1502.55	1460.11	1.091	0.278
4	1571.99	81.096	13.277	1593.2	1506.41	3.567	1.529
5	2233.57	97.101	0.999	2247.07	2214.28	0.318	0.045
6	2924.09	96.921	0.714	2949.16	2877.79	0.811	0.081

Figure 26. The FT-IR spectrum of 3,1-[Rh$_2$(C$_6$H$_5$NCOCH$_3$)$_4$·1,3-dicyanobenzene] showing the

C≡N stretching frequency at 2233.57 cm^{-1}.

Trans-2,2-tetrakis(N-phenylacetamido) dirhodium(II) – Benzonitrile. Prior to taking the ^{1}H NMR for the *trans*-2,2-[$Rh_2(C_6H_5NCOCH_3)_4$·benzonitrile] adduct, an initial NMR of the $CDCl_3$ solvent was first taken in clean, dry NMR tubes to ensure that the tube was clean. These spectra showed peaks as expected (TMS at 0 ppm and the $CHCl_3$ at 7.263 ppm). The $CDCl_3$ from these NMR tubes with known spectra was then used to dissolve a small amount of *trans*-2,2-[$Rh_2(C_6H_5NCOCH_3)_4$·benzonitrile] (see Figure 51 for labeling). The NMR tube was mounted on a JOEL AS400 FT-NMR spectrophotometer and the spectrum gotten by doing 300 scans.

The ^{1}H NMR spectrum for the free benzonitrile (see Figure 50 for labeling) ligand was also taken for comparison purposes.

Figures 27 and 29, below, show the ^{1}H NMR spectrum for the free benzonitrile ligand while Figures 28 and 30, below, show the ^{1}H NMR spectrum for the *trans*-2,2-[$Rh_2(C_6H_5NCOCH_3)_4$·benzonitrile] adduct.
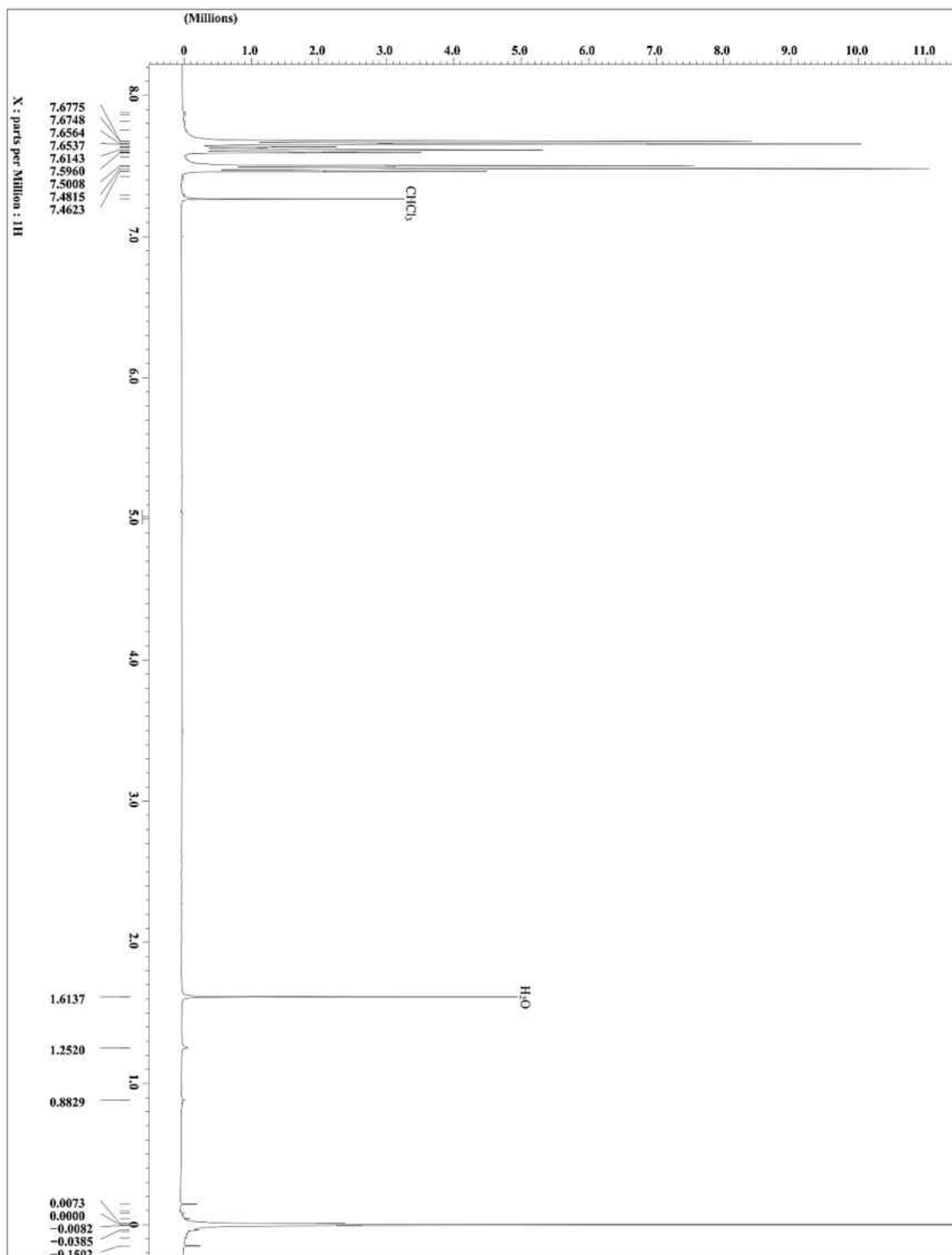
Figure 27. The ^{1}H NMR spectrum of Benzonitrile.
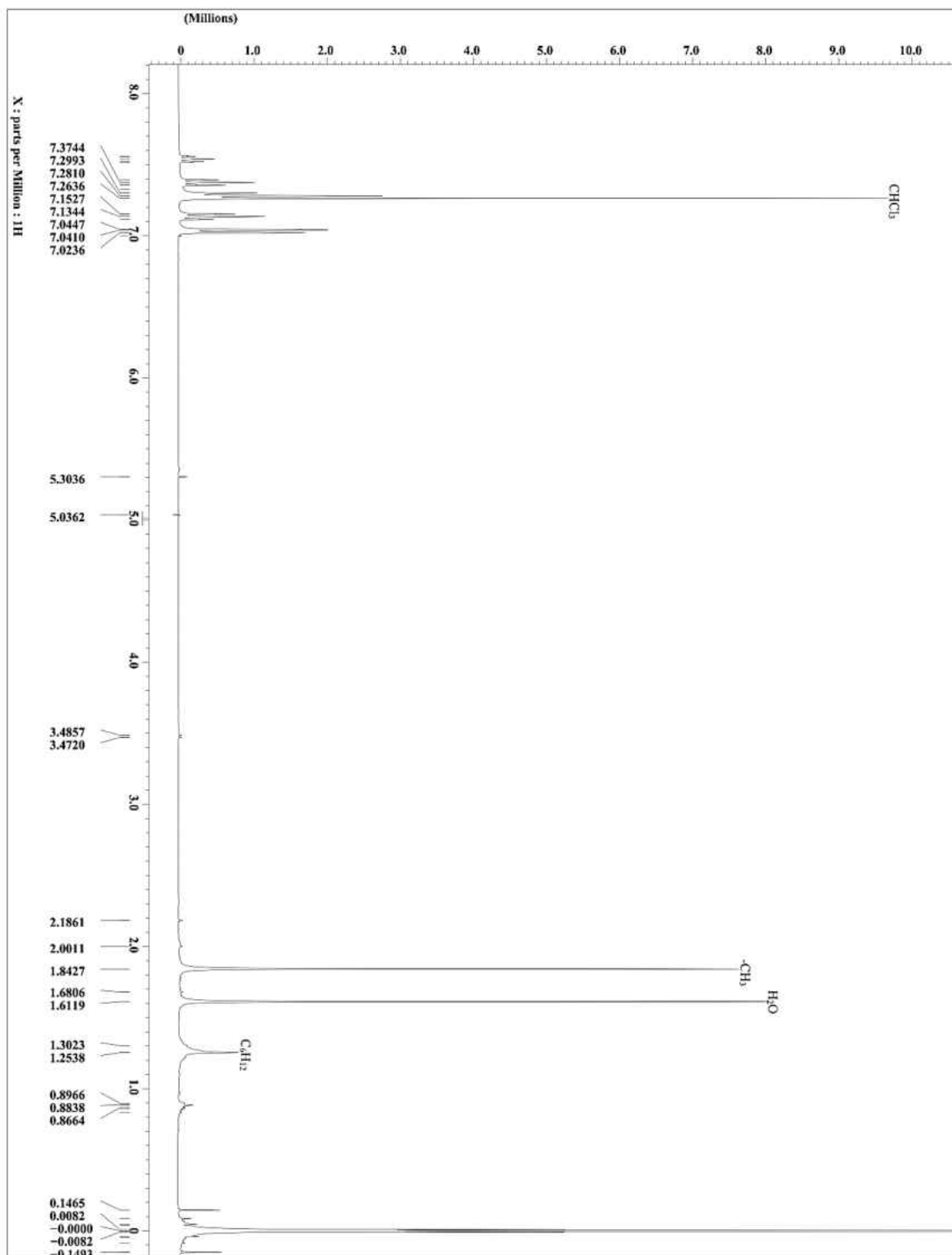
Figure 28. The ^{1}H NMR spectrum of *trans*-2,2-[Rh$_2$(C$_6$H$_5$NCOCH$_3$)$_4$•2benzonitrile].
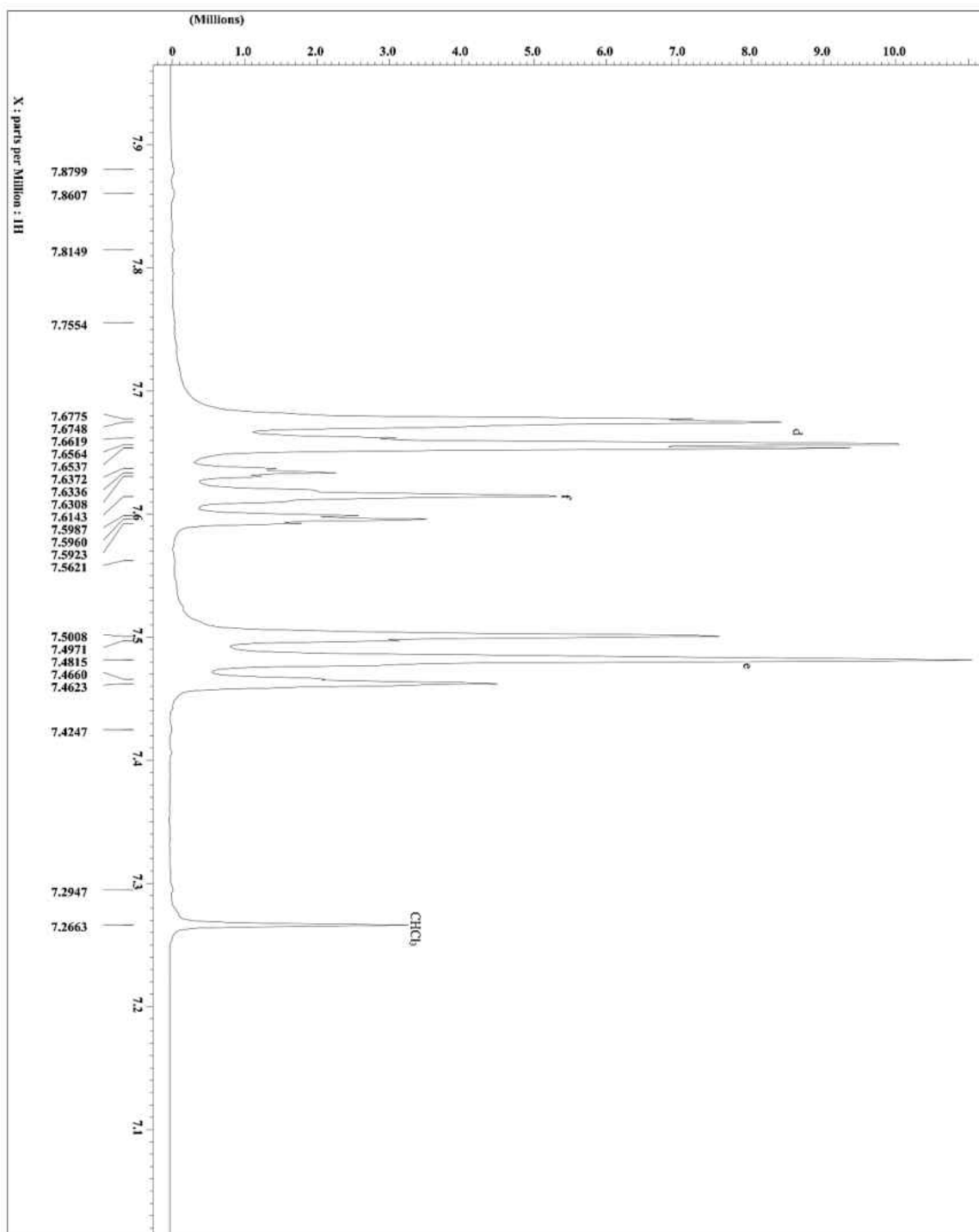
Figure 29. The ^{1}H NMR spectrum of benzonitrile showing the chemical shift region from 7.1 ppm and 7.9 ppm.
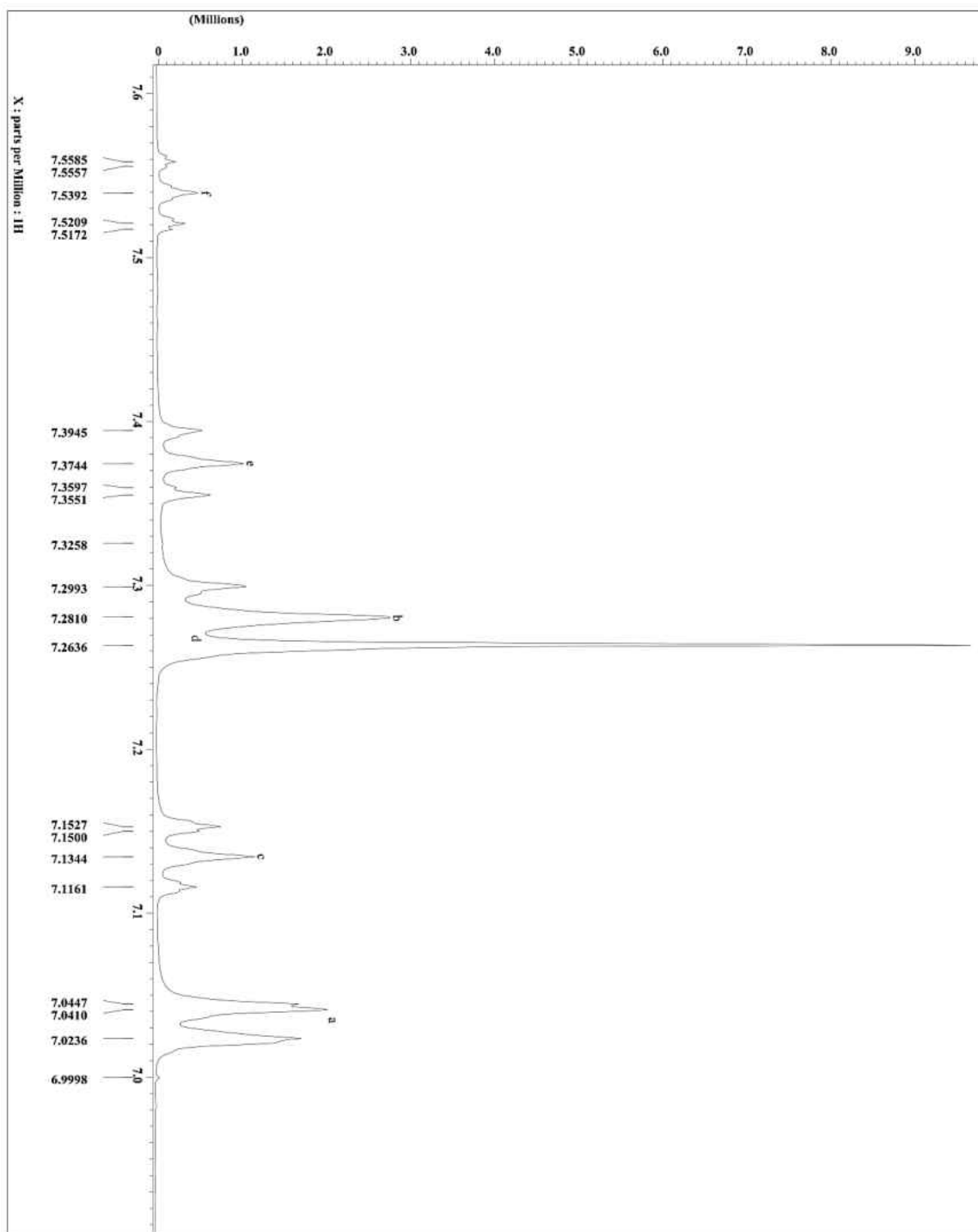
Figure 30. The ^{1}H NMR spectrum of *trans*-2,2-[Rh$_2$(C$_6$H$_5$NCOCH$_3$)$_4$·benzonitrile] showing the chemical shift region from 7.0 ppm to 7.6 ppm.

Trans-2,2-tetrakis(N-phenylacetamido) dirhodium(II) – 2-methyl benzonitrile. Prior to taking the ^{1}H NMR for the *trans*-2,2-[Rh$_2$(C$_6$H$_5$NCOCH$_3$)$_4$•o-tolunitrile] adduct, an initial NMR of the CDCl$_3$ solvent was first taken in clean, dry NMR tubes to ensure that the tube was clean. These spectra showed peaks as expected (TMS at 0 ppm and the CHCl$_3$ at 7.263 ppm). The CDCl$_3$ from these NMR tubes with known spectra was then used to dissolve a small amount of *trans*-2,2-[Rh$_2$(C$_6$H$_5$NCOCH$_3$)$_4$•o-tolunitrile] (see Figure 53 for labeling). The NMR tube was mounted on a JOEL AS400 FT-NMR spectrophotometer and the spectrum gotten by doing 300 scans.

The ^{1}H NMR spectrum for the free o-tolunitrile (see Figure 52 for labeling) ligand was also taken for comparison purposes.

Figures 31 and 33, below, show the ^{1}H NMR spectrum for the free o-tolunitrile ligand while Figures 32 and 34, below, show the ^{1}H NMR spectrum for the *trans*-2,2-[Rh$_2$(C$_6$H$_5$NCOCH$_3$)$_4$•o-tolunitrile] adduct.
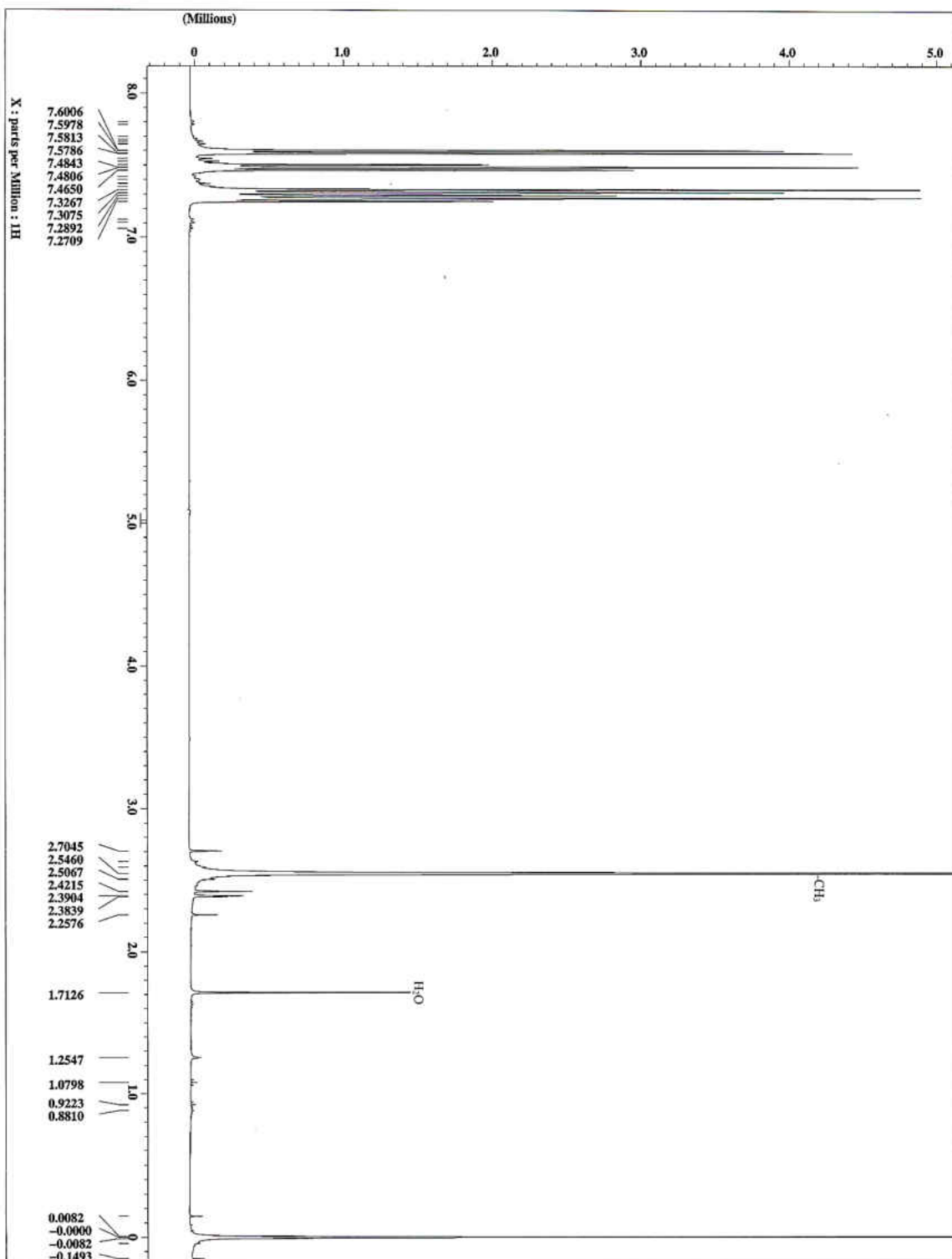
Figure 31. The ^{1}H NMR spectrum of o-tolunitrile.
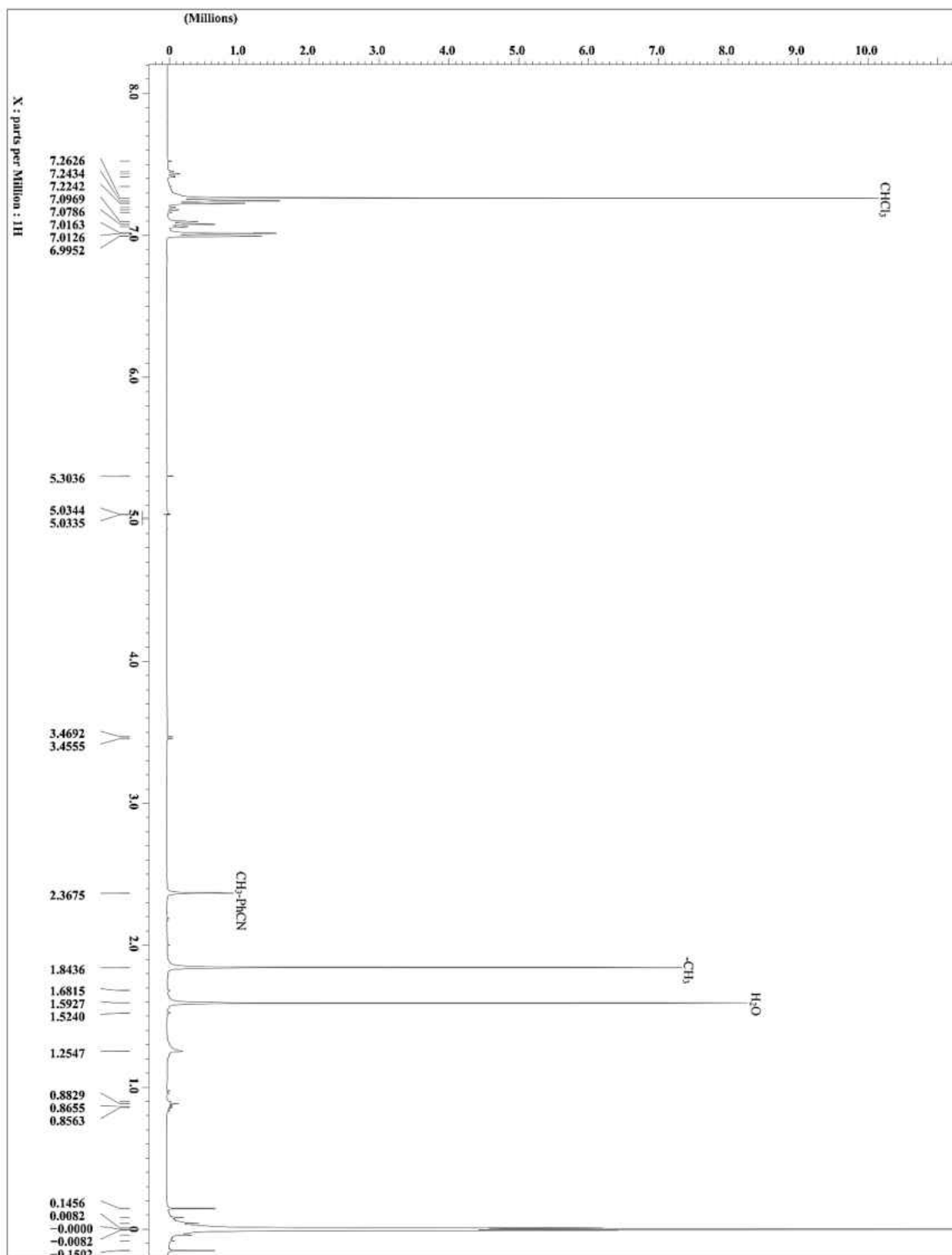
Figure 32. The ^{1}H NMR spectrum of *trans*-2,2-[Rh$_2$(C$_6$H$_5$NCOCH$_3$)$_4$•2o-tolunitrile].
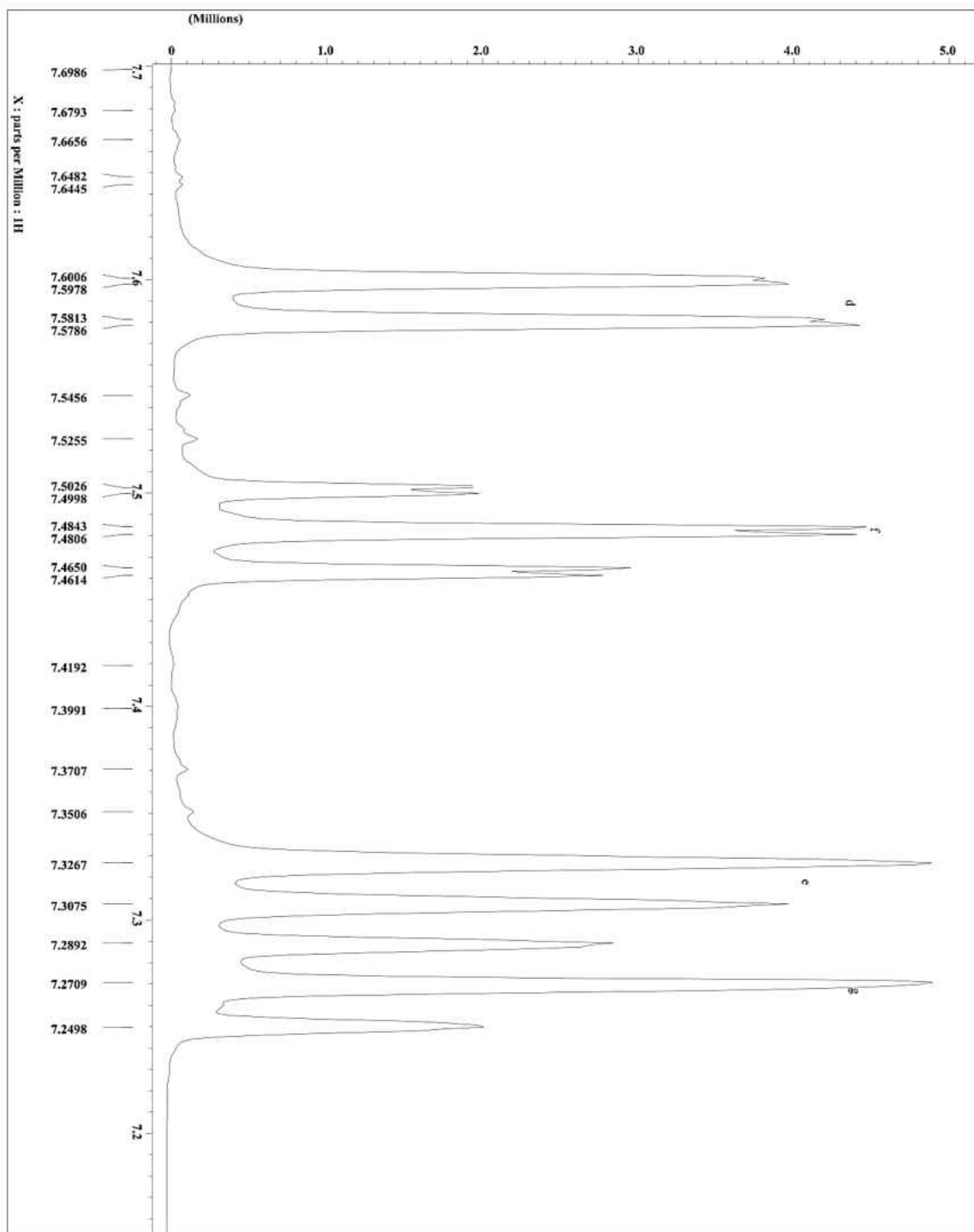
Figure 33. The ^{1}H NMR spectrum of o-tolunitrile showing the chemical shift region from 7.2 ppm to 7.7 ppm.
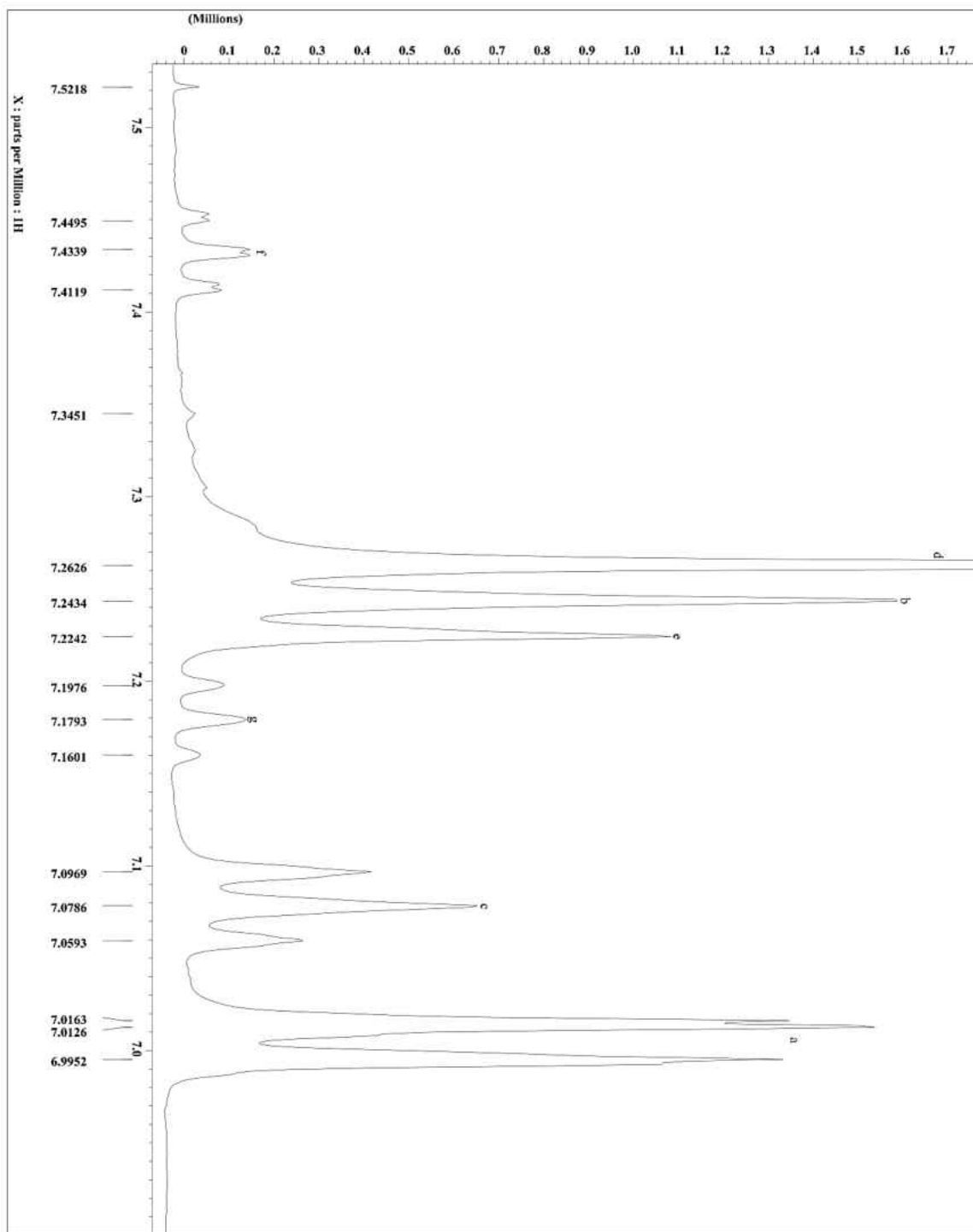
Figure 34. The ^{1}H NMR of *trans*-2,2-[Rh$_2$(C$_6$H$_5$NCOCH$_3$)$_4$·2o-tolunitrile] showing the chemical shift region from 7.0 ppm and 7.5 ppm.

Trans-2,2-tetrakis(N-phenylacetamido) dirhodium(II) – 3-methyl benzonitrile. Prior to taking the ^{1}H NMR for the *trans*-2,2-[Rh$_2$(C$_6$H$_5$NCOCH$_3$)$_4$•m-tolunitrile] adduct, an initial NMR of the CDCl$_3$ solvent was first taken in clean, dry NMR tubes to ensure that the tube was clean. These spectra showed peaks as expected (TMS at 0 ppm and the CHCl$_3$ at 7.263 ppm). The CDCl$_3$ from these NMR tubes with known spectra was then used to dissolve a small amount of *trans*-2,2-[Rh$_2$(C$_6$H$_5$NCOCH$_3$)$_4$•m-tolunitrile] (see Figure 55 for labeling). The NMR tube was mounted on a JOEL AS400 FT-NMR spectrophotometer and the spectrum gotten by doing 300 scans.

The ^{1}H NMR spectrum for the free m-tolunitrile (see Figure 54 for labeling) ligand was also taken for comparison purposes.

Figures 35 and 37, below, show the ^{1}H NMR spectrum for the free m-tolunitrile ligand while Figures 36 and 38, below, show the ^{1}H NMR spectrum for the *trans*-2,2-[Rh$_2$(C$_6$H$_5$NCOCH$_3$)$_4$•m-tolunitrile] adduct.
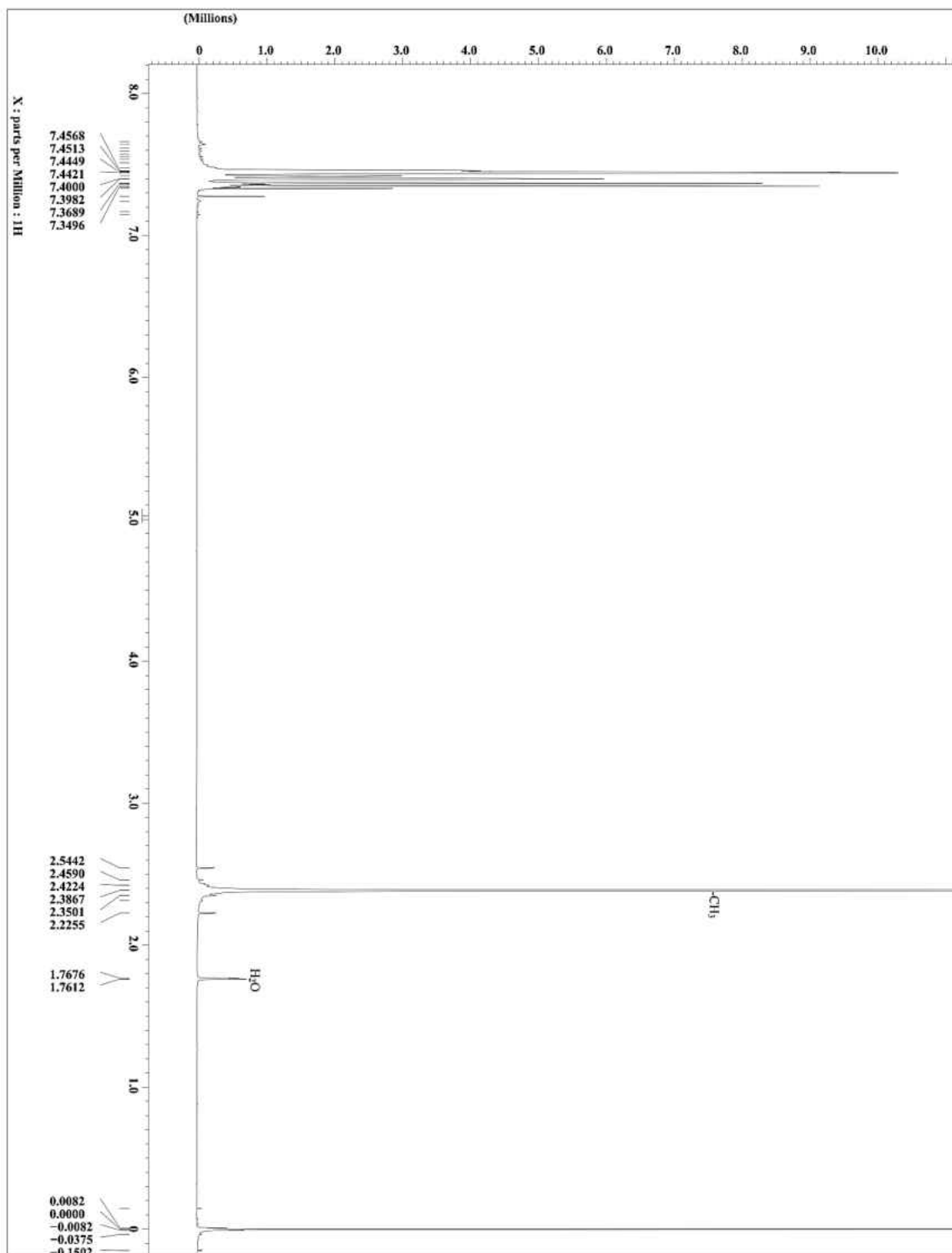
Figure 35. The ^{1}H NMR spectrum of m-tolunitrile.
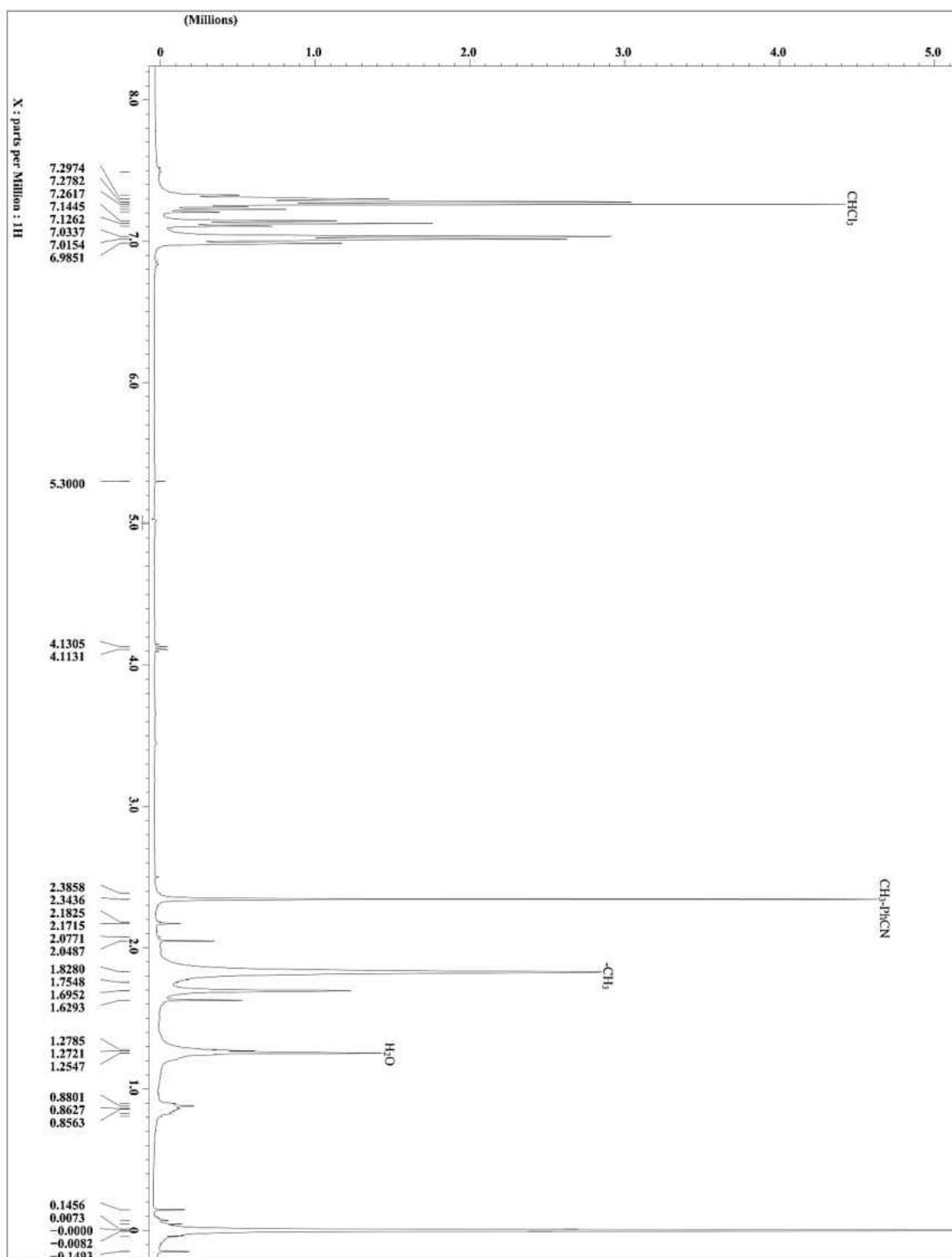
Figure 36. The ^{1}H NMR spectrum of *trans*-2,2-[Rh$_2$(C$_6$H$_5$NCOCH$_3$)$_4$·m-tolunitrile].
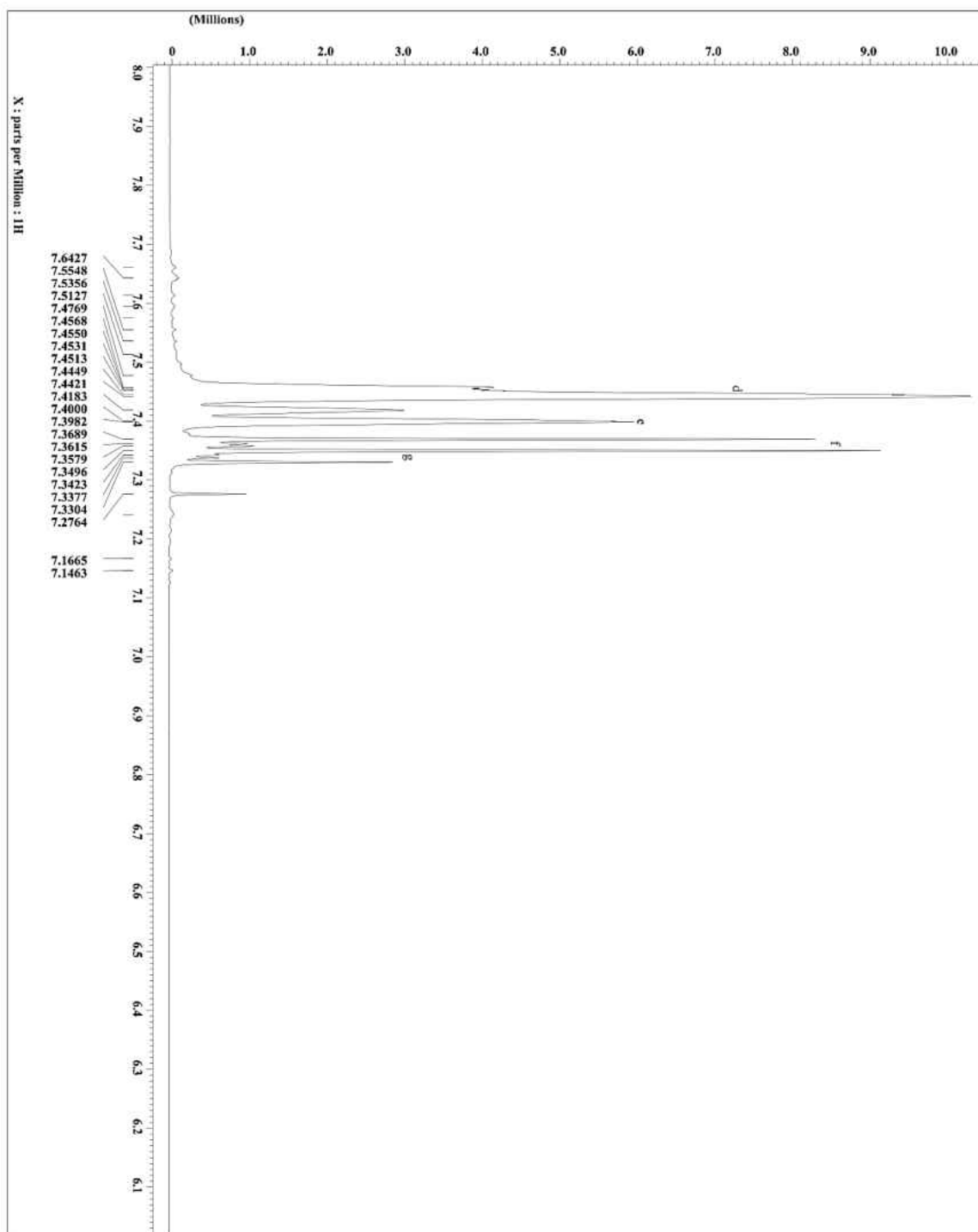
Figure 37. The ^{1}H NMR spectrum of m-tolunitrile showing the chemical shift region from 6.1 ppm to 8.0 ppm.
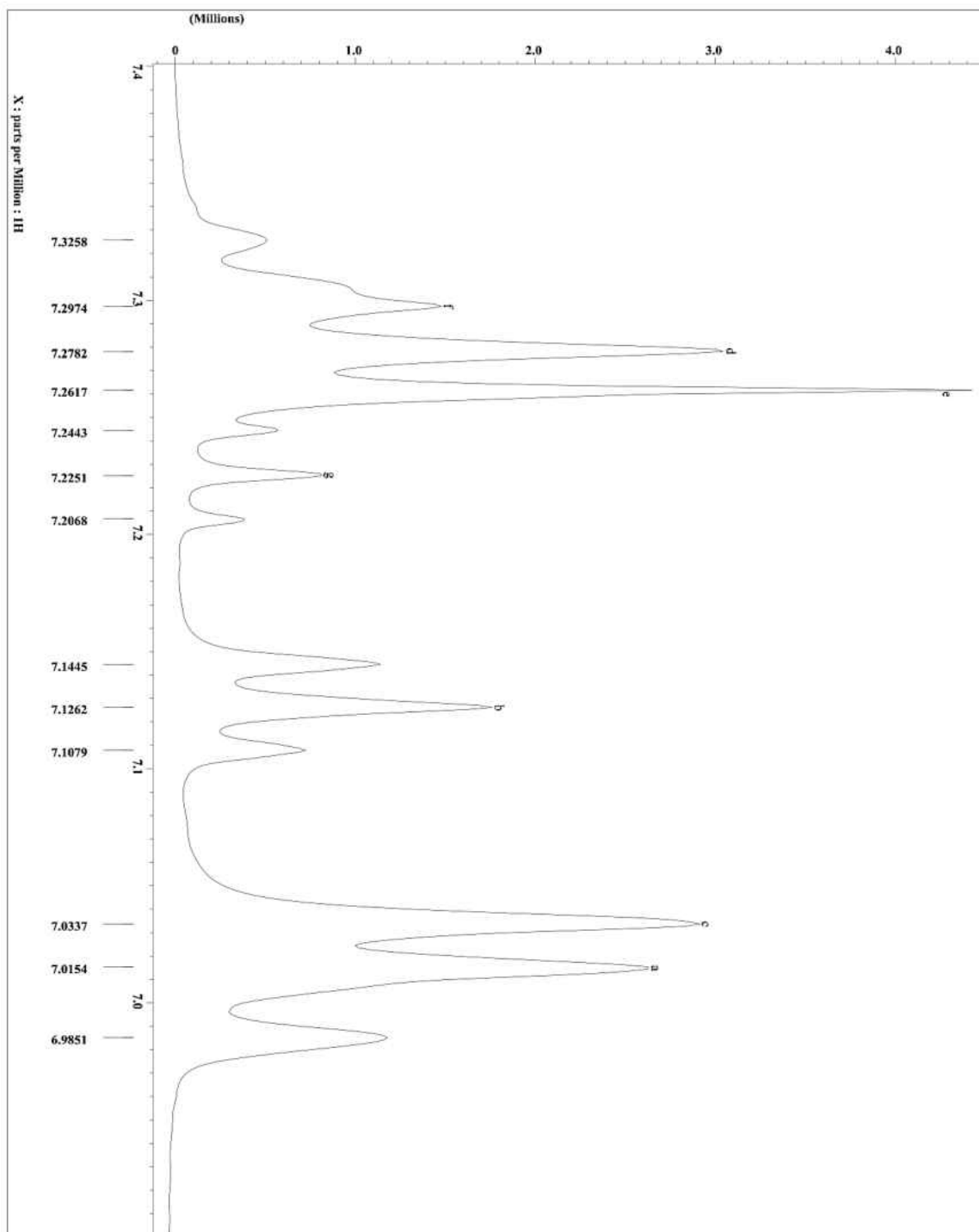
Figure 38. The ^{1}H NMR spectrum of *trans*-2,2-[Rh$_2$(C$_6$H$_5$NCOCH$_3$)$_4$·m-tolunitrile] showing the

chemical shift region from 6.9 ppm and 7.4 ppm.

3,1-tetrakis(N-phenylacetamido) dirhodium(II) – 1,3-dicyanobenzene. Prior to taking the

^{1}H NMR for the 3,1-[Rh$_2$(C$_6$H$_5$NCOCH$_3$)$_4$·1,3-dicyanobenzene] adduct, an initial NMR of the

CDCl$_3$ solvent was first taken in clean, dry NMR tubes to ensure that the tube was clean. These

spectra showed peaks as expected (TMS at 0 ppm and the CHCl$_3$ at 7.263 ppm). The CDCl$_3$

from these NMR tubes with known spectra was then used to dissolve a small amount of 3,1-

[Rh$_2$(C$_6$H$_5$NCOCH$_3$)$_4$·1,3-dicyanobenzene] (see Figure 57 for labeling). The NMR tube was

mounted on a JOEL AS400 FT-NMR spectrophotometer and the spectrum gotten by doing 300

scans.

The ^{1}H NMR spectrum for the free 1,3-dicyanobenzene (see Figure 56 for labeling)

ligand was also taken for comparison purposes.

Figures 39 and 41, below, show the ^{1}H NMR spectrum for the free 1,3-dicyanobenzene

ligand while Figures 40 and 42, below, show the ^{1}H NMR spectrum for the 3,1-

[Rh$_2$(C$_6$H$_5$NCOCH$_3$)$_4$·1,3-dicyanobenzene] adduct.
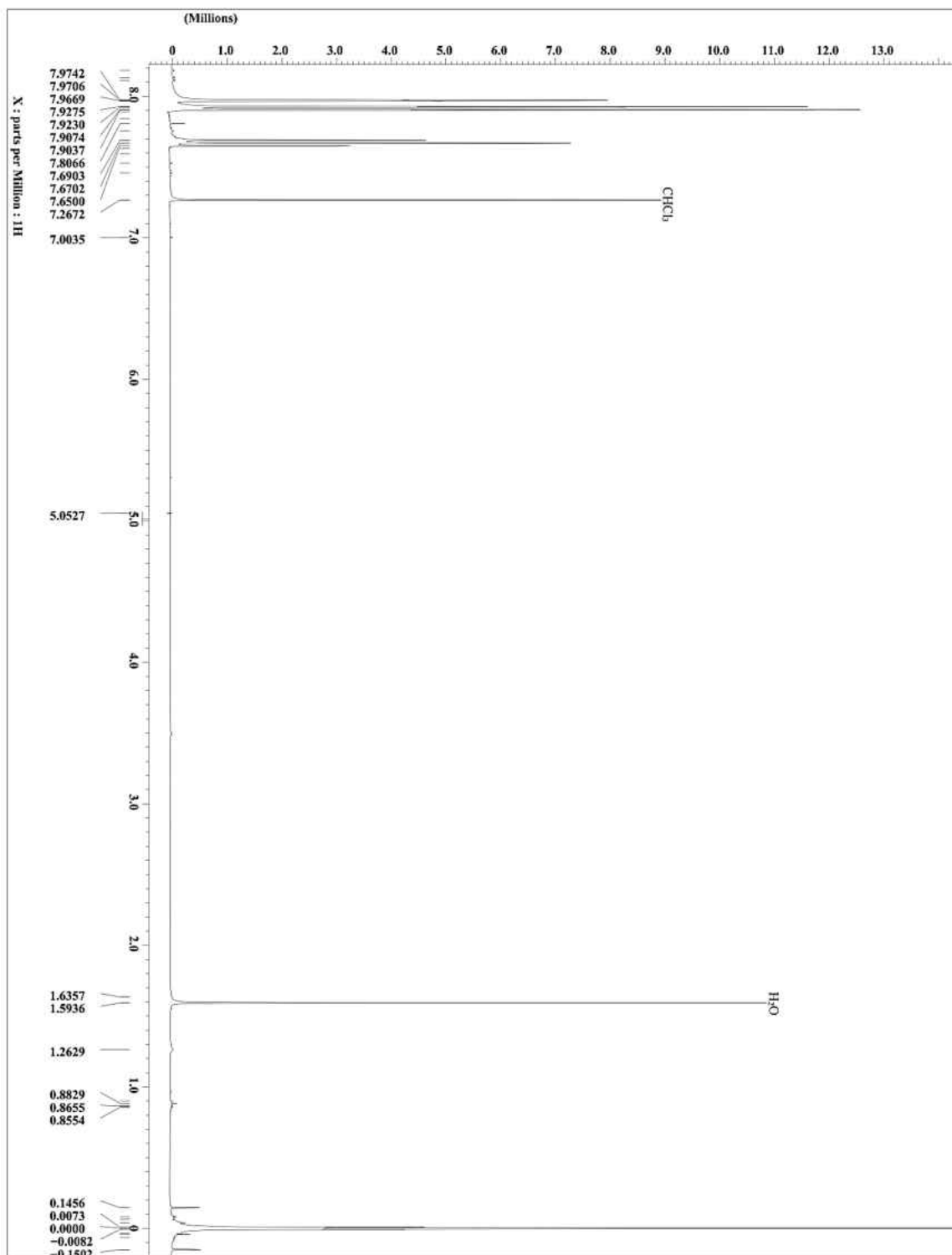
Figure 39. The ^{1}H NMR spectrum of 1,3-dicyanobenzene.
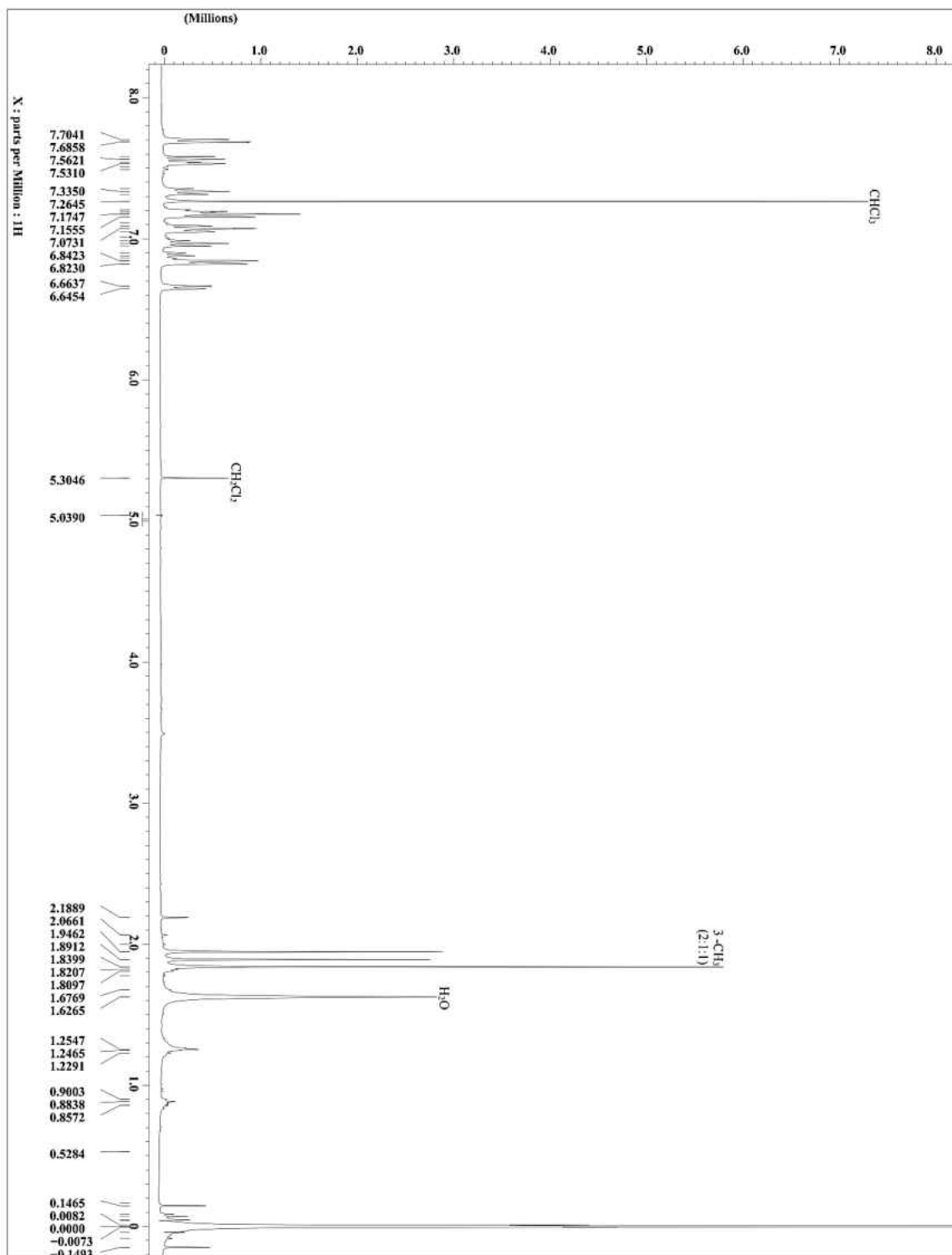
Figure 40. The ^{1}H NMR spectrum of 3,1-[$Rh_2(C_6H_5NCOCH_3)_4 \cdot 1,3$-dicyanobenzene].
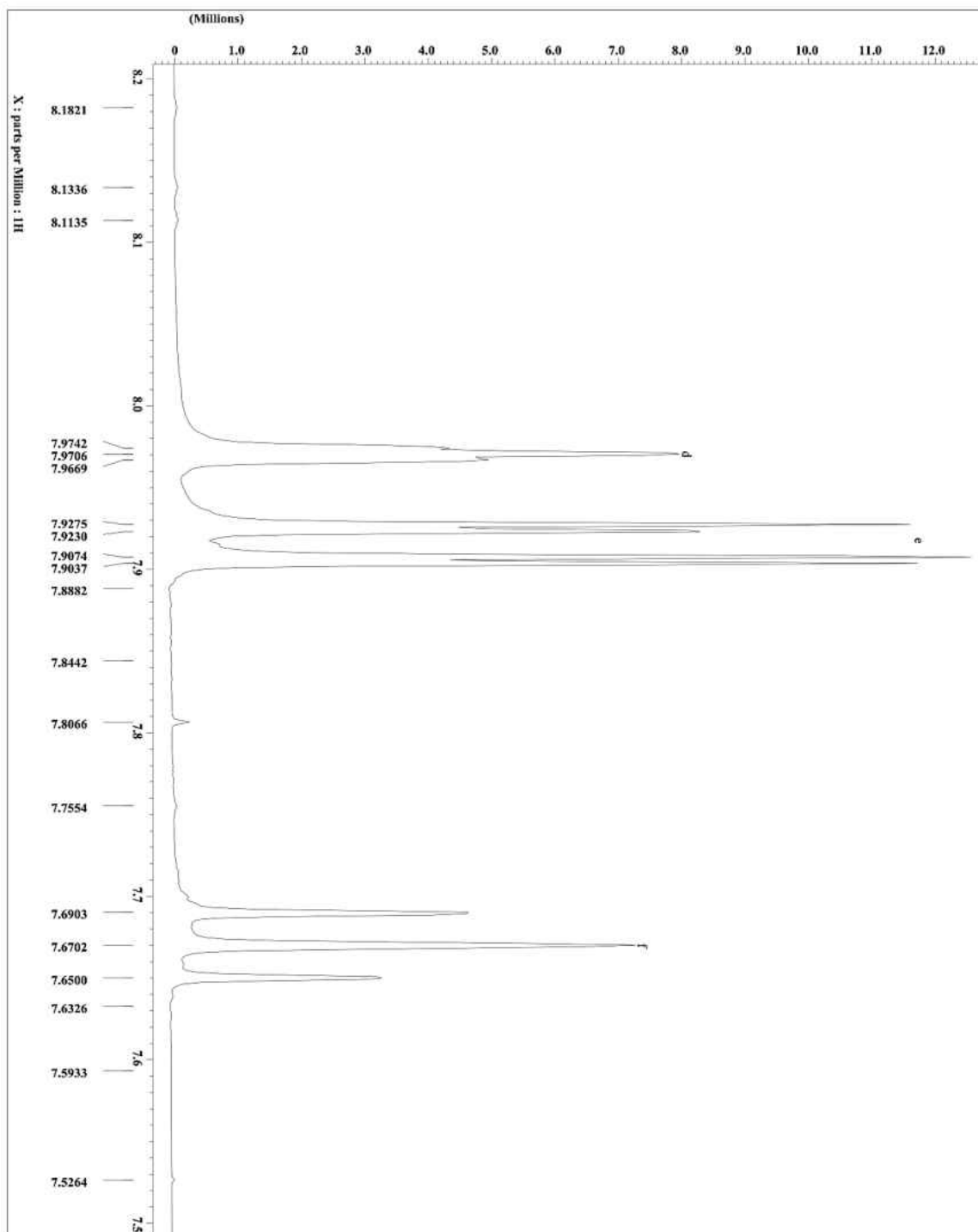
Figure 41. The ^{1}H NMR of 1,3-dicyanobenzene showing the chemical shift region from 7.5 ppm to 8.2 ppm.
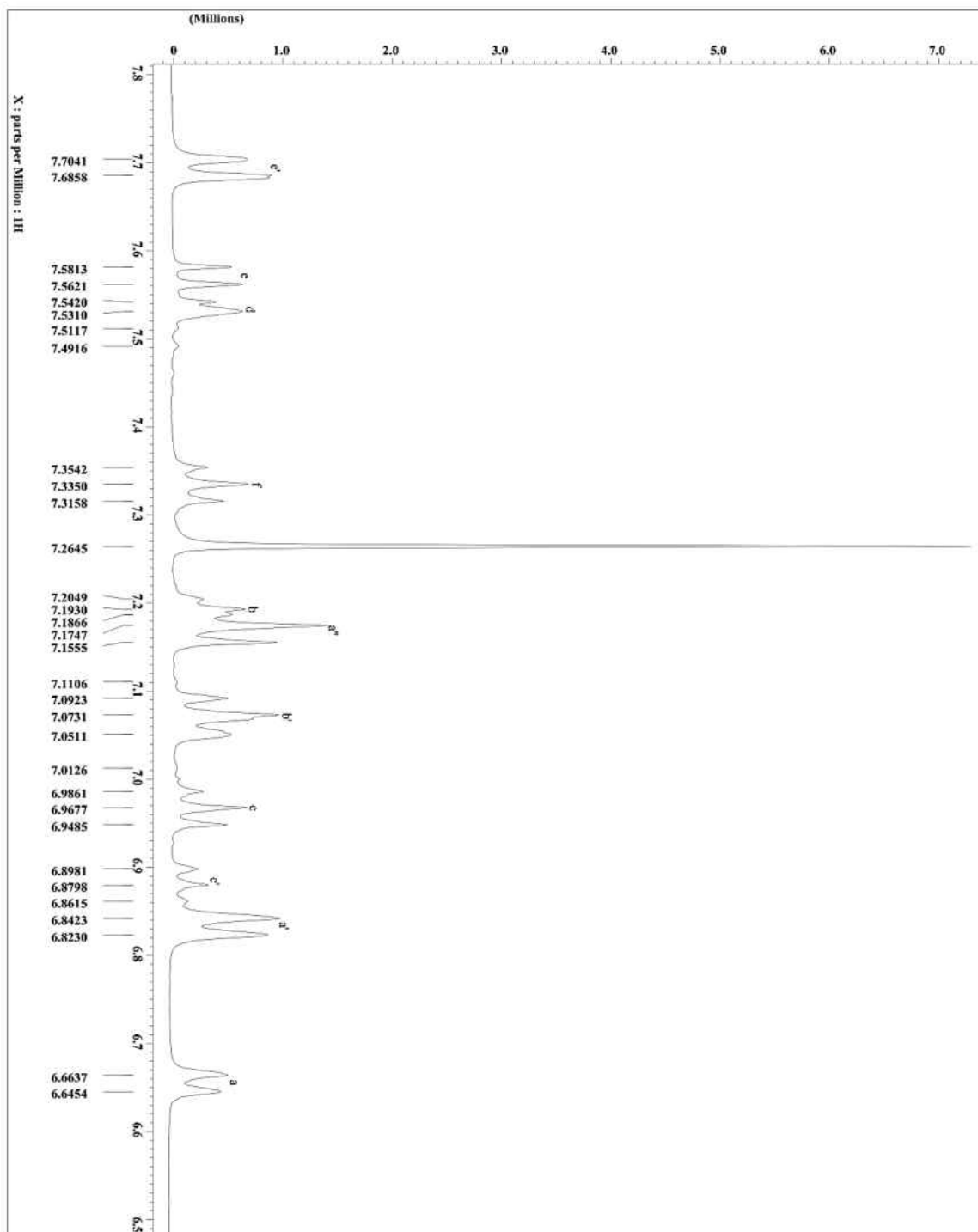
Figure 42. The ^{1}H NMR spectrum of 3,1-[Rh$_2$(C$_6$H$_5$NCOCH$_3$)$_4$·1,3-dicyanobenzene] showing

the chemical shift region from 6.5 ppm to 7.8 ppm.

, X-ray Crystallography

Trans-2,2-tetrakis(N-phenylacetamido) dirhodium(II) – Benzonitrile. A red block crystal

of *trans*-2,2-[$Rh_2(C_6H_5NCOCH_3)_4\cdot 2$benzonitrile] with dimensions of 0.140 x 0.110 x 0.080 mm

was mounted on a mitogen loop. Measurements were taken on a Rigaku XtaLAB mini-

diffractometer. The crystal-to-detector distance was 50.00 mm. The data were collected at a

temperature of 25 ± 1^0C to a maximum 2θ value of 55.0^0. A total of 540 oscillation images were

collected. Three sweeps of data were done using ω oscillations from -60.0 to 120.0^0 in 1.0^0 steps,

using an exposure rate of 30.0 [sec./^{0}]. The detector swing angle was 29.50^0.

Of the 23916 reflections that were collected, 9148 were unique ($R_{int} = 0.1361$);

equivalent reflections were merged. Data were collected and processed using CrystalClear[39]

(Rigaku). The data were corrected for Lorentz and polarization effects.

The structure was solved by direct methods[41] (SHELX97) and expanded using Fourier

techniques. The nonhydrogen atoms were refined anisotropically. Hydrogen atoms were refined

using the riding model. The final cycle of full-matrix least-squares[38] refinement on F^2 was based

on 9106 observed reflections and 527 variable parameters. The calculations were performed

using the CrystalStructure[40] crystallographic software package except for refinement, which was

performed using SHELXL-97.

Figure 43, below, shows the ORTEP of this complex at 30% probability. Hydrogen atoms

are also represented as very small spheres.
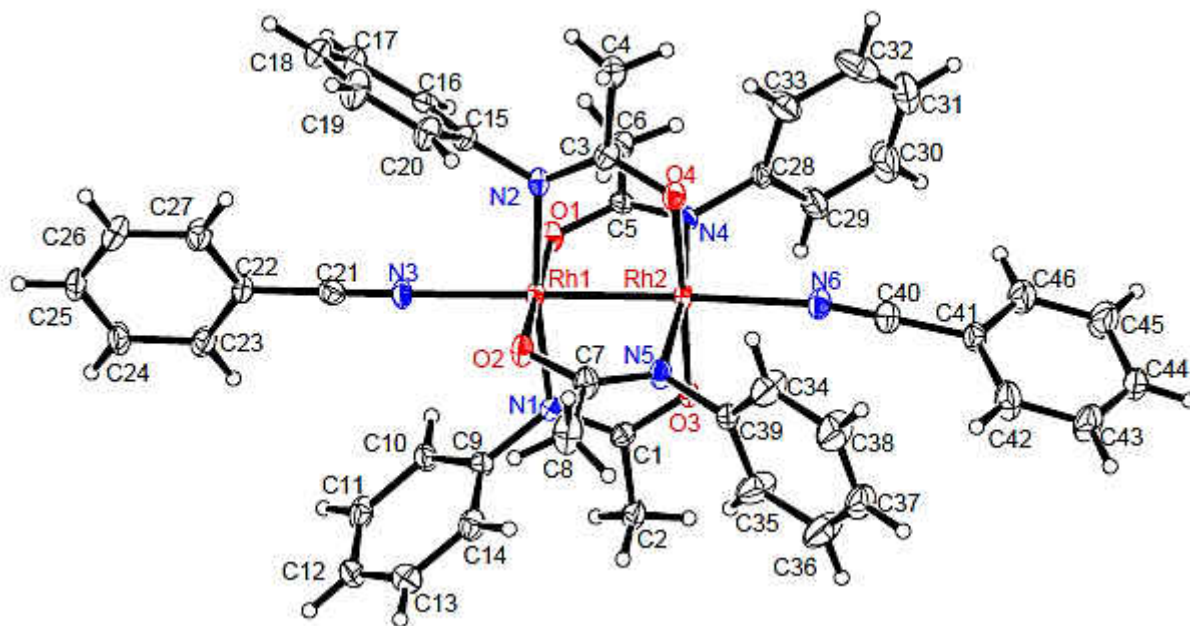
Figure 43. The ORTEP of *trans*-2,2-[$Rh_2(C_6H_5NCOCH_3)_4 \cdot 2$benzonitrile] showing 30% thermal ellipsoids and hydrogen atoms as very small spheres.

Some selected bond angles (Rh – N – C and N – Rh – Rh – O dihedral angles) and bond distances (Rh – Rh, C – N, and Rh – N$_{(ax)}$) for the above complex are shown in Table 3, below.

Table 3. Bond lengths and angles for *trans*-2,2-[Rh$_2$(C$_6$H$_5$NCOCH$_3$)$_4$·2benzonitrile]

Bond lengths	
Rh1 - Rh2	2.4207(8) Å
N3 - C21	1.156(8) Å
N6 - C40	1.130(8) Å
Rh1 - N3	2.199(5) Å
Rh2 - N6	2.238(5) Å
Bond angles	
Rh1 - N3 - C21	177.8(5) [0]
Rh2 - N6 - C40	169.1(6) [0]
Dihedral angles	
O1 - Rh1 -Rh2 - N4	10.84(12) [0]
N1 - Rh1 - Rh2 - O3	12.71(15) [0]
N2 - Rh1 - Rh2 - O4	9.50(14) [0]
N5 - Rh1 - Rh2 - O2	11.26(13) [0]

Trans-2,2-tetrakis-(N-phenylacetamido) dirhodium(II) – 2-methyl benzonitrile. A red long block crystal of tetrakis 2,2-*trans*-[$Rh_2(C_6H_5NCOCH_3)_4 \cdot 2$o-tolunitrile] with dimensions of 0.330 x 0.120 x 0.120 mm was mounted on a mitogen loop. Measurements were taken on a Rigaku XtaLAB mini diffractometer. The crystal-to-detector distance was 50.00 mm. The data were collected at a temperature of 25 ± 1^0C to a maximum 2θ value of 55.0^0. A total of 540 oscillation images were collected. A sweep of data was done using ω oscillations from -60.0 to 120.0^0 in 1.0^0 steps, using an exposure rate of 16.0 [sec./^{0}]. The detector swing angle was 29.50^0.

Of the 23557 reflections that were collected, 10150 were unique ($R_{int} = 0.0386$); equivalent reflections were merged. Data were collected and processed using CrystalClear[39] (Rigaku). The data were corrected for Lorentz and polarization effects.

The structure was solved by direct methods[41] (SHELX97) and expanded using Fourier techniques. The nonhydrogen atoms were refined anisotropically. Hydrogen atoms were refined using the riding model. The final cycle of full-matrix least-squares[42] refinement on F^2 was based on 10137 observed reflections and 547 variable parameters. The calculations were performed using the CrystalStructure[40] crystallographic software package except for refinement, which was performed using SHELXL-97.

Figure 44, below, shows the ORTEP of this complex at 30% probability. Hydrogen atoms are also represented as very small spheres.
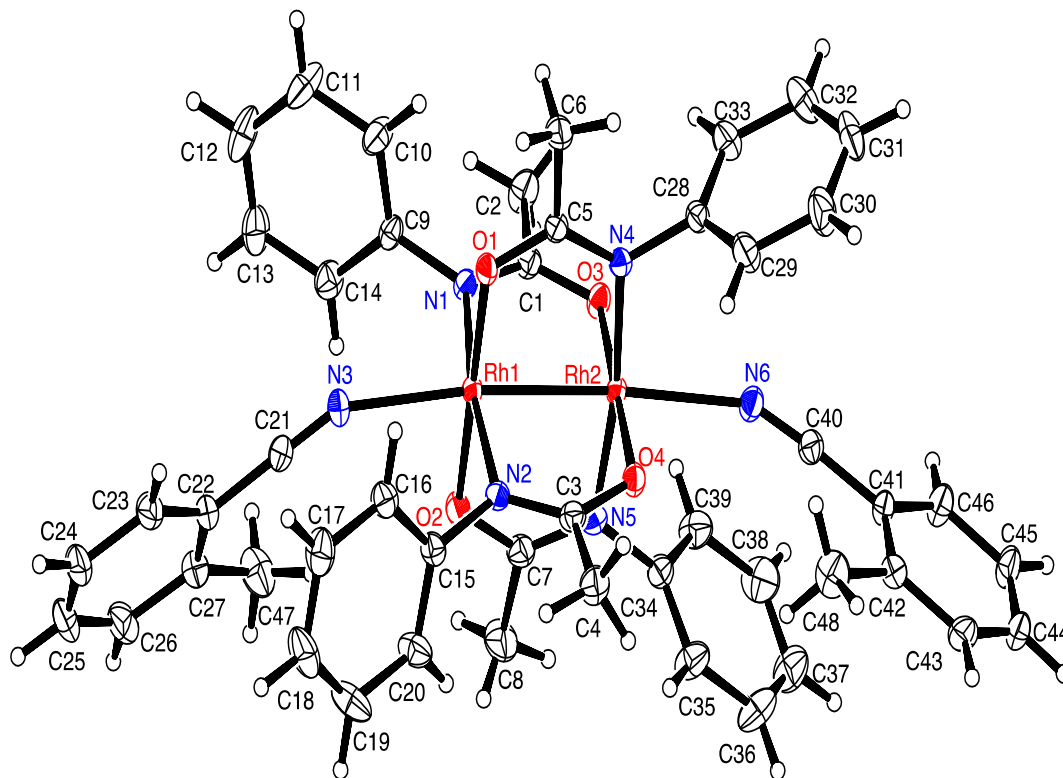
Figure 44. The ORTEP of *trans*-2,2-[$Rh_2(C_6H_5NCOCH_3)_4 \cdot 2$o-tolunitrile] showing 30% thermal ellipsoids and hydrogen atoms as very small spheres.

Some selected bond angles (Rh – N – C and N – Rh – Rh – O dihedral angles) and bond distances (Rh – Rh, C – N, and Rh – N$_{(ax)}$) for the above complex are shown in Table 4, below.

Table 4. Bond lengths and angles for *trans*-2,2-[Rh$_2$(C$_6$H$_5$NCOCH$_3$)$_4$·2o-tolunitrile]

Bond lengths	
Rh1 - Rh2	2.4241(4) Å
N3 - C21	1.133(5) Å
N6 - C40	1.137(5) Å
Rh1 - N3	2.236(3) Å
Rh2 - N6	2.254(3) Å
Bond angles	
Rh1 - N3 - C21	151.6(3) [0]
Rh2 - N6 - C40	1152.5(3) [0]
Dihedral angles	
O1 - Rh1 -Rh2 - N4	4.07(5) [0]
N1 - Rh1 - Rh2 - O3	6.78(7) [0]
N2 - Rh1 - Rh2 - O4	6.82(7) [0]
N5 - Rh1 - Rh2 - O2	4.79(5) [0]

Trans-2,2-tetrakis(N-phenylacetamido) dirhodium(II) – 3-methyl benzonitrile. A blue

block crystal of tetrakis *trans*-2,2-[$Rh_2(C_6H_5NCOCH_3)_4$·m-tolunitrile] with dimensions of 0.160

x 0.080 x 0.070 mm was mounted on a mitogen loop. Measurements were taken on a Rigaku

XtaLAB mini diffractometer. The crystal-to-detector distance was 50.00 mm. The data were

collected at a temperature of 25 ± 1^0C to a maximum 2θ value of 55.0^0. A total of 540 oscillation

images were collected. Three sweeps of data were done using ω oscillations from -60.0 to 120.0^0

in 1.0^0 steps, using an exposure rate of 30.0 [sec./^{0}]. The detector swing angle was 29.50^0.

Of the 18454 reflections that were collected, 8159 were unique ($R_{int} = 0.0646$);

equivalent reflections were merged. The data were collected and processed using CrystalClear[39]

(Rigaku). The data were corrected for Lorentz and polarization effects.

The structure was solved by direct methods[41] (SHELX97) and expanded using Fourier

techniques. The nonhydrogen atoms were refined anisotropically. Hydrogen atoms were refined

using the riding model. The final cycle of full-matrix least-squares[42] refinement on F^2 was based

on 8152 observed reflections and 465 variable parameters. The calculations were performed

using the CrystalStructure[40] crystallographic software package except for refinement, which was

performed using SHELXL-97.

Figure 45, below, shows the ORTEP of this complex at 30% probability. Hydrogen atoms

are also represented as very small spheres.
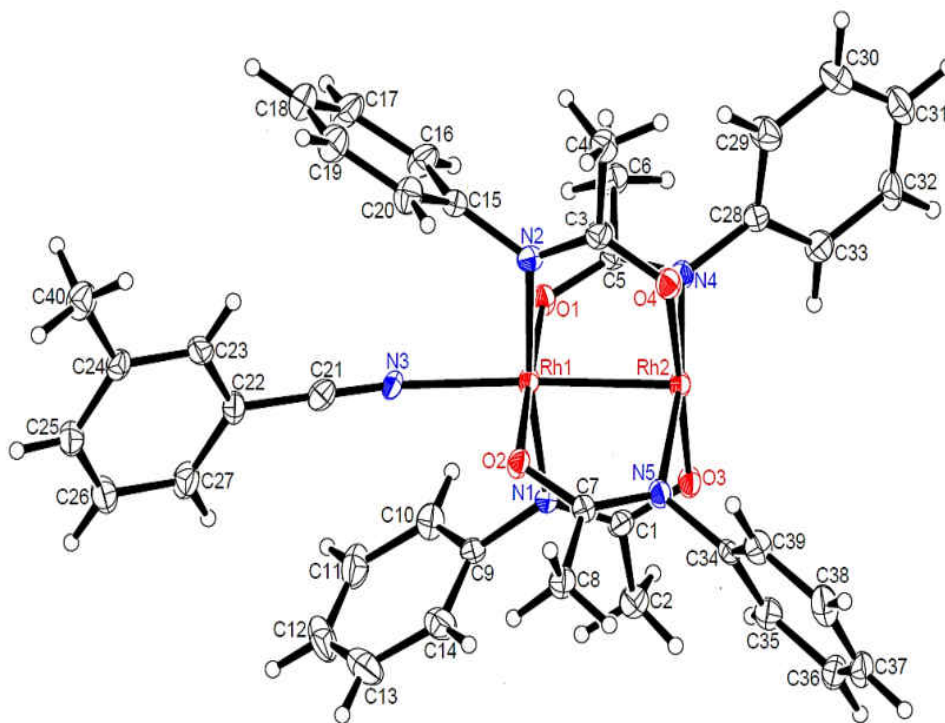
Figure 45. The ORTEP of *trans*-2,2-[Rh$_2$(C$_6$H$_5$NCOCH$_3$)$_4$·m-tolunitrile] showing 30% thermal ellipsoids and hydrogen atoms as small spheres.

Some selected bond angles (Rh – N – C and N – Rh – Rh – O dihedral angles) and bond distances (Rh – Rh, C – N, and Rh – N$_{(ax)}$) for the above complex are shown in Table 5, below.

Table 5. Bond lengths and angles for *trans*-2,2-[Rh$_2$(C$_6$H$_5$NCOCH$_3$)$_4$·m-tolunitrile]

Bond lengths	
Rh1 - Rh2	2.4039(7) Å
N3 - C21	1.140(8) Å
N6 - C40	-
Rh1 - N3	2.160(5) Å
Rh2 - N6	-
Bond angles	
Rh1 - N3 - C21	166.3(4) ^{0}
Rh2 - N6 - C40	-
Dihedral angles	
O1 - Rh1 -Rh2 - N4	14.04(8) ^{0}
N1 - Rh1 - Rh2 - O3	12.55(11) ^{0}
N2 - Rh1 - Rh2 - O4	12.69(11) ^{0}
N5 - Rh1 - Rh2 - O2	13.28(8) ^{0}

3,1-tetrakis(N-phenylacetamido) dirhodium(II) – 1,3-dicyanobenzene. A purple block crystal of the 3,1-[$Rh_2(C_6H_5NCOCH_3)_4$·1,3-dicyanobenzene] with dimensions of 0.21 x 0.18 x 0.11 mm was mounted on a mitogen loop. Measurements were taken on a Rigaku Mercury375R/M CCD (XtaLAB mini) diffractometer. The crystal-to-detector distance was 50.00 mm. The data were collected at a temperature of 25 ± 1^0C to a maximum 2θ value of 55.0^0. A total of 540 oscillation images were collected. Three sweeps of data was done using ω scans from -60.0 to 120.0^0 in 1.0^0 steps, using an exposure rate of 20.0 [sec./^{0}]. The detector swing angle was 29.50^0.

Of the 21660 reflections that were collected, 9390 were unique ($R_{int} = 0.0458$); equivalent reflections were merged. Data were collected and processed using CrystalClear (Rigaku). The data were corrected for Lorentz and polarization effects.

The structure was solved by direct methods and expanded using Fourier techniques. The non hydrogen atoms were refined anisotropically. Hydrogen atoms were refined using the riding model. The final cycle of full-matrix least-squares[42] refinement on F^2 was based on 14070 observed reflections and 500 variable parameters. Calculations were performed using the CrystalStructure crystallographic software package except for refinement, which was performed using SHELXL-97.

Figure 46, below, shows the ORTEP of this complex at 30% probability. Hydrogen atoms are omitted for clarity.
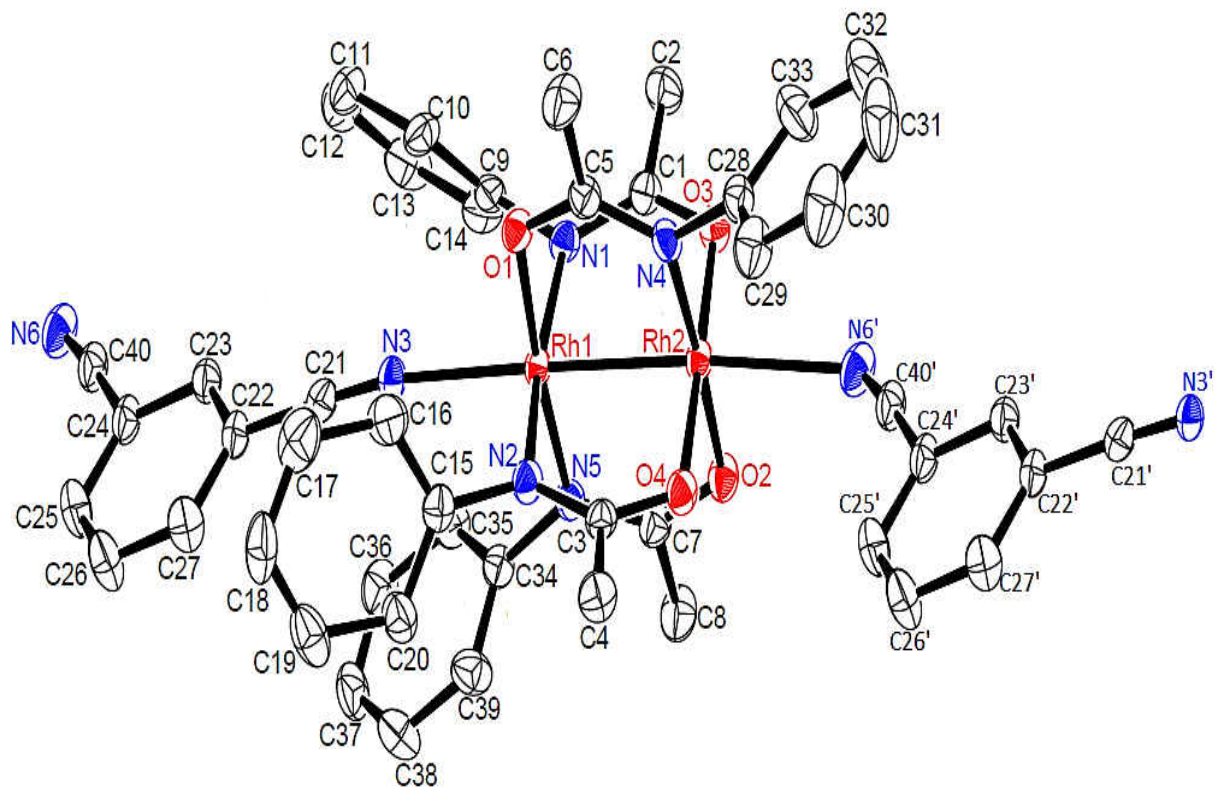
Figure 46. The ORTEP of 3,1-[Rh$_2$(C$_6$H$_5$NCOCH$_3$)$_4$·1,3-dicyanobenzene] showing 30% thermal ellipsoids and hydrogen atoms not shown.

Some selected bond angles (Rh – N – C and N – Rh – Rh – O dihedral angles) and bond distances (Rh – Rh, C – N, and Rh – N$_{(ax)}$) for the above complex are shown in Table 6, below.

Table 6. Bond lengths and angles for 3,1-[Rh$_2$(C$_6$H$_5$NCOCH$_3$)$_4$·1,3-dicyanobenzene]

Bond lengths	
Rh1 - Rh2	2.4146(5) Å
N3 - C21	1.132(6) Å
N6 - C40	1.129(8) Å
Rh1 - N3	2.182(3) Å
Rh2 - N6	2.380(4) Å
Bond angles	
Rh1 - N3 - C21	166.8(3) [0]
Rh2 - N6 - C40	127.7(3) [0]
Dihedral angles	
O1 - Rh1 -Rh2 - N4	6.73(8) [0]
N1 - Rh1 - Rh2 - O3	4.31(8) [0]
N2 - Rh1 - Rh2 - O4	8.47(9) [0]
N5 - Rh1 - Rh2 - O2	6.99(10) [0]

CHAPTER 3

DISCUSSION

The purpose of this research was to understand the relationship between the metal –

carbene bond and the rhodium – nitrile bond. Various nitriles were used to model this metal –

carbene bond because they have the capability of doing σ-bonding and π-back bonding. Studies

were carried out on the 3,1-tetrakis(N-phenylacetamidato) dirhodium(II) and the *trans*-2,2-

tetrakis(N-phenylacetamidato) dirhodium(II) isomers using 1,3-dicyanobenzene, benzonitrile, o-

tolunitrile, m-tolunitrile as axial nitrile ligands. These compounds were synthesized and

characterized by ^{1}H NMR spectroscopy, IR spectroscopy, and X-crystallography. The reason for

doing these studies was to acquire structural knowledge of these dirhodium compounds.

Synthesis of Tetrakis(N-phenylacetamidato) Dirhodium(II)

This synthesis involved the exchange of the equatorial acetate bridging ligands of the

tetrakis(acetato) dirhodium(II), $Rh_2(CH_3CO_2)_4$ with the N-phenylacetamide, $HNPhCOCH_3$. The

mechanism for the ligand exchange is similar to that in Scheme 1 and Equations 3 – 6. The

synthesis was carried out in chlorobenzene (PhCl) solvent because PhCl forms an azeotropic

mixture with acetic acid, CH_3COOH, produced from the ligand exchange. The azeotrope distills

at 128 ^{0}C, which is between the boiling points of PhCl and CH_3COOH, which are 132 ^{0}C and

118 ^{0}C, respectively. The CH_3COOH produced distilled with PhCl as the azeotrope into the

soxhlet extractor and drained into the thimble containing a mixture of sand and Na_2CO_3. The

CH_3COOH is then trapped by the Na_2CO_3 in the thimble.

$$2CH_3COOH + Na_2CO_3 \rightarrow 2CH_3COO^-Na^+ + CO_2 + H_2O \qquad (13)$$

Theoretically, there are 14 possible compounds that can result from this synthesis. However, we isolated only 3 of them (2,2-cis, 2,2-trans, and 3,1- isomers). The tetrakis 4,0- isomer was not isolated in this synthesis. The tetrakis 4,0- isomer along with all other possible byproducts were eluted from the MPLC column and labeled Fraction IV.

Organic impurities and decomposed rhodium material that resulted from this synthesis were removed during the MPLC column separation. The desired isomers that were in the first 3 colored bands were eluted using mixtures of ethylacetate and hexane. The fourth band and rest of the column was eluted with methanol and ethylacetate mixture. The more polar isomers were adsorbed unto the surface of the silica gel (stationary phase). The polarity of the eluent (mobile phase) was increased in order to remove the other fractions. Therefore, the polarity of each isomer increased from band to band. TLC suggested that each band contained one $Rh_2(C_6H_5NCOCH_3)_4$ fraction. The TLC for fraction II showed an excess of N-phenylacetamide that was further removed by sublimation.

Characterization of the Various Isomers by ^1H NMR

When the ^1H NMR of tetrakis(N-phenylacetamide) dirhodium(II) is carried out, the various protons tend to be in chemically different environments. The methyl protons on the acetamide bridge are of higher energy and appear upfield. The protons on the phenyl ring are of lower energy and appear downfield. Resonance effects can be used to explain which protons are more shielded and hence appear at high energy, upfield. Scheme 3, below, shows resonance on the phenyl rings of the acetamide bridge.
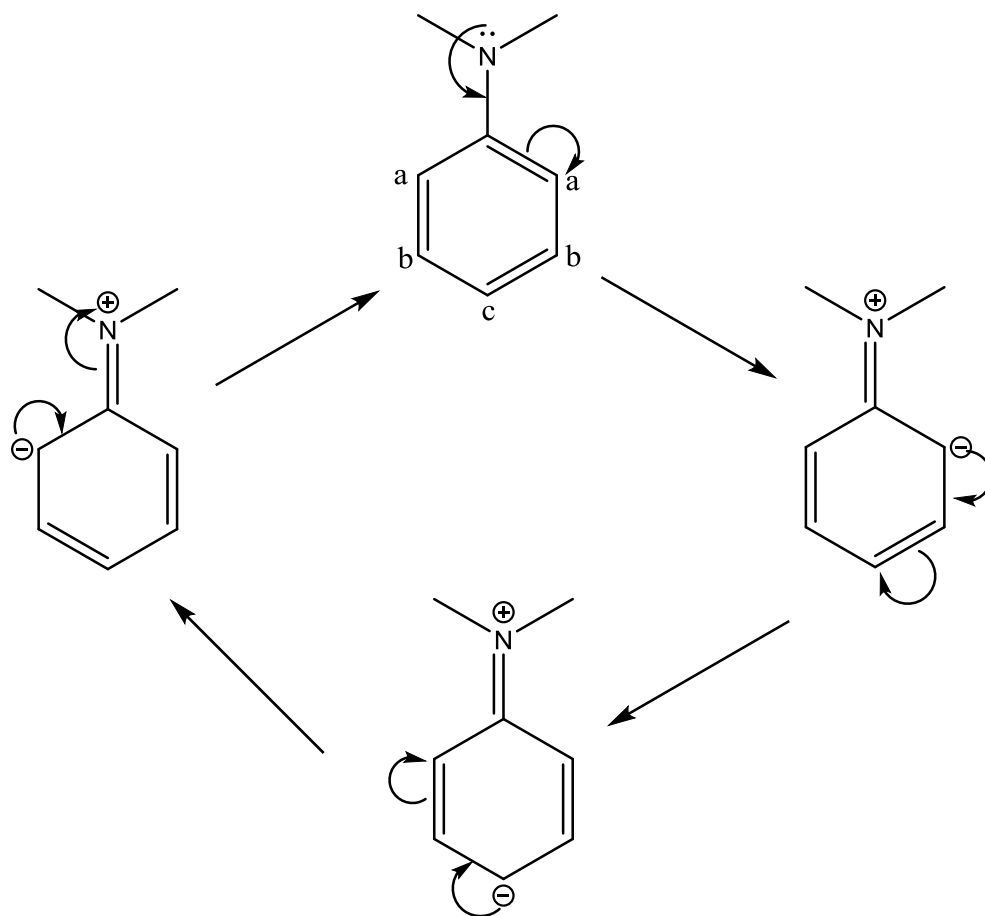
Scheme 3. The resonance of the benzene ring on N-phenylacetamide bridge

Protons 'b' (meta position) are the most deshielded, are low energy, and thus appear furthest downfield on the ^{1}H NMR spectrum. Protons 'a' and 'c' are shielded and high energy. They appear upfield on the spectrum. However, due to the inductive effect of the heteroatom (Nitrogen) on the electron density of the ring, protons 'a' are more shielded than protons 'c' and thus appear slightly upfield when compared to position 'c'.

It is expected that the protons 'a' be split by the coupling with the protons 'b' giving rise to a doublet. The protons 'b' will be split by coupling with the protons 'a' and 'c' giving rise to a triplet. The 'c' protons will be split by coupling with the protons 'b' giving rise to a triplet.

The ratio of the peaks a:b:c should be approximately 2:2:1.

Fraction I – trans-2,2-tetrakis(N-phenylacetamido) dirhodium(II)

Analysis of Fraction I suggests that Fraction I was the isomer with 2 nitrogen atoms bound on each rhodium atom (see Figure 47). On any one Rh atom, the 2 N atoms were *trans* (on opposite sides) to one another. All phenyl protons are in the same environment for each N-phenylacetamide equatorial ligand considered. The protons on any one ring are chemically different and are labeled a, b, and c in Figure 47.
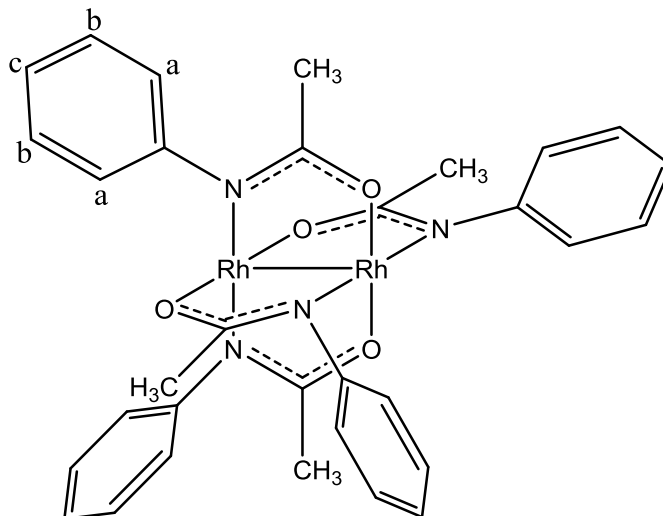
Figure 47. A *trans*-2,2-[Rh$_2$(C$_6$H$_5$NCOCH$_3$)$_4$] showing the various types of Hydrogen atoms for Figures 13 and 14 that show the ^{1}H NMR for the above compound.

Tables 7 and 8, below, show the peaks of interest in the ^{1}H NMR spectra of the *trans*-2,2-[Rh$_2$(C$_6$H$_5$NCOCH$_3$)$_4$] that are presented in Figures 13 and 14.

Table 7. The ^{1}H NMR peaks for *trans*-2,2-[Rh$_2$(C$_6$H$_5$NCOCH$_3$)$_4$] from Figure 13

Chemical shift (ppm)	Peak type	Proton type
1.600	Singlet	H$_2$O
1.859	Singlet	Methyl
7.269	Singlet	CHCl$_3$
7.011 – 7.288	Complex	Phenyl

The peaks a, b, and c at 7.011 ppm, 7.288 ppm and 7.138 ppm respectively correspond to the chemical shifts of the protons on the phenyl rings of the N-phenylacetamide and appear further downfield as expected. The peak at 7.269 ppm represents the chemical shift of the H atom from the trace amount CHCl$_3$ in the CDCl$_3$ used as NMR solvent. The singlet at 1.600 ppm corresponds to the chemical shift of the protons from H$_2$O in the NMR solvent. The singlet at 1.859 ppm corresponds to the chemical shift of the methyl protons on the *trans*-2,2-[Rh$_2$(C$_6$H$_5$NCOCH$_3$)$_4$].

Table 8. The ^{1}H NMR peaks for phenyl protons on *trans*-2,2-[Rh$_2$(C$_6$H$_5$NCOCH$_3$)$_4$] from Figure 14

Chemical shift (ppm)	Peak type	Proton type
7.011	Doublet	a
7.138	Triplet	c
7.269	Singlet	CHCl$_3$
7.288	Triplet	b

The triplet at 7.288 ppm corresponds to the chemical shift of the b-protons split by the effect of the a- and c-protons. These protons are most deshielded from the effects of the heteroatom and thus show up furthest downfield. The triplet at 7.138 ppm corresponds to the chemical shift of the c-proton. This proton is fairly shielded by the effects of the heteroatom and is split by the effect of the 2 b-protons. The most shielded set of protons are the a-protons. They show up more upfield than the previous set of atoms. They correspond to the doublet at 7.011 ppm and are split by the effects of the b-protons.

Fraction II – cis-2,2-tetrakis(N-phenylacetamido) dirhodium(II)

Analysis of Fraction II suggests that Fraction II was the isomer with 2 nitrogen atoms per rhodium atom. However, on any one Rh atom, the 2 N atoms were *cis* (about 90^0) to one another (see Figure 48). All phenyl protons are in the same environment for each N-phenylacetamide equatorial ligand considered. The protons on any one ring are chemically different and are labeled a, b, and c as shown in Figure 48.
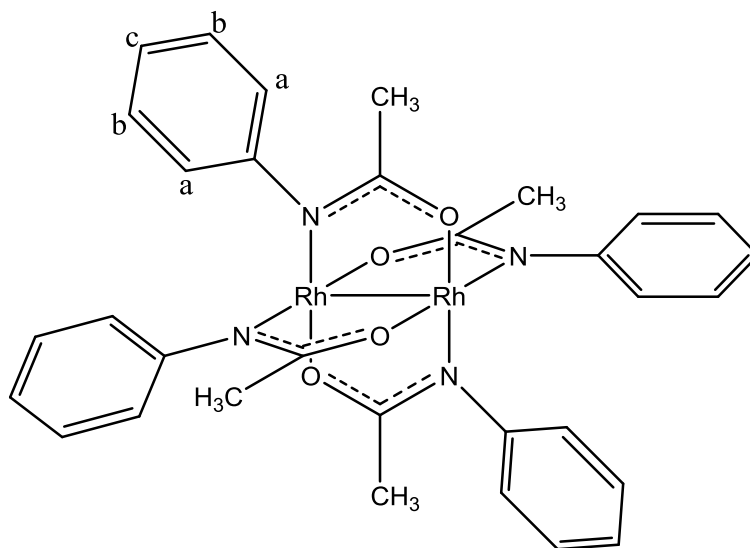
Figure 48. A *cis*-2,2-[Rh₂(C₆H₅NCOCH₃)₄] showing the various types of Hydrogen atoms for Figures 15 and 16 that show the ^{1}H NMR for the above compound.

Tables 9 and 10, below, show the peaks of interest in the ^{1}H NMR spectra of the *cis*-2,2-[Rh₂(C₆H₅NCOCH₃)₄] that are presented in Figures 15 and 16.

Table 9. The ^{1}H NMR peaks for *cis*-2,2-[Rh₂(C₆H₅NCOCH₃)₄] from Figure 15

Chemical shift (ppm)	Peak type	Proton type
1.752	Singlet	H_2O
1.885	Singlet	Methyl
2.032	Complex	Hexane
7.263	Singlet	$CHCl_3$

The peak at 7.263 ppm corresponds to the chemical shift of the $CHCl_3$ in the $CDCl_3$ solvent. The peaks a, b, and c correspond to the chemical shifts of the protons on the phenyl rings of the N-phenylacetamide bridge. The peak at about 2.032 ppm correspond to the protons

of the hexane left over in the sample from the MPLC column, while the peak at 1.752 ppm corresponds to traces of H_2O contained in the NMR solvent. The singlet at 1.885 ppm corresponds to the methyl protons on the N-phenylacetamide bridge.

Table 10. The ^1H NMR peaks for phenyl protons on *cis*-2,2-[Rh$_2$(C$_6$H$_5$NCOCH$_3$)$_4$] from Figure 16

Chemical shift (ppm)	Peak type	Proton type
6.946	Doublet	a
7.113	Triplet	c
7.221	Triplet	b
7.263	Singlet	CHCl$_3$

The triplet at 7.221 ppm corresponds to the chemical shift of the b-protons split by the a- and c- protons. These protons appear furthest downfield as they are the most deshielded from the effects of the heteroatom. The triplet at 7.113 ppm corresponds to the c-proton and is split by the effects of the 2 b-protons. The doublet at 6.946 ppm is most shielded by the effects of the heteroatom and corresponds to a- protons.

Fraction III – 3,1-tetrakis(N-phenylacetamido) dirhodium(II)

Analysis of Fraction III suggests that Fraction III was the isomer with 3 nitrogen atoms attached to 1 rhodium atom, 1 nitrogen atom attached to the other nitrogen atom (see Figure 49). The environments around the 2 phenyl rings trans to one another (on the same Rh atom) but cis to the other phenyl ring on the other Rh atom are in the same chemical environment. However,

the third phenyl ring with protons labeled a" is trans to the phenyl ring on the other Rh atom.

Thus, the chemical environment of these protons is slightly different.
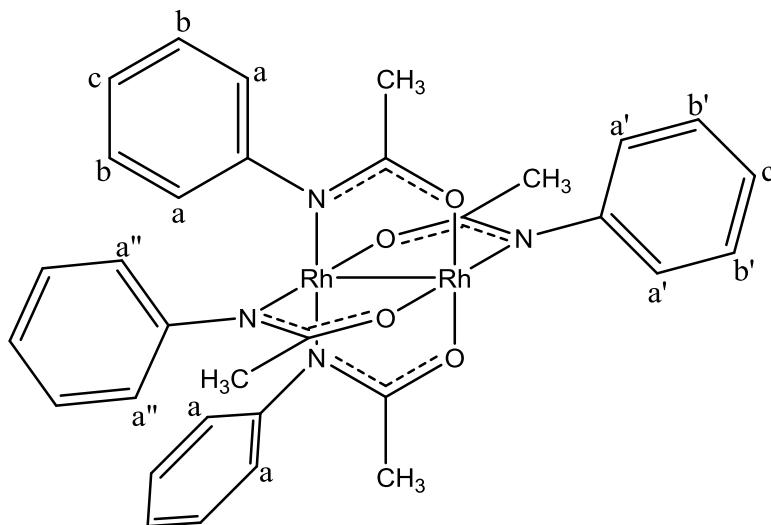
Figure 49. A 3,1-[$Rh_2(C_6H_5NCOCH_3)_4$] showing the various types of Hydrogen atoms for Figures 17 and 18 that show the ^{1}H NMR for the compound above.

Tables 11 and 12, below, show the peaks of interest in the ^{1}H NMR spectra of the 3,1-[$Rh_2(C_6H_5NCOCH_3)_4$] that are presented in Figures 17 and 18.

Table 11. The ^{1}H NMR peaks of 3,1-[$Rh_2(C_6H_5NCOCH_3)_4$] from Figure 17

Chemical shift (ppm)	Peak type	Proton type
1.270	Multiplet	Hexane
1.849	Singlet	Methyl
1.884	Singlet	Methyl
2.030	Singlet	Methyl
2.336	Singlet	Ethylacetate

113

Corrections for the peak positions were done for this spectrum because TMS was not referenced to 0 ppm. 0.0087 units were added to all peak values. The peak at 7.263 ppm corresponds to the chemical shift of $CHCl_3$ in the $CDCl_3$ NMR solvent. The singlets at 1.849 ppm, 1.884 ppm, and 2.030 ppm, in the ratio 2:1:1, correspond to the chemical shift of the methyl protons on the acetamide bridges. The peak at 2.336 ppm and multiplet at 1.27 ppm correspond to the chemical shifts of the ethylacetate and hexane solvents that may have been still contained in the sample.

Table 12. The ^{1}H NMR peaks for phenyl protons on 3,1-[$Rh_2(C_6H_5NCOCH_3)_4$] from Figure 18

Chemical shift (ppm)	Peak type	Proton type
6.505	Doublet	a'
6.660	Doublet	a"
7.028	Doublet	a
7.070	Triplet	c'
7.149	Triplet	c
7.240	Triplet	b'
7.263	Singlet	$CHCl_3$
7.367	Triplet	b

The doublet around 6.505 ppm corresponds to the chemical shift of the a'- protons split by b'-protons. The doublet at 6.660 ppm corresponds to the chemical shift of the a"-protons split by the effects of one neighbor. The triplet 7.367 ppm corresponds to the chemical shift of the b-

protons and is split by the effects of a- and c-protons. The triplet at 7.240 ppm overlaps with the CHCl$_3$ peak at 7.263 ppm. This peak corresponds to the chemical shift of the b'-protons split by the effects of a'- and c'-protons. The triplet at 7.149 ppm corresponds to the chemical shift of c'-protons split by the effect of 2 b'-protons. The triplet at 7.070 ppm overlaps with a doublet around 7.028 ppm correspond to c'-protons split by 2 b'-protons and a-protons split by b-protons respectively.

Formation of Nitrile Adducts

Trans-2,2-tetrakis(N-phenylacetamido) dirhodium(II) – Benzonitrile, **I**

2 mol equivalence of benzonitrile was reacted with 1 mol equivalence of *trans*-2,2-[Rh$_2$(C$_6$H$_5$NCOCH$_3$)$_4$] with the aim of coordinating the ligand in both axial sites of the *trans*-2,2-[Rh$_2$(C$_6$H$_5$NCOCH$_3$)$_4$] isomer. The axial ligand was found to be coordinated to both sides (see pages 131 – 132).

Trans-2,2-tetrakis(N-phenylacetamido) dirhodium(II) – 2-methyl benzonitrile, **II**

2 mol equivalence of o-tolunitrile was reacted with 1 mol equivalence of *trans*-2,2-[Rh$_2$(C$_6$H$_5$NCOCH$_3$)$_4$] with the aim of coordinating the ligand in both axial sites of the *trans*-2,2-[Rh$_2$(C$_6$H$_5$NCOCH$_3$)$_4$] isomer. The axial ligand was found to be coordinated to both sides (see pages 133 – 135).

Trans-2,2-tetrakis(N-phenylacetamido) dirhodium(II) – 3-methyl benzonitrile, **III**

2 mol equivalence of m-tolunitrile was reacted with 1 mol equivalence of tetrakis *trans*-2,2-[Rh$_2$(C$_6$H$_5$NCOCH$_3$)$_4$] with the aim of coordinating the ligand in both axial sites of the *trans*-

2,2-[$Rh_2(C_6H_5NCOCH_3)_4$] isomer. The ligand was found to be coordinated to one side (see pages 136 – 139).

*Tetrakis 3,1-(N-phenylacetamido) dirhodium(II) – 1,3-dicyanobenzene, **IV***

1 mol equivalence of 1,3-dicyanobenzene was reacted with 1 mol equivalence of 3,1-[$Rh_2(C_6H_5NCOCH_3)_4$] with the aim of coordinating the ligand in both axial sites of the 3,1-[$Rh_2(C_6H_5NCOCH_3)_4$] isomer. A linear polymer was found to be synthesized with each C≡N group coordinated to the axial site of the tetrakis 3,1 [$Rh_2(C_6H_5NCOCH_3)_4$] (see pages 140 – 143).

<div align="center">*Characterization of the Various Nitrile Adducts*</div>

Infrared Spectrophotometry

The C≡N stretching frequency usually shows up as a sharp peak between 2500 cm^{-1} and 3000 cm^{-1}. During coordination to the metal, there is σ-bonding from the nitrile to the Rh metal as well as π-back bonding from the filled d-orbitals of the metal to the antibonding orbitals of the nitrile. During σ bonding, there is electron donation to the rhodium metal by the nitrile. The tendency of the C≡N bond to vibrate is reduced as it is connected to 2 different constituents. This causes the stretching frequency of the C≡N in the rhodium – nitrile complex to be higher than the C≡N of the nitrile alone. Peaks resulting from this σ interaction tend to show up at higher wave numbers (higher energy). The π-back bonding interactions populate the antibonding orbitals of the C≡N bond, resulting in a longer bond, hence a weaker one too. Therefore, σ-bonding results in an increase in energy, while π-back bonding results in a decrease in energy.

Trans-2,2-tetrakis(N-phenylacetamido) dirhodium(II) – Benzonitrile, I. The IR spectrum of benzonitrile shows a C≡N stretch at 2227.78 cm^{-1}, as seen in Figure 19. Figure 20 shows the IR spectrum of benzonitrile complexed with a low intensity C≡N stretch at 2362.8 cm^{-1}

Therefore, in this complex, there is an overall increase of σ-bonding to π-back bonding upon complexation as seen when comparing the IR spectra together (see Figures 19 and 20).

Trans-2,2-tetrakis(N-phenylacetamido) dirhodium(II) – 2-methyl benzonitrile, II. The IR spectrum of o-tolunitrile shows a C≡N stretch at 2223.92 cm^{-1}, as seen in Figure 21. Figure 22 shows the IR spectrum of o-tolunitrile complexed with a low intensity C≡N stretch at 2320.37 cm^{-1}

Therefore, in this complex, there is an overall increase of σ-bonding to π-back bonding upon complexation as seen when comparing the IR spectra (see Figures 21 and 22).

Trans-2,2-tetrakis(N-phenylacetamido) dirhodium(II) – 3-methyl benzonitrile, III. The IR spectrum of m-tolunitrile shows a C≡N stretch at 2227.78 cm^{-1}, as seen in Figure 23. Figure 24 show the IR spectrum of m-tolunitrile complexed with a low intensity C≡N stretch at 2241.28 cm^{-1}

Therefore, in this complex, there is an overall increase of σ-bonding to π-back bonding upon complexation as seen when comparing the IR spectra (see Figures 23 and 24).

3,1-tetrakis(N-phenylacetamido) dirhodium(II) – 1,3-dicyanobenzene, IV. The IR spectrum of 1,3-dicyanobenzene shows a C≡N stretch at 2233.57 cm^{-1}, as seen in Figure 25. Figure 26 shows the IR spectrum of 1,3-dicyanobenzene complexed with a low intensity C≡N stretch at 2233.57 cm^{-1}

Thus, in this complex, there is no overall change in amount of σ-bonding to π-back

bonding upon complexation as seen when comparing the IR spectra (see Figures 25 and 26).

^{1}H NMR Spectrophotometry

When the ^{1}H NMR for the nitrile adducts are carried out, the protons on the nitrile appear

downfield. They are lower energy and their relative chemical shift positions downfield can be

explained using resonance. Scheme 4, below, shows the resonance of the benzene ring on due to

the effect of the nitrile group substituent.
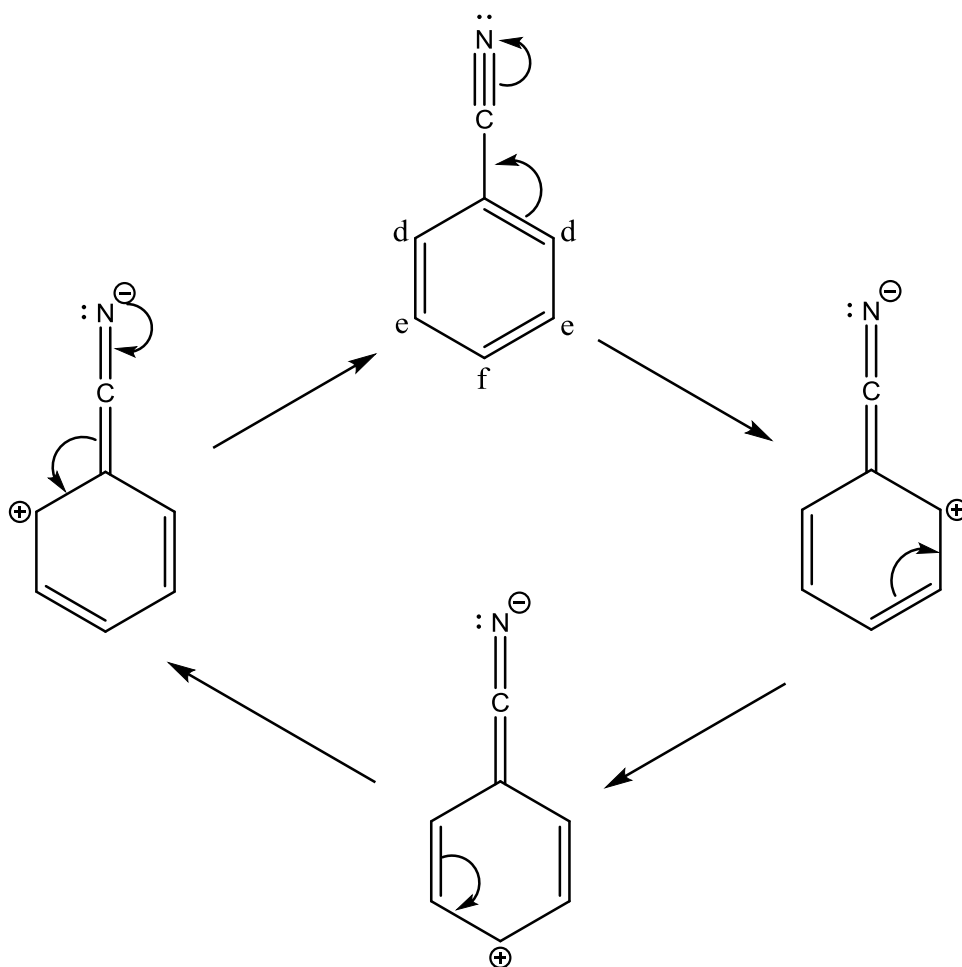
Scheme 4. The resonance of a benzene ring with a nitrile substituent.

The C≡N is a strong electron withdrawing group that pulls π electron density from the ring. The 'd' and 'f' (ortho and para) protons are the most deshielded and due to the proximity of protons 'd' to the C≡N group, these protons further appear at lower energy downfield. The least affected protons by the effect of the electron withdrawing group are the e protons. Thus, they are fairly shielded and appear upfield when compared with protons 'd' and 'f'.

Protons 'd' will be expected to couple with protons 'e' and appear as a doublet. The protons 'e' will couple with the protons 'd' and 'f' giving rise to a triplet and lastly, proton 'f' will couple with the protons 'e' giving rise to a triplet.

Trans-2,2-tetrakis(N-phenylacetamido) dirhodium(II) – Benzonitrile, **I.** The protons on the benzonitrile ligand are chemically different and are labelled d, e, and f in Figure 50.
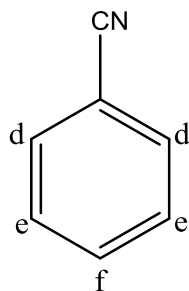
Figure 50. Benzonitrile showing various types of Hydrogen atoms for Figures 27 and 29 that show the ^{1}H NMR for the benzonitrile.

Tables 13 and 14, below, show the peaks of interest in the ^{1}H NMR spectra of the benzonitrile that are presented in Figures 27 and 29.

Table 13. The ^{1}H NMR peaks for benzonitrile from Figure 27

Chemical shift (ppm)	Peak type	Proton type
1.614	Singlet	H_2O
7.266	Singlet	$CHCl_3$

The residual solvent peaks for H_2O and $CHCl_3$ appear as singlets at 1.614 ppm and 7.266 ppm, respectively.

Table 14. The ^{1}H NMR peaks for benzonitrile from Figure 29

Chemical shift (ppm)	Peak type	Proton type
7.266	Singlet	$CHCl_3$
7.481	Triplet	e
7.614	Triplet of triplets	f
7.700	Doublet of doublets	d

Due to the resonance effect of the C≡N (an actively ring deactivating group) on the ring the e-protons are most shielded and appear as a triplet upfield at 7.481 ppm. The f-protons are deshielded with the d-protons most shielded as they are in close proximity to the C≡N group. The f-protons appear as a triplet of triplets with chemical shift at 7.614 ppm and the e-protons appear as a doublet of doublets with a chemical shift of 7.700 ppm.

For the complex (**I**), the chemical environments for the protons on the acetamide bridge and on the ligand differ. They are labelled a, b, c, d, e, and f accordingly (shown in Figure 51).

The protons are the chemically equivalent for any one acetamide bridge considered or any one ligand phenyl ring considered.
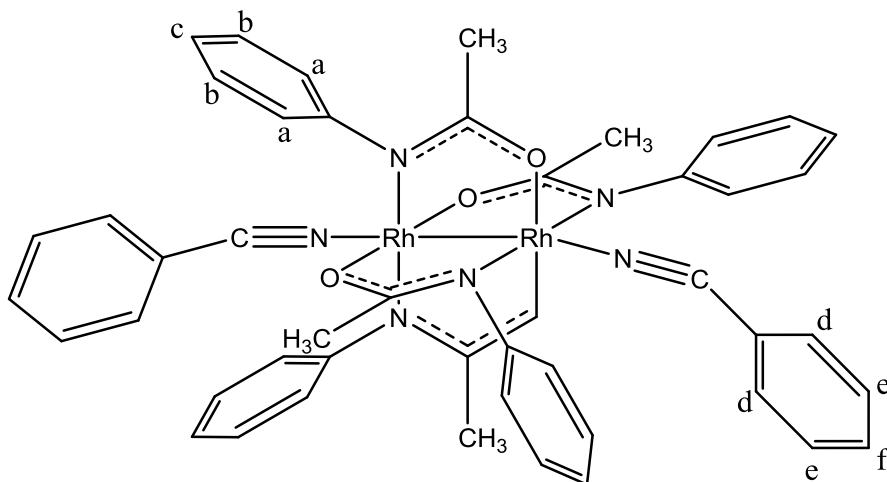
Figure 51. A *trans*-2,2-[Rh$_2$(C$_6$H$_5$NCOCH$_3$)$_4$·2benzonitrile] showing different types of Hydrogen atoms for Figures 28 and 30 that show the ^{1}H NMR for the above compound.

Tables 15 and 16, below, show the peaks of interest in the ^{1}H NMR spectra of the complex (**I**) that are presented in Figures 28 and 30.

Table 15. The ^{1}H NMR peaks for *trans*-2,2-[Rh$_2$(C$_6$H$_5$NCOCH$_3$)$_4$·2benzonitrile] from Figure 28

Chemical shift (ppm)	Peak type	Proton type
1.253 – 1.302	Complex	Hexane
1.616	Singlet	H$_2$O
1.843	Singlet	Methyl
7.263	Singlet	CHCl$_3$

The solvent residual peaks for hexanes, H_2O and $CHCl_3$ appear at 1.253 ppm, 1.302 ppm, 1.616 ppm, and 7.263 ppm. The methyl peaks on the dirhodium core also appear as a singlet at 1.843 ppm.

Table 16. The ^1H NMR peaks for *trans*-2,2-[Rh$_2$(C$_6$H$_5$NCOCH$_3$)$_4$·benzonitrile] from Figure 30

Chemical shift (ppm)	Peak type	Proton type
7.031	Doublet	a
7.134	Triplet	c
7.281	Overlapping triplet	b, d
7.374	Triplet	e
7.539	Triplet	f

Protons a-, b-, and c- are the protons on the phenyl rings attached to the amide bridge while protons d-, e-, and f- are the protons attached to the benzonitrile ligand. Protons a-, b-, and c- still appear as a doublet, triplet, and triplet respectively. However, the b-protons are not clearly seen on the spectrum as they overlap with the solvent peak and others from the benzonitrile ligand. Also, protons d-, e-, and f- appear as a doublet, triplet, and triplet respectively. Instead of d-protons being the most d-shielded in this case, due to their proximity with the Rh atom that has a large electron density, the Rh shields them and the doublet of doublet is actually shifted upfield. In this case, the peaks overlap with both the solvent peak and the b-protons at 7.281 ppm. Peaks a-, c-, e-, and f- appear at 7.031 ppm, 7.134 ppm, 7.374 ppm, and 7.539 ppm respectively.

Trans-2,2-tetrakis(N-phenylacetamido) dirhodium(II) – 2-methyl benzonitrile, **II.** The protons on the 2-methyl benzonitrile ligand are chemically different and are labelled d, e, f, and g in Figure 52.
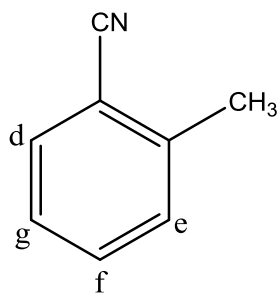
Figure 52. 2-methyl benzonitrile showing various types of Hydrogen atoms for Figures 31 and 33 that show the ^{1}H NMR for o-tolunitrile.

Tables 17 and 18, below, show the peaks of interest in the ^{1}H NMR spectra of the 2-methyl benzonitrile that are presented in Figures 31 and 33.

Table 17. The ^{1}H NMR peaks for o-tolunitrile from Figure 31

Chemical shift (ppm)	Peak type	Proton type
1.713	Singlet	H_2O
2.522	Singlet	Methyl

The methyl peak of the ligand appears as a singlet at 2.522 ppm. The reason it appears relatively down field is that it is directly attached to the phenyl ring and is next to the C≡N group which is ring deactivating due to resonance effects.

Table 18. The ^{1}H NMR peaks for o-tolunitrile from Figure 33

Chemical shift (ppm)	Peak type	Proton type
7.271	Triplet	g
7.317	Doublet	e
7.482	Triplet	f
7.585	Doublet	d

Due to the presence of both the nitrile and methyl groups on the phenyl ring, all protons are now chemically different. The d-protons are most deshielded as they are in close proximity to the nitrile, then the f-protons due to resonance. Due to the effect of the methyl group the g-protons are more shielded than the e-protons hence appear slightly upfield. The g-protons appear as a triplet at 7.271 ppm, the e-protons a doublet at 7.317 ppm, the f-protons a triplet at 7.482 ppm, and the d-protons a doublet at 7.585 ppm.

For the complex (**II**), the chemical environments for the protons on the acetamide bridge and on the ligand differ. They are labelled a, b, c, d, e, f, and g accordingly (shown in Figure 53). The protons are the chemically equivalent for any one acetamide bridge considered or any one ligand phenyl ring considered.
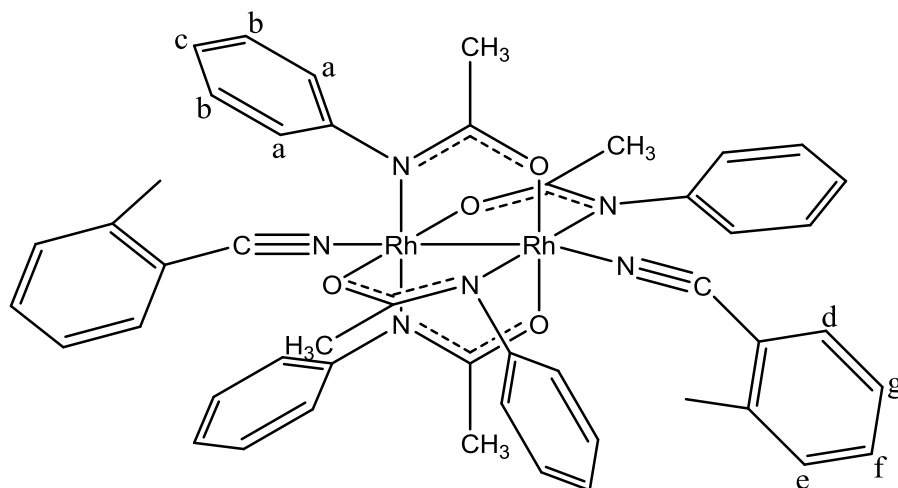
Figure 53. A *trans*-2,2-[Rh₂(C₆H₅NCOCH₃)₄·2o-benzonitrile] showing different types of Hydrogen atoms for Figures 32 and 34 that show the ^{1}H NMR spectra for the above compound.

Tables 19 and 20, below, show the peaks of interest in the ^{1}H NMR spectra of the complex (**II**) that are presented in Figures 32 and 34.

Table 19. The ^{1}H NMR peaks for tetrakis *trans*-2,2-[Rh₂(C₆H₅NCOCH₃)₄·2o-tolunitrile] from Figure 32

Chemical shift (ppm)	Peak type	Proton type
1.593	Singlet	H₂O
1.844	Singlet	Methyl (on bridge)
2.368	Singlet	Methyl (on ligand)
7.262	Singlet	CHCl₃

The solvent residual peaks of H_2O and $CHCl_3$ appear at 1.593 ppm and 7.262 ppm. The methyl groups on the acetamide bridges appear at 1.844 ppm while the methyl group on the ligand appears at 2.368 ppm.

Table 20. The ^{1}H NMR peaks for tetrakis *trans*-2,2-[Rh$_2$(C$_6$H$_5$NCOCH$_3$)$_4$·2o-tolunitrile] from Figure 32

Chemical shift (ppm)	Peak type	Proton type
7.001	Doublet	a
7.079	Triplet	c
7.179	Triplet	g
7.243	Overlapping triplet	b, d, e
7.434	Triplet	f

Protons a-, b-, and c- are due to the protons on the phenyl substituent on the dirhodium core while protons d-, e-, f-, and g- are due to the protons on the o-tolunitrile ligand. Due to the proximity of d-, g-, and e- to the metal center, their chemical shifts are slightly shifted upfield since they get shielded by the electron density of the Rh atom. Due to this shift, the peaks from d- and e- overlap with the triplet from the b-protons at 7.243 ppm. The a-protons appear as a doublet at 7.001 ppm, c-protons a triplet at 7.079ppm, f-protons a triplet at 7.434 ppm and g-protons shielded upfield as a triplet at 7.179 ppm.

*Tetrakis 2,2 trans-(N-phenylacetamido) dirhodium(II) – 3-methyl benzonitrile, **III**.* The protons on the 3-methyl benzonitrile ligand are chemically different and are labelled d, e, f, and g in Figure 54.
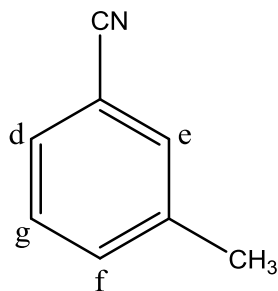
Figure 54. 3-methyl benzonitrile showing different Hydrogen atoms for Figures 35 and 37 that show the ^{1}H NMR of m-tolunitrile.

Tables 21 and 22, below, show the peaks of interest in the ^{1}H NMR spectra of the 3-methyl benzonitrile that are presented in Figures 35 and 37.

Table 21. The ^{1}H NMR peaks for m-tolunitrile from Figure 35

Chemical shift (ppm)	Peak type	Proton type
1.764	Singlet	H_2O
2.422	Singlet	Methyl

In the spectrum above, the methyl protons on the ligand appear as a singlet at 2.422 ppm. The H_2O residual peak appears at 1.764 ppm.

Table 22. The ^{1}H NMR peaks for o-tolunitrile from Figure 37

Chemical shift (ppm)	Peak type	Proton type
7.276	Singlet	$CHCl_3$
7.330 – 7.477	Complex peaks	d, e, f, g

The most shielded protons are the f- and g-protons while the most deshielded protons are the e- and d- protons. The singlet from e- is overlapping with the doublets from d- and f-protons. This multiplex also overlaps with the triplet from the g-protons in the range 7.330 ppm to 7.477 ppm.

For the complex (**III**), the chemical environments for the protons on the acetamide bridge and on the ligand differ. They are labelled a, b, c, d, e, f, and g accordingly (shown in Figure 55). The protons are chemically equivalent for any one acetamide bridge considered or any one ligand phenyl ring considered.
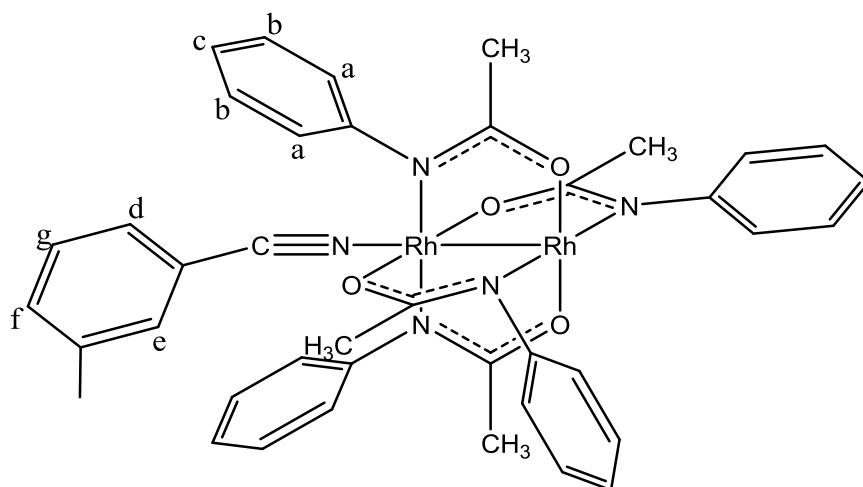
Figure 55. A *trans*-2,2-[Rh$_2$(C$_6$H$_5$NCOCH$_3$)$_4$·2m-benzonitrile] showing different types of Hydrogen atoms for Figures 36 and 38 that show the ^{1}H NMR for the above compound.

Tables 23 and 44, below, show the peaks of interest in the ^{1}H NMR spectra of the complex (**III**) that are presented in Figures 36 and 38.

Table 23. The ^{1}H NMR peaks for tetrakis *trans*-2,2-[Rh$_2$(C$_6$H$_5$NCOCH$_3$)$_4$·2m-tolunitrile]

from Figure 36

Chemical shift (ppm)	Peak type	Proton type
1.272	Singlet	Hexane
1.695	Singlet	H$_2$O
1.828	Singlet	Methyl (on bridge)
2.344	Singlet	Methyl (on ligand)
7.262	Singlet	CHCl$_3$

The solvent residual peaks from hexane, H$_2$O and CHCl$_3$ appear at 1.272 ppm, 1.695 ppm, and 7.262 ppm respectively. The singlets at 1.828 ppm and 2.344 ppm are due to the methyl groups on the dirhodium core and the m-tolunitrile ligand respectively.

Table 24. The ^{1}H NMR peaks for tetrakis *trans*-2,2-[Rh$_2$(C$_6$H$_5$NCOCH$_3$)$_4$·2m-tolunitrile]

from Figure 38

Chemical shift (ppm)	Peak type	Proton type
6.985 – 7.034	Overlapping peaks	a, c
7.126	Triplet	b
7.225	Triplet	g
7.278 – 7.356	Complex peaks	d, e, f

Due to coordination of the m-tolunitrile ligand in only one axial site, the a-, b-, and c-protons on either axial side of the dirhodium core are slightly different. Hence, there is overlapping of the peaks created by the a- and c- protons between 6.985 ppm and 7.034 ppm. Also, the b-protons are slightly shielded and appear as a triplet at 7.126 ppm. The g-protons appear as a triplet at 7.225 ppm while d-, e- and f-protons form a multiplet due to their overlapping from 7.278 ppm to 7.356 ppm.

Tetrakis 3,1-(N-phenylacetamido) dirhodium(II) – 1,3-dicyanobenzene, **IV.** The protons on the 1,3-dicyanobenzene ligand are chemically different and are labelled d, e, and f in Figure 56.
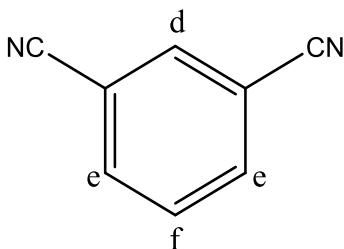
Figure 56. 1,3-dicyanobenzene showing the various types of hydrogen atoms for Figures 39 and 41 that show the ^{1}H NMR for 1,3-dicyanobenzene.

Tables 25 and 26, below, show the peaks of interest in the ^{1}H NMR spectra of the 1,3-dicyanobenzene that are presented in Figures 39 and 41.

Table 25. The ^{1}H NMR peaks of 1,3-dicyanobenzene from Figure 39

Chemical shift (ppm)	Peak type	Proton type
1.594	Singlet	H_2O
7.267	Singlet	$CHCl_3$

The H_2O and $CHCl_3$ peaks residual peaks appear at 1.594 ppm and 7.267 ppm respectively.

Table 26. The ^1H NMR peaks for 1,3-dicyanobenzene from Figure 41

Chemical shift (ppm)	Peak type	Proton type
7.670	Triplet	f
7.915	Doublet	e
7.971	Singlet	d

The d-protons are the most deshielded due to the 2 nitrile groups that sandwich it. Also this peak appears as a singlet at 7.971 ppm, long range coupled with the 2 neighboring e-protons. The e-protons appear as a doublet at 7.915 ppm, due to coupling to the f-protons and is long range coupled to the d-protons. The f-protons are the most shielded and appear as a triplet at 7.670 ppm by coupling with 2 e-protons.

For the complex (**IV**), the chemical environments for the protons on the acetamide bridge and on the ligand differ. They are labelled a, a', a'', b, b', c, c', d, e, e', and f accordingly (shown in Figure 57).
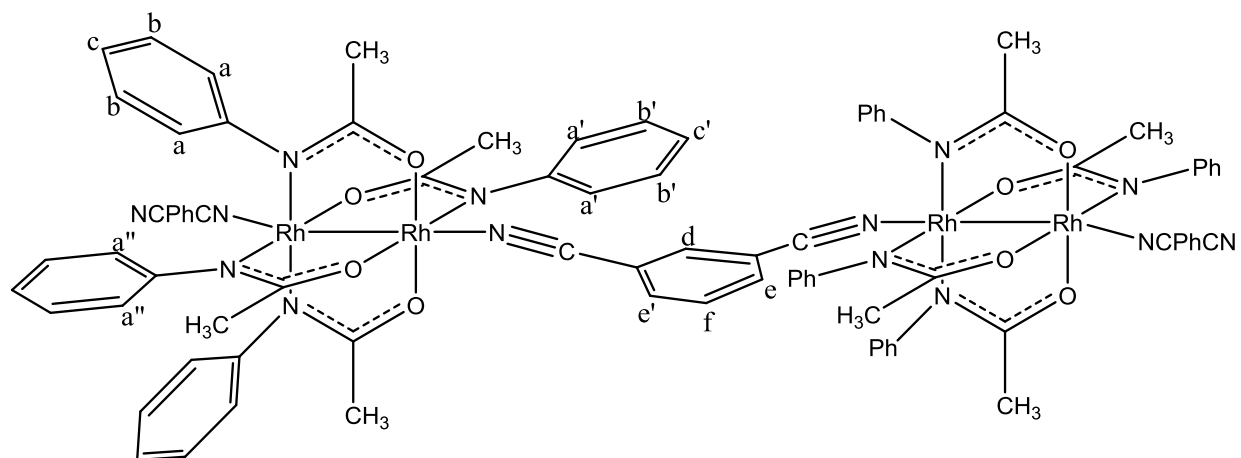
Figure 57. A 3,1-[Rh$_2$(C$_6$H$_5$NCOCH$_3$)$_4$·1,3-dicyanobenzene] showing different types of Hydrogen atoms for Figures 40 and 42 that show the ^{1}H NMR for the above compound.

Tables 27 and 28, below, show the peaks of interest in the ^{1}H NMR spectra of the complex (**IV**) that are presented in Figures 40 and 42.

Table 27. The ^{1}H NMR peaks for 3,1-[Rh$_2$(C$_6$H$_5$NCOCH$_3$)$_4$·1,3-dicyanobenzene] from Figure 40

Chemical shift (ppm)	Peak type	Proton type
1.627	Singlet	H$_2$O
1.840	Singlet	Methyl
1.891	Singlet	Methyl
1.946	Singlet	Methyl
5.305	Singlet	CH$_2$Cl$_2$
7.265	Singlet	CHCl$_3$

The solvent residual peaks for H_2O, CH_2Cl_2, and $CHCl_3$ appear at 1.627 ppm, 5.305 ppm, and 7.265 ppm respectively. The singlets at 1.840 ppm, 1.891 ppm, and 1.946 ppm in the ratio 2:1:1 correspond to the methyl groups on the acetamide bridge.

Table 28. The ^{1}H NMR of 3,1-[Rh$_2$(C$_6$H$_5$NCOCH$_3$)$_4$·1,3-dicyanobenzene] from Figure 42

Chemical shift (ppm)	Peak type	Proton type
6.654	Doublet	a
6.833	Doublet	a'
6.880	Triplet	c'
6.968	Triplet	c
7.073	Triplet	b'
7.165	Doublet	a"
7.193	Triplet	b
7.335	Triplet	f
7.531	Singlet	d
7.572	Doublet	e
7.694	Doublet	e'

The protons are labeled respectively (see Figure 57). The protons on the phenyl ring of the dirhodium core are all now fairly different due to the "3,1" nature of the ligand. The a-, a'-, and a"- protons correspond to the doublets at 6.654 ppm, 6.833 ppm, and 7.165 ppm, respectively. The b- and b'- protons appear as triplets at 7.193 ppm and 7.073 ppm respectively. The c- and c'- protons appear as triplets at 6.968 ppm and 6.880 ppm. The d-proton is a singlet at

7.531 ppm that overlaps slightly with the e-protons at 7.572 ppm. The e'-protons appear as a doublet at 7.694 ppm. The f-protons appear as a clean triplet at 7.335 ppm.

X-ray Crystallography

Tetrakis 2,2 trans-(N-phenylacetamido) dirhodium(II) – Benzonitrile, I. The crystal was mounted on a Rigaku XtaLab mini diffractometer that was run for 12 initial images using the CrystalClear software package. These 12 images were used to calculate the unit cell parameters of the compound ($a = 30.238(7)$ Å, $b = 10.605(2)$ Å, $c = 26.091(6)$ Å, $\beta = 90.539(7)^0$, $V = 8366(4)$ Å^3). This implied the unit cell was monoclinic. Three shells of images were further collected that were then further processed and the data were exported to a Crystal Structure software. The information was further analyzed using the XPLAIN function from the Crystal Structure software package with further narrowed down to the possible space group (C2/c). This implied the unit cell is C-centered and has a 2-fold rotation perpendicular to the c-face. The structure solution was then solved using direct methods (SHELX97) to obtain a portion of the molecule for which further structural revelations were achieved by manually adding the remaining atoms. Least square refinements were run on 25 peaks as the structure was edited until achieving an R_1 value of 0.0686.

An ORTEP of **I** is shown in Figure 43. X-ray structural analysis of **I** showed that benzonitrile ligand coordinated to both sides of tetrakis 2,2 trans-[$Rh_2(C_6H_5NCOCH_3)_4$] as shown in Figure 43. There was a benzonitrile ligand coordinated in each axial site of the dirhodium core.

Figure 58, below, shows the packing of molecules in one unit cell. The unit cell diagram on top is as seen looking down the cell edge a while that on the bottom is as seen looking down the cell edge c. We may clearly see 8 molecules found in the unit cell (Figure 58, top)
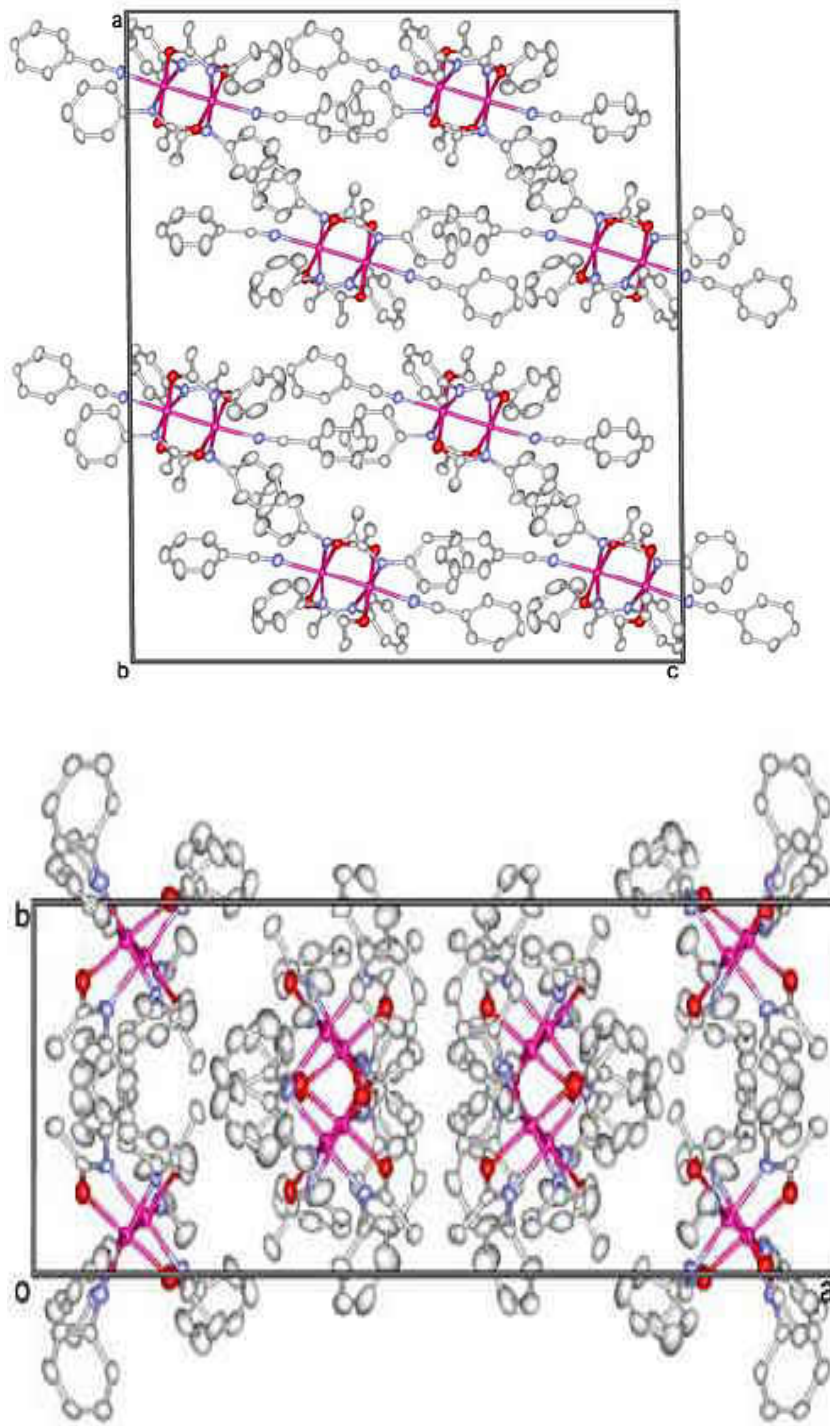
Figure 58. The unit cell diagrams of [Rh$_2$(PhNCOCH$_3$)$_4$·2NCC$_6$H$_5$], with thermal ellipsoids as seen looking down cell edges a and c respectively (hydrogen atoms not shown), showing 8 molecules per unit cell.

The molecule was generated completely with no special geometry present.

*Tetrakis 2,2 trans-(N-phenylacetamido) dirhodium(II) – 2-methyl benzonitrile, **II**.* The crystal was mounted on a Rigaku XtaLab mini diffractometer that was run for 12 initial images using the CrystalClear software package. These 12 images were used to calculate the unit cell parameters of the compound (a = 9.7912(7) Å, b = 14.787(1) Å, c = 16.359(1) Å, α = 103.837(7)^0, β = 99.173(7)^0, γ = 99.772(7)^0, V = 2216.4(3) Å^3). This implied the unit cell was triclinic. Three shells of images were further collected that were then further processed and the data were exported to a Crystal Structure software. The information was further analyzed using the XPLAIN function from the Crystal Structure software package with further narrowed down to the possible space group (P-1). This implied the unit cell is a primitive lattice and is asymmetric. The structure solution was then solved using direct methods (SHELX97) to obtain a portion of the molecule for which further structural revelations were achieved by manually adding the remaining atoms. Least square refinements were run on 25 peaks as the structure was edited until achieving an R_1 value of 0.0368.

An ORTEP of **II** is shown in Figure 44. X-ray structural analysis of **II** showed that o-tolunitrile ligand coordinated to both sides of tetrakis 2,2 *trans*-[$Rh_2(PhNCOCH_3)_4$] (see Figure 44). The compound is triclinic and belongs to the P-1(#2) space group with 2 molecules per assymetric unit. The compound has 4 N-phenylacetamide ligands bridging a dirhodium core, arranged in a 2,2-*trans* manner with respect to the nitrogen atoms; 2 nitrogen atoms and 2 oxygen atoms coordinated to 1 rhodium atom *trans* to one another and the other 2 nitrogen atoms and 2 oxygen atoms coordinated to the other rhodium atom in a similar *trans* arrangement. The torsion angles on any one N-phenylacetamide bridge, N_{eq}—Rh—Rh—O_{eq} vary between 4.07° and 6.83°. The N(3)-Rh(1)-Rh(2)-N(6) (N_{ax}-Rh-Rh-N_{ax}) torsion angle is 71.6°. The N_{eq}—Rh—

Rh—N$_{eq}$ torsion angles are close to 90°. The axial rhodium-nitrogen-carbon bond angles are bent from linearity; 151.6 (3)° and 152.5 (3)°, respectively. The N(3)-C(21) bond distance is 1.133 (5) Å and the N(6)-C(40) bond distance is 1.137 (5) Å. This compound also has a pseudo 4-fold symmetry as seen in Figure 44.

Figure 59, below, shows the unit cell diagrams as seen down the cell edge a (top) and as seen down the cell edge b (bottom). We may clearly see 2 molecules in the unit cell (see Figure 59, top) and 4 half molecules (see Figure 59, bottom) giving a total of 2 molecules in the unit cell.
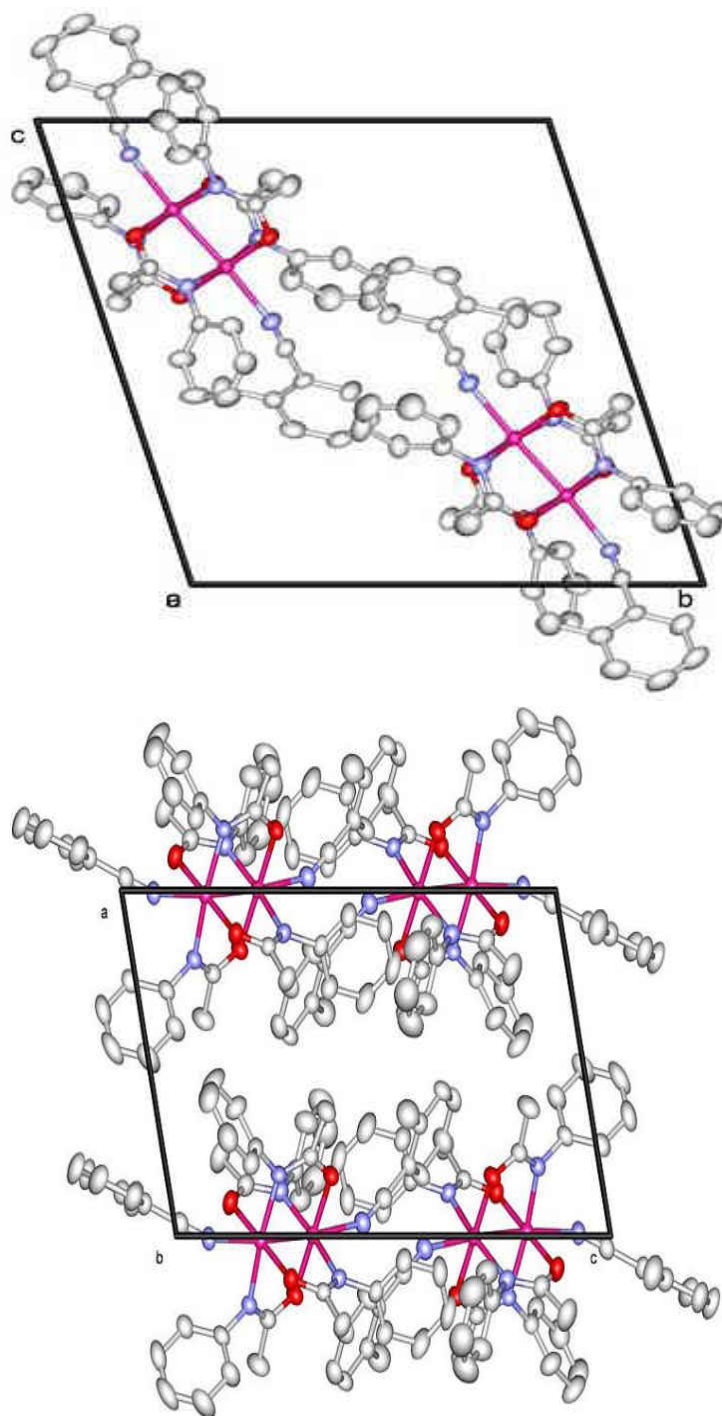
Figure 59. The unit cell diagrams of [Rh$_2$(PhNCOCH$_3$)$_4$·2NC{2-CH$_3$}C$_6$H$_4$], with thermal ellipsoids as seen looking down cell edges a and b (hydrogen atoms not shown), showing 2 molecules per unit cell.

For further crystallographic information, see appendix A.

*Tetrakis 2,2 trans-(N-phenylacetamido) dirhodium(II) – 3-methyl benzonitrile, **III***. The

crystal was mounted on a Rigaku XtaLab mini diffractometer that was run for 12 initial images

using the CrystalClear software package. These 12 images were used to calculate the unit cell

parameters of the compound (a = 11.711(2) Å, b = 13.018(2) Å, c = 13.398(2) Å, α = 72.337(5)^0,

β = 66.780(5)^0, γ = 82.742(6)^0, V = 1788.6(4) Å^3). This implied the unit cell was triclinic. Three

shells of images were further collected that were then further processed and the data were

exported to a Crystal Structure software. The information was further analyzed using the

XPLAIN function from the Crystal Structure software package with further narrowed down to

the possible space group (P-1). This implied the unit cell is a primitive lattice and is asymmetric.

The structure solution was then solved using direct methods (SHELX97) to obtain a portion of

the molecule for which further structural revelations were achieved by manually adding the

remaining atoms. Least square refinements were run on 25 peaks as the structure was edited until

achieving an R$_1$ value of 0.0491.

An ORTEP of **III** is shown in Figure 45. X-ray structural analysis of **III** showed that m-

tolunitrile ligand coordinated to both sides of tetrakis 2,2 *trans*-[Rh$_2$(PhNCOCH$_3$)$_4$] (see Figure

45). The compound is triclinic and belongs to the P-1(#2) space group with 2 molecules per

asymmetric unit. The compound has 4 N-phenylacetamide ligands bridging a dirhodium core,

arranged in a 2,2-*trans* manner with respect to the nitrogen atoms; 2 nitrogen atoms and 2

oxygen atoms coordinated to 1 rhodium atom *trans* to one another and the other 2 nitrogen atoms

and 2 oxygen atoms coordinated to the other rhodium atom in a similar *trans* arrangement. The

torsion angles on any one N-phenylacetamide bridge, N$_{eq}$—Rh—Rh—O$_{eq}$ vary between 12.55°

and 14.04°. The N$_{eq}$—Rh—Rh—N$_{eq}$ torsion angles are close to 90°. Thus, the compound has

pseudo four-fold symmetry along the rhodium-rhodium bond. The Rh—Rh bond distance is 2.4039 (7)   Å. There is a significant deviation from linearity when considering bond angles involving rhodium and the nitrogen of the nitrile. The Rh(1)—N(3)—C(21) bond angle is 166.3 (4)°, while the N(3)—C(21) bond distance is 1.140 (8) Å as seen Figure 45.

Figure 60, below, shows the unit cell diagram as seen looking down the cell edge a (top) and as seen down the cell edge c (bottom). We may clearly see 2 molecules in the unit cell.
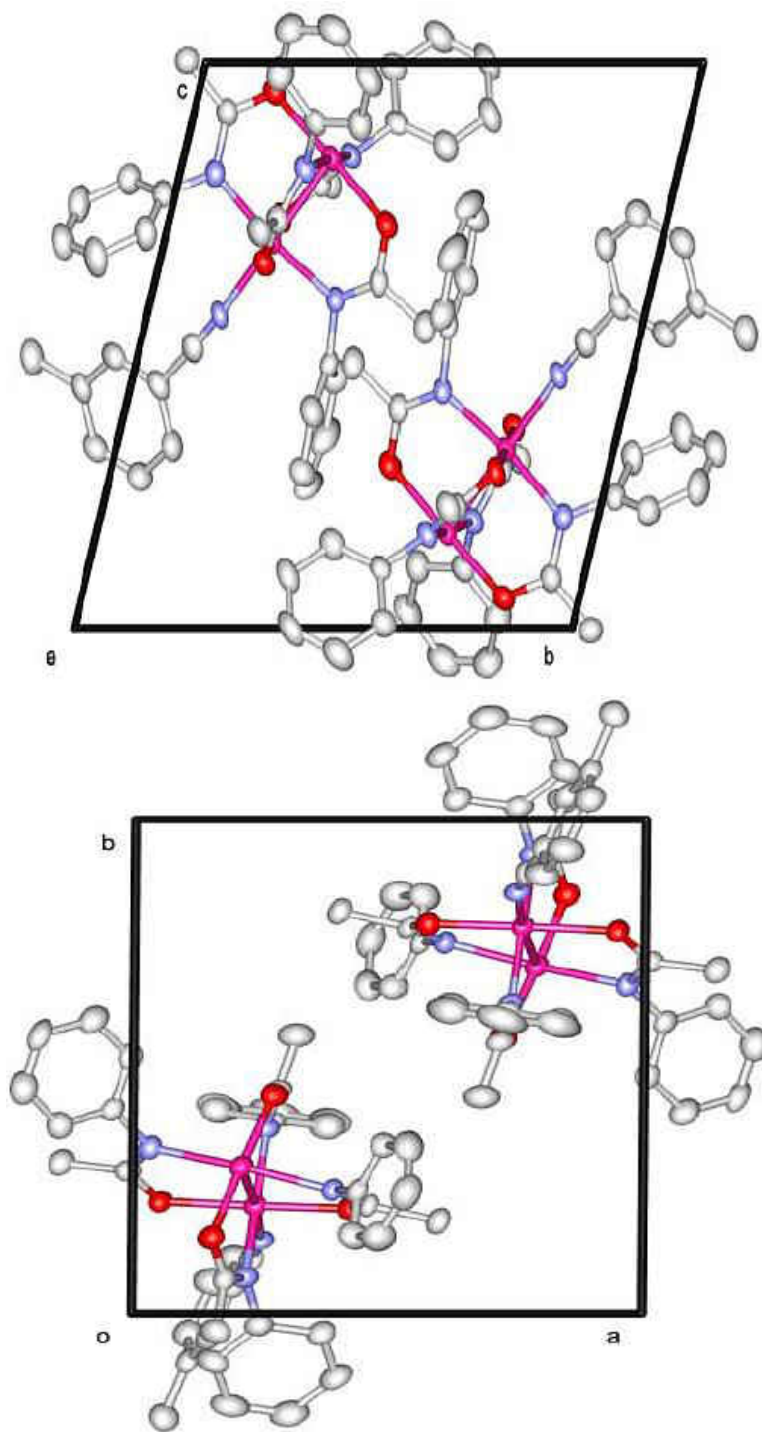
Figure 60. The unit cell diagrams of $[Rh_2(PhNCOCH_3)_4 \cdot NC\{3\text{-}CH_3\}C_6H_4]$, with thermal ellipsoids as seen looking down a and c cell edges respectively (hydrogen atoms not shown), showing 2 molecules per unit cell.

The m-tolunitrile was found to coordinate to only one side. Arguments can be made using packing forces to explain this. One of the N-phenylacetamide phenyl groups in this molecule occupies the axial site of another molecule, thus preventing m-tolunitrile from coordinating to 2 axial sites. Therefore, there is pi-stacking between the phenyl rings (see Figure 61).

pi-stacking of phenyl rings
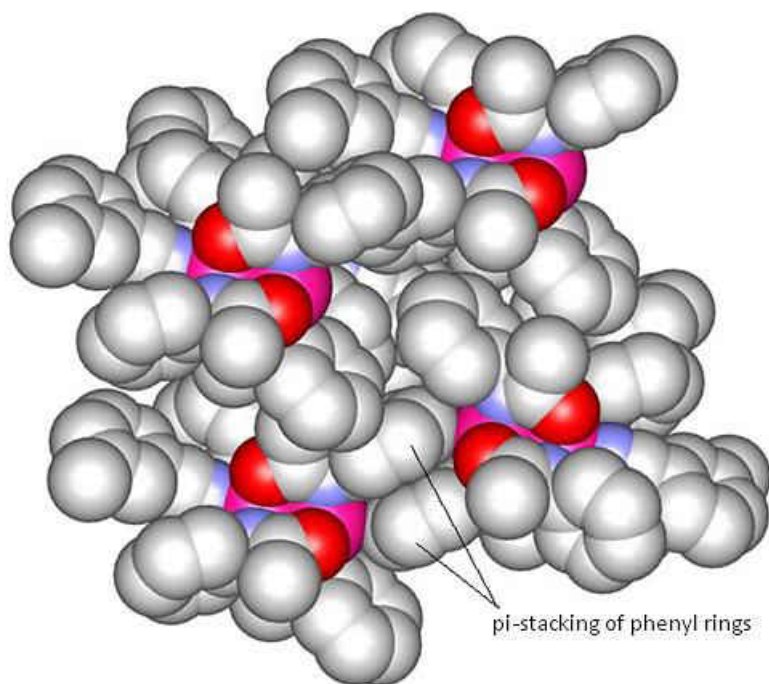
Figure 61. A CPK diagram of [Rh$_2$(PhNCOCH$_3$)$_4$·NC{3-CH$_3$}C$_6$H$_4$] showing a small number of molecules and π-stacking of phenyl rings.

For further crystallographic information, see appendix B.

When the synthesis of **III** was carried out again with excess nitrile ligand (**III$_{(xs)}$**), the expected 1:2, tetrakis(N-phenylacetamidato) dirhodium(II) complex was formed, [Rh$_2$(PhNCOCH$_3$)$_4$·2NC{3-CH$_3$}C$_6$H$_4$] (as seen in Figure 62).
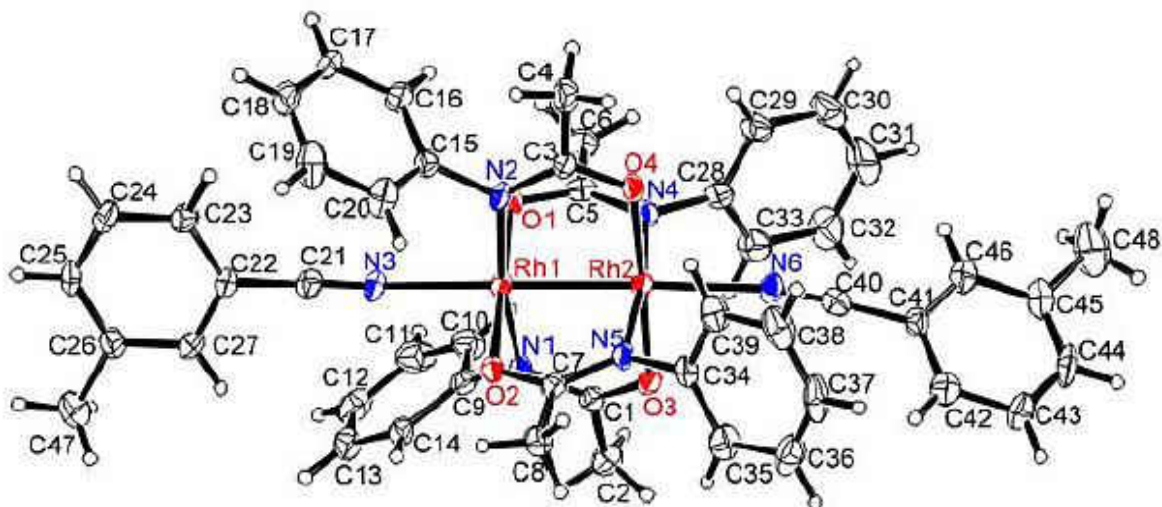
Figure 62. The ORTEP of [Rh$_2$(PhNCOCH$_3$)$_4$·2NC{3-CH$_3$}C$_6$H$_4$] showing 30% thermal ellipsoids and hydrogen atoms shown as very small spheres.

This 1:2 complex was analyzed by X-ray Crystallography (see appendix C for further information) and its structure was obtained. No further characterization was done on this complex. Compounds of this type have been reported.[15,39]

Tetrakis 3,1-(N-phenylacetamido) dirhodium(II) – 1,3-dicyanobenzene, **IV.** The crystal was mounted on a Rigaku XtaLab mini diffractometer that was run for 12 initial images using the CrystalClear software package. These 12 images were used to calculate the unit cell parameters of the compound (a = 11.8846(12) Å, b = 13.3012(14) Å, c = 14.8803(15) Å, α = 77.976(6)^0, β = 74.608(5)^0, γ = 65.476(5)^0, V = 2050.3(4) Å^3). This implied the unit cell was triclinic. Three shells of images were further collected that were then further processed and the data were exported to a Crystal Structure software. The information was further analyzed using the XPLAIN function from the Crystal Structure software package with further narrowed down to the possible space group (P-1). This implied the unit cell is a primitive lattice and is asymmetric. The structure solution was then solved using direct methods (SHELX97) to obtain a

portion of the molecule for which further structural revelations were achieved by manually adding the remaining atoms. Least square refinements were run on 25 peaks as the structure was edited until achieving an R_1 value of 0.0454.

An Ortep of **IV** is shown in Figure 46. X-ray structural analysis of **IV** showed that this compound grew as a linear polymer. This molecule is triclinic and belongs to the space group P-1(#2) with 2 molecules per unit cell. The structure has 4 N-phenylacetamide ligands bridging a dirhodium core. The N-phenylacetamide ligands are arranged in a "3,1" fashion; 3 nitrogen atoms and 1 oxygen atom are coordinated to one of the rhodium atoms; the other 1 nitrogen atom and 3 oxygen atoms are coordinated to the other rhodium atom. It has pseudo 4-fold symmetry. The title compound crystallized as a polymer with Rh-Rh bond length of 2.4146 (5) Å. In one dirhodium unit, each rhodium atom is coordinated to a nitrogen of the 1,3-dicyanobenzene. This causes quite a strain on the rhodium-nitrogen-carbon bond angle such that one rhodium atom has a rhodium-nitrogen-carbon bond angle of 166.8 (3)° and the other rhodium atom has a rhodium-nitrogen-carbon bond angle of 127.7 (3)°. Where the rhodium-nitrogen-carbon bond angle is 166.8 (3)°, the carbon-nitrogen bond distance of the 1,3-dicyanobenzene is 1.132 (6) Å and where the rhodium-nitrogen-carbon bond angle is 127.7 (3)°, the carbon-nitrogen bond distance of the 1,3-dicyanobenzene is 1.129 (8) Å. Considering the distortion of the structure, the solvent was incorporated into the lattice (2 molecules of dichloromethane per unit cell).

Figure 63, below, shows the unit cell diagrams as seen down the cell egdes a (top) and b (bottom) respectively showing 2 molecules of **IV** and 2 solvent molecules in the unit cell, while Figure 64 shows the extended linear chain polymer structure of **IV** formed.
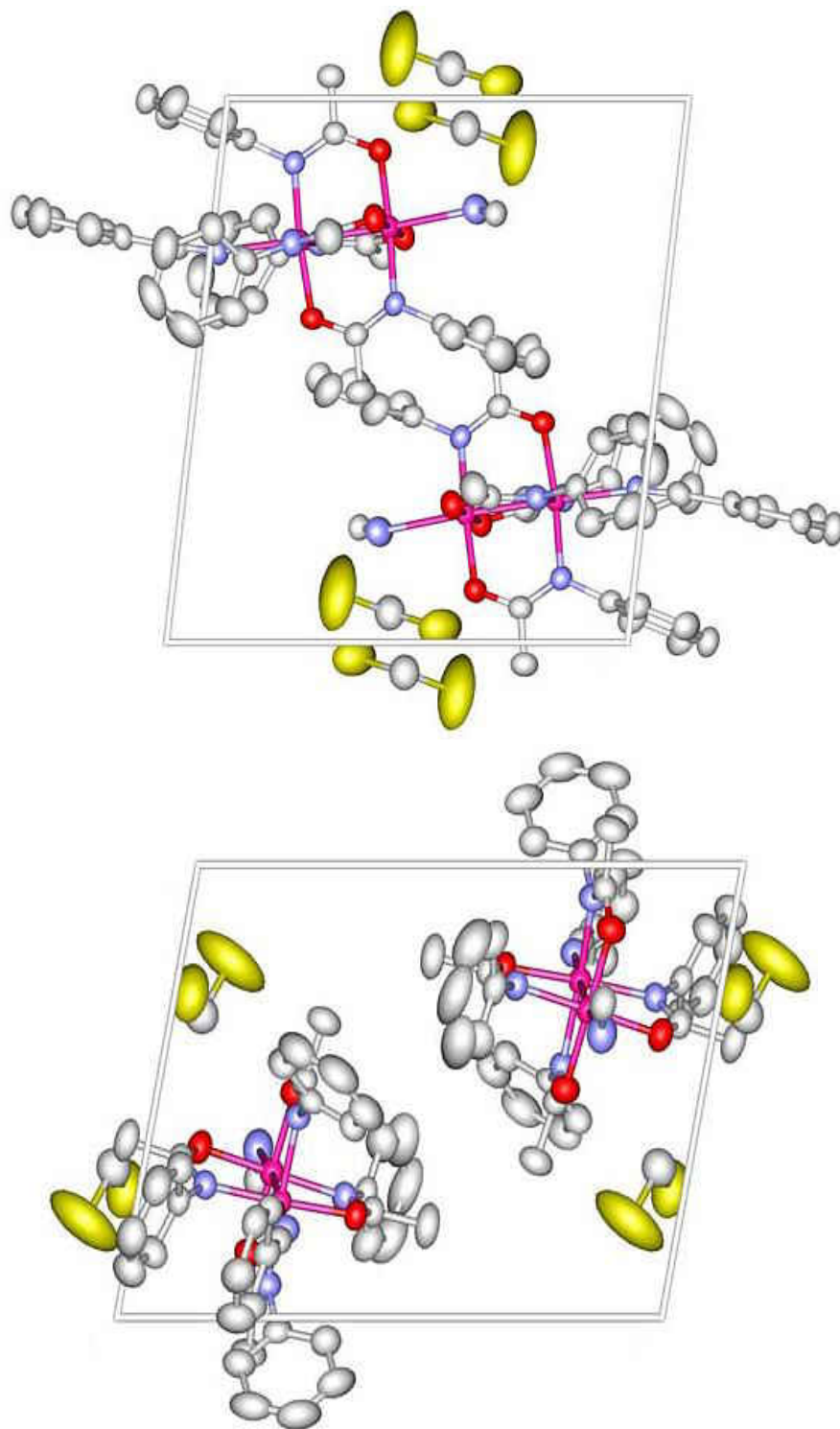
Figure 63. The unit cell diagrams of $[Rh_2(PhNCOCH_3)_4 \cdot 2NC\{3\text{-}CN\}C_6H_4]_\infty$, with thermal ellipsoids as seen looking down a and b cell edges respectively (hydrogen atoms not shown), showing 2 molecules per unit cell and 2 solvent molecules in a unit cell.
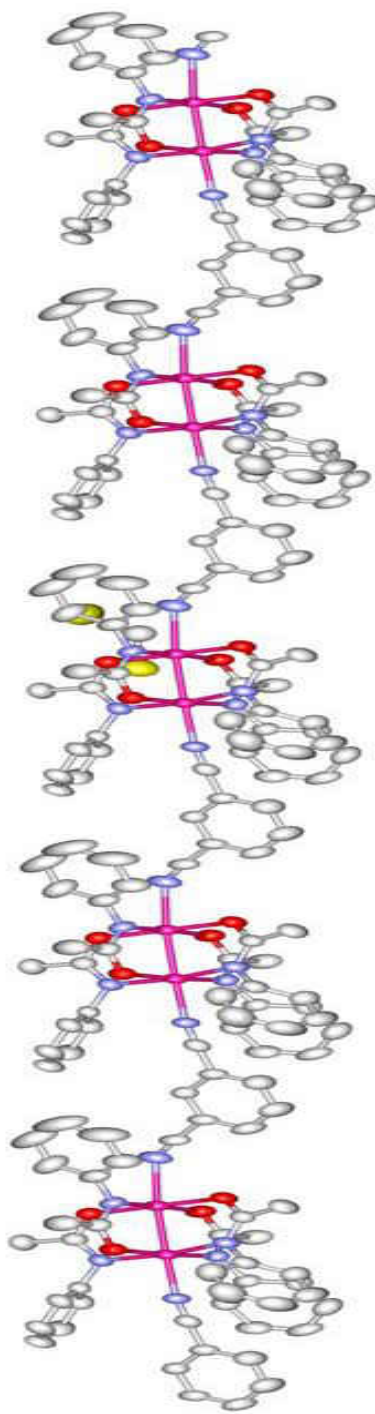
Figure 64. The extended polymer structure of $[Rh_2(PhNCOCH_3)_4 \cdot 2NC\{3\text{-}CN\}C_6H_4]_\infty$

(hydrogen atoms not shown).

For further crystallographic information, see Appendix D.

Nitrile Stretching

Table 29, below, shows the IR stretching frequencies of the C≡N bond of the free nitrile ligand and that contained in the synthesized complexes. Contrary to expected, we see an increase in the stretching frequency for all cases except in the case of compound **IV**. This suggests that for compounds **I**, **II**, and **III**, the nitrile binds strongly to the Rhodium atom through σ-bonding. If there had been stronger π-back bonding, we would have observed a decrease in the C≡N stretching frequency. In the case of compound **IV**, the stretching frequency about stays the same upon complexing the 1,3-dicyanobenzene with 3,1-tetrakis(N-phenylacetamidato) dirhodium(II).

The IR spectra generally showed a trend where, after complexation, the intensity of the nitrile stretching greatly reduced. It showed up as an intense sharp peak in the uncomplexed ligands, and then showed up as very small sharp peaks upon complexation. Possible explanations to this trend where the C≡N peak appears as a small peak may be due to a couple of reasons including a change in dipole (reduction) moment upon complexation and/or the light may not have coupled properly into the crystals when placed on the ATR sample cup.

Table 29. The comparison of C≡N stretching frequencies of the free nitrile ligand with the nitrile containing tetrakis(N-phenylacetamidato) dirhodium(II) complex

	CN Stretching frequency
Free Benzonitrile	2227.78 cm^{-1}
Benzonitrile – I	2362.8 cm^{-1}
Free o-tolunitrile	2223.92 cm^{-1}
o-tolunitrile – II	2320.37 cm^{-1}
Free m-tolunitrile	2227.78 cm^{-1}
m-tolunitrile – III	2241.28 cm^{-1}
Free 1,3-dicyanobenzene	2233.57 cm^{-1}
1,3-dicyanobenzene – IV	2233.57 cm^{-1}

The nitrile stretching frequency seen in the IR region is due the dipolar C≡N bond (C→N). As these nitriles coordinate in the axial site of the tetrakis(N-phenylacetamidato) dirhodium(II) compound, the vibrational frequency and the bond strength are increased. The intensity of absorption is also reduced as the observed nitrile stretch shifts to higher frequency (energy).

To understand the IR spectra, the various ways the nitrile can coordinate to the Rh atom of the tetrakis(N-phenylacetamidato) dirhodium(II) compound are shown in scheme 5 below.
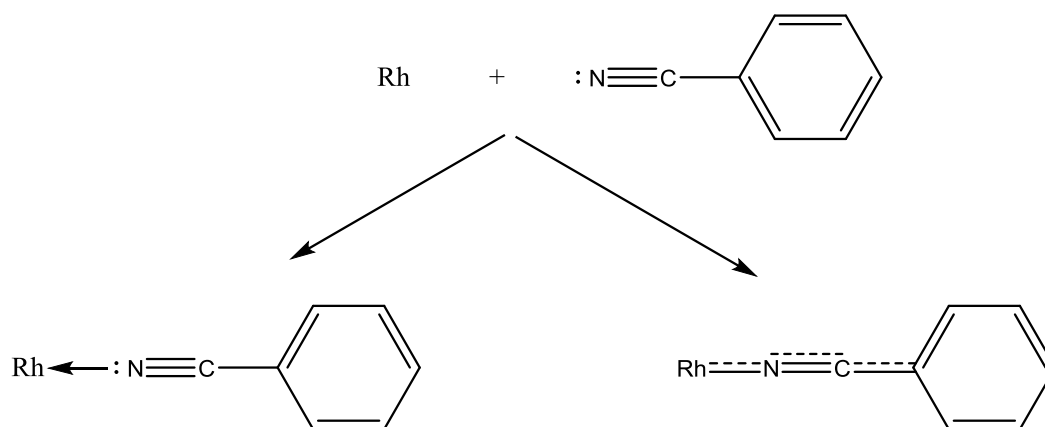
Scheme 5. Possible coordination modes

Here, the nitrile can coordinate to the Rh atom following either pathway. On one hand, the nitrile is pivoted on both sides by the phenyl ring and the Rh atom. This results in an increased stretching frequency and a lower intensity peak. On the other hand, the nitrile may coordinate where the π density of the triple bond is delocalized across the Rh – N – C. In this case the bond order would be reduced leading to a decreased energy nitrile stretch. However, as suggested by the IR these nitriles most likely coordinate via the first pathway thus favoring σ bonding interactions. The π-back bonding and σ bonding appear to balance each other out as seen in compound **IV**, but in the cases of **I**, **II**, and **III**, the IR spectra suggest increased σ bonding interactions.

Chemical Shift Environments

The ^{1}H NMR for these compounds showed that there was not much change in chemical environment when considering the N-phenylacetamide bridge. The protons (a, b, c) on the ring here were neither shielded nor deshieled after ligand coordination in the axial site of the various tetrakis(N-phenylacetamidato) dirhodium(II) compounds. However, while the protons on the free

ligand were deshielded and appeared downfield, they generally became slightly shielded upon complexation with the tetrakis(N-phenylacetamidato) dirhodium(II) compound. This was because upon complexation with [Rh$_2$(PhNCOCH$_3$)$_4$] the protons were in close proximity with the electron rich rhodium atom and the electron withdrawing strength of the group is reduced by rhodium metal's electron density being shared also with the C≡N as seen in Figure 65, below.
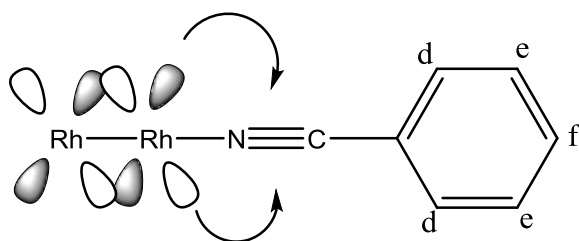
Figure 65. The effect of the rhodium atom on a nitrile containing ligand.

As a net effect, all the peaks on the nitrile are slightly shielded and their chemical shifts appear a little upfield in comparison to the uncomplexed nitrile. The most shielded in this case were the protons on the d positions.

For compound **I**, protons 'e' shift from 7.481 ppm to 7.374 ppm, protons 'f' shift from 7.614 ppm to 7.539 ppm, while protons 'd' are the most affected that shift from 7.700 ppm to 7.281 ppm overlapping with the b protons from the N-phenylacetamide.

For compound **II**, protons 'f' are shifted from 7.482 ppm to 7.434 ppm, protons 'g' are shifted from 7.271 ppm to 7.179 ppm, protons 'd' and 'e' are shifted from 7.585 ppm and 7.317 ppm respectively to overlap with protons 'b' from the N-phenylacetamide at 7.243 ppm.

For compound **III**, protons 'd', 'e', 'f', and 'g', which overlap forming peaks around 7.330 ppm to 7.477 ppm, are shielded after complexation and appear around 7.225 ppm to 7.356 ppm.

In compound **IV**, the chemical environment change around the ligand is most noted as up to 0.4 ppm changes are noticed. This can be expected because the polymer network formed tends to sandwich the ligand on both sides because of the presence of 2 C≡N groups. Thus the ring is affected on both sides by 2 different rhodium atoms. Protons 'd' shift from 7.971 ppm to 7.531 ppm, protons 'e' shift from 7.915 ppm to around 7.572 ppm to 7.694 ppm, protons 'f' shift from 7.670 ppm to 7.335 ppm.

Crystallographic Properties

A comparison of the crystallographic features of all synthesized compounds with general formula, $[Rh_2(C_6H_5NCOCH_3)_4 \cdot x(NC)_nR]$, is shown in Table 30, below. Their Rh – Rh bond distances are within 2.35Å – 2.45Å, which tie with similarly synthesized compounds by Bear and Kadish[40], Niu and coworkers.[37] Niu and coworkers synthesized tetrakis(acetate) dirhodium(II) compounds[37] that have Rh – Rh bond distances within the above stated range.

Table 30. The comparison of tetrakis(N-phenylacetamidato) dirhodium(II) nitrile,

$[Rh_2(C_6H_5NCOCH_3)_4 \cdot x(NC)_nR]$, compounds synthesized in this research

	I (x=2, n=1, R=C_6H_5)	**II** (x=2, n=1, R=2-$CH_3C_6H_4$)	**III** (x=1, n=1, R=3-$CH_3C_6H_4$)	**III(excess ligand)** (x=2, n=1, R=3-$CH_3C_6H_4$)	**IV** (x=1, n=2, R=C_6H_4)
Crystal System	Monoclinic	Triclinic	Triclinic	Orthorhombic	Triclinic
Lattice Type	C-Centered	Primitive	Primitive	Primitive	Primitive
Space Group	C2/c (#15)	P-1 (#2)	P-1 (#2)	Pbcn (#60)	P-1 (#2)
Z value	8	2	2	8	2
Dcalc	1.506 g/cm^3	1.463 g/cm^3	1.596 g/cm^3	1.487 g/cm^3	1.548 g/cm^3
Rh1 - Rh2	2.4207(8) Å	2.4241(4) Å	2.4039(7) Å	2.4230(7) Å	2.4146(5) Å
N3 - C21	1.156(8) Å	1.133(5) Å	1.140(8) Å	1.130(8) Å	1.132(6) Å
N6 - C40	1.130(8) Å	1.137(5) Å	-	1.139(9) Å	1.129(8) Å
Rh1 - N3	2.199(5) Å	2.236(3) Å	2.160(5) Å	2.202(5) Å	2.182(3) Å
Rh2 - N6	2.238(5) Å	2.254(3) Å	-	2.247(5) Å	2.380(4) Å
Rh1 - N3 - C21	177.8 (5) ^{0}	151.6(3) ^{0}	166.3(4) ^{0}	177.7(5) ^{0}	166.8(3) ^{0}
Rh2 - N6 - C40	169.1 (6) ^{0}	152.5(3) ^{0}	-	165.7(5) ^{0}	127.7(3) ^{0}
Rh2 - Rh1 - N3	178.55(14) ^{0}	172.79(7) ^{0}	175.94(11) ^{0}	179.14(13) ^{0}	178.41(10) ^{0}
Rh1 - Rh2 - N6	177.51(14) ^{0}	174.59(6) ^{0}	-	177.47(13) ^{0}	175.39(11) ^{0}
O1 - Rh1 -Rh2 - N4	10.84(12) ^{0}	4.07(5) ^{0}	14.04(8) ^{0}	7.61(11) ^{0}	6.738) ^{0}
N1 - Rh1 - Rh2 - O3	12.71(15) ^{0}	6.78(7) ^{0}	12.55(11) ^{0}	10.80(13) ^{0}	4.31(8) ^{0}
N2 - Rh1 - Rh2 - O4	9.50(14) ^{0}	6.82(7) ^{0}	12.69(11) ^{0}	6.48(13) ^{0}	8.47(9) ^{0}
N5 - Rh1 - Rh2 - O2	11.26(13) ^{0}	4.79(5) ^{0}	13.28(8) ^{0}	8.44(11) ^{0}	6.99(10) ^{0}

Compounds **I** – **IV** were either monoclinic or triclinic. These are very low symmetry crystals systems with not too many symmetry operators. Compound I was C-centered belonging to C2/c space group only differs from compounds **II**, **III**, and **IV** which were primitive belonging to P-1 space group in that the C2/c space group has a 2-fold axis that is perpendicular to the c-face unlike P-1 that is just primitive and asymmetric. No atoms fall in special positions as these space groups are limited by symmetry. Hence, none of the atoms were as a result of symmetry.

During this research all compounds synthesized had Rh – Rh within 2.35 Å – 2.45 Å as seen in previously synthesized compounds of this type[25,36,37,43,44]. An expected C≡N ($C_{sp\ hybridized}$ – N) bond length is about 1.136 Å[41] and the C≡N bond lengths for the compounds synthesized did not differ much (1.129 Å – 1.156 Å). Niu and coworkers synthesized a series of acetates (see table 1.1) that showed C≡N bond lengths ranging from 1.122 Å – 1.140 Å. Each compound had dihedral angles around each acetamide bridge range from 4.07^0 to 14.04^0. Thus, these compounds can be slightly, to very highly sterically, strained around the dirhodium core.

Another steric effect usually imposed on the ring is due to the coordination of the axial ligand. Bent Rh – N – C bond angles ranging from 127.3^0 - 177.8^0 support evidence of this kind of steric strain on the ring imposed by the ligands attached to the axial site of the dirhodium complex. In compound **I**, these angles are close to linear (177.8^0 and 169.1^0) even though bent. This is because of no substituent on the nitrile ligand. In the case of compound **II** where the methyl substituent on the ligand is in ortho position, there is increased steric strain as the methyl group may come in contact with the phenyl ring of the N-phenylacetamide. As a result, the ligand in axial position is forced to bend away from the phenyl resulting in Rh – N – C bond angles as low as 151.6^0 and 152.3^0. Compounds **III** and **IV** are not affected as much as each second substituent on the ring is on the meta position. Thus, for compound **III**, there is not as

much steric strain in the axial positions and, hence, greater angles of 166.3^0. However, in compound **IV**, because the second nitrile coordinates to another tetrakis(N-phenylacetamidato) dirhodium(II) species, on the other end there is even a greater bend or deviation from the expected trend. For packing reasons, the second Rh – N – C bond angle is as low as 127.7^0 (severe angle strain) such that there is a solvent molecule incorporated into the lattice. Comparing the above compounds to those synthesized by Niu and coworkers, the bond angle decrease (greater bend) upon moving from straight chain solvents (acetone and methanol) to ring structured solvents (THF and benzene). Compounds **1** and **2** have the largest angles (178.1^0 and 177.8^0) while compound **3** has an angle of 168.7^0. Compound **4** has an even lower bond angle of 150.6^0. Niu suggested that due to the solvent trapped within the lattice, the electronic considerations maximize packing of the molecules causing this variation in Rh – N – C bond angles. In compound **4**, the benzene molecule packs parallel to the 1,4-dicyanobenzene ligand phenyl ring through π-π interactions causing the Rh – N – C angles not to be linear. In compound **3** also, the interactions of the lone pair electrons of the oxygen on the THF with the phenyl rings of the 1,4-dicyanobenzene ligand, causes these angles also not to be linear.

Comparing compounds **III** and **IV** to compound **I**, because of an almost linear alignment of the substituents in meta position, we see that the Rh – Rh – N bond angles are fairly close to 180^0. However, due to the position of the methyl substituent on the nitrile ligand (ortho position) in compound **II**, the Rh – Rh – N bond angle is not as linear (172.79^0) as expected due to steric constraints on one side. In comparison with the compounds by Niu and coworkers (see table 1), the Rh – Rh – N bond angles are nearly linear also with the exception of compound 5 that had a bond angle of 173.78^0 due to the presence of the solvent molecule in the lattice.

Conclusion

This research reports the first synthesis of a 1:1, tetrakis(N-phenylacetamidato) dirhodium(II) complex with a nitrile (Compound III). This indicates that not all axial sites have to be occupied in these dirhodium(II) complexes to allow for X-ray crystallographic determination. Thus, there is the possibility of mixed axial ligand species in the future and/or dirhodium(II) compounds where one axial site is blocked from catalysis and the other is available for catalysis.

Vapor diffusion was used to grow the X-ray quality crystals used for X-ray diffraction experiments. This method of crystal growth successfully grew crystals with dimensions as small as 0.1x0.1x0.1 mm. Even with the small sizes of the crystals, they still were able to give X-ray diffraction, integration, and structure solutions for these compounds. While X-ray quality crystals for compounds **I**, **II**, and **IV** were grown in dichloromethane, crystals for compound **III** were not of X-ray quality. These compounds were reduced to solid and redissolved in acetone. From this solution, X-ray quality crystals were grown.

All compounds synthesized here had Rh – Rh bond distances, 2.35 Å – 2.45 Å, within reported values for other published compounds with a dirhodium core.

The FT-IR spectra show an overall increase in the C≡N stretching frequency upon complexation of the nitrile with tetrakis(N-phenylacetamidato) dirhodium(II). Thus, although the presence of both σ and π back bonding is anticipated; it is observed that σ bonding prevails. This is, therefore, contrary to the predicted decrease that will occur as a result of π back bonding. Even though the FT-IR spectra suggest the overall presence of σ bonding, it is still proposed that due to the bent Rh – N – C angles, there exists some π-back bonding.[36] As one would expect the

Rh – N – C$_{(axial)}$ to be linear (180^0), X-ray crystallography shows bent angles ranging from 127.7^0 – 177.8^0. This means for severely strained Rh – N – C angles (127.7^0), there may be a possibility that the antibonding orbitals of the nitrile (oriented like p-orbitals) overlap with the filled orbitals on the rhodium metal forming a π-back bond.

X-ray crystallography also supports σ bonding in these systems via examination of the C≡N bond distance and the Rh – Rh – N bond angles. While there is evidence of π-back bonding, we cannot deny the fact that another interaction of the ligand with the rhodium metal is via σ bonding interactions. The C≡N bond distances are approximately 1.136 Å, an expected C≡N bond distance in crystalline compounds containing the C≡N.[45]   The Rh – Rh – N bond angles are nearly linear indicating that there is head-on interaction in the axial site by the nitrile with the rhodium atom through σ bonding.

After determining several crystal structures for these dirhodium(II) complexes, an analysis of these compounds can help us understand their potential applications in catalysis.

The nitrile adducts of *trans*-2,2-tetrakis[Rh$_2$(NPhCOCH$_3$)$_4$] were synthesized with benzonitrile, o-tolunitrile, m-tolunitrile, and mono substituted as well as disubstituted products were formed. A nitrile adduct of 3,1-tetrakis[Rh$_2$(NPhCOCH$_3$)$_4$] was also synthesized with 1,3-dicyanobenzene and a straight chained polymer was observed with coordination in the more sterically strained and less sterically strained "3" and "1" sides.

It was shown that more than one 3,1-tetrakis(N-phenylacetamidato) dirhodium(II) can be linked by 1,3-dicyanobenzene. It was shown that depending on the ligand used to react in the axial site of the tetrakis(N-phenylacetamidato) dirhodium(II), it can form mono-substituted adducts (as seen in Compound **III**), di-substituted adducts (as seen in Compound **II**), or can even

bridge more than one dirhodium(II) compound together into a polymer (as seen in Compound

IV). By manipulating the bulk around the ligand, predictions can be made to achieve a dimer of

dirhodium(II) complexes. The compounds synthesized here show variety in bond distances, bond

angles, and strain that can be very indicative of the rich chemistry this research can afford.

REFERENCES

1. Clark, G. L. *Applied X-rays*; 4th ed.; McGraw-Hill Book Company, Inc, New York, 1955.

2. Partington, J.R. *A History of Chemistry*; Ed.; McGraw-Hill Book Company, Inc, New York, 1931; Vol. 4

3. Lipson, L.S. *Crystals and X-rays*; Wykeham Publications LTD, London, 1970.

4. Hammond, C. *Introduction to Crystallography;* Oxford Science Publications, New York, 1990.

5. Sands, D. E. *Introduction to Crystallography;* Dover Publications, Inc; Mineola, NY, 1994; pp 88, 89.

6. USGS Coastal and Marine Geology program, http://pubs.usgs.gov/of/2001/of01-041/htmldocs/images/beam.jpg (accessed March 12, 2013).

7. *The Hutchinson dictionary of scientific biography*; Helicon Pub., Abingdon, Oxon, c2004.

8. Cotton, F. A.; Murillo, C. A.; Walton, R. A. *Multiple Bonds between Metal Atoms*, 3rd ed.; Springer Science and Business Media, Inc, New York, 2005; 14, 467, 506, 592, 606.

9. Cotton, F. A.; Hillard, E. A.; Murillo, C. A. The First Dirhodium Tetracarboxylate Molecule without Axial Ligation: New Insight into the Electronic Structures of Molecules with Importance in Catalysis and Other Reactions. *J. Am. Chem. Soc.* **2002**, *124*(20), 5658-5660.

10. Ezerskaya, N. A.; Toropchenova, E. S.; Kubrakova, I. V.; Krasheninnikova, S. V.; Kudinova, T. F.; Fomina, T. A.; Kiseleva, I. N. Preparation of binuclear rhodium(II) tetraacetate (initial compound for the coulometric determination of rhodium) under the action of microwave radiation. *J. Anal. Chem.* **2000**, *55*(12), 1132-1135.

11. Legzdins, P.; Mitchell, R. W.; Rempel, G. L.; Ruddick, J. D.; Wilkinson, G. Protonation of ruthenium- and rhodium-bridged carboxyllates and their uses homogeneous hydrogenation catalysts for unsaturated substances. *J. Chem. Soc. A* **1970**, (19), 3322-3326.

12. Doyle, M. P.; Bagheri, V.; Wandless, T. J.; Harn, N. K.; Brinker, D. A.; Eagle, C. T.; Loh, K. L. Exceptionally high trans (anti) stereoselectivity in catalytic cyclopropanation reactions. *J. Am. Chem. Soc*. **1990**, *112*(5), 1906-1912.

13. Eagle, C. T.; Farrar, D. G.; Holder, G. N.; Pennington, W. T.; Bailey, R. D. Structural and electronic properties of (2,2-trans)-dirhodium(II) tetrakis(N-phenylacetamidate). *J. Organomet. Chem.* **2000**, *596*(1-2) 90-94.

14. Duncan, J.; Malinski, T.; Zhu, T.; Hu, Z. S.; Kadish, K. M.; Bear, J. L. Characterization of novel rhodium(II) dimers with N-phenylacetamido bridging ligands. *J. Am Chem. Soc.* **1982**, *104*(20), 5507-5509.

15. Bear, J. L.; Zhu, T. P.; Malinski, T.; Dennis, A, M.; Kadish, K. M. Electrochemical characterization of a rhodium(II) dimer with N-phenylacetamido bridging ligands. *Inorg. Chem.* **1984**, *23*(6), 674-678.

16. Doyle, M. P.; Zhou, Q. L.; Raab, C. E.; Roos, G. H. P.; Simonsen, S. H.; Lynch, V. Synthesis and Structures of (2,2-cis)-Dirhodium(II) Tetrakis[methyl 1-acyl-2-oxoimidazolidine-4(S)-carboxylates]. Chiral Catalysts for Highly Stereoselective Metal Carbene Transformations. *Inorg. Chem.* **1996**, *35*(21), 6064-6073.

17. Doyle, M. P.; Zhou, Q. L.; Raab, C. E.; Roos, G. H. P.; Lynch, V.; Simonsen, S. H. (4,0)-Dirhodium(II) tetrakis[methyl 1-acetyl-2-oxoimidazolidine-4(S)-carboxylate]. Implications for the mechanism of ligand exchange reactions. *Inorg. Chim. Acta.* **1997**, *266*(1), 13-18.

18. Zhu, T. P.; Ahsan, M. Q.; Malinski, T.; Kadish, K. M.; Bear, J. L. Electrochemical studies of a series of dirhodium(II) complexes with acetate and acetamidate bridging ligands. *Inorg. Chem.* **1984**, *23*(1), 2-3.

19. Ahsan, M. Q.; Bernal, I.; Bear, John L. Reaction of tetrakis(acetato)dirhodium with acetamide: crystal and molecular structure of tetrakis(acetamido)diaquadirhodium trihydrate. *Inorg. Chem.* **1986**, *25*(3), 260-265.

20. Doyle, M. P.; McKervey, M. A.; Ye, T. *Modern Catalytic Methods for Organic Synthesis with Diazo Compounds*, John Wiley & Sons, Inc.: New York, 1998.

21. Doyle, M. P.; Ren, T. The influence of ligands on dirhodium(II) on reactivity and selectivity in metal carbene reactions. *Prog. Inorg. Chem.* **2001**, *49*, 113-168.

22. Timmons, D. J.; Doyle, M. P. Catalyst selection for metal carbene transformations. *J. Organometal. Chem.* **2001**, *617-618*, 98-104.

23. Eagle, C. T.; Farrar, D.; Holder, G. N.; Hatley, M. L.; Humphrey, S. L.; Olson, E. V.; Quintos, M.; Sadighi, J.; Wideman, T. cis-Enhanced cyclopropanation catalysts: reaction chemistry of three isomers of $Rh_2[N(C_6H_5)COCH_3]_4$. *Tetrahedron Lett.* **2003,** *44*(12), 2593-2595.

24. O'Malley, S.; Kodadek, T. Asymmetric cyclopropanation of alkenes catalyzed by a chiral wall porphyrin. *Tetrahedron Lett.* **1991**, *32*(22), 2445-2448.

25. Hoye, T. R.; Dinsmore, C. J.; Johnson, D. S.; Korkowski, P. F. Alkyne insertion reactions of metal-carbenes derived from enynyl-α-diazoketones [R'CN$_2$COCR$_2$CH$_2$C≡C(CH$_2$)$_n$-2CH:CH$_2$]. *J. Org. Chem,* **1990**, *55*(15), 4518-4520.

26. Doyle, M. P.; Devora, G. A.; Nefedov, A. O.; High, K. G. Addition/elimination in the rhodium(II) perfluorobutyrate catalyzed hydrosilylation of 1-alkenes. Rhodium hydride promoted isomerization and hydrogenation. *Organometallics* **1992**, *11*(2), 549-555.

27. Doyle, M. P.; High, K. G.; Nesloney, C. L.; Clayton, T. W., Jr; Lin, J. Rhodium(II) perfluorobutyrate catalyzed hydrosilylation of 1-alkynes. Trans addition and rearrangement to allylsilanes. *Organometallics* **1991**, *10*(5), 1225-1226.

28. Doyle, M. P.; High, K. G.; Bagheri, V.; Pieters, R. J.; Lewis, P. J.; Pearson, M. M. Rhodium(II) perfluorobutyrate catalyzed silane alcoholysis. A highly selective route to silyl ethers. *J. Org. Chem.* **1990**, *55*(25), 6082-6086.

29. Doyle, M. P.; Shanklin, M. S. Highly Regioselective and Stereoselective Silylformylation of Alkynes Under Mild Conditions Promoted by Dirhodium(II) Perfluorobutyrate. *Organometallics* **1994**, *13*(4), 1081-1088.

30. Doyle, M. P.; Phillips, I. M.; Hu, W. A New Class of Chiral Lewis Acid Catalysts for Highly Enantioselective Hetero-Diels-Alder Reactions: Exceptionally High Turnover Numbers from Dirhodium(II) Carboxamidates. *J. Am. Chem. Soc.* **2001**, *123*(22), 5366-5367.

31. Eagle, C. T.; Farrar, D. G.; Pfaff, C. U. π-Back-Bonding in Bis(isonitrile) Complexes of Rhodium(II) Acetate: Structural Analogs for Rhodium Carbenoids. *Organometallics* **1998**, *17*(20), 4523-4526.

32. Sargent, A. L.; Rollog, M. E.; Eagle, C. T. Electronic structure of axially ligated rhodium carboxylates. π back-bonding revisited. *Theor. Chem. Acc.*, **1997**, *9*(1-4), 283-288.

33. Chaven, M. Y.; Ashan, M. Q.; Lifsey, R. S.; Bear, J. L.; Kadish, K. M. Reversible carbon monoxide binding by Rh$_2$(O$_2$CCH$_3$)$_n$(HNOCCH$_3$)$_{4-n}$. A spectroscopic and electrochemical investigation. *Inorg. Chem.* **1986**, *25*(18), 3218-3223.

34. Eagle, C. T.; Farrar, D. G.; Pfaff, C. U.; Davies, J. A.; Kluwe, C.; Miller, L. π-Back-Bonding in Bis(isonitrile) Complexes of Rhodium(II) Acetate: Structural Analogs for Rhodium Carbenoids. *Organometallics* , **1998**, *17*(20), 4523-4526.

35. Niu, T.; Lu, J.; Crisci, G.; Jacobson, A. J. Syntheses and structural characterization of the one dimensional polymers: 1∞ [$Rh_2(OAc)_4(NCPhCN)\cdot S$]; S = CH_3COCH_3, CH_3OH, C_2H_5OH, C_4H_8O and C_6H_6. *Polyhedron*, *1998*, *17*(23-24), 4079-4089.

36. Azaroff, L. V. *Introduction to Solids*; McGraw-Hill Book Company, INC, New York, Toronto, London, 1960

37. CrystalClear: Pflugrath, J.W. The finer things in X-ray diffraction data collection. *Acta Cryst. D,* **1999**, *55*(10), 1718-1725.

38. CrystalStructure 4.0: Crystal Structure Analysis Package, Rigaku Corporation (2000-2010). Tokyo, Japan.

39. SHELX97: Sheldrick, G.M. A short history of SHELX. *Acta Cryst. A,* **2008**, *64*(1), 112-122.

40. Least Squares function minimized: (SHELXL97); $\sum w(Fo2 - Fc2)2$ where w = Least Squares weights.

41. Eagle, C.T.; Kpogo, K. K.; Zink, L.C.; Smith, A. E. Tetrakis[μ-N-(2,4,6-trimethylphenyl)acetamidato]-$\kappa 4N$:O;$\kappa 4$O:N-bis[(benzonitrile-κN)rhodium(II)](Rh-Rh). *Acta Cryst. E*, **2012**, *68*(7), m877.

42. Lifsey, R. S.; Lin, X. Q.; Chavan, M. Y.; Ahsan, M. Q.; Kadish, K. M.; Bear, J. L. Reaction of rhodium(II) acetate with N-phenylacetamide: substitution products and geometric isomers. *Inorg. Chem.* **1987**, *26*(6), 830-836.

43. Haynes W. M.; Lide D. R. Ed. *CRC Handbook of Chemistry and Physics;* 92nd ed.; New York, 2011-2012. p 9-8

APPENDIX A

SUPPLEMENTARY INFORMATION FOR **II**

EXPERIMENTAL DETAILS

A. Crystal Data

Empirical Formula	$C_{48}H_{46}N_6O_4Rh_2$
Formula Weight	976.74
Crystal Color, Habit	red, long block
Crystal Dimensions	0.330 X 0.120 X 0.120 mm
Crystal System	triclinic
Lattice Type	Primitive
Lattice Parameters	a = 9.7912(7) Å
	b = 14.787(1) Å
	c = 16.359(1) Å
	α = 103.837(7) ^{o}
	β = 99.173(7) ^{o}
	γ = 99.772(7) ^{o}
	V = 2216.4(3) Å^3
Space Group	P-1 (#2)
Z value	2
D_{calc}	1.463 g/cm^3
F_{000}	996.00
μ(MoKα)	7.932 cm^{-1}

B. Intensity Measurements

Diffractometer	XtaLAB mini
Radiation	MoKα ($\lambda = 0.71075$ Å)
	graphite monochromated
Voltage, Current	50kV, 12mA
Temperature	20.0°C
Detector Aperture	75 mm (diameter)
Data Images	540 exposures
ω oscillation Range	-60.0 - 120.0°
Exposure Rate	16.0 sec./°
Detector Swing Angle	29.50°
ω oscillation Range	-60.0 - 120.0°
Exposure Rate	16.0 sec./°
Detector Swing Angle	29.50°
ω oscillation Range	-60.0 - 120.0°
Exposure Rate	16.0 sec./°
Detector Swing Angle	29.50°
ω oscillation Range	-60.0 - 120.0°
Exposure Rate	16.0 sec./°
Detector Swing Angle	29.50°
ω oscillation Range	-60.0 - 120.0°
Exposure Rate	16.0 sec./°
Detector Swing Angle	29.50°

ω oscillation Range	-60.0 - 120.0^{o}

Exposure Rate   16.0 sec./^{o}

Detector Swing Angle   29.50^{o}

Detector Position   50.00 mm

Pixel Size   0.146 mm

$2\theta_{max}$ 55.0^{o}

No. of Reflections Measured   Total: 23557

                                       Unique: 10137 (R_{int} = 0.0386)

Corrections   Lorentz-polarization

                                        Absorption

                                        (trans. factors: 0.720 - 0.909)

C. Structure Solution and Refinement

Structure Solution   Direct Methods

Refinement   Full-matrix least-squares on F^2

Function Minimized $\Sigma \, w \, (Fo^2 - Fc^2)^2$

Least Squares Weights $w = 1/ [\, \sigma^2(Fo^2) + (0.0257 \cdot P)^2$

                                        $+ 1.5457 \cdot P\,]$

                                        where $P = (Max(Fo^2,0) + 2Fc^2)/3$

$2\theta_{max}$ cutoff   55.0^{o}

Anomalous Dispersion   All non-hydrogen atoms

No. Observations (All reflections)   10137

No. Variables   547

Reflection/Parameter Ratio   18.53

Residuals: R1 (I>2.00σ(I))   0.0368

Residuals: R (All reflections)		0.0541		
Residuals: wR2 (All reflections)		0.0789		
Goodness of Fit Indicator		1.038		
Max Shift/Error in Final Cycle		0.002		
Maximum peak in Final Diff. Map		0.62 e$^-$/Å^3		
Minimum peak in Final Diff. Map		-0.51 e$^-$/Å^3		

Table 1. Atomic coordinates and B_{iso}/B_{eq}

atom	x	y	z	B_{eq}
Rh(1)	1.01287(2)	0.20909(2)	0.80783(2)	1.826(5)
Rh(2)	0.99761(2)	0.27462(2)	0.68511(2)	1.874(5)
O(1)	1.1252(2)	0.1166(2)	0.7524(2)	2.31(4)
O(2)	0.9034(3)	0.3026(2)	0.8638(2)	2.77(4)
O(3)	1.1707(2)	0.3798(2)	0.7488(2)	2.48(4)
O(4)	0.8259(2)	0.1692(2)	0.6218(2)	2.53(4)
N(1)	1.2007(3)	0.3089(2)	0.8577(2)	2.22(4)
N(2)	0.8227(3)	0.1166(2)	0.7420(2)	2.18(4)
N(3)	1.0082(3)	0.1600(2)	0.9267(2)	2.51(5)
N(4)	1.1241(3)	0.1848(2)	0.6416(2)	2.16(4)
N(5)	0.8720(3)	0.3571(2)	0.7447(2)	2.51(5)
N(6)	0.9624(3)	0.3271(2)	0.5666(2)	2.69(5)
C(1)	1.2406(3)	0.3749(2)	0.8200(2)	2.40(5)
C(2)	1.3725(4)	0.4523(3)	0.8583(3)	3.85(7)
C(3)	0.7702(3)	0.1132(2)	0.6622(2)	2.41(5)
C(4)	0.6393(4)	0.0417(3)	0.6085(2)	3.49(7)
C(5)	1.1626(3)	0.1240(2)	0.6823(2)	2.21(5)

C(6)	1.2568(4)	0.0586(3)	0.6509(2)	3.22(6)
C(7)	0.8534(4)	0.3571(2)	0.8218(2)	2.77(6)
C(8)	0.7708(5)	0.4210(3)	0.8705(3)	4.54(9)
C(9)	1.2896(3)	0.3022(2)	0.9327(2)	2.37(5)
C(10)	1.4003(4)	0.2568(3)	0.9263(3)	3.72(7)
C(11)	1.4856(5)	0.2479(3)	0.9991(3)	4.83(9)
C(12)	1.4571(5)	0.2835(3)	1.0785(3)	4.70(9)
C(13)	1.3473(5)	0.3290(3)	1.0857(3)	4.17(8)
C(14)	1.2626(4)	0.3381(3)	1.0133(2)	3.25(6)
C(15)	0.7454(3)	0.0593(2)	0.7849(2)	2.42(5)
C(16)	0.7892(4)	-0.0200(2)	0.8014(2)	2.93(6)
C(17)	0.7152(4)	-0.0741(3)	0.8457(3)	4.02(7)
C(18)	0.5991(5)	-0.0483(3)	0.8741(3)	4.82(9)
C(19)	0.5560(4)	0.0306(3)	0.8590(3)	4.93(9)
C(20)	0.6296(4)	0.0852(3)	0.8156(3)	3.57(7)
C(21)	0.9643(3)	0.1564(2)	0.9861(2)	2.52(5)
C(22)	0.9072(4)	0.1529(3)	1.0620(2)	2.72(6)
C(23)	0.8885(4)	0.0686(3)	1.0857(3)	3.60(7)
C(24)	0.8369(4)	0.0646(3)	1.1588(3)	4.39(8)
C(25)	0.8049(5)	0.1447(4)	1.2067(3)	4.87(9)
C(26)	0.8222(4)	0.2281(3)	1.1829(3)	4.33(8)
C(27)	0.8739(4)	0.2347(3)	1.1099(2)	3.33(6)
C(28)	1.1614(3)	0.1857(2)	0.5609(2)	2.34(5)
C(29)	1.0725(4)	0.1283(3)	0.4856(2)	3.67(7)
C(30)	1.1042(5)	0.1310(3)	0.4068(3)	4.74(9)

C(31)	1.2234(5)	0.1921(3)	0.4025(3)	4.50(8)
C(32)	1.3119(5)	0.2491(3)	0.4771(3)	4.26(8)
C(33)	1.2809(4)	0.2465(3)	0.5562(2)	3.29(6)
C(34)	0.8123(4)	0.4202(2)	0.7027(2)	2.76(6)
C(35)	0.6725(4)	0.3946(3)	0.6589(3)	3.92(7)
C(36)	0.6154(5)	0.4555(3)	0.6174(3)	5.2(1)
C(37)	0.6983(5)	0.5406(3)	0.6186(3)	5.3(1)
C(38)	0.8372(5)	0.5652(3)	0.6605(3)	5.00(9)
C(39)	0.8955(4)	0.5051(3)	0.7022(3)	3.61(7)
C(40)	0.8918(4)	0.3379(2)	0.5090(2)	2.62(6)
C(41)	0.7953(3)	0.3515(2)	0.4392(2)	2.51(5)
C(42)	0.6750(3)	0.2806(2)	0.3979(2)	2.65(6)
C(43)	0.5801(4)	0.2994(3)	0.3338(2)	3.34(7)
C(44)	0.6058(4)	0.3844(3)	0.3127(2)	3.46(7)
C(45)	0.7254(4)	0.4533(3)	0.3527(2)	3.48(7)
C(46)	0.8207(4)	0.4368(3)	0.4165(2)	3.45(7)
C(47)	0.8930(5)	0.3266(3)	1.0843(3)	4.77(9)
C(48)	0.6476(4)	0.1880(3)	0.4222(3)	4.34(8)

$B_{eq} = 8/3\ \pi^2(U_{11}(aa^*)^2 + U_{22}(bb^*)^2 + U_{33}(cc^*)^2 + 2U_{12}(aa^*bb^*)\cos \gamma + 2U_{13}(aa^*cc^*)\cos \beta + 2U_{23}(bb^*cc^*)\cos \alpha)$

Table 2. Anisotropic displacement parameters

atom	U_{11}	U_{22}	U_{33}	U_{12}	U_{13}	U_{23}
Rh(1)	0.0239(2)	0.0247(1)	0.0226(2)	0.00461(9)	0.00514(9)	0.01014(9)
Rh(2)	0.0228(2)	0.0264(2)	0.0247(2)	0.00586(9)	0.00424(9)	0.01214(9)
O(1)	0.034(1)	0.032(1)	0.028(1)	0.0117(9)	0.0094(9)	0.0157(9)
O(2)	0.043(2)	0.039(2)	0.032(2)	0.017(1)	0.015(1)	0.015(1)
O(3)	0.030(1)	0.030(1)	0.033(2)	-0.0005(9)	-0.0001(9)	0.0156(9)
O(4)	0.029(1)	0.038(2)	0.028(1)	-0.0006(9)	0.0017(9)	0.0147(9)
N(1)	0.026(2)	0.029(2)	0.029(2)	0.005(1)	0.002(1)	0.010(1)
N(2)	0.023(2)	0.029(2)	0.031(2)	-0.000(1)	0.004(1)	0.011(1)
N(3)	0.039(2)	0.031(2)	0.025(2)	0.005(2)	0.007(2)	0.011(1)
N(4)	0.027(2)	0.030(2)	0.030(2)	0.008(1)	0.008(1)	0.013(1)
N(5)	0.030(2)	0.034(2)	0.036(2)	0.013(1)	0.009(1)	0.013(1)
N(6)	0.035(2)	0.036(2)	0.033(2)	0.008(2)	0.003(2)	0.015(2)
C(1)	0.027(2)	0.030(2)	0.033(2)	0.003(2)	0.003(2)	0.011(2)
C(2)	0.039(2)	0.045(2)	0.056(3)	-0.009(2)	-0.007(2)	0.025(2)
C(3)	0.027(2)	0.031(2)	0.034(2)	0.006(2)	0.006(2)	0.010(2)
C(4)	0.036(2)	0.048(2)	0.040(2)	-0.006(2)	-0.002(2)	0.011(2)
C(5)	0.026(2)	0.030(2)	0.029(2)	0.005(2)	0.004(2)	0.011(2)
C(6)	0.045(2)	0.048(2)	0.042(2)	0.024(2)	0.019(2)	0.020(2)
C(7)	0.036(2)	0.034(2)	0.038(2)	0.012(2)	0.011(2)	0.011(2)
C(8)	0.073(3)	0.062(3)	0.057(3)	0.040(3)	0.034(2)	0.021(2)
C(9)	0.030(2)	0.026(2)	0.030(2)	0.002(2)	-0.003(2)	0.010(2)
C(10)	0.045(2)	0.055(3)	0.039(2)	0.022(2)	-0.003(2)	0.009(2)
C(11)	0.061(3)	0.059(3)	0.056(3)	0.031(2)	-0.017(2)	0.008(2)

C(12)	0.073(3)	0.044(2)	0.044(3)	0.003(2)	-0.026(2)	0.011(2)
C(13)	0.067(3)	0.052(3)	0.028(2)	0.001(2)	-0.002(2)	0.005(2)
C(14)	0.040(2)	0.042(2)	0.033(2)	0.003(2)	0.001(2)	0.005(2)
C(15)	0.030(2)	0.029(2)	0.029(2)	-0.002(2)	0.005(2)	0.007(2)
C(16)	0.039(2)	0.035(2)	0.037(2)	0.005(2)	0.010(2)	0.011(2)
C(17)	0.063(3)	0.039(2)	0.050(3)	0.002(2)	0.006(2)	0.021(2)
C(18)	0.069(3)	0.057(3)	0.057(3)	-0.011(2)	0.027(3)	0.024(2)
C(19)	0.054(3)	0.061(3)	0.079(3)	0.002(2)	0.041(3)	0.020(3)
C(20)	0.040(2)	0.041(2)	0.061(3)	0.008(2)	0.022(2)	0.018(2)
C(21)	0.037(2)	0.029(2)	0.030(2)	0.008(2)	0.003(2)	0.010(2)
C(22)	0.036(2)	0.042(2)	0.030(2)	0.010(2)	0.010(2)	0.016(2)
C(23)	0.051(2)	0.053(2)	0.049(2)	0.024(2)	0.022(2)	0.028(2)
C(24)	0.060(3)	0.074(3)	0.058(3)	0.026(3)	0.030(2)	0.045(3)
C(25)	0.070(3)	0.090(3)	0.049(3)	0.031(3)	0.036(2)	0.039(3)
C(26)	0.064(3)	0.068(3)	0.043(2)	0.027(2)	0.027(2)	0.015(2)
C(27)	0.042(2)	0.052(2)	0.036(2)	0.011(2)	0.010(2)	0.015(2)
C(28)	0.035(2)	0.030(2)	0.031(2)	0.013(2)	0.013(2)	0.013(2)
C(29)	0.044(2)	0.059(3)	0.034(2)	0.000(2)	0.012(2)	0.012(2)
C(30)	0.067(3)	0.078(3)	0.029(2)	0.005(3)	0.010(2)	0.011(2)
C(31)	0.083(3)	0.063(3)	0.040(2)	0.022(3)	0.035(3)	0.023(2)
C(32)	0.068(3)	0.044(2)	0.057(3)	0.004(2)	0.035(2)	0.019(2)
C(33)	0.044(2)	0.041(2)	0.039(2)	0.002(2)	0.014(2)	0.010(2)
C(34)	0.039(2)	0.036(2)	0.037(2)	0.016(2)	0.011(2)	0.015(2)
C(35)	0.040(2)	0.044(2)	0.065(3)	0.012(2)	0.002(2)	0.021(2)
C(36)	0.057(3)	0.068(3)	0.077(3)	0.032(3)	-0.004(3)	0.025(3)

C(37)	0.079(3)	0.068(3)	0.078(3)	0.046(3)	0.018(3)	0.039(3)
C(38)	0.070(3)	0.044(3)	0.094(4)	0.023(2)	0.029(3)	0.037(3)
C(39)	0.043(2)	0.036(2)	0.061(3)	0.010(2)	0.011(2)	0.018(2)
C(40)	0.034(2)	0.032(2)	0.037(2)	0.006(2)	0.008(2)	0.016(2)
C(41)	0.035(2)	0.036(2)	0.027(2)	0.010(2)	0.004(2)	0.014(2)
C(42)	0.035(2)	0.035(2)	0.031(2)	0.007(2)	0.008(2)	0.009(2)
C(43)	0.030(2)	0.054(2)	0.034(2)	0.003(2)	-0.002(2)	0.005(2)
C(44)	0.044(2)	0.060(3)	0.032(2)	0.020(2)	0.002(2)	0.019(2)
C(45)	0.049(2)	0.045(2)	0.042(2)	0.011(2)	0.001(2)	0.025(2)
C(46)	0.040(2)	0.043(2)	0.043(2)	-0.004(2)	-0.007(2)	0.022(2)
C(47)	0.085(3)	0.046(3)	0.059(3)	0.019(3)	0.033(3)	0.016(2)
C(48)	0.060(3)	0.037(2)	0.064(3)	0.001(2)	0.008(2)	0.019(2)

The general temperature factor expression: $\exp(-2\pi^2(a*^2U_{11}h^2 + b*^2U_{22}k^2 + c*^2U_{33}l^2 + 2a*b*U_{12}hk + 2a*c*U_{13}hl + 2b*c*U_{23}kl))$

Table 3. Bond lengths (Å)

atom	atom	distance	atom	atom	distance
Rh(1)	Rh(2)	2.4241(4)	Rh(1)	O(1)	2.034(2)
Rh(1)	O(2)	2.028(3)	Rh(1)	N(1)	2.061(2)
Rh(1)	N(2)	2.071(2)	Rh(1)	N(3)	2.236(3)
Rh(2)	O(3)	2.0358(17)	Rh(2)	O(4)	2.0279(17)
Rh(2)	N(4)	2.048(3)	Rh(2)	N(5)	2.067(3)
Rh(2)	N(6)	2.254(3)	O(1)	C(5)	1.282(4)
O(2)	C(7)	1.285(5)	O(3)	C(1)	1.278(4)
O(4)	C(3)	1.281(4)	N(1)	C(1)	1.313(5)
N(1)	C(9)	1.421(4)	N(2)	C(3)	1.311(4)
N(2)	C(15)	1.422(4)	N(3)	C(21)	1.133(5)
N(4)	C(5)	1.309(5)	N(4)	C(28)	1.427(4)
N(5)	C(7)	1.302(5)	N(5)	C(34)	1.431(5)
N(6)	C(40)	1.137(5)	C(1)	C(2)	1.506(4)
C(3)	C(4)	1.506(4)	C(5)	C(6)	1.506(5)
C(7)	C(8)	1.512(6)	C(9)	C(10)	1.374(5)
C(9)	C(14)	1.384(5)	C(10)	C(11)	1.388(6)
C(11)	C(12)	1.372(6)	C(12)	C(13)	1.368(7)
C(13)	C(14)	1.382(5)	C(15)	C(16)	1.385(5)
C(15)	C(20)	1.386(5)	C(16)	C(17)	1.391(6)
C(17)	C(18)	1.372(7)	C(18)	C(19)	1.370(7)
C(19)	C(20)	1.385(6)	C(21)	C(22)	1.449(5)
C(22)	C(23)	1.383(6)	C(22)	C(27)	1.395(5)
C(23)	C(24)	1.381(6)	C(24)	C(25)	1.369(6)

C(25)	C(26)	1.371(7)		C(26)	C(27)	1.388(6)
C(27)	C(47)	1.506(6)		C(28)	C(29)	1.380(4)
C(28)	C(33)	1.375(5)		C(29)	C(30)	1.380(6)
C(30)	C(31)	1.372(6)		C(31)	C(32)	1.369(5)
C(32)	C(33)	1.383(6)		C(34)	C(35)	1.382(5)
C(34)	C(39)	1.378(5)		C(35)	C(36)	1.388(7)
C(36)	C(37)	1.370(7)		C(37)	C(38)	1.367(6)
C(38)	C(39)	1.386(7)		C(40)	C(41)	1.437(5)
C(41)	C(42)	1.390(4)		C(41)	C(46)	1.393(5)
C(42)	C(43)	1.399(5)		C(42)	C(48)	1.507(5)
C(43)	C(44)	1.375(6)		C(44)	C(45)	1.367(5)
C(45)	C(46)	1.381(5)				

Table 4. Bond angles (º)

atom	atom	atom	angle	atom	atom	atom	angle
Rh(2)	Rh(1)	O(1)	90.04(7)	Rh(2)	Rh(1)	O(2)	89.97(7)
Rh(2)	Rh(1)	N(1)	85.65(8)	Rh(2)	Rh(1)	N(2)	85.90(8)
Rh(2)	Rh(1)	N(3)	172.79(7)	O(1)	Rh(1)	O(2)	179.24(7)
O(1)	Rh(1)	N(1)	88.29(9)	O(1)	Rh(1)	N(2)	91.45(9)
O(1)	Rh(1)	N(3)	97.10(10)	O(2)	Rh(1)	N(1)	90.95(9)
O(2)	Rh(1)	N(2)	89.31(9)	O(2)	Rh(1)	N(3)	82.90(10)
N(1)	Rh(1)	N(2)	171.55(11)	N(1)	Rh(1)	N(3)	95.47(10)
N(2)	Rh(1)	N(3)	92.95(10)	Rh(1)	Rh(2)	O(3)	89.96(7)
Rh(1)	Rh(2)	O(4)	89.82(7)	Rh(1)	Rh(2)	N(4)	85.66(8)
Rh(1)	Rh(2)	N(5)	85.77(8)	Rh(1)	Rh(2)	N(6)	174.59(6)
O(3)	Rh(2)	O(4)	179.63(9)	O(3)	Rh(2)	N(4)	90.99(8)

O(3)	Rh(2)	N(5)	88.95(9)	O(3)	Rh(2)	N(6)	95.24(9)
O(4)	Rh(2)	N(4)	88.69(8)	O(4)	Rh(2)	N(5)	91.33(9)
O(4)	Rh(2)	N(6)	84.98(9)	N(4)	Rh(2)	N(5)	171.43(11)
N(4)	Rh(2)	N(6)	95.71(10)	N(5)	Rh(2)	N(6)	92.83(11)
Rh(1)	O(1)	C(5)	118.8(2)	Rh(1)	O(2)	C(7)	119.3(2)
Rh(2)	O(3)	C(1)	118.88(19)	Rh(2)	O(4)	C(3)	119.30(16)
Rh(1)	N(1)	C(1)	121.43(19)	Rh(1)	N(1)	C(9)	118.18(19)
C(1)	N(1)	C(9)	120.3(3)	Rh(1)	N(2)	C(3)	120.6(2)
Rh(1)	N(2)	C(15)	119.70(17)	C(3)	N(2)	C(15)	119.6(3)
Rh(1)	N(3)	C(21)	151.6(3)	Rh(2)	N(4)	C(5)	122.2(2)
Rh(2)	N(4)	C(28)	117.2(2)	C(5)	N(4)	C(28)	120.4(3)
Rh(2)	N(5)	C(7)	121.3(3)	Rh(2)	N(5)	C(34)	119.1(2)
C(7)	N(5)	C(34)	119.4(3)	Rh(2)	N(6)	C(40)	152.5(3)
O(3)	C(1)	N(1)	123.2(3)	O(3)	C(1)	C(2)	114.5(3)
N(1)	C(1)	C(2)	122.3(3)	O(4)	C(3)	N(2)	123.5(3)
O(4)	C(3)	C(4)	113.5(3)	N(2)	C(3)	C(4)	123.0(3)
O(1)	C(5)	N(4)	122.9(3)	O(1)	C(5)	C(6)	114.8(3)
N(4)	C(5)	C(6)	122.3(3)	O(2)	C(7)	N(5)	123.3(3)
O(2)	C(7)	C(8)	113.5(3)	N(5)	C(7)	C(8)	123.3(4)
N(1)	C(9)	C(10)	120.7(3)	N(1)	C(9)	C(14)	120.4(3)
C(10)	C(9)	C(14)	118.8(3)	C(9)	C(10)	C(11)	121.1(4)
C(10)	C(11)	C(12)	119.4(4)	C(11)	C(12)	C(13)	120.0(4)
C(12)	C(13)	C(14)	120.6(4)	C(9)	C(14)	C(13)	120.1(4)
N(2)	C(15)	C(16)	120.8(3)	N(2)	C(15)	C(20)	120.3(3)
C(16)	C(15)	C(20)	118.8(4)	C(15)	C(16)	C(17)	120.3(4)

C(16)	C(17)	C(18)	120.1(4)	C(17)	C(18)	C(19)	120.0(5)
C(18)	C(19)	C(20)	120.3(4)	C(15)	C(20)	C(19)	120.5(4)
N(3)	C(21)	C(22)	179.3(4)	C(21)	C(22)	C(23)	119.1(3)
C(21)	C(22)	C(27)	119.3(4)	C(23)	C(22)	C(27)	121.6(4)
C(22)	C(23)	C(24)	119.8(4)	C(23)	C(24)	C(25)	119.1(5)
C(24)	C(25)	C(26)	121.2(4)	C(25)	C(26)	C(27)	121.3(4)
C(22)	C(27)	C(26)	117.0(4)	C(22)	C(27)	C(47)	122.0(4)
C(26)	C(27)	C(47)	121.0(4)	N(4)	C(28)	C(29)	119.8(3)
N(4)	C(28)	C(33)	121.3(3)	C(29)	C(28)	C(33)	118.9(3)
C(28)	C(29)	C(30)	120.6(4)	C(29)	C(30)	C(31)	120.3(3)
C(30)	C(31)	C(32)	119.4(4)	C(31)	C(32)	C(33)	120.5(4)
C(28)	C(33)	C(32)	120.4(3)	N(5)	C(34)	C(35)	120.4(3)
N(5)	C(34)	C(39)	120.2(3)	C(35)	C(34)	C(39)	119.4(4)
C(34)	C(35)	C(36)	120.2(4)	C(35)	C(36)	C(37)	120.0(4)
C(36)	C(37)	C(38)	119.9(5)	C(37)	C(38)	C(39)	120.7(4)
C(34)	C(39)	C(38)	119.8(4)	N(6)	C(40)	C(41)	176.2(4)
C(40)	C(41)	C(42)	119.2(3)	C(40)	C(41)	C(46)	119.6(3)
C(42)	C(41)	C(46)	121.1(3)	C(41)	C(42)	C(43)	117.1(3)
C(41)	C(42)	C(48)	121.2(3)	C(43)	C(42)	C(48)	121.7(3)
C(42)	C(43)	C(44)	121.1(3)	C(43)	C(44)	C(45)	121.5(4)
C(44)	C(45)	C(46)	118.6(4)	C(41)	C(46)	C(45)	120.5(3)

Table 5. Torsion Angles(^{o})

(Those having bond angles > 160 or < 20 degrees are excluded.)

atom1	atom2	atom3	atom4	angle	atom1	atom2	atom3	atom4	angle
Rh(2)	Rh(1)	O(1)	C(5)	5.81(11)	O(1)	Rh(1)	Rh(2)	O(3)	-95.07(5)

O(1)	Rh(1)	Rh(2)	O(4)	84.63(5)	O(1)	Rh(1)	Rh(2)	N(4)	-4.07(5)
O(1)	Rh(1)	Rh(2)	N(5)	175.98(5)	Rh(2)	Rh(1)	O(2)	C(7)	5.09(13)
O(2)	Rh(1)	Rh(2)	O(3)	84.17(6)	O(2)	Rh(1)	Rh(2)	O(4)	-96.13(6)
O(2)	Rh(1)	Rh(2)	N(4)	175.16(5)	O(2)	Rh(1)	Rh(2)	N(5)	-4.79(5)
Rh(2)	Rh(1)	N(1)	C(1)	7.59(17)	Rh(2)	Rh(1)	N(1)	C(9)	-169.94(16)
N(1)	Rh(1)	Rh(2)	O(3)	-6.78(7)	N(1)	Rh(1)	Rh(2)	O(4)	172.92(7)
N(1)	Rh(1)	Rh(2)	N(4)	84.21(7)	N(1)	Rh(1)	Rh(2)	N(5)	-95.74(7)
Rh(2)	Rh(1)	N(2)	C(3)	8.12(16)	Rh(2)	Rh(1)	N(2)	C(15)	-169.14(16)
N(2)	Rh(1)	Rh(2)	O(3)	173.48(7)	N(2)	Rh(1)	Rh(2)	O(4)	-6.82(7)
N(2)	Rh(1)	Rh(2)	N(4)	-95.53(7)	N(2)	Rh(1)	Rh(2)	N(5)	84.53(7)
O(1)	Rh(1)	N(1)	C(1)	97.76(18)	O(1)	Rh(1)	N(1)	C(9)	-79.77(16)
N(1)	Rh(1)	O(1)	C(5)	-79.84(13)	O(1)	Rh(1)	N(2)	C(3)	-81.82(18)
O(1)	Rh(1)	N(2)	C(15)	100.92(17)	N(2)	Rh(1)	O(1)	C(5)	91.71(13)
O(1)	Rh(1)	N(3)	C(21)	-164.3(4)	N(3)	Rh(1)	O(1)	C(5)	-175.14(12)
O(2)	Rh(1)	N(1)	C(1)	-82.30(18)	O(2)	Rh(1)	N(1)	C(9)	100.16(17)
N(1)	Rh(1)	O(2)	C(7)	90.74(15)	O(2)	Rh(1)	N(2)	C(3)	98.14(18)
O(2)	Rh(1)	N(2)	C(15)	-79.12(17)	N(2)	Rh(1)	O(2)	C(7)	-80.81(15)
O(2)	Rh(1)	N(3)	C(21)	16.4(4)	N(3)	Rh(1)	O(2)	C(7)	-173.86(14)
N(1)	Rh(1)	N(3)	C(21)	106.7(4)	N(3)	Rh(1)	N(1)	C(1)	-165.26(18)
N(3)	Rh(1)	N(1)	C(9)	17.21(17)	N(2)	Rh(1)	N(3)	C(21)	-72.5(4)
N(3)	Rh(1)	N(2)	C(3)	-179.01(18)	N(3)	Rh(1)	N(2)	C(15)	3.73(17)
Rh(1)	Rh(2)	O(3)	C(1)	8.56(14)	Rh(1)	Rh(2)	O(4)	C(3)	8.06(15)
Rh(1)	Rh(2)	N(4)	C(5)	3.89(13)	Rh(1)	Rh(2)	N(4)	C(28)	179.46(12)
Rh(1)	Rh(2)	N(5)	C(7)	6.31(14)	Rh(1)	Rh(2)	N(5)	C(34)	-177.96(13)
O(3)	Rh(2)	N(4)	C(5)	93.78(15)	O(3)	Rh(2)	N(4)	C(28)	-90.65(13)

N(4)	Rh(2)	O(3)	C(1)	-77.10(16)	O(3)	Rh(2)	N(5)	C(7)	-83.72(16)
O(3)	Rh(2)	N(5)	C(34)	92.01(15)	N(5)	Rh(2)	O(3)	C(1)	94.32(16)
O(3)	Rh(2)	N(6)	C(40)	-147.8(4)	N(6)	Rh(2)	O(3)	C(1)	-172.93(15)
O(4)	Rh(2)	N(4)	C(5)	-86.03(15)	O(4)	Rh(2)	N(4)	C(28)	89.54(13)
N(4)	Rh(2)	O(4)	C(3)	93.73(17)	O(4)	Rh(2)	N(5)	C(7)	96.04(16)
O(4)	Rh(2)	N(5)	C(34)	-88.24(15)	N(5)	Rh(2)	O(4)	C(3)	-77.70(17)
O(4)	Rh(2)	N(6)	C(40)	32.5(4)	N(6)	Rh(2)	O(4)	C(3)	-170.42(17)
N(4)	Rh(2)	N(6)	C(40)	120.7(4)	N(6)	Rh(2)	N(4)	C(5)	-170.86(14)
N(6)	Rh(2)	N(4)	C(28)	4.72(13)	N(5)	Rh(2)	N(6)	C(40)	-58.6(4)
N(6)	Rh(2)	N(5)	C(7)	-178.92(15)	N(6)	Rh(2)	N(5)	C(34)	-3.19(14)
Rh(1)	O(1)	C(5)	N(4)	-4.5(3)	Rh(1)	O(1)	C(5)	C(6)	174.46(11)
Rh(1)	O(2)	C(7)	N(5)	-1.6(4)	Rh(1)	O(2)	C(7)	C(8)	178.38(12)
Rh(2)	O(3)	C(1)	N(1)	-5.1(4)	Rh(2)	O(3)	C(1)	C(2)	175.66(14)
Rh(2)	O(4)	C(3)	N(2)	-4.0(4)	Rh(2)	O(4)	C(3)	C(4)	177.07(14)
Rh(1)	N(1)	C(1)	O(3)	-3.2(4)	Rh(1)	N(1)	C(1)	C(2)	175.97(17)
Rh(1)	N(1)	C(9)	C(10)	96.2(3)	Rh(1)	N(1)	C(9)	C(14)	-81.3(3)
C(1)	N(1)	C(9)	C(10)	-81.4(4)	C(1)	N(1)	C(9)	C(14)	101.2(4)
C(9)	N(1)	C(1)	O(3)	174.2(3)	C(9)	N(1)	C(1)	C(2)	-6.6(5)
Rh(1)	N(2)	C(3)	O(4)	-4.4(4)	Rh(1)	N(2)	C(3)	C(4)	174.48(17)
Rh(1)	N(2)	C(15)	C(16)	-75.3(3)	Rh(1)	N(2)	C(15)	C(20)	100.8(3)
C(3)	N(2)	C(15)	C(16)	107.4(3)	C(3)	N(2)	C(15)	C(20)	-76.5(4)
C(15)	N(2)	C(3)	O(4)	172.9(3)	C(15)	N(2)	C(3)	C(4)	-8.3(5)
Rh(2)	N(4)	C(5)	O(1)	-0.5(3)	Rh(2)	N(4)	C(5)	C(6)	-179.35(13)
Rh(2)	N(4)	C(28)	C(29)	-86.7(3)	Rh(2)	N(4)	C(28)	C(33)	89.7(3)
C(5)	N(4)	C(28)	C(29)	89.0(3)	C(5)	N(4)	C(28)	C(33)	-94.6(3)

C(28)	N(4)	C(5)	O(1)	-176.0(2)	C(28)	N(4)	C(5)	C(6)	5.2(4)
Rh(2)	N(5)	C(7)	O(2)	-4.3(4)	Rh(2)	N(5)	C(7)	C(8)	175.70(15)
Rh(2)	N(5)	C(34)	C(35)	100.6(3)	Rh(2)	N(5)	C(34)	C(39)	-76.5(3)
C(7)	N(5)	C(34)	C(35)	-83.6(3)	C(7)	N(5)	C(34)	C(39)	99.3(4)
C(34)	N(5)	C(7)	O(2)	180.0(3)	C(34)	N(5)	C(7)	C(8)	-0.0(4)
N(1)	C(9)	C(10)	C(11)	-178.4(3)	N(1)	C(9)	C(14)	C(13)	178.3(3)
C(10)	C(9)	C(14)	C(13)	0.8(5)	C(14)	C(9)	C(10)	C(11)	-1.0(5)
C(9)	C(10)	C(11)	C(12)	1.3(6)	C(10)	C(11)	C(12)	C(13)	-1.4(6)
C(11)	C(12)	C(13)	C(14)	1.2(6)	C(12)	C(13)	C(14)	C(9)	-0.9(5)
N(2)	C(15)	C(16)	C(17)	178.1(2)	N(2)	C(15)	C(20)	C(19)	-178.6(2)
C(16)	C(15)	C(20)	C(19)	-2.4(4)	C(20)	C(15)	C(16)	C(17)	1.9(4)
C(15)	C(16)	C(17)	C(18)	-0.7(4)	C(16)	C(17)	C(18)	C(19)	-0.1(5)
C(17)	C(18)	C(19)	C(20)	-0.4(5)	C(18)	C(19)	C(20)	C(15)	1.7(5)
C(21)	C(22)	C(23)	C(24)	178.7(3)	C(21)	C(22)	C(27)	C(26)	-178.8(3)
C(21)	C(22)	C(27)	C(47)	1.1(4)	C(23)	C(22)	C(27)	C(26)	0.5(5)
C(23)	C(22)	C(27)	C(47)	-179.6(3)	C(27)	C(22)	C(23)	C(24)	-0.6(5)
C(22)	C(23)	C(24)	C(25)	0.1(5)	C(23)	C(24)	C(25)	C(26)	0.5(6)
C(24)	C(25)	C(26)	C(27)	-0.6(6)	C(25)	C(26)	C(27)	C(22)	0.0(5)
C(25)	C(26)	C(27)	C(47)	-179.8(3)	N(4)	C(28)	C(29)	C(30)	177.5(3)
N(4)	C(28)	C(33)	C(32)	-177.3(3)	C(29)	C(28)	C(33)	C(32)	-0.8(5)
C(33)	C(28)	C(29)	C(30)	0.9(6)	C(28)	C(29)	C(30)	C(31)	-1.1(7)
C(29)	C(30)	C(31)	C(32)	1.1(7)	C(30)	C(31)	C(32)	C(33)	-1.0(7)
C(31)	C(32)	C(33)	C(28)	0.8(6)	N(5)	C(34)	C(35)	C(36)	-179.3(3)
N(5)	C(34)	C(39)	C(38)	179.3(3)	C(35)	C(34)	C(39)	C(38)	2.3(5)
C(39)	C(34)	C(35)	C(36)	-2.2(5)	C(34)	C(35)	C(36)	C(37)	1.0(6)

C(35)	C(36)	C(37)	C(38)	0.2(7)	C(36)	C(37)	C(38)	C(39)	-0.1(7)
C(37)	C(38)	C(39)	C(34)	-1.1(7)	C(40)	C(41)	C(42)	C(43)	176.4(3)
C(40)	C(41)	C(42)	C(48)	-2.9(5)	C(40)	C(41)	C(46)	C(45)	-176.6(3)
C(42)	C(41)	C(46)	C(45)	0.8(5)	C(46)	C(41)	C(42)	C(43)	-1.1(5)
C(46)	C(41)	C(42)	C(48)	179.7(3)	C(41)	C(42)	C(43)	C(44)	0.3(5)
C(48)	C(42)	C(43)	C(44)	179.6(3)	C(42)	C(43)	C(44)	C(45)	0.7(6)
C(43)	C(44)	C(45)	C(46)	-1.0(6)	C(44)	C(45)	C(46)	C(41)	0.2(6)

APPENDIX B

SUPPLEMENTARY INFORMATION FOR **III**

EXPERIMENTAL DETAILS

A. Crystal Data

Empirical Formula	$C_{40}H_{39}N_5O_4Rh_2$
Formula Weight	859.59
Crystal Color, Habit	blue, block
Crystal Dimensions	0.160 X 0.080 X 0.070 mm
Crystal System	triclinic
Lattice Type	Primitive
Lattice Parameters	$a = 11.711(2)$ Å
	$b = 13.018(2)$ Å
	$c = 13.398(2)$ Å
	$\alpha = 72.337(5)$ º
	$\beta = 66.780(5)$ º
	$\gamma = 82.742(6)$ º
	$V = 1788.6(4)$ Å^3
Space Group	P-1 (#2)
Z value	2
D_{calc}	1.596 g/cm^3
F_{000}	872.00
$\mu(MoK\alpha)$	9.699 cm^{-1}

B. Intensity Measurements

Diffractometer	XtaLAB mini
Radiation	MoKα ($\lambda = 0.71075$ Å)
	graphite monochromated
Voltage, Current	50kV, 12mA
Temperature	20.0°C
Detector Aperture	75 mm (diameter)
Data Images	540 exposures
ω oscillation Range	-60.0 - 120.0°
Exposure Rate	30.0 sec./°
Detector Swing Angle	29.50°
ω oscillation Range	-60.0 - 120.0°
Exposure Rate	30.0 sec./°
Detector Swing Angle	29.50°
ω oscillation Range	-60.0 - 120.0°
Exposure Rate	30.0 sec./°
Detector Swing Angle	29.50°
ω oscillation Range	-60.0 - 120.0°
Exposure Rate	30.0 sec./°
Detector Swing Angle	29.50°
ω oscillation Range	-60.0 - 120.0°
Exposure Rate	30.0 sec./°
Detector Swing Angle	29.50°

ω oscillation Range	-60.0 - 120.0^o
Exposure Rate	30.0 sec./^{o}
Detector Swing Angle	29.50^o
Detector Position	50.00 mm
Pixel Size	0.146 mm
$2\theta_{max}$	55.0^o
No. of Reflections Measured	Total: 18454
	Unique: 8152 (R_{int} = 0.0646)
Corrections	Lorentz-polarization
	Absorption
	(trans. factors: 0.774 - 0.934)

C. Structure Solution and Refinement

Structure Solution	Direct Methods (SHELX97)
Refinement	Full-matrix least-squares on F^2
Function Minimized	$\Sigma\, w\, (F_o^2 - F_c^2)^2$
Least Squares Weights	$w = 1/[\,\sigma^2(F_o^2) + (0.0355 \cdot P)^2$
	$+ 1.4525 \cdot P\,]$
	where $P = (Max(F_o^2,0) + 2F_c^2)/3$
$2\theta_{max}$ cutoff	55.0^o
Anomalous Dispersion	All non-hydrogen atoms
No. Observations (All reflections)	8152
No. Variables	465
Reflection/Parameter Ratio	17.53
Residuals: R1 (I>2.00σ(I))	0.0491

Residuals: R (All reflections)			0.0859	
Residuals: wR2 (All reflections)			0.1014	
Goodness of Fit Indicator			1.036	
Max Shift/Error in Final Cycle			0.001	
Maximum peak in Final Diff. Map			0.73 e$^-$/Å^3	
Minimum peak in Final Diff. Map			-0.84 e$^-$/Å^3	

Table 1. Atomic coordinates and B_{iso}/B_{eq}

atom	x	y	z	B_{eq}
Rh(1)	0.75888(3)	0.78295(3)	0.31657(3)	1.820(8)
Rh(2)	0.78739(3)	0.70206(3)	0.16908(3)	1.898(8)
O(1)	0.5727(3)	0.7891(3)	0.3547(3)	2.26(6)
O(2)	0.9464(3)	0.7740(3)	0.2746(3)	2.20(6)
O(3)	0.7241(3)	0.5592(3)	0.2870(3)	2.37(6)
O(4)	0.8450(3)	0.8477(3)	0.0536(3)	2.32(6)
N(1)	0.7375(4)	0.6280(3)	0.4193(3)	1.95(7)
N(2)	0.7778(4)	0.9297(3)	0.1961(3)	2.21(7)
N(3)	0.7472(4)	0.8541(3)	0.4465(3)	2.12(7)
N(4)	0.6066(4)	0.7502(3)	0.1894(3)	2.07(7)
N(5)	0.9662(4)	0.6646(3)	0.1649(3)	2.08(7)
C(1)	0.7162(5)	0.5487(4)	0.3882(4)	2.34(9)
C(2)	0.6808(6)	0.4375(4)	0.4681(5)	3.4(1)
C(3)	0.8186(4)	0.9336(4)	0.0883(4)	2.26(8)
C(4)	0.8348(5)	1.0383(4)	-0.0036(4)	2.88(9)
C(5)	0.5351(4)	0.7824(4)	0.2789(4)	2.21(8)
C(6)	0.4015(5)	0.8138(4)	0.2993(5)	2.8(1)

C(7)	1.0112(5)	0.7110(4)	0.2149(4)	2.20(8)
C(8)	1.1421(5)	0.6944(4)	0.2126(5)	2.79(9)
C(9)	0.7292(5)	0.6104(4)	0.5329(4)	2.22(8)
C(10)	0.6181(6)	0.6223(4)	0.6170(5)	3.5(1)
C(11)	0.6129(7)	0.6134(5)	0.7252(5)	4.2(2)
C(12)	0.7197(8)	0.5942(5)	0.7473(5)	4.8(2)
C(13)	0.8304(7)	0.5843(5)	0.6624(6)	4.6(2)
C(14)	0.8359(5)	0.5908(4)	0.5556(5)	3.3(1)
C(15)	0.7489(5)	1.0255(4)	0.2322(4)	2.44(9)
C(16)	0.6271(5)	1.0417(4)	0.3019(5)	3.2(1)
C(17)	0.5972(6)	1.1305(5)	0.3443(5)	4.0(2)
C(18)	0.6871(6)	1.2047(5)	0.3164(5)	3.9(2)
C(19)	0.8052(6)	1.1884(5)	0.2493(5)	3.9(2)
C(20)	0.8391(5)	1.0991(4)	0.2068(5)	3.1(1)
C(21)	0.7661(5)	0.8925(4)	0.5044(4)	2.56(9)
C(22)	0.8003(5)	0.9440(4)	0.5701(4)	2.45(9)
C(23)	0.8454(5)	1.0478(4)	0.5196(4)	2.60(9)
C(24)	0.8896(4)	1.0983(4)	0.5751(4)	2.43(9)
C(25)	0.8889(5)	1.0417(4)	0.6811(4)	3.0(1)
C(26)	0.8412(5)	0.9386(5)	0.7323(5)	3.4(1)
C(27)	0.7967(5)	0.8882(4)	0.6777(5)	3.3(1)
C(28)	0.5585(4)	0.7519(4)	0.1057(4)	2.22(8)
C(29)	0.5649(5)	0.8446(5)	0.0197(5)	3.4(1)
C(30)	0.5160(5)	0.8463(5)	-0.0588(5)	3.7(1)
C(31)	0.4636(5)	0.7554(5)	-0.0556(5)	3.8(2)

C(32)	0.4599(5)	0.6628(5)	0.0288(5)	3.3(1)
C(33)	0.5075(5)	0.6603(4)	0.1093(5)	2.83(9)
C(34)	1.0411(4)	0.5882(4)	0.1067(4)	2.01(8)
C(35)	1.0073(5)	0.4806(4)	0.1481(5)	2.74(9)
C(36)	1.0814(5)	0.4060(5)	0.0935(5)	3.2(1)
C(37)	1.1859(5)	0.4369(5)	-0.0012(5)	3.1(1)
C(38)	1.2172(5)	0.5445(5)	-0.0452(5)	3.6(1)
C(39)	1.1456(5)	0.6206(5)	0.0087(4)	2.80(9)
C(40)	0.9358(5)	1.2124(4)	0.5211(5)	3.4(1)

$B_{eq} = 8/3\ \pi^2(U_{11}(aa^*)^2 + U_{22}(bb^*)^2 + U_{33}(cc^*)^2 + 2U_{12}(aa^*bb^*)\cos\gamma + 2U_{13}(aa^*cc^*)\cos\beta + 2U_{23}(bb^*cc^*)\cos\alpha)$

Table 2. Anisotropic displacement parameters

atom	U_{11}	U_{22}	U_{33}	U_{12}	U_{13}	U_{23}
Rh(1)	0.0237(2)	0.0238(2)	0.0254(2)	0.0019(2)	-0.0106(2)	-0.0111(2)
Rh(2)	0.0221(2)	0.0280(2)	0.0274(2)	0.0038(2)	-0.0115(2)	-0.0138(2)
O(1)	0.023(2)	0.035(2)	0.029(2)	0.001(2)	-0.008(2)	-0.014(2)
O(2)	0.025(2)	0.029(2)	0.038(2)	0.003(2)	-0.014(2)	-0.019(2)
O(3)	0.033(2)	0.032(2)	0.033(2)	0.000(2)	-0.015(2)	-0.015(2)
O(4)	0.028(2)	0.035(2)	0.026(2)	0.003(2)	-0.008(2)	-0.013(2)
N(1)	0.029(2)	0.022(2)	0.027(2)	0.003(2)	-0.015(2)	-0.008(2)
N(2)	0.029(2)	0.025(2)	0.031(3)	0.003(2)	-0.014(2)	-0.008(2)
N(3)	0.031(3)	0.023(2)	0.031(3)	0.004(2)	-0.012(2)	-0.015(2)
N(4)	0.023(2)	0.030(2)	0.030(2)	0.003(2)	-0.011(2)	-0.013(2)
N(5)	0.025(2)	0.032(2)	0.028(2)	0.004(2)	-0.013(2)	-0.014(2)
C(1)	0.031(3)	0.024(3)	0.037(3)	0.004(2)	-0.016(3)	-0.010(2)
C(2)	0.058(4)	0.033(3)	0.045(4)	0.000(3)	-0.025(3)	-0.011(3)
C(3)	0.022(3)	0.031(3)	0.033(3)	0.003(2)	-0.010(2)	-0.010(3)
C(4)	0.041(3)	0.036(3)	0.028(3)	-0.004(3)	-0.009(3)	-0.007(3)
C(5)	0.018(3)	0.031(3)	0.035(3)	0.006(2)	-0.009(2)	-0.012(2)
C(6)	0.027(3)	0.041(3)	0.040(3)	0.008(3)	-0.011(3)	-0.018(3)
C(7)	0.033(3)	0.027(3)	0.029(3)	0.001(2)	-0.016(3)	-0.009(2)
C(8)	0.029(3)	0.041(3)	0.043(3)	0.006(3)	-0.016(3)	-0.021(3)
C(9)	0.038(3)	0.018(3)	0.028(3)	-0.000(2)	-0.016(3)	-0.003(2)
C(10)	0.054(4)	0.041(3)	0.044(4)	0.001(3)	-0.022(3)	-0.017(3)
C(11)	0.075(5)	0.045(4)	0.036(4)	-0.008(3)	-0.010(3)	-0.017(3)
C(12)	0.113(6)	0.044(4)	0.035(4)	-0.031(4)	-0.040(4)	0.005(3)

C(13)	0.085(5)	0.043(4)	0.062(5)	-0.018(4)	-0.053(4)	0.007(3)
C(14)	0.045(4)	0.038(3)	0.046(4)	-0.004(3)	-0.026(3)	-0.005(3)
C(15)	0.039(3)	0.027(3)	0.031(3)	0.003(2)	-0.018(3)	-0.008(2)
C(16)	0.033(3)	0.035(3)	0.052(4)	0.005(3)	-0.014(3)	-0.018(3)
C(17)	0.046(4)	0.041(4)	0.068(4)	0.014(3)	-0.020(3)	-0.028(3)
C(18)	0.067(4)	0.038(4)	0.056(4)	0.008(3)	-0.030(4)	-0.023(3)
C(19)	0.065(4)	0.032(3)	0.057(4)	-0.009(3)	-0.028(4)	-0.011(3)
C(20)	0.043(3)	0.035(3)	0.039(3)	-0.008(3)	-0.010(3)	-0.010(3)
C(21)	0.025(3)	0.033(3)	0.036(3)	0.004(2)	-0.005(3)	-0.014(3)
C(22)	0.027(3)	0.038(3)	0.036(3)	0.004(2)	-0.014(3)	-0.021(3)
C(23)	0.031(3)	0.041(3)	0.031(3)	0.011(3)	-0.015(3)	-0.015(3)
C(24)	0.024(3)	0.034(3)	0.039(3)	0.006(2)	-0.011(3)	-0.020(3)
C(25)	0.041(3)	0.044(3)	0.037(3)	0.004(3)	-0.017(3)	-0.020(3)
C(26)	0.057(4)	0.043(4)	0.035(3)	-0.005(3)	-0.022(3)	-0.013(3)
C(27)	0.052(4)	0.033(3)	0.044(4)	-0.005(3)	-0.018(3)	-0.015(3)
C(28)	0.019(3)	0.037(3)	0.031(3)	0.007(2)	-0.009(2)	-0.015(3)
C(29)	0.038(3)	0.046(4)	0.050(4)	-0.004(3)	-0.025(3)	-0.010(3)
C(30)	0.052(4)	0.052(4)	0.038(3)	0.002(3)	-0.026(3)	-0.005(3)
C(31)	0.038(3)	0.077(5)	0.042(4)	0.013(3)	-0.022(3)	-0.029(4)
C(32)	0.034(3)	0.056(4)	0.053(4)	-0.002(3)	-0.022(3)	-0.031(3)
C(33)	0.031(3)	0.035(3)	0.047(3)	0.001(3)	-0.018(3)	-0.015(3)
C(34)	0.026(3)	0.033(3)	0.025(3)	0.007(2)	-0.017(2)	-0.012(2)
C(35)	0.026(3)	0.042(3)	0.041(3)	0.003(3)	-0.015(3)	-0.017(3)
C(36)	0.041(3)	0.044(3)	0.050(4)	0.010(3)	-0.024(3)	-0.028(3)
C(37)	0.027(3)	0.058(4)	0.051(4)	0.016(3)	-0.020(3)	-0.038(3)

187

C(38)	0.034(3)	0.068(4)	0.042(4)	0.002(3)	-0.013(3)	-0.029(3)
C(39)	0.030(3)	0.043(3)	0.033(3)	-0.000(3)	-0.010(3)	-0.013(3)
C(40)	0.039(3)	0.043(4)	0.055(4)	-0.003(3)	-0.017(3)	-0.021(3)

The general temperature factor expression: $\exp(-2\pi^2(a^{*2}U_{11}h^2 + b^{*2}U_{22}k^2 + c^{*2}U_{33}l^2 + 2a^*b^*U_{12}hk + 2a^*c^*U_{13}hl + 2b^*c^*U_{23}kl))$

Table 3. Bond lengths (Å)

atom	atom	distance	atom	atom	distance
Rh(1)	Rh(2)	2.4039(7)	Rh(1)	O(1)	2.030(4)
Rh(1)	O(2)	2.038(3)	Rh(1)	N(1)	2.049(4)
Rh(1)	N(2)	2.064(4)	Rh(1)	N(3)	2.160(5)
Rh(2)	O(3)	2.037(3)	Rh(2)	O(4)	2.041(3)
Rh(2)	N(4)	2.064(4)	Rh(2)	N(5)	2.071(4)
O(1)	C(5)	1.284(8)	O(2)	C(7)	1.285(6)
O(3)	C(1)	1.288(7)	O(4)	C(3)	1.295(7)
N(1)	C(1)	1.306(8)	N(1)	C(9)	1.433(7)
N(2)	C(3)	1.317(7)	N(2)	C(15)	1.426(7)
N(3)	C(21)	1.140(8)	N(4)	C(5)	1.319(6)
N(4)	C(28)	1.434(8)	N(5)	C(7)	1.302(8)
N(5)	C(34)	1.441(6)	C(1)	C(2)	1.508(6)
C(3)	C(4)	1.508(6)	C(5)	C(6)	1.502(7)
C(7)	C(8)	1.511(8)	C(9)	C(10)	1.373(7)
C(9)	C(14)	1.375(9)	C(10)	C(11)	1.396(10)
C(11)	C(12)	1.372(12)	C(12)	C(13)	1.370(9)
C(13)	C(14)	1.383(11)	C(15)	C(16)	1.394(7)
C(15)	C(20)	1.386(8)	C(16)	C(17)	1.386(9)
C(17)	C(18)	1.381(10)	C(18)	C(19)	1.352(8)
C(19)	C(20)	1.394(9)	C(21)	C(22)	1.444(9)
C(22)	C(23)	1.382(7)	C(22)	C(27)	1.390(8)
C(23)	C(24)	1.392(9)	C(24)	C(25)	1.385(8)
C(24)	C(40)	1.505(7)	C(25)	C(26)	1.383(8)

189

C(26)	C(27)	1.385(10)		C(28)	C(29)	1.379(7)	
C(28)	C(33)	1.379(8)		C(29)	C(30)	1.375(10)	
C(30)	C(31)	1.383(10)		C(31)	C(32)	1.372(8)	
C(32)	C(33)	1.387(10)		C(34)	C(35)	1.386(7)	
C(34)	C(39)	1.388(6)		C(35)	C(36)	1.397(8)	
C(36)	C(37)	1.363(6)		C(37)	C(38)	1.380(8)	
C(38)	C(39)	1.397(8)					

Table 4. Bond angles (º)

atom	atom	atom	angle	atom	atom	atom	angle
Rh(2)	Rh(1)	O(1)	89.67(11)	Rh(2)	Rh(1)	O(2)	88.45(11)
Rh(2)	Rh(1)	N(1)	85.16(13)	Rh(2)	Rh(1)	N(2)	86.69(13)
Rh(2)	Rh(1)	N(3)	175.94(11)	O(1)	Rh(1)	O(2)	178.11(16)
O(1)	Rh(1)	N(1)	88.22(14)	O(1)	Rh(1)	N(2)	89.88(14)
O(1)	Rh(1)	N(3)	94.37(15)	O(2)	Rh(1)	N(1)	91.42(14)
O(2)	Rh(1)	N(2)	90.22(14)	O(2)	Rh(1)	N(3)	87.51(15)
N(1)	Rh(1)	N(2)	171.64(19)	N(1)	Rh(1)	N(3)	94.64(15)
N(2)	Rh(1)	N(3)	93.62(16)	Rh(1)	Rh(2)	O(3)	90.07(11)
Rh(1)	Rh(2)	O(4)	88.87(11)	Rh(1)	Rh(2)	N(4)	85.68(13)
Rh(1)	Rh(2)	N(5)	86.52(13)	O(3)	Rh(2)	O(4)	177.98(12)
O(3)	Rh(2)	N(4)	89.73(13)	O(3)	Rh(2)	N(5)	90.83(13)
O(4)	Rh(2)	N(4)	88.47(13)	O(4)	Rh(2)	N(5)	90.83(13)
N(4)	Rh(2)	N(5)	172.18(18)	Rh(1)	O(1)	C(5)	117.4(3)
Rh(1)	O(2)	C(7)	119.2(4)	Rh(2)	O(3)	C(1)	117.6(4)
Rh(2)	O(4)	C(3)	118.7(3)	Rh(1)	N(1)	C(1)	121.5(4)
Rh(1)	N(1)	C(9)	118.1(3)	C(1)	N(1)	C(9)	119.9(4)

Rh(1)	N(2)	C(3)	120.0(4)	Rh(1)	N(2)	C(15)	118.6(3)
C(3)	N(2)	C(15)	121.4(4)	Rh(1)	N(3)	C(21)	166.3(4)
Rh(2)	N(4)	C(5)	119.9(4)	Rh(2)	N(4)	C(28)	120.8(3)
C(5)	N(4)	C(28)	119.3(4)	Rh(2)	N(5)	C(7)	119.5(3)
Rh(2)	N(5)	C(34)	120.6(4)	C(7)	N(5)	C(34)	119.9(4)
O(3)	C(1)	N(1)	122.7(4)	O(3)	C(1)	C(2)	114.6(5)
N(1)	C(1)	C(2)	122.6(5)	O(4)	C(3)	N(2)	122.5(4)
O(4)	C(3)	C(4)	115.0(5)	N(2)	C(3)	C(4)	122.5(5)
O(1)	C(5)	N(4)	123.4(5)	O(1)	C(5)	C(6)	115.0(5)
N(4)	C(5)	C(6)	121.6(6)	O(2)	C(7)	N(5)	122.9(5)
O(2)	C(7)	C(8)	112.8(5)	N(5)	C(7)	C(8)	124.3(5)
N(1)	C(9)	C(10)	120.9(5)	N(1)	C(9)	C(14)	119.4(4)
C(10)	C(9)	C(14)	119.4(6)	C(9)	C(10)	C(11)	120.5(7)
C(10)	C(11)	C(12)	119.8(6)	C(11)	C(12)	C(13)	119.3(7)
C(12)	C(13)	C(14)	121.2(8)	C(9)	C(14)	C(13)	119.7(5)
N(2)	C(15)	C(16)	118.6(5)	N(2)	C(15)	C(20)	122.3(4)
C(16)	C(15)	C(20)	119.0(5)	C(15)	C(16)	C(17)	120.1(6)
C(16)	C(17)	C(18)	120.5(5)	C(17)	C(18)	C(19)	119.2(6)
C(18)	C(19)	C(20)	121.9(6)	C(15)	C(20)	C(19)	119.2(5)
N(3)	C(21)	C(22)	175.1(5)	C(21)	C(22)	C(23)	117.9(5)
C(21)	C(22)	C(27)	121.1(5)	C(23)	C(22)	C(27)	120.8(6)
C(22)	C(23)	C(24)	120.6(5)	C(23)	C(24)	C(25)	118.6(5)
C(23)	C(24)	C(40)	120.5(5)	C(25)	C(24)	C(40)	120.9(6)
C(24)	C(25)	C(26)	120.6(7)	C(25)	C(26)	C(27)	121.0(6)
C(22)	C(27)	C(26)	118.4(5)	N(4)	C(28)	C(29)	120.2(5)

N(4)	C(28)	C(33)	120.4(4)	C(29)	C(28)	C(33)	119.4(6)
C(28)	C(29)	C(30)	119.9(6)	C(29)	C(30)	C(31)	121.2(5)
C(30)	C(31)	C(32)	118.5(7)	C(31)	C(32)	C(33)	120.8(6)
C(28)	C(33)	C(32)	120.1(5)	N(5)	C(34)	C(35)	119.5(4)
N(5)	C(34)	C(39)	121.2(5)	C(35)	C(34)	C(39)	119.2(5)
C(34)	C(35)	C(36)	119.6(4)	C(35)	C(36)	C(37)	121.4(5)
C(36)	C(37)	C(38)	119.2(6)	C(37)	C(38)	C(39)	120.6(5)
C(34)	C(39)	C(38)	120.0(5)				

Table 5. Torsion Angles(^{o})

(Those having bond angles > 160 or < 20 degrees are excluded.)

atom1	atom2	atom3	atom4	angle	atom1	atom2	atom3	atom4	angle
Rh(2)	Rh(1)	O(1)	C(5)	-19.40(19)	O(1)	Rh(1)	Rh(2)	O(3)	-75.69(8)
O(1)	Rh(1)	Rh(2)	O(4)	102.59(8)	O(1)	Rh(1)	Rh(2)	N(4)	14.04(8)
O(1)	Rh(1)	Rh(2)	N(5)	-166.52(8)	Rh(2)	Rh(1)	O(2)	C(7)	-17.26(19)
O(2)	Rh(1)	Rh(2)	O(3)	104.11(8)	O(2)	Rh(1)	Rh(2)	O(4)	-77.62(8)
O(2)	Rh(1)	Rh(2)	N(4)	-166.17(8)	O(2)	Rh(1)	Rh(2)	N(5)	13.28(8)
Rh(2)	Rh(1)	N(1)	C(1)	-15.8(3)	Rh(2)	Rh(1)	N(1)	C(9)	172.6(3)
N(1)	Rh(1)	Rh(2)	O(3)	12.55(11)	N(1)	Rh(1)	Rh(2)	O(4)	-169.17(11)
N(1)	Rh(1)	Rh(2)	N(4)	102.28(11)	N(1)	Rh(1)	Rh(2)	N(5)	-78.28(11)
Rh(2)	Rh(1)	N(2)	C(3)	-12.2(3)	Rh(2)	Rh(1)	N(2)	C(15)	169.3(3)
N(2)	Rh(1)	Rh(2)	O(3)	-165.59(11)	N(2)	Rh(1)	Rh(2)	O(4)	12.69(11)
N(2)	Rh(1)	Rh(2)	N(4)	-75.86(11)	N(2)	Rh(1)	Rh(2)	N(5)	103.59(11)
O(1)	Rh(1)	N(1)	C(1)	74.0(3)	O(1)	Rh(1)	N(1)	C(9)	-97.5(3)
N(1)	Rh(1)	O(1)	C(5)	-104.6(3)	O(1)	Rh(1)	N(2)	C(3)	-101.9(3)
O(1)	Rh(1)	N(2)	C(15)	79.7(3)	N(2)	Rh(1)	O(1)	C(5)	67.3(3)

N(3)	Rh(1)	O(1)	C(5)	160.9(2)	O(2)	Rh(1)	N(1)	C(1)	-104.2(3)
O(2)	Rh(1)	N(1)	C(9)	84.3(3)	N(1)	Rh(1)	O(2)	C(7)	67.9(3)
O(2)	Rh(1)	N(2)	C(3)	76.2(3)	O(2)	Rh(1)	N(2)	C(15)	-102.2(3)
N(2)	Rh(1)	O(2)	C(7)	-103.9(3)	N(3)	Rh(1)	O(2)	C(7)	162.4(2)
N(3)	Rh(1)	N(1)	C(1)	168.2(3)	N(3)	Rh(1)	N(1)	C(9)	-3.3(3)
N(3)	Rh(1)	N(2)	C(3)	163.8(3)	N(3)	Rh(1)	N(2)	C(15)	-14.7(3)
Rh(1)	Rh(2)	O(3)	C(1)	-13.9(2)	Rh(1)	Rh(2)	O(4)	C(3)	-17.8(3)
Rh(1)	Rh(2)	N(4)	C(5)	-13.5(3)	Rh(1)	Rh(2)	N(4)	C(28)	164.9(3)
Rh(1)	Rh(2)	N(5)	C(7)	-14.4(2)	Rh(1)	Rh(2)	N(5)	C(34)	165.9(2)
O(3)	Rh(2)	N(4)	C(5)	76.6(3)	O(3)	Rh(2)	N(4)	C(28)	-105.0(3)
N(4)	Rh(2)	O(3)	C(1)	-99.6(3)	O(3)	Rh(2)	N(5)	C(7)	-104.4(3)
O(3)	Rh(2)	N(5)	C(34)	75.9(3)	N(5)	Rh(2)	O(3)	C(1)	72.6(3)
O(4)	Rh(2)	N(4)	C(5)	-102.5(3)	O(4)	Rh(2)	N(4)	C(28)	75.9(3)
N(4)	Rh(2)	O(4)	C(3)	67.9(3)	O(4)	Rh(2)	N(5)	C(7)	74.4(3)
O(4)	Rh(2)	N(5)	C(34)	-105.2(3)	N(5)	Rh(2)	O(4)	C(3)	-104.3(3)
Rh(1)	O(1)	C(5)	N(4)	14.3(5)	Rh(1)	O(1)	C(5)	C(6)	-165.8(2)
Rh(1)	O(2)	C(7)	N(5)	10.9(5)	Rh(1)	O(2)	C(7)	C(8)	-167.30(18)
Rh(2)	O(3)	C(1)	N(1)	5.6(6)	Rh(2)	O(3)	C(1)	C(2)	-174.3(3)
Rh(2)	O(4)	C(3)	N(2)	13.3(6)	Rh(2)	O(4)	C(3)	C(4)	-165.1(3)
Rh(1)	N(1)	C(1)	O(3)	9.7(6)	Rh(1)	N(1)	C(1)	C(2)	-170.4(3)
Rh(1)	N(1)	C(9)	C(10)	83.8(5)	Rh(1)	N(1)	C(9)	C(14)	-90.3(4)
C(1)	N(1)	C(9)	C(10)	-87.9(5)	C(1)	N(1)	C(9)	C(14)	98.0(5)
C(9)	N(1)	C(1)	O(3)	-178.9(4)	C(9)	N(1)	C(1)	C(2)	1.0(7)
Rh(1)	N(2)	C(3)	O(4)	1.9(7)	Rh(1)	N(2)	C(3)	C(4)	-179.8(3)
Rh(1)	N(2)	C(15)	C(16)	-63.4(6)	Rh(1)	N(2)	C(15)	C(20)	112.0(4)

C(3)	N(2)	C(15)	C(16)	118.1(5)	C(3)	N(2)	C(15)	C(20)	-66.4(7)
C(15)	N(2)	C(3)	O(4)	-179.7(5)	C(15)	N(2)	C(3)	C(4)	-1.4(7)
Rh(2)	N(4)	C(5)	O(1)	2.3(6)	Rh(2)	N(4)	C(5)	C(6)	-177.5(3)
Rh(2)	N(4)	C(28)	C(29)	-92.3(4)	Rh(2)	N(4)	C(28)	C(33)	86.5(4)
C(5)	N(4)	C(28)	C(29)	86.2(5)	C(5)	N(4)	C(28)	C(33)	-95.1(5)
C(28)	N(4)	C(5)	O(1)	-176.1(4)	C(28)	N(4)	C(5)	C(6)	4.0(6)
Rh(2)	N(5)	C(7)	O(2)	5.3(5)	Rh(2)	N(5)	C(7)	C(8)	-176.8(3)
Rh(2)	N(5)	C(34)	C(35)	-67.2(5)	Rh(2)	N(5)	C(34)	C(39)	111.8(4)
C(7)	N(5)	C(34)	C(35)	113.2(5)	C(7)	N(5)	C(34)	C(39)	-67.9(6)
C(34)	N(5)	C(7)	O(2)	-175.1(3)	C(34)	N(5)	C(7)	C(8)	2.9(6)
N(1)	C(9)	C(10)	C(11)	-174.9(4)	N(1)	C(9)	C(14)	C(13)	173.7(4)
C(10)	C(9)	C(14)	C(13)	-0.5(7)	C(14)	C(9)	C(10)	C(11)	-0.8(7)
C(9)	C(10)	C(11)	C(12)	1.0(8)	C(10)	C(11)	C(12)	C(13)	0.1(9)
C(11)	C(12)	C(13)	C(14)	-1.4(9)	C(12)	C(13)	C(14)	C(9)	1.6(8)
N(2)	C(15)	C(16)	C(17)	176.0(4)	N(2)	C(15)	C(20)	C(19)	-176.9(4)
C(16)	C(15)	C(20)	C(19)	-1.5(8)	C(20)	C(15)	C(16)	C(17)	0.4(8)
C(15)	C(16)	C(17)	C(18)	1.1(9)	C(16)	C(17)	C(18)	C(19)	-1.5(10)
C(17)	C(18)	C(19)	C(20)	0.3(10)	C(18)	C(19)	C(20)	C(15)	1.2(9)
C(21)	C(22)	C(23)	C(24)	-174.6(4)	C(21)	C(22)	C(27)	C(26)	174.2(4)
C(23)	C(22)	C(27)	C(26)	-1.0(7)	C(27)	C(22)	C(23)	C(24)	0.8(7)
C(22)	C(23)	C(24)	C(25)	0.9(7)	C(22)	C(23)	C(24)	C(40)	-178.5(4)
C(23)	C(24)	C(25)	C(26)	-2.2(7)	C(40)	C(24)	C(25)	C(26)	177.2(4)
C(24)	C(25)	C(26)	C(27)	2.0(8)	C(25)	C(26)	C(27)	C(22)	-0.3(8)
N(4)	C(28)	C(29)	C(30)	-178.5(4)	N(4)	C(28)	C(33)	C(32)	179.4(4)
C(29)	C(28)	C(33)	C(32)	-1.9(6)	C(33)	C(28)	C(29)	C(30)	2.7(7)

C(28)	C(29)	C(30)	C(31)	-2.2(7)	C(29)	C(30)	C(31)	C(32)	0.7(8)
C(30)	C(31)	C(32)	C(33)	0.1(7)	C(31)	C(32)	C(33)	C(28)	0.5(7)
N(5)	C(34)	C(35)	C(36)	-178.5(5)	N(5)	C(34)	C(39)	C(38)	179.4(5)
C(35)	C(34)	C(39)	C(38)	-1.7(9)	C(39)	C(34)	C(35)	C(36)	2.6(9)
C(34)	C(35)	C(36)	C(37)	-0.9(10)	C(35)	C(36)	C(37)	C(38)	-1.6(10)
C(36)	C(37)	C(38)	C(39)	2.5(10)	C(37)	C(38)	C(39)	C(34)	-0.8(10)

APPENDIX C

SUPPLEMENTARY INFORMATION FOR III$_{(xs)}$

EXPERIMENTAL DETAILS

A. Crystal Data

Empirical Formula	$C_{48}H_{46}N_6O_4Rh_2$
Formula Weight	976.74
Crystal Color, Habit	red, block
Crystal Dimensions	0.260 X 0.140 X 0.080 mm
Crystal System	orthorhombic
Lattice Type	Primitive
Lattice Parameters	a = 10.5721(8) Å
	b = 25.985(2) Å
	c = 31.751(2) Å
	V = 8723(1) Å^3
Space Group	Pbcn (#60)
Z value	8
D$_{calc}$	1.487 g/cm^3
F$_{000}$	3984.00
μ(MoKα)	8.062 cm^{-1}

B. Intensity Measurements

Diffractometer	XtaLAB mini
Radiation	MoKα (λ = 0.71075 Å)
	graphite monochromated
Voltage, Current	50kV, 12mA

Temperature	20.0ºC
Detector Aperture	75 mm (diameter)
Data Images	540 exposures
ω oscillation Range	-60.0 - 120.0º
Exposure Rate	16.0 sec./º
Detector Swing Angle	29.50º
ω oscillation Range	-60.0 - 120.0º
Exposure Rate	16.0 sec./º
Detector Swing Angle	29.50º
ω oscillation Range	-60.0 - 120.0º
Exposure Rate	16.0 sec./º
Detector Swing Angle	29.50º
ω oscillation Range	-60.0 - 120.0º
Exposure Rate	16.0 sec./º
Detector Swing Angle	29.50º
ω oscillation Range	-60.0 - 120.0º
Exposure Rate	16.0 sec./º
Detector Swing Angle	29.50º
ω oscillation Range	-60.0 - 120.0º
Exposure Rate	16.0 sec./º
Detector Swing Angle	29.50º
Detector Position	50.00 mm
Pixel Size	0.146 mm

$2\theta_{max}$	55.0º
No. of Reflections Measured	Total: 74531
	Unique: 9967 (R_{int} = 0.2014)
Corrections	Lorentz-polarization
	Absorption
	(trans. factors: 0.670 - 0.938)

C. Structure Solution and Refinement

Structure Solution	Direct Methods
Refinement	Full-matrix least-squares on F^2
Function Minimized	$\Sigma\, w\, (F_o^2 - F_c^2)^2$
Least Squares Weights	$w = 1/[\,\sigma^2(F_o^2) + (0.0218 \cdot P)^2$
	$+\ 17.8402 \cdot P\,]$
	where $P = (Max(F_o^2,0) + 2F_c^2)/3$
$2\theta_{max}$ cutoff	55.0º
Anomalous Dispersion	All non-hydrogen atoms
No. Observations (All reflections)	9967
No. Variables	546
Reflection/Parameter Ratio	18.25
Residuals: R1 (I>2.00σ(I))	0.0617
Residuals: R (All reflections)	0.1582
Residuals: wR2 (All reflections)	0.1121
Goodness of Fit Indicator	1.014
Max Shift/Error in Final Cycle	0.002
Maximum peak in Final Diff. Map	0.63 e$^-$/Å^3

Minimum peak in Final Diff. Map $\qquad$ -0.70 e$^-$/Å^3

Table 1. Atomic coordinates and B$_{iso}$/B$_{eq}$

atom	x	y	z	B$_{eq}$
Rh1	0.36822(4)	0.56988(2)	0.88692(2)	2.31(1)
Rh2	0.42317(4)	0.48344(2)	0.86492(2)	2.30(1)
O1	0.2478(4)	0.5767(2)	0.8374(2)	2.92(8)
O2	0.4869(4)	0.5613(2)	0.9371(1)	2.73(8)
O3	0.2960(4)	0.4555(2)	0.9075(2)	2.63(8)
O4	0.5503(4)	0.5126(2)	0.8230(2)	3.03(9)
N1	0.2202(5)	0.5366(2)	0.9191(2)	2.5(1)
N2	0.5153(5)	0.5931(2)	0.8485(2)	2.5(1)
N3	0.3211(5)	0.6486(2)	0.9074(2)	3.0(1)
N4	0.2800(5)	0.4916(2)	0.8214(2)	2.7(1)
N5	0.5593(5)	0.4851(2)	0.9113(2)	2.56(9)
N6	0.4675(5)	0.4019(2)	0.8464(2)	3.0(1)
C1	0.2134(6)	0.4860(3)	0.9225(2)	2.6(2)
C2	0.1061(6)	0.4609(3)	0.9462(2)	3.6(2)
C3	0.5733(6)	0.5613(3)	0.8240(2)	2.8(2)
C4	0.6747(7)	0.5776(3)	0.7934(2)	4.7(2)
C5	0.2210(6)	0.5355(3)	0.8171(2)	3.0(2)
C6	0.1091(6)	0.5405(3)	0.7875(2)	3.9(2)
C7	0.5619(6)	0.5226(3)	0.9388(2)	2.5(1)
C8	0.6562(6)	0.5237(3)	0.9747(2)	3.2(2)
C9	0.1137(6)	0.5666(3)	0.9311(2)	3.0(2)
C10	0.0056(7)	0.5678(3)	0.9058(2)	4.1(2)

C11	-0.0970(8)	0.5964(3)	0.9167(3)	5.2(2)
C12	-0.0962(8)	0.6244(3)	0.9526(3)	4.9(2)
C13	0.0097(8)	0.6246(3)	0.9784(3)	4.3(2)
C14	0.1146(7)	0.5959(3)	0.9676(2)	3.3(2)
C15	0.5426(6)	0.6472(3)	0.8458(2)	2.8(2)
C16	0.4930(8)	0.6763(3)	0.8141(2)	5.0(2)
C17	0.5212(9)	0.7281(3)	0.8111(3)	6.3(3)
C18	0.5977(9)	0.7506(3)	0.8395(3)	5.3(2)
C19	0.6467(7)	0.7225(3)	0.8715(3)	5.3(2)
C20	0.6195(6)	0.6703(3)	0.8747(3)	4.4(2)
C21	0.2973(6)	0.6894(3)	0.9165(2)	2.8(2)
C22	0.2640(6)	0.7413(2)	0.9290(2)	2.7(2)
C23	0.3043(6)	0.7824(3)	0.9048(2)	3.4(2)
C24	0.2667(7)	0.8315(3)	0.9161(3)	4.1(2)
C25	0.1867(6)	0.8388(3)	0.9499(2)	3.6(2)
C26	0.1438(7)	0.7980(3)	0.9739(2)	3.5(2)
C27	0.1846(6)	0.7486(3)	0.9633(2)	3.3(2)
C28	0.2465(6)	0.4479(3)	0.7970(2)	2.8(2)
C29	0.3018(7)	0.4394(3)	0.7585(2)	3.7(2)
C30	0.2691(8)	0.3967(4)	0.7355(3)	5.2(2)
C31	0.1822(9)	0.3620(4)	0.7513(3)	6.2(3)
C32	0.1295(8)	0.3700(3)	0.7896(3)	5.6(2)
C33	0.1604(7)	0.4130(3)	0.8125(2)	4.2(2)
C34	0.6478(6)	0.4443(2)	0.9127(2)	2.7(2)
C35	0.6373(7)	0.4056(3)	0.9419(2)	4.1(2)

C36	0.7223(8)	0.3641(3)	0.9409(3)	5.3(2)
C37	0.8161(8)	0.3615(3)	0.9118(3)	5.5(2)
C38	0.8267(7)	0.3999(4)	0.8826(3)	5.5(2)
C39	0.7426(7)	0.4411(3)	0.8824(3)	4.1(2)
C40	0.4685(6)	0.3584(3)	0.8421(2)	3.0(2)
C41	0.4648(6)	0.3029(3)	0.8381(2)	2.9(2)
C42	0.5131(7)	0.2729(3)	0.8696(3)	4.2(2)
C43	0.4980(8)	0.2201(3)	0.8673(3)	5.3(2)
C44	0.4370(8)	0.1984(3)	0.8331(3)	5.1(2)
C45	0.3904(7)	0.2274(3)	0.8010(3)	4.3(2)
C46	0.4061(7)	0.2810(3)	0.8035(2)	4.0(2)
C47	0.0544(7)	0.8059(3)	1.0107(2)	5.5(2)
C48	0.3251(8)	0.2035(3)	0.7634(3)	7.9(3)

$B_{eq} = 8/3 \ \pi^2(U_{11}(aa^*)^2 + U_{22}(bb^*)^2 + U_{33}(cc^*)^2 + 2U_{12}(aa^*bb^*)\cos \gamma + 2U_{13}(aa^*cc^*)\cos \beta + 2U_{23}(bb^*cc^*)\cos \alpha)$

Table 2. Anisotropic displacement parameters

atom	U_{11}	U_{22}	U_{33}	U_{12}	U_{13}	U_{23}
Rh1	0.0319(3)	0.0216(3)	0.0342(3)	0.0015(3)	0.0010(3)	0.0005(3)
Rh2	0.0335(3)	0.0222(3)	0.0316(3)	0.0010(2)	-0.0034(3)	-0.0009(3)
O1	0.045(3)	0.028(3)	0.038(3)	0.004(2)	-0.006(2)	0.003(2)
O2	0.042(3)	0.027(3)	0.035(3)	0.003(2)	-0.001(2)	-0.005(2)
O3	0.039(3)	0.023(3)	0.038(3)	-0.001(2)	-0.002(2)	0.003(2)
O4	0.044(3)	0.029(3)	0.042(3)	0.002(2)	0.010(2)	-0.007(2)
N1	0.035(4)	0.025(3)	0.037(3)	0.004(3)	0.002(3)	-0.001(3)
N2	0.034(3)	0.018(3)	0.045(3)	-0.000(3)	0.004(3)	0.001(3)
N3	0.040(4)	0.021(3)	0.053(4)	0.001(3)	0.003(3)	0.001(3)
N4	0.039(4)	0.030(3)	0.034(3)	0.002(3)	-0.007(3)	-0.002(3)
N5	0.037(4)	0.025(3)	0.035(3)	0.004(3)	-0.002(3)	-0.003(3)
N6	0.039(4)	0.028(3)	0.047(4)	0.001(3)	-0.013(3)	-0.004(3)
C1	0.035(4)	0.033(4)	0.029(4)	-0.005(4)	-0.004(3)	0.001(4)
C2	0.040(5)	0.042(4)	0.053(4)	-0.002(4)	0.001(4)	0.007(4)
C3	0.042(4)	0.025(4)	0.040(4)	0.001(4)	0.004(4)	0.002(3)
C4	0.076(6)	0.037(4)	0.067(5)	0.002(4)	0.032(5)	-0.006(4)
C5	0.037(4)	0.047(5)	0.029(4)	-0.001(4)	-0.001(3)	0.009(4)
C6	0.052(5)	0.056(5)	0.040(4)	0.001(4)	-0.008(4)	0.001(4)
C7	0.033(4)	0.029(4)	0.035(4)	-0.001(3)	0.002(3)	0.002(3)
C8	0.042(4)	0.038(4)	0.044(4)	-0.001(3)	-0.006(4)	-0.007(3)
C9	0.043(5)	0.031(4)	0.040(4)	0.005(4)	0.013(4)	0.008(4)
C10	0.041(5)	0.066(5)	0.048(5)	0.011(4)	0.010(4)	0.001(4)

C11	0.057(6)	0.083(6)	0.056(5)	0.017(5)	0.010(5)	0.017(5)
C12	0.050(6)	0.053(5)	0.083(6)	0.020(4)	0.028(5)	0.025(5)
C13	0.067(6)	0.034(4)	0.062(5)	0.001(4)	0.036(5)	-0.002(4)
C14	0.050(5)	0.031(4)	0.043(4)	-0.007(4)	0.011(4)	0.000(3)
C15	0.039(4)	0.029(4)	0.037(4)	0.002(3)	0.007(3)	-0.001(3)
C16	0.114(7)	0.037(5)	0.039(5)	-0.004(5)	-0.027(5)	0.002(4)
C17	0.16(1)	0.029(5)	0.044(5)	0.010(5)	-0.007(6)	0.009(4)
C18	0.100(8)	0.034(5)	0.069(6)	-0.019(5)	0.032(6)	-0.001(5)
C19	0.048(5)	0.047(5)	0.108(8)	-0.014(4)	-0.010(5)	-0.024(5)
C20	0.047(5)	0.040(4)	0.081(6)	0.001(4)	-0.015(4)	-0.003(4)
C21	0.032(4)	0.031(4)	0.045(4)	-0.009(3)	0.005(3)	0.002(4)
C22	0.034(4)	0.024(4)	0.042(4)	-0.000(3)	0.000(4)	-0.001(3)
C23	0.042(5)	0.038(4)	0.050(4)	-0.004(4)	0.014(4)	0.005(4)
C24	0.066(6)	0.028(4)	0.063(5)	-0.006(4)	0.005(5)	0.003(4)
C25	0.053(5)	0.025(4)	0.058(5)	0.005(4)	-0.004(4)	-0.011(4)
C26	0.050(5)	0.039(4)	0.045(4)	0.003(4)	0.007(4)	-0.007(4)
C27	0.052(5)	0.029(4)	0.043(4)	-0.006(4)	0.005(4)	0.007(4)
C28	0.032(4)	0.041(4)	0.032(4)	0.003(3)	-0.010(3)	0.002(3)
C29	0.058(5)	0.052(5)	0.031(4)	0.006(4)	-0.007(4)	-0.000(4)
C30	0.071(7)	0.085(7)	0.043(5)	0.026(5)	-0.019(5)	-0.019(5)
C31	0.074(7)	0.082(7)	0.080(7)	0.003(6)	-0.044(6)	-0.039(6)
C32	0.063(6)	0.064(6)	0.085(7)	-0.031(5)	-0.009(5)	-0.017(5)
C33	0.053(5)	0.059(5)	0.047(5)	-0.015(4)	-0.009(4)	-0.002(4)
C34	0.027(4)	0.032(4)	0.044(4)	0.004(3)	-0.016(4)	-0.011(3)
C35	0.049(5)	0.048(5)	0.057(5)	0.019(4)	-0.022(4)	-0.002(4)

C36	0.077(7)	0.042(5)	0.082(6)	0.010(5)	-0.028(6)	0.000(5)
C37	0.060(6)	0.051(6)	0.100(7)	0.028(5)	-0.040(6)	-0.032(6)
C38	0.051(6)	0.077(6)	0.081(7)	0.021(5)	-0.004(5)	-0.028(6)
C39	0.041(5)	0.054(5)	0.063(5)	0.006(4)	0.004(4)	-0.012(4)
C40	0.036(4)	0.044(5)	0.034(4)	-0.003(4)	0.001(3)	-0.005(4)
C41	0.040(5)	0.029(4)	0.043(4)	-0.004(3)	0.004(4)	-0.005(4)
C42	0.060(5)	0.044(5)	0.056(5)	0.001(4)	-0.001(4)	-0.004(4)
C43	0.093(7)	0.034(5)	0.075(6)	0.018(5)	0.008(6)	0.004(5)
C44	0.077(6)	0.021(4)	0.097(7)	-0.005(4)	0.016(6)	-0.012(5)
C45	0.043(5)	0.044(5)	0.077(6)	-0.000(4)	0.002(4)	-0.017(5)
C46	0.054(5)	0.040(4)	0.059(5)	0.005(4)	0.001(4)	-0.003(4)
C47	0.084(7)	0.062(6)	0.064(5)	0.010(5)	0.021(5)	-0.009(5)
C48	0.088(7)	0.085(7)	0.126(9)	-0.015(6)	-0.024(6)	-0.043(7)

The general temperature factor expression: $\exp(-2\pi^2(a*^2U_{11}h^2 + b*^2U_{22}k^2 + c*^2U_{33}l^2 + 2a*b*U_{12}hk + 2a*c*U_{13}hl + 2b*c*U_{23}kl))$

Table 3. Bond lengths (Å)

atom	atom	distance	atom	atom	distance
Rh1	Rh2	2.4230(7)	Rh1	O1	2.031(4)
Rh1	O2	2.041(4)	Rh1	N1	2.059(5)
Rh1	N2	2.067(5)	Rh1	N3	2.202(5)
Rh2	O3	2.040(4)	Rh2	O4	2.037(4)
Rh2	N4	2.061(5)	Rh2	N5	2.060(5)
Rh2	N6	2.247(5)	O1	C5	1.282(8)
O2	C7	1.283(7)	O3	C1	1.272(7)
O4	C3	1.289(7)	N1	C1	1.321(8)
N1	C9	1.421(8)	N2	C3	1.289(8)
N2	C15	1.438(8)	N3	C21	1.130(8)
N4	C5	1.307(8)	N4	C28	1.420(8)
N5	C7	1.307(8)	N5	C34	1.415(8)
N6	C40	1.139(9)	C1	C2	1.510(9)
C3	C4	1.508(9)	C5	C6	1.515(9)
C7	C8	1.516(9)	C9	C10	1.396(9)
C9	C14	1.387(9)	C10	C11	1.360(11)
C11	C12	1.354(12)	C12	C13	1.387(11)
C13	C14	1.381(10)	C15	C16	1.364(9)
C15	C20	1.365(9)	C16	C17	1.381(10)
C17	C18	1.345(12)	C18	C19	1.352(12)
C19	C20	1.391(10)	C21	C22	1.449(9)
C22	C23	1.381(9)	C22	C27	1.387(9)
C23	C24	1.383(9)	C24	C25	1.379(10)

C25	C26	1.384(9)	C26	C27	1.395(9)
C26	C47	1.515(10)	C28	C29	1.373(9)
C28	C33	1.378(9)	C29	C30	1.372(11)
C30	C31	1.381(12)	C31	C32	1.356(13)
C32	C33	1.372(11)	C34	C35	1.372(9)
C34	C39	1.391(9)	C35	C36	1.402(11)
C36	C37	1.358(12)	C37	C38	1.367(12)
C38	C39	1.391(11)	C40	C41	1.449(9)
C41	C42	1.368(9)	C41	C46	1.383(9)
C42	C43	1.382(9)	C43	C44	1.382(12)
C44	C45	1.362(11)	C45	C46	1.405(10)
C45	C48	1.512(12)			

Table 4. Bond angles (^{o})

atom	atom	atom	angle	atom	atom	atom	angle
Rh2	Rh1	O1	90.43(11)	Rh2	Rh1	O2	88.67(11)
Rh2	Rh1	N1	86.31(13)	Rh2	Rh1	N2	85.40(13)
Rh2	Rh1	N3	179.14(13)	O1	Rh1	O2	178.51(15)
O1	Rh1	N1	86.77(17)	O1	Rh1	N2	89.36(17)
O1	Rh1	N3	90.33(17)	O2	Rh1	N1	91.99(17)
O2	Rh1	N2	91.75(17)	O2	Rh1	N3	90.57(17)
N1	Rh1	N2	170.83(18)	N1	Rh1	N3	94.13(19)
N2	Rh1	N3	94.21(18)	Rh1	Rh2	O3	88.90(11)
Rh1	Rh2	O4	90.06(11)	Rh1	Rh2	N4	85.51(14)
Rh1	Rh2	N5	86.67(13)	Rh1	Rh2	N6	177.47(13)
O3	Rh2	O4	178.90(16)	O3	Rh2	N4	89.83(17)

O3	Rh2	N5	89.66(17)	O3	Rh2	N6	88.58(16)
O4	Rh2	N4	90.46(17)	O4	Rh2	N5	89.91(17)
O4	Rh2	N6	92.46(17)	N4	Rh2	N5	172.16(19)
N4	Rh2	N6	94.30(18)	N5	Rh2	N6	93.50(18)
Rh1	O1	C5	117.2(4)	Rh1	O2	C7	119.8(4)
Rh2	O3	C1	118.6(4)	Rh2	O4	C3	118.3(4)
Rh1	N1	C1	120.0(4)	Rh1	N1	C9	120.4(4)
C1	N1	C9	118.7(5)	Rh1	N2	C3	121.8(4)
Rh1	N2	C15	118.1(4)	C3	N2	C15	119.6(5)
Rh1	N3	C21	177.7(5)	Rh2	N4	C5	120.8(4)
Rh2	N4	C28	117.8(4)	C5	N4	C28	121.4(5)
Rh2	N5	C7	120.5(4)	Rh2	N5	C34	117.9(4)
C7	N5	C34	121.6(5)	Rh2	N6	C40	165.7(5)
O3	C1	N1	123.5(6)	O3	C1	C2	115.6(6)
N1	C1	C2	120.8(6)	O4	C3	N2	123.6(6)
O4	C3	C4	113.2(5)	N2	C3	C4	123.2(6)
O1	C5	N4	124.7(6)	O1	C5	C6	114.4(6)
N4	C5	C6	120.9(6)	O2	C7	N5	123.0(6)
O2	C7	C8	114.9(5)	N5	C7	C8	122.1(5)
N1	C9	C10	120.4(6)	N1	C9	C14	121.3(6)
C10	C9	C14	118.3(6)	C9	C10	C11	121.2(7)
C10	C11	C12	120.2(7)	C11	C12	C13	120.3(7)
C12	C13	C14	119.9(7)	C9	C14	C13	120.0(6)
N2	C15	C16	120.6(6)	N2	C15	C20	120.6(6)
C16	C15	C20	118.7(6)	C15	C16	C17	120.6(7)

atom1	atom2	atom3	angle	atom1	atom2	atom3	angle
C16	C17	C18	120.4(7)	C17	C18	C19	119.9(7)
C18	C19	C20	120.2(8)	C15	C20	C19	120.1(7)
N3	C21	C22	178.4(7)	C21	C22	C23	119.4(6)
C21	C22	C27	119.2(6)	C23	C22	C27	121.2(6)
C22	C23	C24	118.6(6)	C23	C24	C25	120.4(6)
C24	C25	C26	121.6(6)	C25	C26	C27	118.0(6)
C25	C26	C47	121.7(6)	C27	C26	C47	120.3(6)
C22	C27	C26	120.2(6)	N4	C28	C29	120.6(6)
N4	C28	C33	119.8(6)	C29	C28	C33	119.7(6)
C28	C29	C30	119.7(7)	C29	C30	C31	120.3(7)
C30	C31	C32	119.9(8)	C31	C32	C33	120.2(8)
C28	C33	C32	120.3(7)	N5	C34	C35	121.1(6)
N5	C34	C39	119.9(6)	C35	C34	C39	118.8(6)
C34	C35	C36	119.7(7)	C35	C36	C37	121.4(7)
C36	C37	C38	119.0(8)	C37	C38	C39	120.8(8)
C34	C39	C38	120.2(7)	N6	C40	C41	177.2(7)
C40	C41	C42	119.5(6)	C40	C41	C46	119.4(6)
C42	C41	C46	120.9(6)	C41	C42	C43	118.9(7)
C42	C43	C44	120.2(7)	C43	C44	C45	122.0(7)
C44	C45	C46	117.6(7)	C44	C45	C48	121.9(7)
C46	C45	C48	120.4(7)	C41	C46	C45	120.4(6)

Table 5. Torsion Angles(º)

(Those having bond angles > 160 or < 20 degrees are excluded.)

atom1	atom2	atom3	atom4	angle	atom1	atom2	atom3	atom4	angle
Rh2	Rh1	O1	C5	12.2(3)	O1	Rh1	Rh2	O3	-97.53(11)

O1	Rh1	Rh2	O4	82.84(11)	O1	Rh1	Rh2	N4	-7.61(11)
O1	Rh1	Rh2	N5	172.75(11)	Rh2	Rh1	O2	C7	10.6(3)
O2	Rh1	Rh2	O3	81.29(11)	O2	Rh1	Rh2	O4	-98.34(11)
O2	Rh1	Rh2	N4	171.20(11)	O2	Rh1	Rh2	N5	-8.44(11)
Rh2	Rh1	N1	C1	9.0(3)	Rh2	Rh1	N1	C9	-159.7(3)
N1	Rh1	Rh2	O3	-10.80(13)	N1	Rh1	Rh2	O4	169.58(13)
N1	Rh1	Rh2	N4	79.12(13)	N1	Rh1	Rh2	N5	-100.52(13)
Rh2	Rh1	N2	C3	7.8(4)	Rh2	Rh1	N2	C15	-179.5(3)
N2	Rh1	Rh2	O3	173.15(14)	N2	Rh1	Rh2	O4	-6.48(13)
N2	Rh1	Rh2	N4	-96.94(14)	N2	Rh1	Rh2	N5	83.42(14)
O1	Rh1	N1	C1	99.7(4)	O1	Rh1	N1	C9	-69.1(3)
N1	Rh1	O1	C5	-74.1(3)	O1	Rh1	N2	C3	-82.7(4)
O1	Rh1	N2	C15	90.0(3)	N2	Rh1	O1	C5	97.6(3)
N3	Rh1	O1	C5	-168.2(3)	O2	Rh1	N1	C1	-79.5(4)
O2	Rh1	N1	C9	111.7(3)	N1	Rh1	O2	C7	96.8(3)
O2	Rh1	N2	C3	96.3(4)	O2	Rh1	N2	C15	-91.0(3)
N2	Rh1	O2	C7	-74.8(3)	N3	Rh1	O2	C7	-169.0(3)
N3	Rh1	N1	C1	-170.2(4)	N3	Rh1	N1	C9	21.0(4)
N3	Rh1	N2	C3	-173.0(4)	N3	Rh1	N2	C15	-0.3(4)
Rh1	Rh2	O3	C1	16.6(3)	Rh1	Rh2	O4	C3	7.7(3)
Rh1	Rh2	N4	C5	5.6(4)	Rh1	Rh2	N4	C28	-173.4(3)
Rh1	Rh2	N5	C7	9.6(3)	Rh1	Rh2	N5	C34	-171.2(3)
O3	Rh2	N4	C5	94.5(4)	O3	Rh2	N4	C28	-84.4(3)
N4	Rh2	O3	C1	-68.9(3)	O3	Rh2	N5	C7	-79.3(4)
O3	Rh2	N5	C34	99.9(3)	N5	Rh2	O3	C1	103.2(3)

N6	Rh2	O3	C1	-163.2(3)	O4	Rh2	N4	C5	-84.5(4)
O4	Rh2	N4	C28	96.6(3)	N4	Rh2	O4	C3	93.2(3)
O4	Rh2	N5	C7	99.7(4)	O4	Rh2	N5	C34	-81.2(3)
N5	Rh2	O4	C3	-79.0(3)	N6	Rh2	O4	C3	-172.5(3)
N6	Rh2	N4	C5	-177.0(4)	N6	Rh2	N4	C28	4.1(4)
N6	Rh2	N5	C7	-167.9(4)	N6	Rh2	N5	C34	11.3(3)
Rh1	O1	C5	N4	-11.6(8)	Rh1	O1	C5	C6	166.4(3)
Rh1	O2	C7	N5	-6.1(7)	Rh1	O2	C7	C8	172.9(3)
Rh2	O3	C1	N1	-14.4(7)	Rh2	O3	C1	C2	167.2(3)
Rh2	O4	C3	N2	-3.9(8)	Rh2	O4	C3	C4	176.3(3)
Rh1	N1	C1	O3	1.3(8)	Rh1	N1	C1	C2	179.6(3)
Rh1	N1	C9	C10	95.5(6)	Rh1	N1	C9	C14	-83.4(6)
C1	N1	C9	C10	-73.4(7)	C1	N1	C9	C14	107.7(6)
C9	N1	C1	O3	170.3(5)	C9	N1	C1	C2	-11.4(8)
Rh1	N2	C3	O4	-4.1(8)	Rh1	N2	C3	C4	175.7(4)
Rh1	N2	C15	C16	-95.1(6)	Rh1	N2	C15	C20	85.3(6)
C3	N2	C15	C16	77.8(7)	C3	N2	C15	C20	-101.8(7)
C15	N2	C3	O4	-176.8(5)	C15	N2	C3	C4	3.0(8)
Rh2	N4	C5	O1	2.6(8)	Rh2	N4	C5	C6	-175.3(3)
Rh2	N4	C28	C29	-92.3(6)	Rh2	N4	C28	C33	85.9(6)
C5	N4	C28	C29	88.8(7)	C5	N4	C28	C33	-93.0(7)
C28	N4	C5	O1	-178.5(5)	C28	N4	C5	C6	3.6(8)
Rh2	N5	C7	O2	-4.3(8)	Rh2	N5	C7	C8	176.7(3)
Rh2	N5	C34	C35	-102.9(5)	Rh2	N5	C34	C39	72.8(6)
C7	N5	C34	C35	76.3(7)	C7	N5	C34	C39	-108.0(6)

C34	N5	C7	O2	176.6(5)	C34	N5	C7	C8	-2.4(8)
N1	C9	C10	C11	-179.7(5)	N1	C9	C14	C13	179.9(5)
C10	C9	C14	C13	1.0(9)	C14	C9	C10	C11	-0.7(10)
C9	C10	C11	C12	-0.1(11)	C10	C11	C12	C13	0.6(11)
C11	C12	C13	C14	-0.4(11)	C12	C13	C14	C9	-0.5(10)
N2	C15	C16	C17	-178.8(5)	N2	C15	C20	C19	179.1(5)
C16	C15	C20	C19	-0.5(10)	C20	C15	C16	C17	0.7(10)
C15	C16	C17	C18	-0.2(12)	C16	C17	C18	C19	-0.6(13)
C17	C18	C19	C20	0.8(12)	C18	C19	C20	C15	-0.3(11)
C21	C22	C23	C24	177.1(5)	C21	C22	C27	C26	-175.3(5)
C23	C22	C27	C26	-0.0(9)	C27	C22	C23	C24	1.8(9)
C22	C23	C24	C25	-2.5(10)	C23	C24	C25	C26	1.4(10)
C24	C25	C26	C27	0.4(10)	C24	C25	C26	C47	-179.1(6)
C25	C26	C27	C22	-1.1(9)	C47	C26	C27	C22	178.4(5)
N4	C28	C29	C30	179.4(5)	N4	C28	C33	C32	-178.5(5)
C29	C28	C33	C32	-0.3(10)	C33	C28	C29	C30	1.2(9)
C28	C29	C30	C31	-0.8(11)	C29	C30	C31	C32	-0.4(12)
C30	C31	C32	C33	1.3(12)	C31	C32	C33	C28	-1.0(11)
N5	C34	C35	C36	176.4(5)	N5	C34	C39	C38	-177.3(5)
C35	C34	C39	C38	-1.5(9)	C39	C34	C35	C36	0.6(9)
C34	C35	C36	C37	0.5(11)	C35	C36	C37	C38	-0.7(12)
C36	C37	C38	C39	-0.2(12)	C37	C38	C39	C34	1.3(11)
C40	C41	C42	C43	173.8(5)	C40	C41	C46	C45	-173.7(5)
C42	C41	C46	C45	2.7(10)	C46	C41	C42	C43	-2.6(10)
C41	C42	C43	C44	1.2(11)	C42	C43	C44	C45	0.1(12)

C43	C44	C45	C46	-0.1(11)		C43	C44	C45	C48	179.2(7)
C44	C45	C46	C41	-1.3(10)		C48	C45	C46	C41	179.4(6)

APPENDIX D

SUPPLEMENTARY INFORMATION FOR **IV**

EXPERIMENTAL DETAILS

A. Crystal Data

Empirical Formula	$C_{41}H_{38}N_6O_4Rh_2Cl_2$
Formula Weight	955.51
Crystal Color, Habit	purple, block
Crystal Dimensions	0.21 X 0.18 X 0.11 mm
Crystal System	triclinic
Lattice Type	Primitive
Lattice Parameters	a = 11.8846(12) Å
	b = 13.3012(14) Å
	c = 14.8803(15) Å
	α = 77.976(6) º
	β = 74.608(5) º
	γ = 65.476(5) º
	V = 2050.3(4) Å^3
Space Group	P-1 (#2)
Z value	2
D_{calc}	1.548 g/cm^3
F_{000}	964.00
μ(MoKα)	9.812 cm^{-1}

B. Intensity Measurements

Diffractometer	Rigaku Mercury375R/M CCD (XtaLAB mini)
Radiation	MoKα (λ = 0.71075 Å)
	graphite monochromated
Voltage, Current	50kV, 12mA
Temperature	20.0°C
Detector Aperture	75 mm (diameter)
Data Images	540 exposures
ω oscillation Range (=54.0, =0.0)	-60.0 - 120.0°
Exposure Rate	20.0 sec./°
Detector Swing Angle	29.50°
ω oscillation Range (=54.0, =120.0)	-60.0 - 120.0°
Exposure Rate	20.0 sec./°
Detector Swing Angle	29.50°
ω oscillation Range (=54.0, =240.0)	-60.0 - 120.0°
Exposure Rate	20.0 sec./°
Detector Swing Angle	29.50°
ω oscillation Range (=54.0, =0.0)	-60.0 - 120.0°
Exposure Rate	20.0 sec./°
Detector Swing Angle	29.50°
ω oscillation Range (=54.0, =120.0)	-60.0 - 120.0°
Exposure Rate	20.0 sec./°
Detector Swing Angle	29.50°

ω oscillation Range (=54.0, =240.0)	-60.0 - 120.0°
Exposure Rate	20.0 sec./°
Detector Swing Angle	29.50°
Detector Position	50.00 mm
Pixel Size	0.146 mm
$2\theta_{max}$	55.0°
No. of Reflections Measured	Total: 21660
	Unique: 9317 (R_{int} = 0.0458)
Corrections	Lorentz-polarization
	Absorption
	(trans. factors: 0.621 - 0.898)

C. Structure Solution and Refinement

Structure Solution	Direct Methods
Refinement	Full-matrix least-squares on F^2
Function Minimized	$\Sigma\, w\, (F_o^2 - F_c^2)^2$
Least Squares Weights	$w = 1/\,[\,\sigma^2(F_o^2) + (0.0407 \cdot P)^2$
	$+ 1.3081 \cdot P\,]$
	where $P = (Max(F_o^2,0) + 2F_c^2)/3$
$2\theta_{max}$ cutoff	55.0°
Anomalous Dispersion	All non-hydrogen atoms
No. Observations (All reflections)	14070
No. Variables	500
Reflection/Parameter Ratio	28.14
Residuals: R1 (I>2.00σ(I))	0.0454

Residuals: R (All reflections)		0.0722		
Residuals: wR2 (All reflections)		0.1037		
Goodness of Fit Indicator		1.027		
Max Shift/Error in Final Cycle		0.001		
Maximum peak in Final Diff. Map		0.72 e$^-$/Å^3		
Minimum peak in Final Diff. Map		-0.63 e$^-$/Å^3		

Table 1. Atomic coordinates and B_{iso}/B_{eq}

atom	x	y	z	B_{eq}
Rh(1)	0.25565(3)	0.80902(2)	0.26175(2)	2.394(7)
Rh(2)	0.32060(3)	0.61760(2)	0.23662(2)	2.618(7)
Cl(1)	0.7161(2)	0.58958(16)	0.02749(13)	8.87(5)
Cl(2)	0.7865(3)	0.35902(17)	0.0912(3)	15.35(13)
O(1)	0.2262(2)	0.7630(2)	0.40441(17)	3.07(5)
O(2)	0.3760(3)	0.6572(2)	0.09580(18)	3.49(5)
O(3)	0.4964(3)	0.5856(2)	0.2528(2)	3.52(5)
O(4)	0.1427(3)	0.6518(2)	0.2211(2)	3.35(5)
N(1)	0.4429(3)	0.7676(3)	0.2660(2)	2.83(6)
N(2)	0.0733(3)	0.8249(3)	0.2655(2)	3.14(6)
N(3)	0.1947(3)	0.9835(3)	0.2809(2)	3.10(6)
N(4)	0.2666(3)	0.5880(3)	0.3775(2)	3.11(6)
N(5)	0.2931(3)	0.8402(2)	0.1183(2)	2.91(6)
N(6)	0.3729(4)	0.4341(3)	0.2037(3)	4.53(8)
C(1)	0.5232(4)	0.6645(3)	0.2664(3)	3.14(7)
C(2)	0.6544(4)	0.6289(4)	0.2827(4)	4.58(10)
C(3)	0.0524(4)	0.7426(3)	0.2465(3)	3.01(7)

216

C(4)	-0.0783(4)	0.7471(4)	0.2537(4)	4.47(10)
C(5)	0.2340(4)	0.6635(3)	0.4340(3)	3.30(7)
C(6)	0.2028(5)	0.6398(4)	0.5393(3)	5.26(11)
C(7)	0.3503(4)	0.7592(3)	0.0641(3)	3.25(7)
C(8)	0.3915(5)	0.7815(4)	-0.0403(3)	4.82(10)
C(9)	0.4780(4)	0.8505(3)	0.2860(3)	2.89(7)
C(10)	0.4233(4)	0.8949(4)	0.3703(3)	3.84(8)
C(11)	0.4530(5)	0.9769(4)	0.3901(4)	5.11(11)
C(12)	0.5368(5)	1.0153(4)	0.3262(5)	5.89(13)
C(13)	0.5906(5)	0.9724(4)	0.2422(4)	5.35(12)
C(14)	0.5612(4)	0.8904(4)	0.2208(3)	4.11(9)
C(15)	-0.0296(4)	0.9220(3)	0.2989(3)	3.26(7)
C(16)	-0.0518(5)	0.9394(4)	0.3913(4)	4.98(10)
C(17)	-0.1442(5)	1.0360(5)	0.4241(4)	6.31(14)
C(18)	-0.2152(5)	1.1150(5)	0.3661(5)	6.06(14)
C(19)	-0.1954(5)	1.0993(4)	0.2752(5)	5.53(12)
C(20)	-0.1013(4)	1.0029(4)	0.2398(4)	4.31(9)
C(21)	0.1700(4)	1.0763(3)	0.2727(3)	3.16(7)
C(22)	0.1418(4)	1.1944(3)	0.2546(3)	3.24(7)
C(23)	0.2377(4)	1.2326(3)	0.2452(3)	3.25(7)
C(24)	0.2101(4)	1.3457(3)	0.2225(3)	3.52(8)
C(25)	0.0928(5)	1.4183(4)	0.2088(4)	4.61(10)
C(26)	-0.0009(5)	1.3786(4)	0.2188(4)	5.27(11)
C(27)	0.0235(4)	1.2666(4)	0.2407(3)	4.40(9)
C(28)	0.2722(4)	0.4786(3)	0.4160(3)	3.74(8)

C(29)	0.1671(5)	0.4533(4)	0.4354(4)	5.08(11)
C(30)	0.1766(8)	0.3454(5)	0.4713(4)	7.47(17)
C(31)	0.2866(9)	0.2655(5)	0.4862(4)	8.6(2)
C(32)	0.3918(9)	0.2891(5)	0.4640(5)	8.5(2)
C(33)	0.3866(6)	0.3955(4)	0.4289(4)	5.97(13)
C(34)	0.2570(4)	0.9526(3)	0.0752(3)	3.07(7)
C(35)	0.3307(4)	1.0130(4)	0.0668(3)	3.68(8)
C(36)	0.2911(5)	1.1233(4)	0.0301(3)	4.70(10)
C(37)	0.1786(5)	1.1746(4)	0.0009(4)	5.07(11)
C(38)	0.1051(5)	1.1153(4)	0.0076(4)	5.27(11)
C(39)	0.1444(4)	1.0049(4)	0.0442(3)	4.37(9)
C(40)	0.3066(4)	0.3903(3)	0.2117(3)	3.73(8)
C(41)	0.6694(5)	0.4769(4)	0.0549(4)	5.56(11)

$B_{eq} = 8/3\, \pi^2 (U_{11}(aa^*)^2 + U_{22}(bb^*)^2 + U_{33}(cc^*)^2 + 2U_{12}(aa^*bb^*)\cos\gamma + 2U_{13}(aa^*cc^*)\cos\beta + 2U_{23}(bb^*cc^*)\cos\alpha)$

Table 2. Anisotropic displacement parameters

atom	U_{11}	U_{22}	U_{33}	U_{12}	U_{13}	U_{23}
Rh(1)	0.03429(17)	0.02606(15)	0.03416(17)	-0.01529(12)	-0.00533(12)	-0.00463(12)
Rh(2)	0.03976(19)	0.02643(16)	0.03592(18)	-0.01624(13)	-0.00486(13)	-0.00480(13)
Cl(1)	0.1714(19)	0.1151(14)	0.0871(12)	-0.1021(14)	-0.0134(12)	-0.0016(10)
Cl(2)	0.187(3)	0.0807(13)	0.360(5)	-0.0246(15)	-0.195(3)	0.0069(19)
O(1)	0.0492(16)	0.0366(14)	0.0332(14)	-0.0208(12)	-0.0039(12)	-0.0046(12)
O(2)	0.0587(18)	0.0346(15)	0.0387(15)	-0.0212(13)	-0.0021(13)	-0.0057(12)
O(3)	0.0425(16)	0.0350(15)	0.0564(18)	-0.0132(12)	-0.0089(13)	-0.0103(13)
O(4)	0.0431(16)	0.0351(14)	0.0562(18)	-0.0189(13)	-0.0121(13)	-0.0090(13)
N(1)	0.0348(17)	0.0367(17)	0.0408(18)	-0.0175(14)	-0.0064(14)	-0.0072(14)
N(2)	0.0402(19)	0.0343(17)	0.051(2)	-0.0189(15)	-0.0096(15)	-0.0066(15)
N(3)	0.0442(20)	0.0293(17)	0.049(2)	-0.0180(15)	-0.0082(15)	-0.0076(15)
N(4)	0.0464(20)	0.0274(16)	0.0394(18)	-0.0118(14)	-0.0079(15)	0.0008(14)
N(5)	0.0448(19)	0.0308(16)	0.0374(18)	-0.0173(14)	-0.0097(14)	-0.0013(14)
N(6)	0.081(3)	0.049(2)	0.058(2)	-0.040(2)	-0.012(2)	-0.0091(19)
C(1)	0.039(2)	0.039(2)	0.043(2)	-0.0171(18)	-0.0060(17)	-0.0056(18)
C(2)	0.045(3)	0.053(3)	0.079(3)	-0.011(2)	-0.024(2)	-0.014(2)
C(3)	0.044(2)	0.037(2)	0.039(2)	-0.0201(18)	-0.0106(17)	-0.0032(17)
C(4)	0.042(3)	0.055(3)	0.085(4)	-0.025(2)	-0.018(2)	-0.013(3)
C(5)	0.050(2)	0.037(2)	0.038(2)	-0.0188(19)	-0.0082(18)	-0.0010(18)
C(6)	0.107(4)	0.058(3)	0.038(3)	-0.040(3)	-0.007(3)	-0.002(2)
C(7)	0.051(2)	0.039(2)	0.036(2)	-0.0213(19)	-0.0066(18)	-0.0043(18)
C(8)	0.091(4)	0.049(3)	0.038(2)	-0.030(3)	0.002(2)	-0.005(2)
C(9)	0.036(2)	0.0330(20)	0.046(2)	-0.0150(16)	-0.0159(17)	-0.0015(17)

C(10)	0.051(3)	0.053(3)	0.052(3)	-0.022(2)	-0.017(2)	-0.013(2)
C(11)	0.067(3)	0.057(3)	0.086(4)	-0.020(3)	-0.034(3)	-0.026(3)
C(12)	0.079(4)	0.050(3)	0.124(5)	-0.032(3)	-0.054(4)	-0.010(3)
C(13)	0.065(3)	0.060(3)	0.095(4)	-0.042(3)	-0.034(3)	0.019(3)
C(14)	0.050(3)	0.058(3)	0.058(3)	-0.031(2)	-0.014(2)	0.001(2)
C(15)	0.032(2)	0.043(2)	0.055(3)	-0.0193(18)	-0.0028(18)	-0.0142(20)
C(16)	0.048(3)	0.072(3)	0.061(3)	-0.013(2)	-0.008(2)	-0.018(3)
C(17)	0.048(3)	0.100(5)	0.087(4)	-0.018(3)	0.008(3)	-0.051(4)
C(18)	0.045(3)	0.059(3)	0.127(5)	-0.013(3)	0.000(3)	-0.050(4)
C(19)	0.043(3)	0.046(3)	0.119(5)	-0.016(2)	-0.018(3)	-0.004(3)
C(20)	0.044(3)	0.045(3)	0.072(3)	-0.011(2)	-0.013(2)	-0.010(2)
C(21)	0.041(2)	0.043(2)	0.042(2)	-0.0199(18)	-0.0055(17)	-0.0118(19)
C(22)	0.049(2)	0.0302(20)	0.045(2)	-0.0166(18)	-0.0041(18)	-0.0108(17)
C(23)	0.048(2)	0.033(2)	0.043(2)	-0.0147(17)	-0.0091(18)	-0.0070(17)
C(24)	0.063(3)	0.032(2)	0.043(2)	-0.024(2)	-0.0053(20)	-0.0089(18)
C(25)	0.064(3)	0.029(2)	0.073(3)	-0.013(2)	-0.009(2)	-0.003(2)
C(26)	0.049(3)	0.038(3)	0.101(4)	-0.006(2)	-0.015(3)	-0.008(3)
C(27)	0.045(3)	0.048(3)	0.073(3)	-0.020(2)	-0.005(2)	-0.010(2)
C(28)	0.066(3)	0.034(2)	0.035(2)	-0.017(2)	-0.0035(20)	-0.0028(18)
C(29)	0.080(4)	0.054(3)	0.060(3)	-0.038(3)	0.004(3)	-0.006(2)
C(30)	0.137(6)	0.070(4)	0.085(4)	-0.070(4)	0.019(4)	-0.014(3)
C(31)	0.183(9)	0.044(3)	0.064(4)	-0.037(5)	0.022(5)	-0.001(3)
C(32)	0.150(7)	0.049(4)	0.077(5)	-0.005(4)	-0.013(4)	0.011(3)
C(33)	0.081(4)	0.051(3)	0.070(4)	-0.006(3)	-0.018(3)	0.006(3)
C(34)	0.048(2)	0.034(2)	0.033(2)	-0.0190(18)	-0.0037(17)	-0.0011(16)

C(35)	0.056(3)	0.045(2)	0.046(2)	-0.028(2)	-0.0109(20)	-0.0003(19)
C(36)	0.087(4)	0.047(3)	0.053(3)	-0.042(3)	-0.005(3)	-0.001(2)
C(37)	0.091(4)	0.031(2)	0.059(3)	-0.018(3)	-0.010(3)	0.002(2)
C(38)	0.062(3)	0.052(3)	0.075(4)	-0.011(2)	-0.025(3)	0.008(3)
C(39)	0.056(3)	0.054(3)	0.061(3)	-0.026(2)	-0.021(2)	0.005(2)
C(40)	0.069(3)	0.032(2)	0.044(2)	-0.025(2)	-0.008(2)	-0.0036(18)
C(41)	0.077(4)	0.058(3)	0.079(4)	-0.025(3)	-0.020(3)	-0.009(3)

The general temperature factor expression: $\exp(-2\pi^2(a^{*2}U_{11}h^2 + b^{*2}U_{22}k^2 + c^{*2}U_{33}l^2 + 2a^*b^*U_{12}hk + 2a^*c^*U_{13}hl + 2b^*c^*U_{23}kl))$

Table 3. Fragment Analysis

fragment: 1 CHAIN fragment

Rh1	Rh2	O1	O2	O3
O4	N1	N2	N3	N4
N5	N6	C1	C2	C3
C4	C5	C6	C7	C8
C9	C10	C11	C12	C13
C14	C15	C16	C17	C18
C19	C20	C21	C22	C23
C24	C25	C26	C27	C28
C29	C30	C31	C32	C33
C34	C35	C36	C37	C38
C39	C40			

fragment: 2

Cl1	Cl2	C41

Table 4. Bond lengths (Å)

atom	atom	distance		atom	atom	distance
Rh(1)	Rh(2)	2.4146(5)		Rh(1)	O(1)	2.061(2)
Rh(1)	N(1)	2.074(3)		Rh(1)	N(2)	2.074(4)
Rh(1)	N(3)	2.182(3)		Rh(1)	N(5)	2.051(3)
Rh(2)	O(2)	2.049(2)		Rh(2)	O(3)	2.023(3)
Rh(2)	O(4)	2.037(3)		Rh(2)	N(4)	2.028(3)
Rh(2)	N(6)	2.380(4)		Cl(1)	C(41)	1.743(7)
Cl(2)	C(41)	1.709(5)		O(1)	C(5)	1.276(5)
O(2)	C(7)	1.275(5)		O(3)	C(1)	1.282(6)

O(4)	C(3)	1.285(4)	N(1)	C(1)	1.306(4)
N(1)	C(9)	1.436(6)	N(2)	C(3)	1.317(7)
N(2)	C(15)	1.429(4)	N(3)	C(21)	1.132(6)
N(4)	C(5)	1.312(6)	N(4)	C(28)	1.429(5)
N(5)	C(7)	1.318(5)	N(5)	C(34)	1.430(5)
N(6)	C(40)	1.129(8)	C(1)	C(2)	1.501(7)
C(3)	C(4)	1.505(7)	C(5)	C(6)	1.509(6)
C(7)	C(8)	1.505(6)	C(9)	C(10)	1.379(6)
C(9)	C(14)	1.383(6)	C(10)	C(11)	1.382(9)
C(11)	C(12)	1.370(8)	C(12)	C(13)	1.367(9)
C(13)	C(14)	1.390(9)	C(15)	C(16)	1.381(7)
C(15)	C(20)	1.379(6)	C(16)	C(17)	1.379(7)
C(17)	C(18)	1.354(8)	C(18)	C(19)	1.355(11)
C(19)	C(20)	1.397(6)	C(21)	C(22)	1.444(6)
C(22)	C(23)	1.394(7)	C(22)	C(27)	1.375(6)
C(23)	C(24)	1.386(6)	C(24)	C(25)	1.367(6)
C(24)	C(40)[1]	1.456(8)	C(25)	C(26)	1.382(9)
C(26)	C(27)	1.378(7)	C(28)	C(29)	1.370(9)
C(28)	C(33)	1.382(7)	C(29)	C(30)	1.392(9)
C(30)	C(31)	1.338(11)	C(31)	C(32)	1.354(15)
C(32)	C(33)	1.385(9)	C(34)	C(35)	1.382(8)
C(34)	C(39)	1.382(7)	C(35)	C(36)	1.380(6)
C(36)	C(37)	1.367(8)	C(37)	C(38)	1.373(10)
C(38)	C(39)	1.380(7)			

Symmetry Operators:

(1) X,Y+1,Z

Table 5. Bond angles (^{o})

atom	atom	atom	angle	atom	atom	atom	angle
Rh(2)	Rh(1)	O(1)	89.30(8)	Rh(2)	Rh(1)	N(1)	85.77(10)
Rh(2)	Rh(1)	N(2)	86.50(10)	Rh(2)	Rh(1)	N(3)	178.41(10)
Rh(2)	Rh(1)	N(5)	85.76(9)	O(1)	Rh(1)	N(1)	87.28(12)
O(1)	Rh(1)	N(2)	88.29(12)	O(1)	Rh(1)	N(3)	92.03(12)
O(1)	Rh(1)	N(5)	174.94(11)	N(1)	Rh(1)	N(2)	171.13(13)
N(1)	Rh(1)	N(3)	95.16(14)	N(1)	Rh(1)	N(5)	91.27(13)
N(2)	Rh(1)	N(3)	92.66(14)	N(2)	Rh(1)	N(5)	92.49(14)
N(3)	Rh(1)	N(5)	92.92(12)	Rh(1)	Rh(2)	O(2)	90.01(8)
Rh(1)	Rh(2)	O(3)	90.11(8)	Rh(1)	Rh(2)	O(4)	89.14(8)
Rh(1)	Rh(2)	N(4)	86.34(10)	Rh(1)	Rh(2)	N(6)	175.39(11)
O(2)	Rh(2)	O(3)	88.91(12)	O(2)	Rh(2)	O(4)	91.28(12)
O(2)	Rh(2)	N(4)	176.10(15)	O(2)	Rh(2)	N(6)	87.64(13)
O(3)	Rh(2)	O(4)	179.23(12)	O(3)	Rh(2)	N(4)	89.75(13)
O(3)	Rh(2)	N(6)	93.80(14)	O(4)	Rh(2)	N(4)	90.02(13)
O(4)	Rh(2)	N(6)	86.95(14)	N(4)	Rh(2)	N(6)	96.10(13)
Rh(1)	O(1)	C(5)	118.4(3)	Rh(2)	O(2)	C(7)	118.6(2)
Rh(2)	O(3)	C(1)	119.8(2)	Rh(2)	O(4)	C(3)	119.7(3)
Rh(1)	N(1)	C(1)	121.0(3)	Rh(1)	N(1)	C(9)	118.6(2)
C(1)	N(1)	C(9)	119.3(4)	Rh(1)	N(2)	C(3)	120.5(2)
Rh(1)	N(2)	C(15)	118.6(3)	C(3)	N(2)	C(15)	120.6(4)
Rh(1)	N(3)	C(21)	166.8(3)	Rh(2)	N(4)	C(5)	122.3(3)
Rh(2)	N(4)	C(28)	118.1(3)	C(5)	N(4)	C(28)	119.5(3)

Rh(1)	N(5)	C(7)	121.8(2)	Rh(1)	N(5)	C(34)	119.6(2)
C(7)	N(5)	C(34)	118.6(3)	Rh(2)	N(6)	C(40)	127.7(3)
O(3)	C(1)	N(1)	122.7(4)	O(3)	C(1)	C(2)	114.6(3)
N(1)	C(1)	C(2)	122.7(5)	O(4)	C(3)	N(2)	122.2(4)
O(4)	C(3)	C(4)	115.1(4)	N(2)	C(3)	C(4)	122.7(3)
O(1)	C(5)	N(4)	122.9(3)	O(1)	C(5)	C(6)	114.5(4)
N(4)	C(5)	C(6)	122.7(4)	O(2)	C(7)	N(5)	122.9(3)
O(2)	C(7)	C(8)	115.3(4)	N(5)	C(7)	C(8)	121.8(4)
N(1)	C(9)	C(10)	119.3(4)	N(1)	C(9)	C(14)	121.4(4)
C(10)	C(9)	C(14)	119.3(5)	C(9)	C(10)	C(11)	120.4(4)
C(10)	C(11)	C(12)	120.5(5)	C(11)	C(12)	C(13)	119.5(7)
C(12)	C(13)	C(14)	120.8(5)	C(9)	C(14)	C(13)	119.6(5)
N(2)	C(15)	C(16)	119.1(4)	N(2)	C(15)	C(20)	121.9(4)
C(16)	C(15)	C(20)	118.9(4)	C(15)	C(16)	C(17)	120.6(5)
C(16)	C(17)	C(18)	120.4(6)	C(17)	C(18)	C(19)	119.9(5)
C(18)	C(19)	C(20)	120.9(5)	C(15)	C(20)	C(19)	119.2(5)
N(3)	C(21)	C(22)	175.7(4)	C(21)	C(22)	C(23)	119.2(3)
C(21)	C(22)	C(27)	119.6(5)	C(23)	C(22)	C(27)	121.0(4)
C(22)	C(23)	C(24)	118.1(4)	C(23)	C(24)	C(25)	121.5(5)
C(23)	C(24)	C(40)[1]	120.5(4)	C(25)	C(24)	C(40)[1]	118.0(4)
C(24)	C(25)	C(26)	119.4(4)	C(25)	C(26)	C(27)	120.6(4)
C(22)	C(27)	C(26)	119.4(5)	N(4)	C(28)	C(29)	120.8(4)
N(4)	C(28)	C(33)	119.7(5)	C(29)	C(28)	C(33)	119.3(5)
C(28)	C(29)	C(30)	119.3(5)	C(29)	C(30)	C(31)	121.4(9)
C(30)	C(31)	C(32)	119.5(7)	C(31)	C(32)	C(33)	121.1(7)

C(28)	C(33)	C(32)	119.3(7)	N(5)	C(34)	C(35)	121.2(4)
N(5)	C(34)	C(39)	120.4(5)	C(35)	C(34)	C(39)	118.4(4)
C(34)	C(35)	C(36)	120.6(5)	C(35)	C(36)	C(37)	120.5(6)
C(36)	C(37)	C(38)	119.6(4)	C(37)	C(38)	C(39)	120.1(5)
C(34)	C(39)	C(38)	120.8(6)	N(6)	C(40)	C(24)[2]	173.8(4)
Cl(1)	C(41)	Cl(2)	110.9(4)				

Symmetry Operators:

(1) X,Y+1,Z   (2) X,Y-1,Z

Table 6. Torsion Angles(°)

(Those having bond angles > 160 degrees are excluded.)

atom1	atom2	atom3	atom4	angle	atom1	atom2	atom3	atom4	angle
Rh(2)	Rh(1)	O(1)	C(5)	-7.85(18)	O(1)	Rh(1)	Rh(2)	O(3)	-83.01(8)
O(1)	Rh(1)	Rh(2)	O(4)	96.80(8)	O(1)	Rh(1)	Rh(2)	N(4)	6.73(8)
O(1)	Rh(1)	Rh(2)	N(6)	128.8(2)	Rh(2)	Rh(1)	N(1)	C(1)	-8.0(2)
N(1)	Rh(1)	Rh(2)	O(2)	-84.60(9)	N(1)	Rh(1)	Rh(2)	O(3)	4.31(8)
N(1)	Rh(1)	Rh(2)	N(4)	94.05(9)	N(1)	Rh(1)	Rh(2)	N(6)	-143.8(2)
Rh(2)	Rh(1)	N(2)	C(3)	-6.1(2)	N(2)	Rh(1)	Rh(2)	O(2)	99.75(9)
N(2)	Rh(1)	Rh(2)	O(4)	8.47(9)	N(2)	Rh(1)	Rh(2)	N(4)	-81.60(9)
N(2)	Rh(1)	Rh(2)	N(6)	40.5(2)	Rh(2)	Rh(1)	N(5)	C(7)	-9.3(3)
N(5)	Rh(1)	Rh(2)	O(2)	6.99(10)	N(5)	Rh(1)	Rh(2)	O(3)	95.90(10)
N(5)	Rh(1)	Rh(2)	O(4)	-84.29(10)	N(5)	Rh(1)	Rh(2)	N(6)	-52.2(2)
O(1)	Rh(1)	N(1)	C(1)	81.5(2)	O(1)	Rh(1)	N(1)	C(9)	-87.0(2)
N(1)	Rh(1)	O(1)	C(5)	-93.6(2)	O(1)	Rh(1)	N(2)	C(3)	-95.5(2)
O(1)	Rh(1)	N(2)	C(15)	77.8(2)	N(2)	Rh(1)	O(1)	C(5)	78.7(2)
N(1)	Rh(1)	N(3)	C(21)	87.4(13)	N(3)	Rh(1)	N(1)	C(9)	4.8(2)
N(1)	Rh(1)	N(5)	C(7)	76.3(3)	N(1)	Rh(1)	N(5)	C(34)	-103.4(3)
N(5)	Rh(1)	N(1)	C(1)	-93.7(2)	N(5)	Rh(1)	N(1)	C(9)	97.8(2)
N(2)	Rh(1)	N(3)	C(21)	-96.8(13)	N(3)	Rh(1)	N(2)	C(15)	-14.1(2)
N(2)	Rh(1)	N(5)	C(7)	-95.7(3)	N(2)	Rh(1)	N(5)	C(34)	84.6(3)
N(5)	Rh(1)	N(2)	C(3)	79.5(2)	N(5)	Rh(1)	N(2)	C(15)	-107.2(2)
N(3)	Rh(1)	N(5)	C(34)	-8.2(3)	N(5)	Rh(1)	N(3)	C(21)	-4.2(13)
Rh(1)	Rh(2)	O(2)	C(7)	-7.3(2)	Rh(1)	Rh(2)	O(3)	C(1)	-2.27(19)
Rh(1)	Rh(2)	O(4)	C(3)	-14.22(18)	Rh(1)	Rh(2)	N(4)	C(5)	-8.2(2)

O(2)	Rh(2)	O(3)	C(1)	87.7(2)	O(3)	Rh(2)	O(2)	C(7)	-97.4(2)
O(2)	Rh(2)	O(4)	C(3)	-104.21(20)	O(4)	Rh(2)	O(2)	C(7)	81.8(2)
O(2)	Rh(2)	N(6)	C(40)	-113.7(4)	O(3)	Rh(2)	N(4)	C(5)	81.9(3)
O(3)	Rh(2)	N(4)	C(28)	-94.1(2)	N(4)	Rh(2)	O(3)	C(1)	-88.6(2)
O(3)	Rh(2)	N(6)	C(40)	157.5(3)	O(4)	Rh(2)	N(4)	C(5)	-97.4(3)
O(4)	Rh(2)	N(4)	C(28)	86.6(2)	N(4)	Rh(2)	O(4)	C(3)	72.1(2)
O(4)	Rh(2)	N(6)	C(40)	-22.3(3)	N(4)	Rh(2)	N(6)	C(40)	67.4(4)
N(6)	Rh(2)	N(4)	C(28)	-0.3(3)	Rh(1)	O(1)	C(5)	N(4)	3.8(5)
Rh(2)	O(2)	C(7)	N(5)	2.2(6)	Rh(2)	O(3)	C(1)	N(1)	-3.4(5)
Rh(2)	O(4)	C(3)	N(2)	13.4(5)	Rh(1)	N(1)	C(1)	O(3)	8.8(5)
Rh(1)	N(1)	C(9)	C(10)	60.5(4)	Rh(1)	N(1)	C(9)	C(14)	-116.4(3)
C(1)	N(1)	C(9)	C(10)	-108.2(4)	C(1)	N(1)	C(9)	C(14)	74.9(4)
C(9)	N(1)	C(1)	C(2)	-2.9(5)	Rh(1)	N(2)	C(3)	O(4)	-3.1(5)
Rh(1)	N(2)	C(15)	C(16)	-64.9(4)	Rh(1)	N(2)	C(15)	C(20)	109.9(4)
C(3)	N(2)	C(15)	C(16)	108.4(5)	C(3)	N(2)	C(15)	C(20)	-76.8(5)
C(15)	N(2)	C(3)	C(4)	3.1(5)	Rh(2)	N(4)	C(5)	O(1)	4.5(6)
Rh(2)	N(4)	C(28)	C(29)	-96.7(3)	Rh(2)	N(4)	C(28)	C(33)	79.5(5)
C(5)	N(4)	C(28)	C(29)	87.2(5)	C(5)	N(4)	C(28)	C(33)	-96.7(4)
C(28)	N(4)	C(5)	C(6)	0.6(6)	Rh(1)	N(5)	C(7)	O(2)	6.5(6)
Rh(1)	N(5)	C(34)	C(35)	81.4(3)	Rh(1)	N(5)	C(34)	C(39)	-96.0(4)
C(7)	N(5)	C(34)	C(35)	-98.3(5)	C(7)	N(5)	C(34)	C(39)	84.2(5)
C(34)	N(5)	C(7)	C(8)	7.1(6)	Rh(2)	N(6)	C(40)	C(24)[1]	16(4)
C(10)	C(9)	C(14)	C(13)	1.7(6)	C(14)	C(9)	C(10)	C(11)	-1.2(6)
C(9)	C(10)	C(11)	C(12)	0.2(6)	C(10)	C(11)	C(12)	C(13)	0.4(8)
C(11)	C(12)	C(13)	C(14)	0.1(8)	C(12)	C(13)	C(14)	C(9)	-1.1(7)

C(16)	C(15)	C(20)	C(19)	-1.0(7)	C(20)	C(15)	C(16)	C(17)	0.1(8)
C(15)	C(16)	C(17)	C(18)	0.5(10)	C(16)	C(17)	C(18)	C(19)	-0.1(10)
C(17)	C(18)	C(19)	C(20)	-0.8(10)	C(18)	C(19)	C(20)	C(15)	1.4(9)
C(23)	C(22)	C(27)	C(26)	-1.2(7)	C(27)	C(22)	C(23)	C(24)	0.8(6)
C(22)	C(23)	C(24)	C(25)	-0.5(6)	C(23)	C(24)	C(25)	C(26)	0.7(7)
C(25)	C(24)	C(40)^2	N(6)^2	15(4)	C(24)	C(25)	C(26)	C(27)	-1.1(8)
C(25)	C(26)	C(27)	C(22)	1.3(8)	C(29)	C(28)	C(33)	C(32)	-2.1(7)
C(33)	C(28)	C(29)	C(30)	2.7(7)	C(28)	C(29)	C(30)	C(31)	-0.9(9)
C(29)	C(30)	C(31)	C(32)	-1.5(10)	C(30)	C(31)	C(32)	C(33)	2.2(11)
C(31)	C(32)	C(33)	C(28)	-0.4(10)	C(35)	C(34)	C(39)	C(38)	-1.4(6)
C(39)	C(34)	C(35)	C(36)	1.3(6)	C(34)	C(35)	C(36)	C(37)	-0.4(6)
C(35)	C(36)	C(37)	C(38)	-0.4(7)	C(36)	C(37)	C(38)	C(39)	0.3(7)
C(37)	C(38)	C(39)	C(34)	0.6(7)					

Symmetry Operators:

(1) X,Y-1,Z (2) X,Y+1,Z

VITA

NKONGHO ATEM-TAMBE

Personal Data:	Date of Birth: July 5, 1987
	Place of Birth: Yaounde, Centre Region, Cameroon
	Marital Status: Single
Education:	- M.S. in Chemistry, East Tennessee State University, Johnson City, Tennessee, May 2013.
	- B.S. in Chemistry (Honors Student), Minor in Material Science, University of Buea, Cameroon, December 2008.
Academic Presentations:	- ETSU Boland Research Syposium, East Tennessee State University, Johnson City, TN, April 2013.
	- South Eastern Regional Meeting of the American Chemical Society, SERMACS 2012, Raleigh, NC, November 2012.
	- Appalachian Research Symposium, East Tennessee State University, Johnson City, TN, April 2011.
Publications:	- Eagle, C. T.; Quarshie, F.; Ketron, M. E.; Atem-Tambe, N. "Cis-tetrakis [N-phenylacetamidato]-$K^4N{:}O;K^4O{:}N$-bis[(benzonitrile-KN) dirhoidium(II)] (Rh–Rh)".
	- Eagle, C. T.; Atem-Tambe, N.; Kpogo, K. K.; Tan, J.; Quarshie, F. "(3-Methylbenzonitrile-KN) tetrakis(μ-N-phenylacetamidato)-$K^4N{:}O;K^4O{:}N$-dirhodium(II) (Rh–Rh)".

Professional Experience: - Graduate Assistant/ Teaching Associate, Department of

Chemistry, East Tennessee State University,

2011 – 2013.

- Lab Assistant, Office of Information Technology (OIT),

East Tennessee State University, Johnson City, TN, 2010.

- Office Assistant, Cameroon General Certificate of

Examination Board, Buea, Cameroon, 2009.

Professional Associations: - American Chemical Society.

- Graduate and Professional Student Association (GPSA),

East Tennessee State University.

Honors and Awards: - Margaret Sells Endowment Scholarship for Scholastic

Achievement, East Tennessee state University, 2011.

- Honor Roll Academic Award for Freshman Year,

University of Buea, Cameroon, 2007.